HELICOPTER FLIGHT CONTROL

BY

INDIVIDUAL CHANNEL DESIGN

A DISSERTATION

SUBMITTED TO THE DEPARTMENT OF

ELECTRONICS AND ELECTRICAL ENGINEERING

OF GLASGOW UNIVERSITY

IN PARTIAL FULFILLMENT OF THE REQUIREMENTS

FOR THE DEGREE OF

DOCTOR OF PHILOSOPHY

By

Jesus U. Liceaga-Castro

February 1995

Abstract

Using the multivariable analysis framework known as Individual Channel Design (ICD), the analysis and design of a flight control system for a typical single main rotor helicopter is presented. As the ICD approach is more in the spirit of classical control theory (analysis followed by design), first the helicopter system model is analysed in order to determine the structural characteristics that can facilitate or impede the subsequent control design. Aspects such as loop interaction and right half plane poles and zeros are analysed. Three flight regimes are studied: Forward flight at 80 and 30 knots, and hover. The models for these flight conditions are initially given in the form of linear state space representations. The structural problems associated to these models, which cannot be remedied by simple feedback, are easily removed by ICD techniques resulting in control systems which are compatible with Level 1 handling qualities requirements. Additionally, assessments are performed on the basis of linear higher-order models. Also, the 30 knots design is assessed along a range of different speeds (20 to 40 knots), in order to determine the possibilities to derive scheduling control systems using ICD.

TO MY PARENTS

PROFESSOR JESUS LICEAGA ANGELES

AND

PROFESSOR ARTEMIA CASTRO LINARES

Acknowledgements

Firstly I would like to thank Doctor John O'Reilly for his considerable help, supervision and criticism to this work. I also would like to express my deepest gratitude to Doctor William Leithead from Strathclyde University, with which I had long and very helpful discussions along the development of this work.

I am indebted to the Consejo Nacional de Ciencia y Tecnologia (Mexico) for funding this work.

I would also like to thank the Control Group of the Department of Mechanical Engineering for allowing me to *abuse* their computing resources, and to Mrs Yasmine Mather for her assistance in the use of these facilities.

Finally I wish to thank Irma I. and Silvia I. Liceaga for their constant help, encouragement and support.

Contents

List of Tables

List of Figures

Chapter 1

Introduction

An unaugmented (open-loop except for the pilot) helicopter in either the hover (low speed) or forward flight regime demands a high work load on the part of the pilot. Augmentation in the form of an active control system to ease pilot work load and to meet stringent handling quality requirements is considered necessary, particularly in situations where high-performance manoeuvring is required. In addition, the high level of nonlinearity, cross-coupling characteristics, and unmodelled rotor dynamics of a typical single main rotor helicopter model make the active control law design a difficult and challenging problem. In past years, considerable attention has been paid to the design of active controllers for satisfactory rotor craft handling qualities. This problem has been tackled using different approaches ranging from classical (SISO) techniques, eigenstructure assignment methods, linear quadratic control, and H_∞ optimisation. For instance, Enns [7] designs a successful control system based on SISO techniques, the LQG control system design of Gribble [11] which present adequate robustness properties along different flight speeds or the H_∞ optimisation design by Yue *et al* [35] which gave rise to a successful piloted flight simulation trial.

As indicated by Manness *et al* [21], it is important to establish whether or not a specific approach is suitable for application to the helicopter flight control. That is, some approaches require full access to the state vector which is not yet possible.

In particular, it is suggested to avoid the use of lateral, longitudinal and vertical velocities, since there is not proper measurement equipment for them. Under this consideration the use of full state feedback is not possible. Thus applications which require full state feedback such as eigenstructure assignments methods may be not realistic. Also, the use of designs based on low-order rigid body dynamics may be affected by neglected high order rotor dynamics, Chen *et al* [5]. Frequency-domain modelling and analysis, as noted by Tischler [31], are effective for developing the physical understanding needed to implement high-bandwidth helicopter flight controllers. Therefore, any approach applied to the helicopter problem should be capable of providing information in terms of frequency domain responses.

On the other hand, in modern control theory the methods or approaches represent the most important part in the control system design, even more than the plant to be controlled or the problem of control itself. Simple inspection of recent conferences publications shows that control theory has been moving away from its original engineering context. This has resulted in a lack of transparency from an engineering point of view. In other words, the controllers obtained from the new control theories are not always realistic in terms of implementation. A second characteristic of the new approach is the change with respect to the classical control theory of how the problem is initially tackled, i.e, *design followed by analysis,* not according to the engineering context in which it is highly desirable to recognise physical and dynamical constraints. In particular, it is highly desirable to be able to identify *a priori* those dynamical characteristics of the multivariable system which are likely to facilitate or impede subsequent control systems design of whatever type. This point is further supported by Manness *et al* [21], where it is argued that a thorough comprehension of the systems dynamics is necessary before any control technique can be used to greatest effect. Indeed, a thorough understanding of the structure of the underlying system dynamics should lead to improved control system design. This is the first objective of the present work; a second objective is to focus on the multivariable design issues once the major

structural attributes of the dynamical system have been elucidated by multivariable analysis. The approach, therefore, is very much in the spirit of classical control *analysis followed by design* but for a strongly-coupled multivariable system. As such, the approach adopted here is in contradistinction to previous works Yue *et al* [35], Manness *et al* [21], Enns [7], Inmocenti *et al* [9], Hughes *et al* [8], Townsend [32] and Walker *et al* [34], each of which primarily focuses attention on a particular multivariable design method (e.g. , eigenstructure assignment, H_∞ optimisation, etc) followed by some assessment of the performance of that particular control design. That is not to criticise these various works. It is just that the multivariable analysis framework of the type described herein was simply not available.

It is worthwhile, therefore, and the purpose of this work, to examine in a fundamental way the structural and robustness issues underlying the multivariable helicopter flight control problem for a typical main rotor helicopter in forward flight and hover with a view to simple effective classically inspired feedback design. It is understood by structural issues, the fundamental potentially performance limiting features of the system such as loop interaction, right-half plane poles (RHPP's) and right-half plane zeros (RHPZ's), Leithead *et al* [15].

The frequency-domain multivariable analysis and design framework used is Individual Channel Design (ICD), O'Reilly and Leithead [27, 13, 15, 16, 14, 17, 18]. ICD is an appropriate framework for exploring the structural and robustness issues in helicopter control for the following reasons. First, it is shown [27], [14] that individual SISO signal transmission channels arise naturally from the customer (handling quality) specification on selected plant outputs with no loss of structural (loop interaction) information. Second, ICD is not a design method *per se* ; rather, it is a global structural analysis framework wherein the possibilities and limitations for control design of a particular strongly cross-coupled multivariable system are made apparent from the outset. Third, structural and robustness

issues are exposed by simple graphical Nyquist-type indicators.

The thesis is organised as follows. After a description of the helicopter flight control problem and model in Chapter 2, Chapter 3 reviews ICD as a framework for multivariable structural analysis. Chapter 4 provides an in depth ICD analysis of the helicopter control problem at 80 knots forward flight covering structural issues, principally the potential for decoupled control design on the basis of decoupled longitudinal and lateral dynamics. In Chapter 5, the multivariable designs by ICD for the helicopter longitudinal dynamics and lateral dynamics with an assessment of the total design on the full helicopter system are presented. Following the results of Chapter 4 and 5, in Chapter 6 the ICD analysis and control system design for the helicopter model at 30 knots is presented. This design unlike the 80 knots case is carried out on the basis of the full $4x4$ system. It includes the assessment of the resulting control system in terms of a higher order model which includes approximations of the rotor and actuator dynamics, and the evaluation of the control system along a range of different speeds (20 to 40 knots). The ICD analysis and design for the helicopter in hover together with an assessment on the basis of a higher order model is presented in Chapter 7. The conclusions are presented in Chapter 8.

Chapter 2

Helicopter Control Problem and Model

2.1 Introduction

In this chapter the main characteristics of the helicopter model system are described together with the tracking outputs and flight conditions selected to which the ICD approach is applied. A brief discussion of the dynamical and physical characteristics problems of the model is provided. These characteristics are further analysed in the classical text of Prouty [33] and by Tischler [31]. Also, as is well known, one of the main problems in the design of flight control systems for helicopters is the requirements or specifications of design. However, after the publication of Tischler [31], which provides a highly detailed assessment of flight control system design, this specification problem is considerably reduced. Hence, following this report a set of design objectives can be defined.

2.2 Helicopter control problem

An understanding of the dynamic characteristics of the aircraft is important in assessing the handling or flying qualities of an aircraft as well as for designing

controllers (autopilots). Flying qualities of an aircraft, specifically of a helicopter, are dependent upon pilot opinion, that is, the pilot's likes or dislikes with regards to various vehicle motions. It is possible to design a helicopter that has excellent performance but is considered to be unsatisfactory by the pilot. From the early 1960's to the present, there has been a considerable amount of research directed toward quantifying pilot opinion in terms of helicopter motion characteristics, such as frequency and damping ratio of the helicopter's various modes of motion. Thus, it is important to understand the dynamic characteristics of a helicopter and the relationship of the motion to the vehicle's aerodynamical characteristics and to pilot opinion, Nelson [26].

Like any aircraft in steady flight, the helicopter must be in equilibrium with respect to three forces and three moments acting along and around three orthogonal axes through its center of gravity. The analysis can be based on one of three possible systems of axes: wind axes, stability axes, or body axes. Although each system is valid, there are two reasons for using body axes system in helicopter analysis. First, the other systems lose their significance in hover. Second, when stability augmentation is used, the use of gyros or bob-weights whose displacements are measured with respect to the airframe are required. Also, the analysis of the effects of these devices is easiest in the body axes system, Prouty [33].

The aerodynamic moments and forces in the body axis system that are acting on the helicopter due to the main rotor, the tail rotor tailplane fin and fuselage, can be converted into equations of motion by accounting for forces and moments corresponding to inertia effects associated with accelerations, either linear or angular, and combination of velocities.

$$\mathbf{X} = G.W.sin\theta + \frac{G.W.}{g}(\dot{u} - vr + wq) \tag{2.1}$$

$$\mathbf{Y} = -G.W.sin\Phi + \frac{G.W.}{g}(\dot{v} + ur - wp) \tag{2.2}$$

$$\mathbf{Z} = -G.W.cos\Phi + \frac{G.W.}{g}(\dot{w} - uq + vp) \tag{2.3}$$

$$\mathbf{L} = I_{xx}\dot{p} - qr(I_{yy} - I_{zz}) \tag{2.4}$$

$$\mathbf{M} = I_{yy}\dot{q} - pr(I_{zz} - I_{xx}) \tag{2.5}$$

$$\mathbf{N} = I_{zz}\dot{r} - pq(I_{xx} - I_{yy}) \tag{2.6}$$

where **X**, **Y** and **Z** are the longitudinal force (forward), lateral force (right) and vertical force (down) respectively; **L**, **M** and **N** represent the rolling moment, pitching moment and yawing moment respectively, *G.W.* the weight, I_{jj} angular momentums and u, v, w, p, q and r are the translational and rotational variables as indicated in Figures(2.1)-(2.3) and Table 2.1.

u	Longitudinal velocity
v	Lateral velocity
w	Vertical velocity
p	Pitch rate
q	Roll rate
r	Yaw rate

Table 2.1: Translational and rotational variables

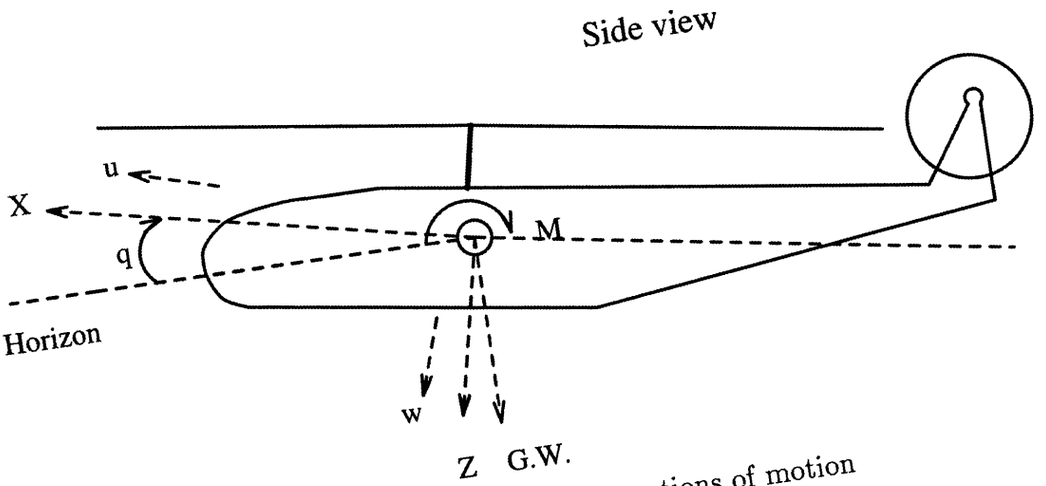

Figure 2.1: Parameters in equations of motion

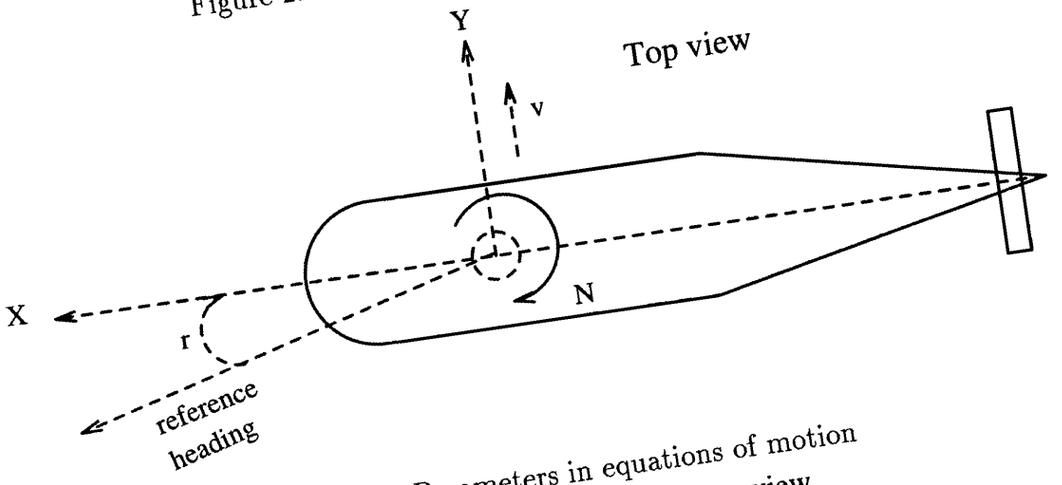

Figure 2.2: Parameters in equations of motion

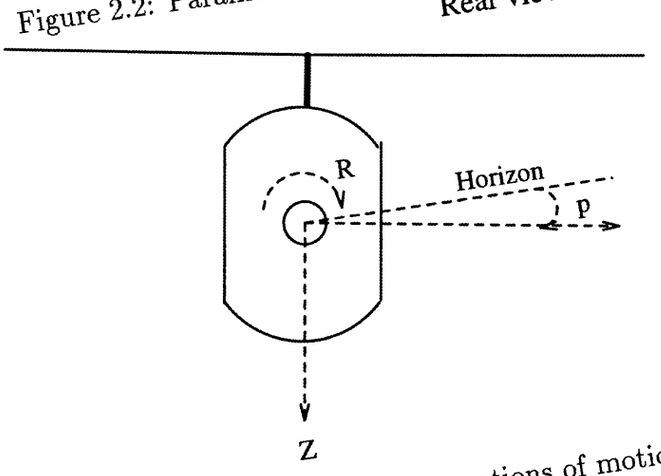

Figure 2.3: Parameters in equations of motion

From a rigorous standpoint, the set of six equations of motion should be augmented with three more equations representing the coning, longitudinal flapping, and lateral flapping of the rotor, which is not attached very rigidly to the airframe. However, the time constant for the flapping of conventional rotor blades corresponds to one-quarter to one-half of a rotor revolution. This rapid response justifies the use of the *quasi-static* assumption, which eliminates blade motions as separate degrees of freedom and simulates replacing the rotor with a black box at the top of the mast, which essentially produces forces and moments instantaneously in response to changes in flight conditions or control inputs. There are some studies, however, in which the coning and the cyclic flapping of the rotor on a short basis cannot be ignored. These include the prediction of the immediate response to gust or to a control input or the design of a high gain stability and control augmentation system (SCAS), Prouty [33].

The six body equations of equilibrium converted to linear partial differential equations of motion for small perturbations from steady, level flight are:

$$\begin{aligned} -\frac{G.W.}{g}\dot{u} + \frac{\delta X}{\delta u}u + \frac{\delta X}{\delta v}v + \frac{\delta X}{\delta w}w + (\frac{\delta X}{\delta q} - \frac{G.W.}{g}\bar{V}_o\Phi)q \\ -G.W.\Phi + \frac{\delta X}{\delta p}p + \frac{\delta X}{\delta r}r = -\frac{\delta X}{\delta \theta_o}\theta_o - \frac{\delta X}{\delta \theta_t}\theta_t - \frac{\delta X}{\delta \theta_l}\theta_l - \frac{\delta X}{\delta \theta_L}\theta_l \end{aligned} \quad (2.7)$$

$$\begin{aligned} -\frac{G.W.}{g}\dot{v} + \frac{\delta Y}{\delta u}u + \frac{\delta Y}{\delta v}v + \frac{\delta Y}{\delta w}w + (\frac{\delta Y}{\delta p} - \frac{G.W.}{g}\bar{V}_o\Phi)p \\ -G.W.\Phi + \frac{\delta Y}{\delta q}q + (\frac{\delta Y}{\delta r} - \frac{G.W.}{g}\bar{V}_o)r = -\frac{\delta Y}{\delta \theta_o}\theta_o - \frac{\delta Y}{\delta \theta_t}\theta_t - \frac{\delta Y}{\delta \theta_l}\theta_l - \frac{\delta Y}{\delta \theta_L}\theta_l \end{aligned} \quad (2.8)$$

$$\begin{aligned} \frac{\delta Z}{\delta u}u + \frac{\delta Z}{\delta v}v + \frac{\delta Z}{\delta w}w + (\frac{\delta Z}{\delta \dot{w}} - \frac{G.W.}{g})\dot{w} \\ +(\frac{\delta Z}{\delta q} + \frac{G.W.}{g}\bar{V}_o)q + \frac{\delta Z}{\delta p}p + \frac{\delta Z}{\delta r}r = -\frac{\delta Z}{\delta \theta_o}\theta_o - \frac{\delta Z}{\delta \theta_t}\theta_t - \frac{\delta Z}{\delta \theta_l}\theta_l - \frac{\delta Z}{\delta \theta_L}\theta_l \end{aligned} \quad (2.9)$$

$$\frac{\delta L}{\delta u}u + \frac{\delta L}{\delta v}v + \frac{\delta L}{\delta w}w + \frac{\delta L}{\delta q}q - I_{xx}\dot{p} + \frac{\delta L}{\delta p}p + \frac{\delta L}{\delta r}r = -\frac{\delta L}{\delta \theta_o}\theta_o - \frac{\delta L}{\delta \theta_t}\theta_t - \frac{\delta L}{\delta \theta_l}\theta_l - \frac{\delta L}{\delta \theta_L}\theta_l \quad (2.10)$$

$$\frac{\delta M}{\delta u}u + \frac{\delta M}{\delta v}v + \frac{\delta M}{\delta w}w + \frac{\delta M}{\delta \dot{w}}\dot{w} + \frac{\delta M}{\delta q}q - I_{yy}\dot{q} + \frac{\delta M}{\delta p}p + \frac{\delta M}{\delta r}r = -\frac{\delta M}{\delta \theta_o}\theta_o - \frac{\delta M}{\delta \theta_t}\theta_t - \frac{\delta M}{\delta \theta_l}\theta_l - \frac{\delta M}{\delta \theta_L}\theta_l \quad (2.11)$$

$$\frac{\delta N}{\delta u}u + \frac{\delta N}{\delta v}v + \frac{\delta N}{\delta w}w + \frac{\delta N}{\delta q}q - I_{zz}\dot{r} + \frac{\delta N}{\delta p}p + \frac{\delta N}{\delta r}r = -\frac{\delta N}{\delta \theta_o}\theta_o - \frac{\delta N}{\delta \theta_t}\theta_t - \frac{\delta N}{\delta \theta_l}\theta_l - \frac{\delta N}{\delta \theta_L}\theta_l \quad (2.12)$$

Note that the terms associated with the control inputs - main rotor collective, tail rotor, longitudinal cyclic and lateral cyclic- have all been gathered on the right-hand side in order to separate free from forced motion. In order to understand the problem which helicopters represent to the pilots, it is important to analyse the effects of these inputs (controllers) on the motion variables of Table 2.1, and how they are operated by the pilot.

Collective control

With the rotor blades free to flap and to lag-lead, the stresses have been reduced enough to permit the generation of thrust to balance the weight of the vehicle. If additional thrust is desired, e.g., to climb or to accelerate, the rotational velocity of the rotor could be increased so as to increase the velocity of air flow over the blades. However, this requires a changing of the engine speed and most helicopters engines have a very narrow band of high efficiency speed, so that producing thrust changes by changing engine speed is usually inefficient.

An alternative is to vary the angle of attack of the rotor blades since the developed lift is a direct function of the angle of attack. The angle of attack is varied by changing the pitch angle of the blades by displacement of the feathering

hinges.

If the lift is uniform about the rotor disc, e.g., the same forward as aft, and it is desired to increase lift uniformly, the pitch angle of all the blades must be changed by the same amount at the same time. This is called a collective change. The usual manner of accomplishing this change is by the use of a swash plate assembly. This assembly consists of a stationary part and a rotating part that turns with the rotor and follows the vertical motion of the stationary plate. Such a device is shown in Figure(2.4).

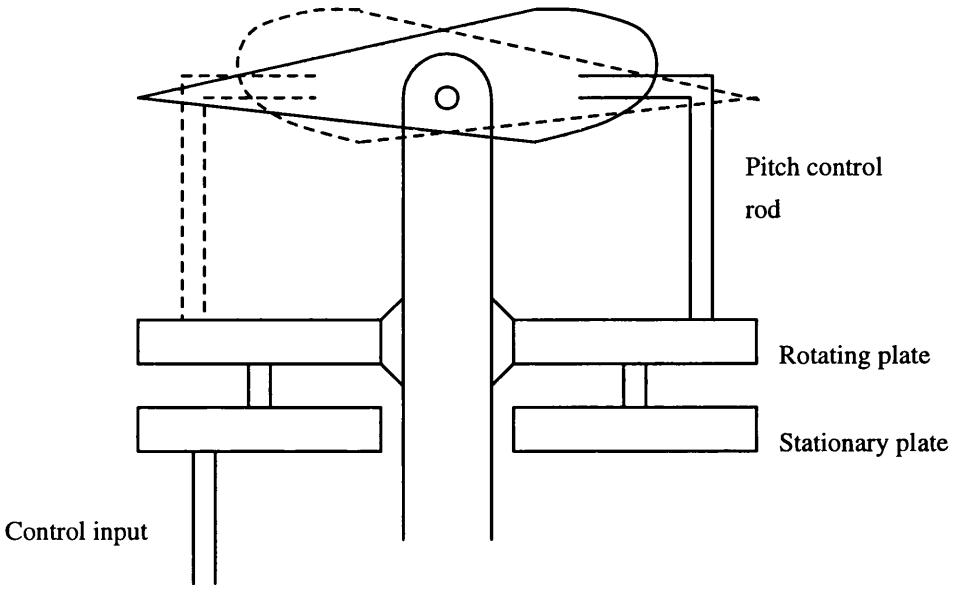

Figure 2.4: Collective control

If the pilot's controller, called the collective, is moved upward, the stationary plate is deflected upward and the rotating plate follows this motion through a set of followers. The raising of the rotating plate increases the pitch of all the blades at every point in the rotation cycle through the pitch control rods. This increase in pitch angle produces an increase in angle of attack and an increase in lift (thrust force).

Within the limits of power available and the settings of the blades, the use of collective control permits the vehicle to raise or descend vertically in still air, or to hold a fixed altitude, called hover. It is known that the rotor blades can produce a thrust force that is normal to the tip path plane of the coned blades. Suppose

that one could tilt the tip path plane and the thrust vector forward as shown in Figure(2.5). From this figure is possible to see that if the vertical component of the thrust is to remain constant in order to balance the weight, one must increase the thrust slightly as the thrust vector is tilted from vertical.

It is also possible to observe from Figure(2.5) that, in addition to the vertical component that balances the weight, there is now a horizontal component that acts as a propelling force and the helicopter moves forward, Layton [25].

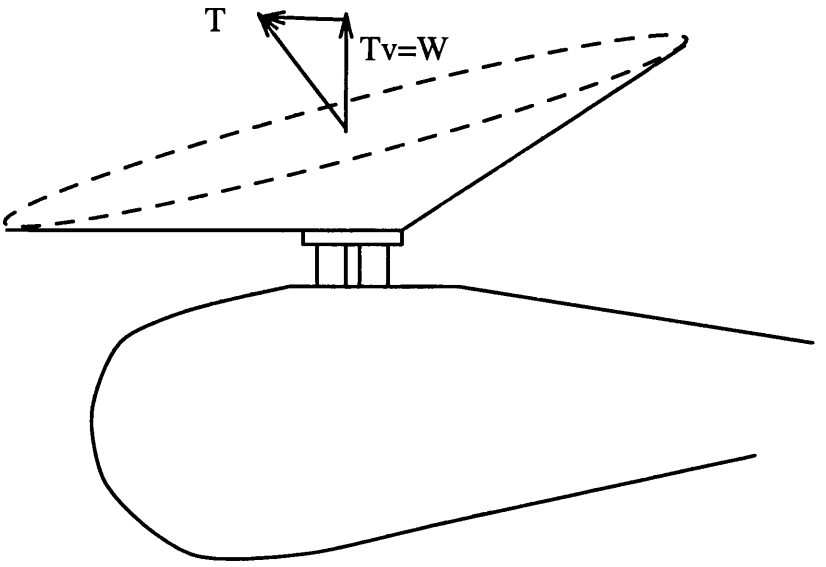

Figure 2.5: Collective controller

Once the vehicle moves forward, a new problem is introduced. In hover, the velocity across each blade is due only to the rotational velocity of the blades. Now as the helicopter moves forward, forward velocity, V_f, which is constant and always in the same direction, must be summed with the rotational velocities which change direction around the disc. At any point in the rotation, the sum of the flight velocity and the velocity due to rotation must be summed as shown in Figure(2.6).

From Figure(2.6) it is possible to see that the forward flight velocity apparently has no effect at aft (180°) and forward (0°) points, is additive at the midposition of the advancing blade (90°) and is subtractive at the midposition of the retreating blade (270°).

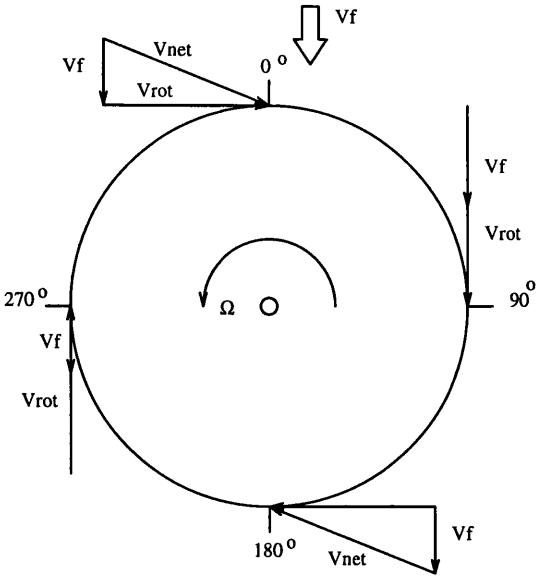

Figure 2.6: Forward and rotational velocities

Considering just the blade positions at 90° degree and the 270° degree points, there is a region of reverse flow on the retreating (270°) blade, starting at the hub and extending outward toward the tip. As the blade moves through the left side of the rotational path, this region is a circle whose radius is function of the rotational velocity and the forward speed.

Cyclic control (lateral/longitudinal)

In forward flight with increased velocity resultant on the advancing side and decreased velocity resultant on the retreating blades, an asymmetry of lift will occur. To balance the lift it is necessary to decrease the lift on the advancing blade side and/or increase the lift on the side of the retreating blades. The changes in lift vary from essentially zero at 0° degrees, to maximum at 90°, to zero at 180° degrees, to a maximum at 270° degrees. and back to zero at 360° degrees. From this, one may observe that the lift change must be cyclic and therefore the pitch change must also be cyclic. This change in pitch angle can be effected by using the same mechanism that was used for the collective control, but now, rather than moving the stationary plate up and down relative to the rotor shaft, it is tilted,

as shown in Figure(2.7).

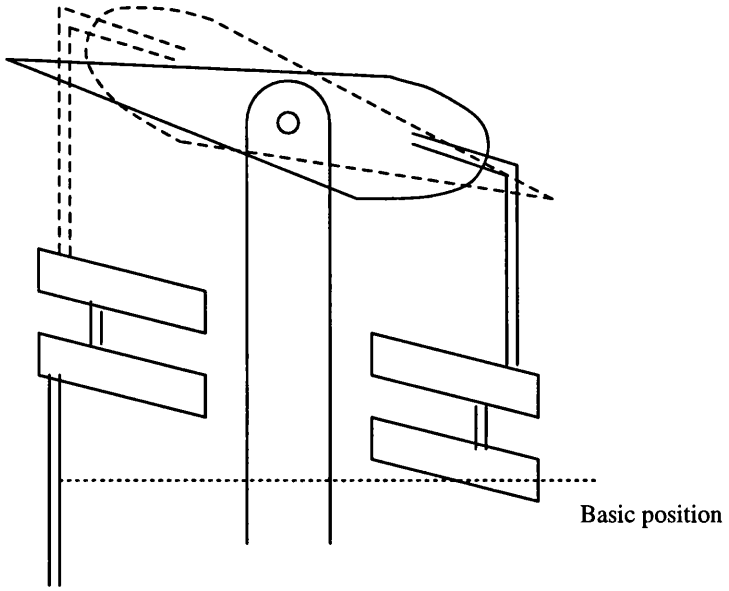

Figure 2.7: Cyclic controller

This cyclic control blade pitch not only permits the balancing of lift loads in forward or sidewise flight, but also permits the balance of any desired forces. For instance, if the lift is increased at rear of the rotor cone at the expense of the lift at the front of the rotor cone, the cone will tilt forward of the vertical, thereby creating a propulsive component of the thrust, as in Figure(2.5). Although the cyclic is used to control larger unbalances in forward flight, small deviations occur by the flapping motion of the blades.

Also, as the cyclic control permits flight in fore and aft directions, as well as lateral, the cyclic acts as a directional control. Recall that as the cyclic is changed the collective setting, as well as the engine power, must be changed to provide the weight balance component of thrust. It is noted, therefore, that the cyclic control and the collective control must be coordinated. To move from hover to forward flight, the pilot moves the cyclic control forward and, at the same time, increases the collective to furnish the required increase in thrust. As the helicopter moves forward, the velocity of forward flight tends to blow the rotor cone aft slightly, thus requiring additional forward movement of the cyclic to maintain the desired forward component, Layton [25].

Anti-torque tail rotor controller

With a single rotor vehicle, turning is accomplished by changing the thrust of the anti-torque rotor. The thrust of the anti-torque rotor is directly related to the power of the main rotor, and, although the anti-torque tail rotor is directly driven from the main rotor transmission system, the thrust is separately controlled. Similar to the main rotor, the thrust of the anti-torque or tail rotor is changed by collective change of the tail rotor blade pitch angles. A coupling between the main rotor collective and the tail rotor, called a collective-yaw coupler, provides a signal to the tail rotor in order that the tail rotor may maintain a pitch setting that provides the anti-torque thrust.

If it is desired to change the heading of a single-rotor helicopter, this may be obtained by changing the pitch of the tail rotor blades. Increasing the tail rotor thrust above the required for anti-torque stability will result in the nose of the helicopter moving to the left. Reducing the thrust will cause the nose of the helicopter to move to the right. This directional control is accomplished through rudder pedals. Displacement of the rudder pedal causes a movement of the tail rotor collective control, Lardinelli [12].

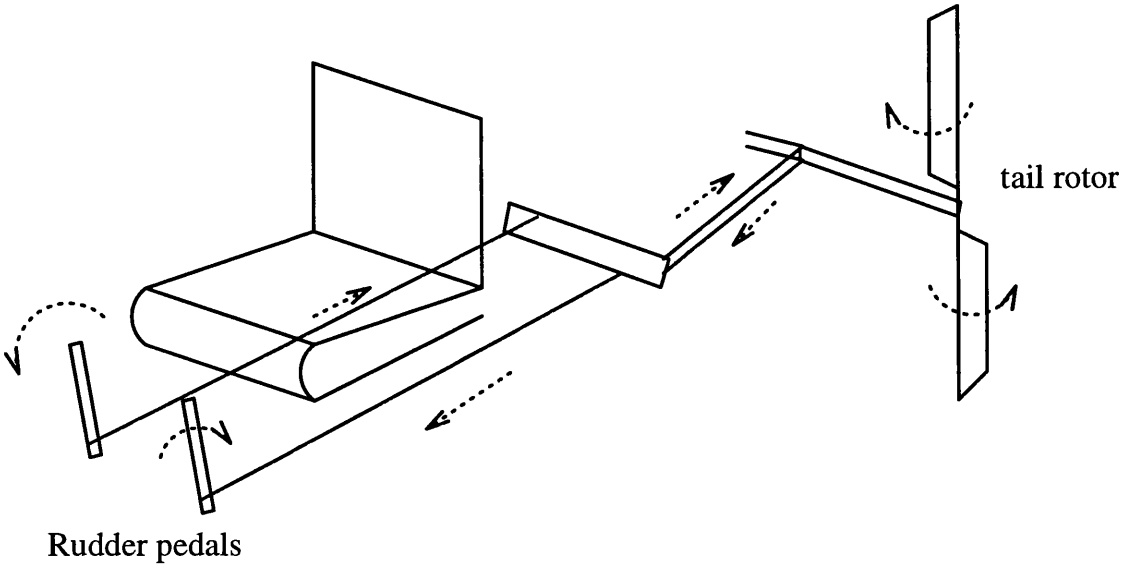

Figure 2.8: Tail rotor controller

From the previous analysis of the helicopter controllers, it is clear that the helicopter presents high cross-coupling characteristics whose source is associated with the fact that the main rotor is used to generate both thrust and control moments. Thus, any change of the tip-path-plane orientation intended to produce a change in the flight condition will create a series of effects which influence all the forces and moments applied to the rotor hub. Therefore, augmentation in the form of an active control system to ease the pilot work is necessary. However, due to the non-linearities of the system, the tremendous dynamical changes for different flight conditions, the inability to measure all the variables, the unmodelled rotor and actuator dynamics, and the inherent cross coupling effects between the lateral and longitudinal dynamics the control design represents a great challenge.

Several approaches have been used to tackle this problem ($H\infty$, LQG, eigenstructure assignment methods and SISO techniques). However, only control systems based on SISO techniques have actually been applied. This is due to the lack of *transparency* of the so called modern control techniques. For instances, in the case of the $H\infty$, the selection of the weighting matrices and their relation to system model constraints is not clear. Moreover, there may be more than one set of weighting matrices which produce the same results. Also, procedures to adjust control parameters to improve the design are not yet available. For the case of eigenstructure assignment methods, it is known that the resulting controllers are very sensitive to parametric uncertainty, and most of them require full state access which is not yet possible. With the methods used in practice (a SISO approach) designs are obtained heuristically, whose lengthy and expensive procedures can only be alleviated by *serendipity* .

The method proposed to solve this problem is the new approach known as ICD. The reason why ICD is an appropriate method for the helicopter flight control problem are: transparency, i.e, it is based on SISO techniques without losing the multivariable characteristic of the problem. Therefore, it is a multivariable

approach which uses the highly successful classical control results. It is a framework of analysis wherein the possibilities and limitations for control system design can be exposed. It represents a powerful tool for control system design in which control adjustment can be easily performed.

2.3 Helicopter model

In control system theory, the plant model represents an important part in the design of control systems. These models to which control is to be applied may have different forms or presentations. They may be represented by non-linear state space forms, linearised state space representations or transfer function matrices. For the case of linearised systems represented by linear time-invariant state space representations, the equations are given by

$$\dot{x} = Ax + Bu \tag{2.13}$$

$$y = Cx + Du \tag{2.14}$$

were the vector u represents the inputs to the system, the vector x represents the state variables and the vector y represents the outputs.

For any given system there may be many different state space representations thus the system in equations(2.13) and (2.14) is not unique. However, the transfer function matrix associated with any of the possible state representations is unique and is given by

$$G(s) = C(sI - A)^{-1}B + D \tag{2.15}$$

In general the transfer function matrix $G(s)$ represents the nominal open-loop signal transmission between the inputs and the outputs. This model will have both gain and phase uncertainties associated with unmodelled dynamics.

The helicopter is a typical example of a system which is multivariable in form having four control inputs in terms of the conventional collective, longitudinal cyclic, lateral cyclic and tail rotor controls. The helicopter models used throughout this work were obtained from the HELISTAB flight mechanics program Padfield [28] and Smith [29]. They are in the form of a linearised state space representation as given by equations(2.13) and (2.14) for a typical single main rotor combat helicopter with the system matrix A assuming quasi-static rotor flapping.

The rigid body dynamics with quasi steady rotor representation are characterised by strong cross coupling effects, non-minimum phase zeros and significant non-linearities. The problem in considering rotor dynamics is that feedback rotor state information with sufficient integrity for control purposes is not currently available. Also the rotor dynamics have non-minimum phase zeros well into the the right half plane which strongly attract poles, Chen *et al* [5]. Therefore, any control law design must take into account the unmodelled rotor dynamics.

The turbine engine dynamics are presently controlled by a shaft speed governor which introduces additional lag into the system as well as yaw-to collective coupling. This is because the governor perceives yawing motions as shaft speed variations, and as a result, changes the torque and hence the lift and height of the vehicle, Pandfiel [28] and Manness *et al* [22]. The actuators controlling blade pitch on both main and tail rotors can be conveniently represented by first order lags, with both authority and rate limits on the output blade angle, which implies the need for small control signal amplitudes in order to avoid nonlinearities.

A number of different models of the helicopter dynamics have been used for control law designs. However, as indicated by Enns [7] and Manness *et al* [22], linear low order rigid body dynamics systems represent the prime focus of a flight control law design since the associated states variables are the controlled quantities of the closed-loop system.

One characteristic of the helicopter model is that the nature of the system's

dynamics can be broken up into two distinct flight regimes: the hover and forward flight (where the dynamics modes of the rotorcraft often approach those of the fixed wing aircraft). So, the flight conditions selected in this work are the forward flight at low and high speed and the hover. However, the 80 knots forward flight represent the basis of this work. The reasons for this choice are

(i) the dynamics change less rapidly than in the neighbourhood of the hover;

(ii) HELISTAB is known to be more accurate in this flight condition as the hover is more affected by the inflow dynamics which are not considered in HELISTAB;

(iii) the multivariable structure and robustness properties of this linear rigid body helicopter model should provide much insight into how the Individual Channel Design framework might usefully be applied to more taxing flight regime including hover and rapid manoeuvre.

Because the requirements given in the handling qualities are usually given by the pilots, these can be considered subjective specifications. As a consequence their translation into control is difficult and can yield different sets of design specifications depending on selected tracking output variables. Hence, one of the must important aspects in helicopter flight control is the set of outputs selected to track the pilot's input commands. As indicated in Chapter 3, for the case of the ICD approach as well to helicopter applications, the number of outputs required must be equal to the number of inputs. Therefore, four tracking variables must be selected and associated with particular pilot inceptors.

There are eight possible sets of tracking variables which appear to be compatible with the forward flight handling quality requirements and the results of a Royal Aerospace Establishment piloted simulation study, Buckingham *et al* [2].

$$S_1 = \left\{\dot{h}, q, \Omega, \beta\right\}$$

$$S_2 = \left\{\dot{h}, q, p, \beta\right\}$$

$$S_3 = \{\Gamma, q, \Omega, \beta\}$$

$$S_4 = \{\Gamma, q, p, \beta\}$$

$$S_5 = \left\{\dot{h}, \theta, \Omega, \beta\right\}$$

$$S_6 = \left\{\dot{h}, \theta, p, \beta\right\}$$

$$S_7 = \{\Gamma, \theta, \Omega, \beta\}$$

$$S_8 = \{\Gamma, \theta, p, \beta\}$$

These sets of outputs can be paired to each input inceptor as indicated in Table 2.2

inceptor	output
Vertical	$\dot{h}$ - Height rate Γ - Flight path angle
Longitudinal	q - Pitch rate θ - Pitch attitude
Lateral	Ω - Turn rate p - roll rate
pedals	β - side slip angle

Table 2.2: Inceptor-tracking output possibilities

The set of outputs S_5 is selected as its associated transfer function matrix is minimum phase (the transmission zeros of the system are all in the left half plane), reducing the difficulties in the exploration of the ICD to the design of high performance helicopter flight control systems. For the hover condition, the set of outputs selected for an Attitude Command Attitude Hold (ACAH) response type are

$$S_h = \left\{\dot{h}, \theta, \phi, r\right\}$$

The reason for this choice is that unlike a Translational Rate Command with Position Hold (TRCPH) response type, the ACAH is minimum phase, Manness *et*

al [22], which increases the possibilities of designing a high performance control system.

The requirements for the control system defined in the handling qualities specifications, Anonymous [1], which describes the desired performance for the control system, involves both time and frequency domains properties, such as time constants, damping ratios, bandwidth and phase delay. These parameters restrict the channel bandwidths to values larger than 2rad/sec, but due to model accuracy deterioration at higher frequencies the bandwidths are also restricted to values of less than 10rad/sec, Enns [7]. In general, the required channels bandwidths for forward flight conditions specify values between 2 to 4 rad/sec, and 3.5 to 5.3 rad/sec for hover. The time responses must present a damping ratio of at least 0.35, and maximum cross-coupling values of ± 0.3. In particular the height rate response should have a qualitative first-order appearance for at least 5 sec. The bandwidths are defined as the frequency at which the overall augmented-vehicle response to the input of the pilot, exhibits 45 deg of phase margin or 6 dB's of gain margin, whichever is less. These stability margins refer to the augmented-vehicle as an open-loop element in the pilot/vehicle closed-loop system, Tischler [31]. Also, phase delays are determined by

$$\pi_p = -\frac{\Phi_{2\omega_{180}} + 180^o}{57.3(2\omega_{180})}$$

where $\Phi_{2\omega_{180}}$ represent the phase value at the double of the frequency at which the phase reaches -180^o degrees, Tischler [30]. The requirements specify time delays of no more than 0.32sec.

Despite the fact that the report ADS-33C [1], does not specify (clearly), stability as a handling quality requirement, Tischler [31] indicates stability as a highly desirable condition. Therefore, the control system must retain stability and performance under perturbations and large parameter uncertainties, in particular to the unmodelled high frequency rotor and actuators dynamics.

2.4 Conclusions

The purpose of this chapter is to give a brief description of the helicopter problem together with the selected flight conditions and outputs to which the ICD approach is applied. The choice of tracking outputs was based on the fact that the resulting model systems are minimum phase. Following the description and the physical restrictions for helicopter models, widely described by Manness *et al* [21], low order rigid body dynamics are selected as the basis for the helicopter control system designs, although the resulting designs are assessed on the basis of higher order models. Also the requirements to achieve Level 1 handling qualities are defined.

Chapter 3

Review of Individual Channel Design

3.1 Introduction

In this chapter the most important aspects of the Individual Channel Design (ICD) are presented. It includes the basic development of the approach in terms of a 2-input 2-output system, together with the extension to the general case of m-input m-output systems. Also some aspects of design within the ICD such as weak feedback, pre/post-compensation and a new application for feedforward control are shown. The details of how these technique are applied to the particular problem of the helicopter are discussed in the chapters concerning the control system design for the helicopter. For further details of the ICD approach, the reader is refered to Leithead and O'Reilly [27, 13, 15, 16, 14, 18, 17].

3.2 ICD analysis for 2-input 2-output systems

Multivariable systems are defined as those systems with more than one input and more than one output. For this reason, they are also called multiple-input multiple-output (MIMO) systems. An important set of MIMO systems are square

MIMO systems, i.e, those systems with the same number of inputs and outputs. The Individual Channel Design approach is based in the possibility of relating the inputs and outputs of a square system by pairs, that is input i and output i form the channel i. This is further supported by the requirements of design stated in the customer specifications which establish particular characteristics for individual signal transmission between each specified output and its associated reference signal.

A typical block diagram of a control system for a MIMO system is shown in Figure(3.1). Where $G(s)$ is the matrix transfer function representing the plant, $K(s)$ is the controller transfer function matrix, $U(s)$ is the input vector and $Y(s)$ is the output vector. Each of the elements y_i of the output vector $Y(s)$ will be influenced by the elements u_i of the input vector $U(s)$ depending on the structural characteristics of the plant $G(s)$. When the outputs y_i are mainly influenced by their corresponded input u_i, then the cross-coupling is weak and the system is effectively a set of single input single output (SISO) systems that can be analysed and designed on the basis of the diagonal elements of the plant matrix $G(s)$. These designs can be carried out using the highly successful tools of classical control theory, in which the requirements of design and the physical constrains can be assessed by the well established methods of Nyquist and Bode. On the other hand, when the influence of the input signals u_i are not restricted to their corresponded output y_i a set of problems arise; phase and gain margins may have a different meaning and can not be applied directly; each element of the controller matrix $K(s)$ is dependent on the other individual controllers and it is not clear how the structure of the system may influence on the structure of the controller.

3.2.1 Structure of 2-input 2-output systems

Consider the standard multivariable feedback control of Figure(3.1). Assume the plant $G(s)$ a 2-input 2-output system and $K(s)$ a diagonal controller matrix. Then

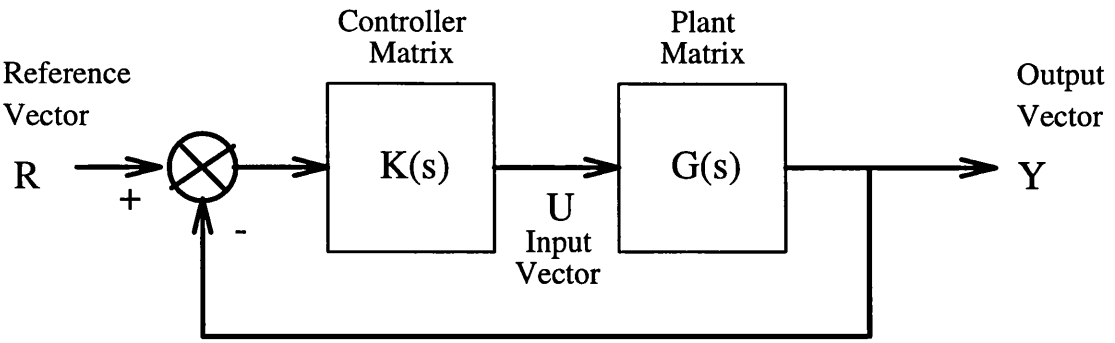

Figure 3.1: Standard multivariable control problem

the feedback system can be redrawn as in Figure(3.2), where k_i are the diagonal elements of the controller matrix $K(s)$ and g_{ij} are the elements of the plant matrix $G(s)$. The signal transmission from reference r_1 to its associated output y_1 in Figure(3.2), has two parallel paths; one directly through $g_{11}(s)$; and the other via $g_{21}(s)$, the bottom feedback subsystem, and $g_{12}(s)$. Also, from Figure(3.2), the forward cross-signal transmission from the second reference r_2 to y_1 is via the bottom feedback subsystem and $g_{12}(s)$. These signal transmission from r_1 to y_1 and r_2 to y_1 can be described as in Figure(3.3). Simple algebraic manipulation result in a more compact form as depicted in Figure(3.4). Therefore, Channel $C_1(s)$ has an open-loop SISO transmittance, O'Reilly and Leithead [27]

$$C_1(s) = k_1 g_{11}(1 - \gamma h_2) = k_1 g_{11}(1 - \gamma_1) \tag{3.1}$$

where the multivariable structure function γ is defined by

$$\gamma(s) = \frac{g_{12}g_{21}}{g_{11}g_{22}} \tag{3.2}$$

$$h_2(s) = \frac{k_2 g_{22}}{1 + k_2 g_{22}} \tag{3.3}$$

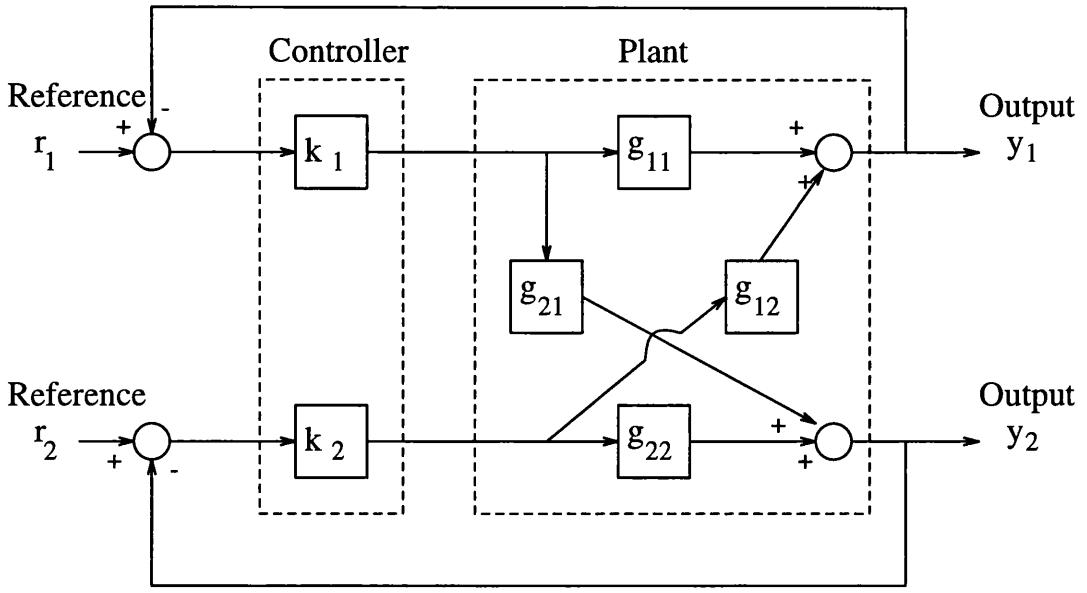

Figure 3.2: 2-input 2-output multivariable control problem with diagonal controller

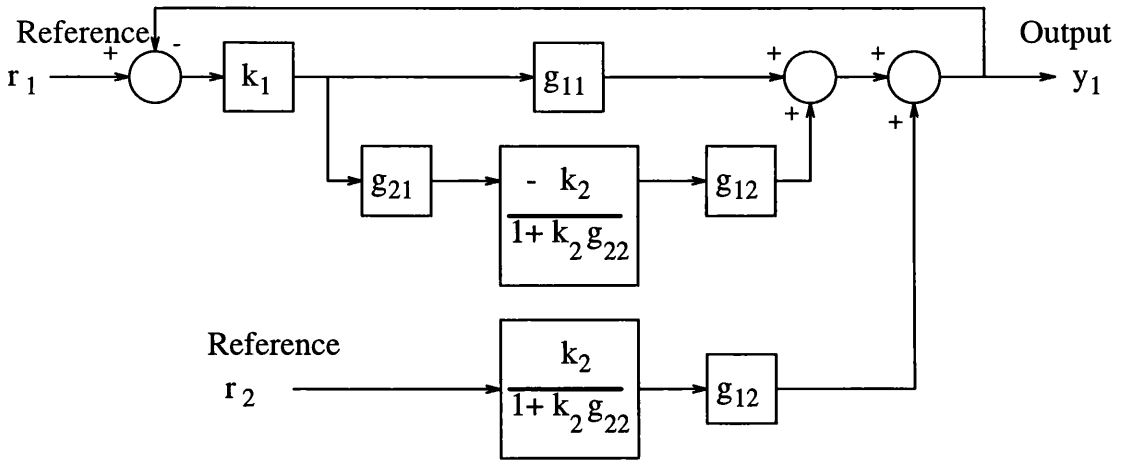

Figure 3.3: Signal transmissions to output y_1

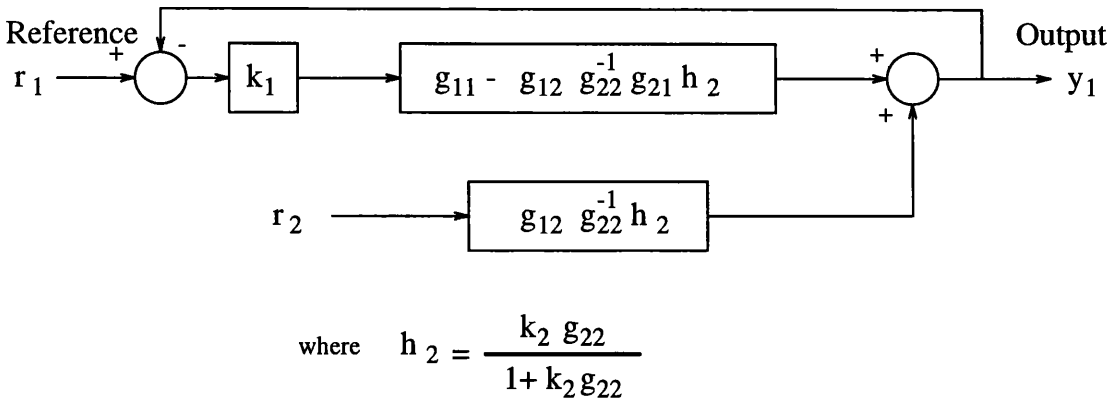

Figure 3.4: Compact form of signal transmissions to output y_1

and is subject to the disturbance

$$d_1(s) = \frac{g_{12}}{g_{22}} h_2 r_2(s) \tag{3.4}$$

Similarly from Figure(3.5), Channel $C_2(s)$ has an open-loop signal transmittance, O'Reilly and Leithead [27]

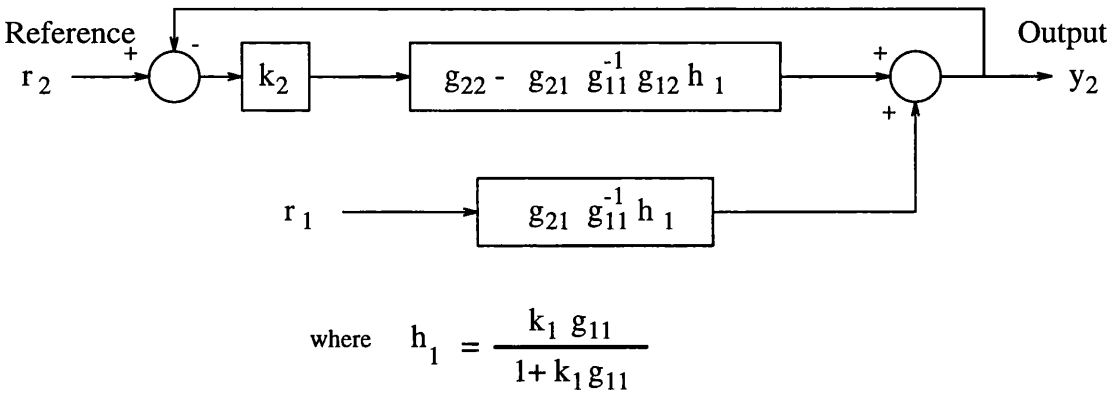

Figure 3.5: Compact form of signal transmissions to output y_2

$$C_2(s) = k_2 g_{22}(1 - \gamma h_1) = k_2 g_{22}(1 - \gamma_2) \tag{3.5}$$

where

$$h_1(s) = \frac{k_1 g_{11}}{1 + k_1 g_{11}} \tag{3.6}$$

and is subject to the disturbance

$$d_2(s) = \frac{g_{21}}{g_{11}} h_1 r_1(s) \tag{3.7}$$

The channel C_1 and C_2 transmittances in equations(3.1) and (3.5) are together structurally equivalent to the original 2-input 2-output open loop-system system transfer function matrix $G(s)K(s)$ depicted in Figure(3.2). The multivariable nature of the SISO channels transmittances is described by the complex transfer function $\gamma(s)$. When the magnitude of $\gamma(s)$ is large the system is highly coupled. Also, no assumptions are made as to the nature of any of the transfer functions g_{ij} and h_i; i.e. they do not need to be stable or minimum phase.

The closed-loop response of Channel C_1 in Figure(3.4) is described by

$$y_1(s) = T_1(s) r_1(s) + D_1(s) r_2(s) \tag{3.8}$$

where

$$T_1(s) = \frac{k_1 g_{11}(1 - \gamma_1)}{(1 + k_1 g_{11}(1 - \gamma_1))} \tag{3.9}$$

and

$$D_1(s) = \frac{g_{12} h_2}{g_{22}(1 + k_1 g_{11}(1 - \gamma_1))} \tag{3.10}$$

If k_1 is a stabilising controller for Channel C_1 and the reference signals r_1 and r_2 are stable, then the response y_1 is stable. Hence, r_2 can be treated as a normal disturbance acting on the SISO system Channel C_1.

Similarly, the closed-loop response of Channel C_2 in Figure(3.5) is described by

$$y_2(s) = T_2(s)r_2(s) + D_2(s)r_1(s) \tag{3.11}$$

where

$$T_2(s) = \frac{k_2 g_{22}(1-\gamma_2)}{(1+k_2 g_{22}(1-\gamma_2))} \tag{3.12}$$

and

$$D_2(s) = \frac{g_{21}h_1}{g_{11}(1+k_2 g_{22}(1-\gamma_2))} \tag{3.13}$$

Similar to r_2, the signal reference r_1 can be treated as a normal disturbance acting on the SISO system Channel C_2.

The set of closed-loop poles for Channel C_1 and Channel C_2 are the same since the closed-loop poles of Channels C_1 and C_2 are the zeros of $(1-\gamma h_2)$ and $(1-\gamma h_1)$ respectively and these two set of poles are the same since $\gamma h_1 + \gamma h_2 = \gamma h_2 h_1$.

3.2.2 Channels pole-zero structure

Consider the open-loop transmittances $g_{11}(1-\gamma h_2)$ and $g_{22}(1-\gamma h_1)$ for Channels C_1 and C_2 respectively. Provided that no pole-zero cancellation occurs, the pole-zero structure of Channel C_1 and Channel C_2 is given in Table(3.1), Leithead and O'Reilly [13]

Transmittance	Zeros	Poles
Channel C_1	zeros of $(1-\gamma_1)$	poles of $g_{11}, g_{12}, g_{21}, h_2$
channel C_2	zeros of $(1-\gamma_2)$	poles of $g_{22}, g_{12}, g_{21}, h_1$

Table 3.1: Open-loop individual channel poles-zeros for a 2x2 system

In some circumstances, not all the zeros and poles indicated in Table(3.1) are present in the open-loop channels transmittances since pole-zero cancellation within γh_1 and γh_2 or cancellation between the poles and zeros within $(1-\gamma h_1)$ and $(1-\gamma h_2)$ may occur.

From equations(3.1) and (3.5) is clear that Channels $C_1(s)$ and $C_2(s)$ can be used to assess the dynamical performance of the system using the standard frequency domain bandwidths and crossover frequencies. In this way phase and gain margins can be used to measure transient dynamic behaviour but not robustness.

The possible closed-loop dynamical performance of the individual channels is adversely affected by the presence of right hand plane zeros (RHPZ's) and these are related to $\gamma_1(s)$ and $\gamma_2(s)$. As it is shown in Table(3.1), the number of RHPZ's of the ith Channel C_i is the number of RHPZ's of $(1-\gamma_i)$ and is determined by Result 3.1, Leithead and O'Reilly [15]

Result 3.1 *Suppose that the Nyquist plot of the multivariable structure function $\gamma_i(s)$, encircles the (1,0) point N times more in a clockwise direction than in an anti-clockwise direction. Then, Z, the number of RHPZ's of $(1-\gamma_i)$, is given by*

$$N = Z - P \tag{3.14}$$

where P is the number of RHPP's of $\gamma_i(s)$.

In this way any actual restriction in performance due to non-minimum phase behaviour in Channel C_i can be detected from the Nyquist plot of γ_i. Moreover, any potential restriction in performance due to RHP transmission zeros can be detected from the Nyquist plot of $\gamma(s)$ as the multivariable transmission zeros defined as the zeros of $|G|$ are the same as the zeros of $(1-\gamma)$. Also, when high performance controllers are required, the subsystem transfer functions $h_1(s)$ and $h_2(s)$ are close to one over most of the significant dynamics of Channels $C_1(s)$ and $C_2(s)$, and both $\gamma_1(s)$ and $\gamma_2(s)$ are essentially $\gamma(s)$. Then, the multivariable structure function $\gamma(s)$ is a good indicator of possible performance restrictions.

3.2.3 Robust channel stability margins

As in the SISO case, it is important to extend the use of gain and phase margins to measure robustness to plant uncertainty in the MIMO case. However, in the case

of 2-input 2-output systems and in general for MIMO systems, the structure of the channels may not be fixed. Therefore, it is important to establish the necessary conditions to guarantee the existence of fixed stabilising controllers for a family of two-inputs two-output plants, Leithead and O'Reilly [13]

Result 3.2 *There exist fixed stabilising controllers, $k_1(s)$ and $k_2(s)$, for a family of two-input two-output plants, G(s), provided:*

(i) each plant $G(s) = [g_{ij}(s)]$ possesses no RHP or purely, imaginary zeros and the individual transfer functions $g_{11}(s)$ and $g_{22}(s)$ possess no zeros in some open neighbourhood of the imaginary axis;

(ii) the limit of $\gamma(s)$, as s tends to plus infinity, is not in some open neighbourhood of one for each plant $G(s)$;

(iii) $\lim_{s\to\infty}(g_{11}g_{22} - g_{12}g_{21}) \to qs^{-m}$ *for q of fixed sign and some integer m (q and m may be different for each plant), and;*

either

$\lim_{s\to\infty} g_{22}(s) \to q_2 s^{-m_2}$ *for q_2 of fixed sign and some integer m_2 (q_2 and m_2 may be different for each plant)(which necessitates the bandwidth of h_1 being chosen less than the bandwidth of h_2).*

or

$\lim_{s\to\infty} g_{11}(s) \to q_1 s^{-m_1}$ *for q_1 of fixed sign and some integer m_1 (q_1 and m_1 may be different for each plant)(which necessitates the bandwidth of h_2 being chosen less than the bandwidth of h_1).*

Moreover, the gains $k_1(s)$ and $k_2(s)$, are stable and minimum phase and arbitrarily high bandwidth and, if the plants have no transmission zeros in some open neighbourhood of the imaginary axis, arbitrarily small sensitivity are possible. Hence, the structures of the plant only weakly influence the controller gains.

Condition (iii) in Result 3.2 is a high frequency condition but it may be replaced by the equivalent low frequency conditions $(iii)'$ and $(iv)'$ given by

$(iii)'$ $\lim_{s\to 0} g_{11}(s) = q_1 s^{-m_1}$ *for some integer* m_1 *(*q_1 *and* m_1 *may be different for each plant),*

$\lim_{s\to 0} g_{22}(s) = q_2 s^{-m_2}$ *for some integer* m_2 *(*q_2 *and* m_2 *may be different for each plant),*

$\lim_{s\to 0} \gamma(s) = q s^{m}$ *for some integer* m *(*q *and* m *may be different for each plant);*

$(iv)'$ *either*

$$\begin{cases} \textit{sign of } \lim_{s\to 0+} g_{11}(s) = \alpha(-1)^{P_1 - Z_1} \textit{when } \lim_{s\to\infty} \gamma(s) < 1 \\ \textit{sign of } \lim_{s\to 0+} g_{11}(s) = -\alpha(-1)^{P_1 - Z_1} \textit{when } \lim_{s\to\infty} \gamma(s) > 1 \\ \textit{sign of } \lim_{s\to 0+} g_{22}(s) = \beta(-1)^{P_2 - Z_2} \end{cases}$$

(which necessitates the bandwidth of Channel C_1 *being chosen less than the bandwidth of Channel* C_2*),*

or

$$\begin{cases} \textit{sign of } \lim_{s\to 0+} g_{22}(s) = \beta(-1)^{P_2 - Z_2} \textit{when } \lim_{s\to\infty} \gamma(s) < 1 \\ \textit{sign of } \lim_{s\to 0+} g_{11}(s) = -\beta(-1)^{P_2 - Z_2} \textit{when } \lim_{s\to\infty} \gamma(s) > 1 \\ \textit{sign of } \lim_{s\to 0+} g_{11}(s) = \alpha(-1)^{P_1 - Z_1} \end{cases}$$

(which necessitates the bandwidth of Channel C_2 *being chosen less than the bandwidth of Channel* C_2*),*

The integers P_1 and Z_1 are respectively the numbers of RHPP's and RHPZ's of $g_{11}(s)$ and the integers P_2 and Z_2 are respectively the numbers of RHPP's and RHPZ's of $g_{22}(s)$. Also, $\alpha = +1$ for all plants in the family or $\alpha = -1$ for plants in the family, and $\beta = +1$ for plants in the family or $\beta = -1$ for plants in the family.

The importance of Result 3.2 is that it supports the use of phase and gain margins as measures of robustness for 2-input 2-output systems, i.e., the family of plants can be interpreted as the set of all possible representations of an uncertain multivariable plant to be stabilised by a diagonal controller.

Similar to the SISO case, the gain and phase margins of the open loop channel transmittances $C_i(s)$ in equation(3.1) or (3.5), indicate the maximum phase or gain change (due to changes in the controller $k_i(s)$), the channel transmittance $k_i g_{ii}(1 - \gamma h_i)$ can be modified before changing the number of encirclements to the point (1,0), by the Nyquist plot. It may appear that the closed-loop system may not remain stable since changes in the control $k_i(s)$ may introduce sufficient structural changes in $h_i(s)$ to induce changes in the right number of encirclements to the point (-1,0) by the Nyquist plots of the other open-loop channel. However, as it was shown above all the closed-loop transmittances have the same set of poles. Therefore, provided any one of the channels is stable is sufficient to guarantee the closed-loop stability of the other channel. In this way, Channel $C_i(s)$ stability to changes in $k_i(s)$ is sufficient to guarantee closed-loop stability in Channel C_j to changes in $h_i(s)$. Hence, gain and phase margins in the open-loop transmittances $k_i g_{ii}(1 - \gamma h_i)$ are robustness measures of robustness to changes in the controller. However, it does not imply that the gain and phase margins are measures of robustness to plant uncertainty. This establish the following result, Leithead and O'Reilly [15].

Result 3.3 *For a 2-input 2-output system, robustness of the closed-loop system stability to changes in the controller does not imply robustness to uncertainty in the plant.*

Consider the SISO individual channel of equation(3.1) or (3.5) The uncertainty affecting Channel $C_i(s) = k_i g_{ii}(1 - \gamma h_j)$ is the product of the uncertainty of two scalar transfer functions i.e., the uncertainty of $k_i g_{ii}$ due to $g_{ii}(s)$ and the uncertainty of $(1 - \gamma h_j)$ due to $\gamma h_j(s)$. However, the uncertainty of $(1 - \gamma h_j)$ can

not be related to the uncertainty of γh_j directly. Consider the Nyquist plot of γh_j in Figure(3.6). The two circles indicate the absolute uncertainty in γh_j at the frequencies ω_1 and ω_2. From this figure it is clear that the relative uncertainty in $(1 - \gamma h_j)$ is less than the relative uncertainty γh_j at frequency ω_1 whereas the relative uncertainty in $(1 - \gamma h_j)$ is much greater than the relative uncertainty γh_j at frequency ω_2. In this way, the traditional gain and phase margins for a plant of fixed structure are measure of robustness to plant uncertainty, if the Nyquist plot of $\gamma h_j(s)$ is near the point (1,0) only at frequencies greater than the channels crossover frequencies. The former establishes Result 3.4, O'Reilly and Leithead [27]

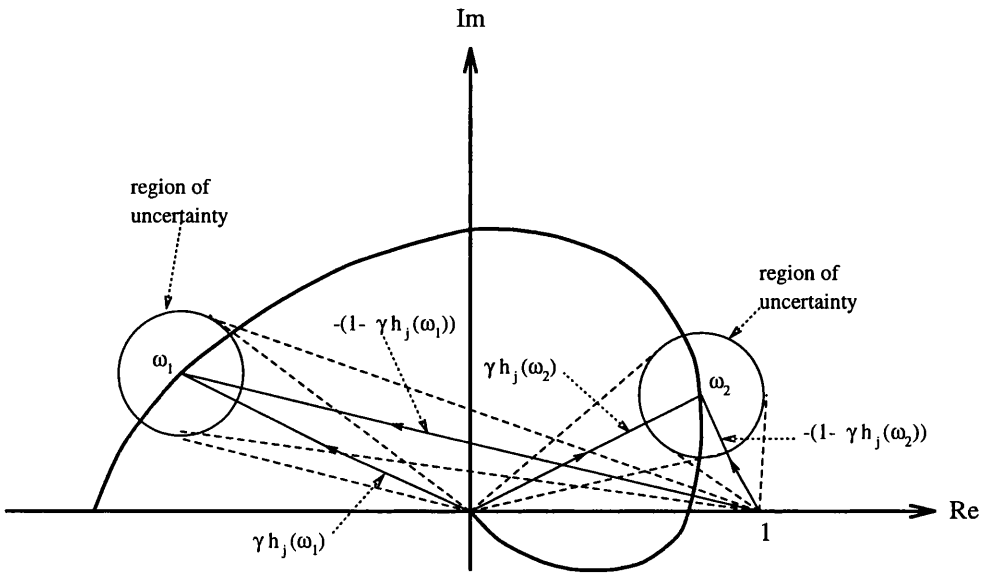

Figure 3.6: Uncertainty in phasors γh_j and $(1 - \gamma h_j)$

Result 3.4 *The phase and gain margins associated with the open-loop channel transmittances* $k_i g_{ii}(1 - \gamma h_j)$, $i, j = 1, 2 (i \neq j)$, *are measures of robustness of the closed-loop system to plant uncertainty provided that the Nyquist plots of the multivariable structure functions* γh_j *do not go near the point (1,0) except at frequencies significantly greater that the gain crossover frequencies of each channel.*

In Result 3.4 was establish as a restriction for robustness that the Nyquist plot of multivariable structure function γh_i must be nowhere near the point (1,0) at frequencies close to and below the channel crossover frequencies. Otherwise two phenomena will cause lack of stability robustness in the closed-loop system. If the Nyquist plot of γh_i goes near the point (1,0) at frequencies below the channel C_j gain crossover frequency, then the region of uncertainty of γh_i may include it. Therefore, by Result 3.1 it is uncertain as to whether or not the open-loop channel transmittance C_j is minimum phase. This may result in the introduction of RHPP's in the closed-loop channel transmittance at frequencies less than the channel crossover frequency. This phenomenon is known as *excessive structural sensitivity.* The second phenomenon is when the multivariable structure function γh_i goes near to the point (1,0) at frequencies close to the channel crossover frequency. Then the phase and gain uncertainty of $(1 - \gamma h_i)$ is very large that is reflected in the open-loop channel transmittance C_j. In this case it is said that the system exhibits *excessive phase uncertainty* .

3.3 ICD analysis for m-input m-output systems

As in the case of 2-input 2-output systems reviewed in Section 3.2 the dynamical performance of the closed-loop system for a m-input m-output multivariable system is strongly influenced by the structure of the system. In this section the structure of the general case of m-input m-output multivariable systems is presented.

3.3.1 Structure of m-input m-output systems

In Section 3.2.1 the 2-input 2-output multivariable control system was decomposed into two SISO equivalent individual channels. In this section the general m-input m-output system is decomposed into two multiple channels M_1 and M_2 as depicted in Figure(3.7). Where multiple channel M_1 contains m_1 inputs and m_1

outputs whereas multiple channel M_2 contains m_2 inputs and m_2 outputs. Where $m_1 + m_2 = m$. The choice of the m_1 and m_2 individual channels assigned to the multiple channels may be freely made. The partitioning of the system is such that.

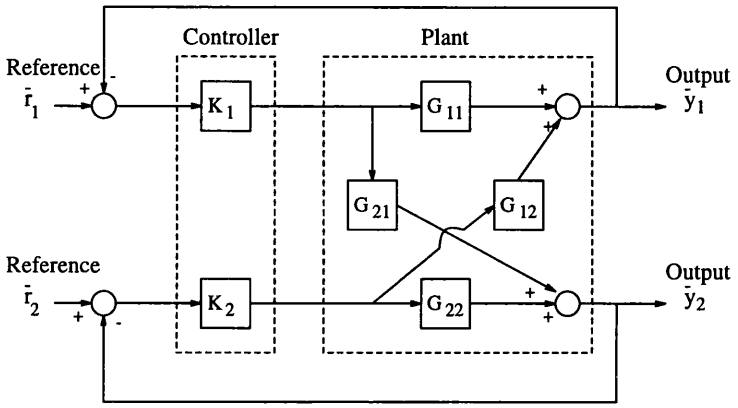

Figure 3.7: Partitioned m-input m-output multivariable system with diagonal controller

$$G(s) = \begin{bmatrix} G_{11}(s) & \vdots & G_{12}(s) \\ \dots & \dots & \dots \\ G_{21}(s) & \vdots & G_{22}(s) \end{bmatrix} \quad ; \quad K(s) = \begin{bmatrix} K_1(s) & \vdots & 0 \\ \dots & \dots & \dots \\ 0 & \vdots & K_2(s) \end{bmatrix} \tag{3.15}$$

$$r(s) = \begin{bmatrix} r_1(s) \\ \dots \\ r_2(s) \end{bmatrix} \quad ; \quad y(s) = \begin{bmatrix} y_1(s) \\ \dots \\ y_2(s) \end{bmatrix} \tag{3.16}$$

where $G(s)$ is the plant matrix transfer function and $K(s)$ is the controller. Since $K(s)$ is assumed a diagonal controller, $K_1(s)$ and $K_2(s)$ are both diagonal controllers. Consider the forward signal transmission from the reference vector $\bar{r}_1$

to its associated output vector $\bar{y}_1$ in Figure(3.7). This transmission follows two paths: one directly through $G_{11}(s)$; and the other via $G_{21}(s)$, the bottom of the system and $G_{12}(s)$ as it is shown in Figure(3.8). Therefore, similar to the 2-input 2-output case the block diagram of Figure(3.7) can be decomposed into two equivalent multiple channels as shown in Figures(3.9) and (3.10). Multiple Channel M_1 has the forward path m_1-input m_1-output transmittance matrix

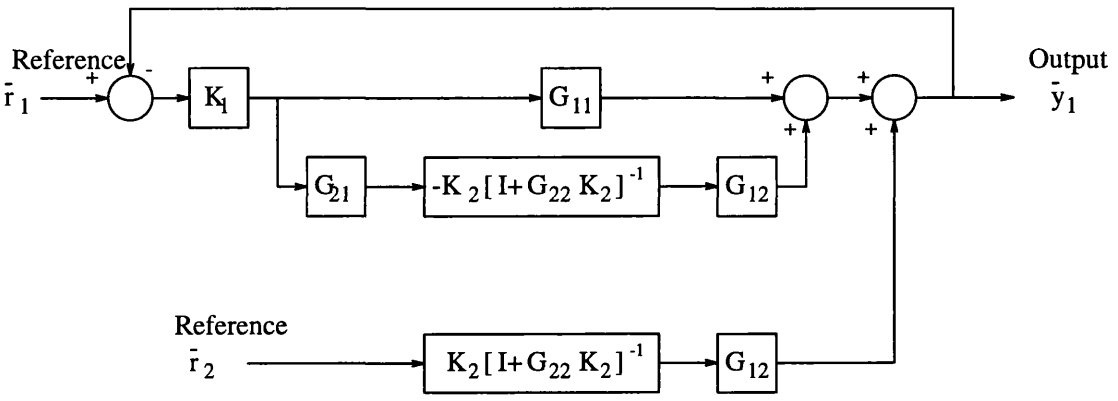

Figure 3.8: Signal transmissions to output $\bar{y}_1$

$$M_1(s) = \left(I - G_{12}G_{22}^{-1}H_2G_{21}G_{11}^{-1}\right)G_{11}K_1 \tag{3.17}$$

where the multiple subsystem transfer function matrix $H_2(s)$ is given by

$$H_2(s) = G_{22}K_2\left[I + G_{22}K_2\right]^{-1} \tag{3.18}$$

and is subjected to the cross-reference disturbance

$$D_1 = G_{12}G_{22}^{-1}H_2 \tag{3.19}$$

Similarly, Multiple-Channel M_2 has the forward path m_2-input m_2-output transmittance matrix

$$M_2(s) = \left(I - G_{21}G_{11}^{-1}H_1G_{12}G_{22}^{-1}\right)G_{22}K_2 \tag{3.20}$$

where the multiple-subsystem transfer function matrix $H_1(s)$ is given by

$$H_1(s) = G_{11}K_1\left[I + G_{11}K_1\right]^{-1} \tag{3.21}$$

and is subjected to the cross-reference disturbance

$$D_2 = G_{21}G_{11}^{-1}H_1 \tag{3.22}$$

The Multiple-Channel M_1 transmittance (3.17) and the Multiple-Channel M_2 transmittance (3.20) are together structurally equivalent to the original m-input m-output open-loop system transfer function matrix $G(s)K(s)$.

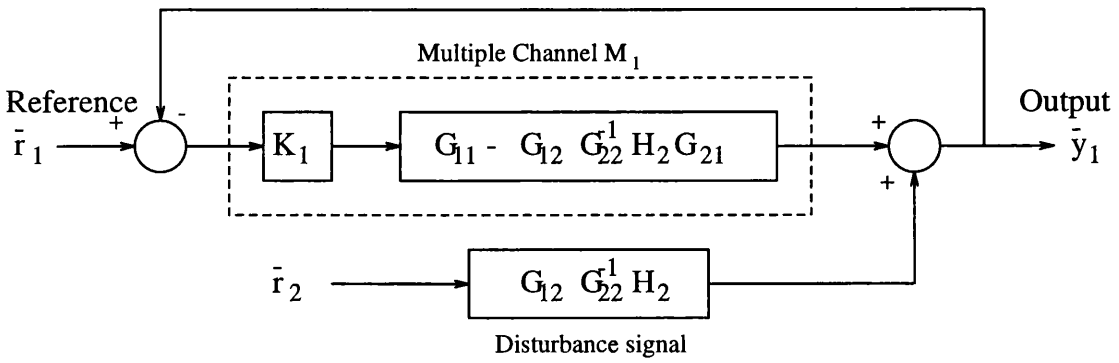

Figure 3.9: m_1-input m_1-output Multiple Channel M_1

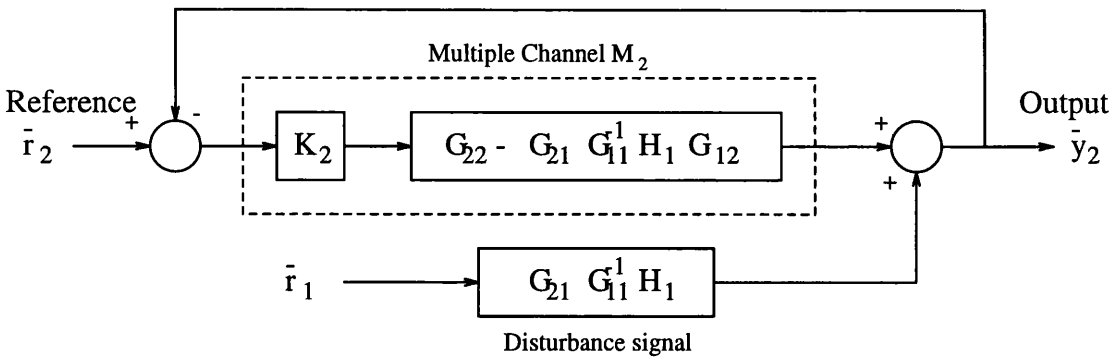

Figure 3.10: m_1-input m_1-output Multiple Channel M_2

3.3.2 Multiple channels pole-zero structure

Consider the open-loop transmittance matrix $(G_{11} - G_{12}G_{22}^{-1}H_2G_{21})$ in multiple channel M_1 in equation (3.17). Assuming no pole-zero cancellation between G_{ij}, the poles of $(G_{11} - G_{12}G_{22}^{-1}H_2G_{21})$ are the poles of G_{11} and $-G_{12}G_{22}^{-1}H_2G_{21}$. The poles of $G_{12}G_{22}^{-1}H_2G_{21}$ are the poles of G_{12} and G_{21} and the zeros of $H_2^{-1}G_{22}$. However, the zeros of $H_2^{-1}G_{22}$ are the poles of H_2 since the zeros of G_{22} are also zeros of H_2.Thus, the poles of $(G_{11} - G_{12}G_{22}^{-1}H_2G_{21})$ are the poles of G_{11}, G_{12}, G_{21} and H_2. On the other hand, due to $(G_{11} - G_{12}G_{22}^{-1}H_2G_{21}) = (I - G_{12}G_{22}^{-1}H_2G_{21}G_{11}^{-1})G_{11}$ the zeros of G_{11} are poles of $(-G_{12}G_{22}^{-1}H_2G_{21}G_{11}^{-1})$ and the zeros of $(G_{11} - G_{12}G_{22}^{-1}H_2G_{21})$ are zeros of $(I - G_{12}G_{22}^{-1}H_2G_{21}G_{11}^{-1})$. Multiple channel M_2 in equation (3.20) has similar pole-zero structure. Hence, the pole-zero structure of the multiples channels is given in the following result, Leithead and O'Reilly [14]

Result 3.5 *Provided that no pole-zero cancellation occurs, the pole-zero structure for the open-loop multiple channels is specified as indicated in Table 3.2*

	Zeros	Poles
Multiple Channel M_1	zeros of $(I - G_{12}G_{22}^{-1}H_2G_{21}G_{11}^{-1})$	poles of G_{11}, G_{12}, G_{21},H_2
Multiple Channel M_2	zeros of $(I - G_{21}G_{11}^{-1}H_1G_{12}G_{22}^{-1})$	poles of G_{22}, G_{12}, G_{21},H_1

Table 3.2: Open-loop multiple channel poles-zeros structure

Similar to the case of individual channels for a 2-input 2-output system, not all the zeros and poles indicated in Table 3.2 are present in the open-loop multiple channels since pole-zero cancellation may occurs. Also, provided no pole-zero cancellation occurs, the transmission zeros defined as the zeros of $|G(s)|$ are the same as the zeros of $(I - G_{12}G_{22}^{-1}G_{21}G_{11}^{-1})$ or $(I - G_{21}G_{11}^{-1}G_{12}G_{22}^{-1})$.

3.3.3 Individual channel structure for m-input m-output systems

The structure of individual channels for m-input m-output systems is a particular case of the multiple channels described in Section 3.3.1. Consider the following partitioning of the system $G(s)$

$$G(s) = \left[\begin{array}{c|ccc} g_{11} & g_{12} & \cdots & g_{1m} \\ \hline g_{21} & g_{22} & \cdots & g_{2m} \\ \vdots & \vdots & & \vdots \\ g_{m1} & g_{m2} & \cdots & g_{mm} \end{array}\right] ; \; K(s) = \left[\begin{array}{c|ccc} k_1 & 0 & \cdots & 0 \\ \hline 0 & k_2 & \cdots & 0 \\ \vdots & \vdots & & \vdots \\ 0 & 0 & \cdots & k_m \end{array}\right] \tag{3.23}$$

Under this partitioning multiple channel M_1 will contain only the signal transmittance containing the scalar reference input one r_1 related to the scalar output one y_1 i.e. channel C_1 can be interpreted as the multiple channel M_1 with

$$G_{11}(s) = g_{11}(s);\ G_{12}(s) = [g_{12}(s), \ldots, g_{1m}(s)]\ ;\ K_1(s) = k_1(s) \tag{3.24}$$

$$G_{21}(s) = \begin{bmatrix} g_{21}(s) \\ \vdots \\ g_{m1}(s) \end{bmatrix}\ ;\ G_{22}(s) = \begin{bmatrix} g_{22}(s) & \ldots & g_{2m}(s) \\ \vdots & & \vdots \\ g_{m2}(s) & \ldots & g_{mm}(s) \end{bmatrix} \tag{3.25}$$

$$K_2(s) = \begin{bmatrix} k_2(s) & \ldots & 0 \\ \vdots & & \vdots \\ 0 & \ldots & k_m(s) \end{bmatrix} \tag{3.26}$$

From (3.17), channel $C_1(s)$ has the open-loop SISO transmittance

$$C_1(s) = k_1 g_{11}(1 - \gamma_1) \tag{3.27}$$

where

$$\gamma_1(s) =: G_{12}G_{22}^{-1}G_{21}G_{11}^{-1} \tag{3.28}$$

also

$$\gamma_1(s) =: G_{12}G_{22}^{-1}G_{21}G_{11}^{-1} = -\left|\begin{array}{c|c} 0 & G_{12} \\ \hline G_{21} & \bar{G}_{22} \end{array}\right| / g_{11}\left|\bar{G}_{22}\right| \tag{3.29}$$

where

$$\bar{G}_{22} = H_2^{-1}G_{22} = [K_2^{-1} + G_{22}] \tag{3.30}$$

which by (3.23) is

$$\gamma_1 = -\begin{vmatrix} 0 & g_{12} & \cdots & g_{1m} \\ g_{21} & g_{22}/h_2 & \cdots & g_{2m} \\ \vdots & \vdots & & \vdots \\ g_{m1} & g_{m2} & \cdots & g_{mm}/h_m \end{vmatrix} / g_{11} \begin{vmatrix} g_{22}/h_2 & \cdots & g_{2m} \\ \vdots & & \vdots \\ g_{m2} & \cdots & g_{mm}/h_m \end{vmatrix} \tag{3.31}$$

Channel $C_1(s)$ is subjected to the scalar disturbance

$$d_1(s) = G_{12}G_{22}^{-1}H_2.\bar{r}_2 = -\begin{vmatrix} 0 & G_{12} \\ \bar{r}_2 & \bar{G}_{22} \end{vmatrix} / \left|\bar{G}_{22}\right| \tag{3.32}$$

In order to simplify equations(3.27), (3.31), and (3.32) and to generalise this procedure to the other $m-1$ individual channels, some definitions are required. Define the matrix $\bar{G}^{i_1 i_2 \cdots i_r}$ as the matrix obtained from $\bar{G}(s) = [K^{-1} + G]$ by eliminating the i_1th row and column, the i_2th row and column and so on up to the i_rth row and column. Define the matrix $\bar{G}_j^{i_1 i_2 \cdots i_r}$ as the matrix obtained by setting diagonal element g_{jj}/h_j of $\bar{G}(s)$ to zero before eliminating the rows and columns as in the definition of $\bar{G}^{i_1 i_2 \cdots i_r}$. Define R_j as the matrix obtained by replacing the jth column of $\bar{G}(s)$ by $\bar{r}$ and setting $r_j = 0$. With these definitions the multivariable structure function in equation(3.31) for channel $C_1(s)$ is

$$\gamma_1(s) = -\left|\bar{G}_1\right| / g_{11} \left|\bar{G}^1\right| \tag{3.33}$$

where $|\ .\ |$ denotes the matrix determinant. The disturbance of equation(3.32) is rewritten as

$$d_1(s) = -\left|R_1\right| / \left|\bar{G}^1\right| \tag{3.34}$$

Therefore, by allocating in multiple channel M_1 the other input-output pairs, it follows that the m individual channels $C_m(s)$ has the open-loop SISO transmittances

$$C_i(s) = k_i g_{ii}(1 - \gamma_i) \quad ; \quad i = 1, ..., m \tag{3.35}$$

where

$$\gamma_i(s) = -\left|\bar{G}_i\right| / g_{ii} \left|\bar{G}^i\right| \tag{3.36}$$

and are subjected to the disturbances

$$d_i(s) = -\left|R_i\right| / \left|\bar{G}^i\right| \tag{3.37}$$

The pole-zero structure of the individual channels for a m-input m-output system can be obtain as an special case of Result 3.5 and equations (3.24), (3.25) and (3.26). This are summarised in the following result, Leithead and O'Reilly [14]

Result 3.6 *Provided no pole-zero cancellation occurs, the pole-zero structure for open-loop channels $C_i(s)$ is specified as follows:*

(i) the zeros of channel $C_i(s)$ are the zeros of $(1 - \gamma_i)$;

(ii) The poles of channel $C_i(s)$ are the zeros of $\bar{G}^i$, the poles of g_{ii} and those poles of $\bar{G}_i$ which are not poles of $\bar{G}^i$.

It is also important to determine the number of RHPZ's of the m individual channels $C_i(s)$; $i = 1, ..., m$, and as was stated in Result 3.6 the number of RHPZ's of channel $C_i(s)$ are the number of zeros of $(1 - \gamma_i)$ and these can be determined using Result 3.1.

3.3.4 Existence of stabilising controllers for m-input m-output systems

Fundamental indicators of the potential performance and coupling of the multivariable system, equivalent to the multivariable structure function $\gamma(s)$ for 2-input 2-output systems, are provided by the multivariable structure functions $\Gamma_i(s)$, $i = 1, ..., m$, Leithead and O'Reilly [14]. The multivariable structure functions Γ_i, $i = 1, ..., m$ are defined by

$$\Gamma_i(s) = - \mid G_i^{12...(i-1)} \mid / g_{ii} \mid G^{12...(i-1)i} \mid \tag{3.38}$$

where $G^{12...i}$ is the transfer function matrix obtained from the plant matrix G by eliminating the first row and column, the second row and column and so on up to the ith row and column; $G_i^{12...(i-1)}$ is the transfer function matrix obtained from G by setting the diagonal element g_{ii} of G to zero before eliminating rows and columns as in the definition of $G^{12...i}$. By definition (3.38), $\Gamma_m(s) = 0$.

Together with structure of the multiple channels (3.17) and (3.17), the coupling characteristics of the system need to be known when designing the controller matrix as the following result shows, Leithead and O'Reilly [14].

Result 3.7 *Consider an m-input m-output plant partitioned into m_1-input m_1-output Multiple-Channel M_1 and m_2-input and m_2-output Multiple-Channel M_2 as in equations(3.17) and (3.17). Construct*

$$G_{11}^* = \left(I - G_{12}G_{22}^{-1}G_{21}G_{11}^{-1}\right) G_{11}$$

Then, the two multiple-channels couple weakly and the Multiple-Channel M_1 can be designed on the basis of G_{11} alone provided:

(i) the diagonal elements of G_{11}^* do not differ significantly from those of G_{11};

(ii) *the multivariable structure functions* $\Gamma_i(s)$ *of the* m_1*-input* m_1*-output system* G_{11}^* *do not differ significantly from those of* G_{11}*;*

(iii) *the structure (that is, the RHPP's and RHPZ's) of* G_{11}^* *does not differ significantly from that of* G_{11}*.*

It should be noted that decoupling of the system so that Multiple-Channel M_1 *can be designed on the basis of* G_{11} *alone does not necessarily mean that Multiple-Channel* M_2 *can be designed on the basis of* G_{22} *alone.*

It just remains to establish an equivalent result to Result 3.2 for m-input m-output systems which states the conditions for the existence of fixed natural controllers for a family of plants $\{G(s)\}$, Leithead and O'Reilly [14].

Result 3.8 *There exist stabilising controllers* k_j, $j = 1, 2, ..., m$ *for a family of m-input m-output plants* $\{G(s)\}$*, provided:*

(i) *each plant* $G(s) = [g_{ij}(s)]$ *possesses no RHP or purely imaginary transmission zeros and the individual transfer functions* G_{jj}, $j = 1, 2, ..., m$ *possesses no zeros in some open neighbourhood of the imaginary axis;*

(ii) *the* $(1 - \Gamma_j(s))$, $j = 1, 2, ..., m$ *possess no zeros on the imaginary axis;*

(iii) *the* $\lim_{s\to\infty} |\Gamma_j(s)| \neq 1$, $j = 1, 2, ..., m$*;*

(iv) $\lim_{s\to\infty} |G(s)| \to q_1 s^{-n_1}$ *for some integer* n_1*;*

$\lim_{s\to\infty} |G^1(s)| \to q_2 s^{-n_2}$ *for some integer* n_2*;*

$\lim_{s\to\infty} |G^{12}(s)| \to q_2 s^{-n_2}$ *for some integer* n_2*;*

$\vdots$

$\lim_{s\to\infty} \left|G^{12...(m-1)}(s)\right| \to q_2 s^{-n_m}$ *for some integer* n_m*.*

If the limit of $\Gamma_j(s)$ *as* s *tends to plus infinity is greater than one, significant bandwidth separation of the subsystem transfer functions* $h_i(s)$, $i = 1, ..., j$, *from the remaining subsystems transfer functions* $h_i(s)$, $i = j+1, ..., m$, *is required with the bandwidths of the* $h_i(s)$, $i = 1, ..., j$, *all less than the bandwidths of the other* $h_i(s)$, $i = j+1, ..., m$. *The* $h_j(s)$ *for which the limit of* $\Gamma_j(s)$ *as* s *tends to plus infinity is greater than one possess one more RHPP than the* $g_{jj}(s)$ *possess RHPZ's. Otherwise, the* $h_j(s)$ *possess the same number of RHPP's as the* $g_{jj}(s)$ *possess RHPZ's. Moreover, the controllers* k_j, $j = 1, ..., m$, *are stable and minimum phase; arbitrarily high bandwidth and arbitrarily small sensitivity are possible for each* $h_j(s)$ *and the closed-loop of each individual channel.*

3.4 Structure of state space models

In many applications the systems are originally represented by the matrix triple (A, B, C) such that the model assumes the finite order state space form

$$\dot{x} = Ax + Bu \tag{3.39}$$

$$y = Cx \tag{3.40}$$

where $x(t)$ is an nx1 vector of states variables, $u(t)$ is an mx1 vector of inputs and $y(t)$ is an mx1 vector of outputs. The transfer function matrix in the complex frequency s associated to the state space representation of equations(3.39) and (3.40) is given by

$$G(s) = C(sI - A)^{-1}B \tag{3.41}$$

By the definitions of the vectors $y(t)$ and $u(t)$ it is assumed that the transfer function matrix $G(s)$ is square, mxm.

The system described in equation(3.41) present several structural characteristics. Firstly, the system $G(s)$ has a characteristic polynomial; i.e. all the individual transfer functions in $G(s)$ have the same set of poles. Therefore, $G(s)$ can be re-written as

$$G(s) = N(s)/\Phi(s) \tag{3.42}$$

where N(s) is an mxm matrix containing the numerators of the individual transfer functions of (3.41) and

$$\Phi(s) = |sI - A| \tag{3.43}$$

is the characteristic polynomial, the roots of which are the poles of every individual transfer function of $G(s)$.

Secondly, the elements of $N(s)$ in (3.42) are not independent and satisfy the following identity. Consider the determinant of the plant (3.41)

$$|G(s)| = |N(s)| / \Phi(s)^m \tag{3.44}$$

But from (3.41)

$$|G(s)| = \left|C(sI - A)^{-1}B\right| = \left|(sI - A)^{-1}\right| . \left|\begin{array}{c|c} (sI - A) & -B \\ \hline C & 0 \end{array}\right|$$

$$= \tilde{N}(s)/\Phi(s) \tag{3.45}$$

where $\tilde{N}(s)$ is a polynomial in s and $\Phi(s)$ is the system characteristic polynomial defined in (3.43). Comparing equations (3.44) and (3.45), it follows that $\Phi^{m-1}(s)$ is a factor of $|N(s)|$; that is, there are zeros of $|N(s)|$ which directly cancel the poles

or roots of $\Phi(s)$. The cancellation is exact and is imposed by the mathematical structure of the system and in some sense these cancellation of poles and zeros is fictitious. Assuming that matrices A, B and C are full rank, it can be ascertained from (3.45) that the degree of $\tilde{N}(s)$ is $(n-m)$; that is, the system has $(n-m)$ transmission zeros.

Similar pole-zero cancellations occurs for any pxp subsystem matrix of the system transfer function $G(s)$ obtained by deleting $(m-p)$ rows and columns of $G(s)$. This shows that each root of the characteristic polynomial of $G(s)$ occurs at most as a single pole of the transfer function matrix $G(s)$ or any sub-matrix of $G(s)$.

3.4.1 Multiple Channel pole-zero structure

The multiple channels pole-zero structure for systems originally represented in state space forms can be determined by Table 3.2 and equation(3.44). From Table 3.2 the zeros of multiple Channel $M_1(s)$ are given by

$$\left|I - G_{12}G_{22}^{-1}H_2G_{21}G_{11}^{-1}\right| = \left|G_{11}^{-1}\right|\left|\bar{G}_{22}\right|^{-1}\left|\begin{array}{c|c} G_{11} & G_{12} \\ \hline G_{21} & \bar{G}_{22} \end{array}\right| \tag{3.46}$$

which by (3.30) and (3.44)

$$\left|\bar{G}_{22}\right| = \bar{N}_{22}(s)/\Phi(s)\theta_2(s) \tag{3.47}$$

and

$$\left|\begin{array}{c|c} G_{11} & G_{12} \\ \hline G_{21} & \bar{G}_{22} \end{array}\right| = \bar{N}_2(s)/\Phi(s)\theta_2(s) \tag{3.48}$$

is equal to

$$(\Phi(s)/N_{11}(s))(\Phi(s)\theta_2(s)/\bar{N}_{22}(s))(\bar{N}_2(s)/\Phi(s)\theta_2(s)) =$$

$$(\Phi(s)\bar{N}_2(s)/N_{11}(s)\bar{N}_{22}(s)) \tag{3.49}$$

where $\theta_2(s)$ is the polynomial formed by the product of the zeros of $k_{m_1+1}, k_{m_1+2}...k_m$. Hence

$$\left|(I - G_{12}G_{22}^{-1}H_2G_{21}G_{11}^{-1})G_{11}\right| = \left|I - G_{12}G_{22}^{-1}H_2G_{21}G_{11}^{-1}\right| |G_{11}|$$

$$= \bar{N}_2(s)/\bar{N}_{22}(s) \tag{3.50}$$

Therefore, the zeros of multiple channel M_1 are the zeros of $(I-G_{12}G_{22}^{-1}H_2G_{21}G_{11}^{-1})$ which are not also poles of the transfer function matrix $G(s)$. Also, the poles of multiple channel M_1 are the poles of $H_2(s)$. Multiple channel M_2 has similar pole-zero structure, Leithead and O'Reilly [18].

Result 3.9 *When a system is represented by a state space model, the pole-zero structure for the open-loop multiple channels $M_1(s)$ and $M_2(s)$ are as specified in Table 3.3*

	Zeros	Poles
Multiple Channel M_1	zeros of $(I - G_{12}G_{22}^{-1}H_2G_{21}G_{11}^{-1})$ which are not poles of $G(s)$	poles of H_2
Multiple Channel M_2	zeros of $(I - G_{21}G_{11}^{-1}H_1G_{12}G_{22}^{-1})$ which are not poles of $G(s)$	poles of H_1

Table 3.3: Open-loop multiple channel poles-zeros structure for state space models

It must be noted, that not all the zeros of $(I - G_{12}G_{22}^{-1}H_2G_{21}G_{11})$ and $(I - G_{21}G_{11}^{-1}H_1G_{12}G_{22})$ are the zeros of the open-loop multiple channels M_1 and M_2 respectively. Those zeros of $(I - G_{12}G_{22}^{-1}H_2G_{21}G_{11})$ and $(I - G_{21}G_{11}^{-1}H_1G_{12}G_{22})$ which coincide with the characteristic polynomial $\Phi(s)$ of (3.43), are fictitious.

3.4.2 Individual pole-zero structure

The structure of the individual channels for systems represented by a state space model, is obtained as a special case of the structure of the multiple channels of Table 3.3. Consider the individual channel $C_1(s)$ to be the single-input single-output multiple channel $M_1(s)$. With multiple channel $M_2(s)$ a (m-1)-input (m-1)-output transmittance. The channel C_1 SISO transmittance is given by

$$C_1(s) = g_{11}(1 - \gamma_1) = (1 - G_{12}G_{22}^{-1}G_{21}G_{11}^{-1})G_{11} \tag{3.51}$$

From the analysis of Result 3.9, the poles of $g_{11}(s)$ are the zeros of $(1 - \gamma_1)$ and from (3.51) the zeros of $g_{11}(s)$ are the poles of $(1 - \gamma_1)$. Hence, the zeros of the individual channel $C_1(s)$ are those zeros of $(1 - \gamma_1)$ which are not poles of $G(s)$, and the poles are those poles of γ_1 that are not zeros of $g_{11}(s)$, i.e. the poles of $H_2(s)$. All the m individual channels have similar pole-zeros structure.. This is summarised in the following result, Leithead and O'Reilly [18]

Result 3.10 *When a system is represented by a state space model, the pole-zero structure for the open-loop individual channels $C_i(s)$, $i = 1, ..., m$, is as specified below.*

(i) Zeros of C_i are the zeros of $(1 - \gamma_j)$ that are not poles of $G(s)$;

(ii) Poles of channel C_i are the poles of γ_i that are not zeros of g_{ii}.

Since $(1 - \gamma_j)$ has a fictitious set of zeros, specifically the factors of the system characteristic polynomial $\Phi(s)$, which cancel with the poles of the individual transfer functions $g_{ij}(s)$, the number of the encirclements of the point (1,0) by the Nyquist plot of $\gamma_i(s)$ now indicates the number of RHP channels zeros plus the number of RHP roots of $\Phi(s)$. Therefore, in the case of systems represented by a state space model, Result 3.1 has to be rewritten as indicated in Result 3.10, Leithead and O'Reilly [18].

Result 3.11 *When a system is represented by a state space model, the number of RHPZ's of channel C_i, is given by*

$$Z = N + P - Q$$

where N is the net number of clockwise encirclements to the point (1,0) by the Nyquist plot of the multivariable structure function γ_i, P is the number of RHPP;s of γ_i, and Q is the number of RHP poles of the plant.

3.5 Assessment of some aspects of design within ICD

Throughout the ICD review was assumed a very simple control system structure, i.e. as indicated in Figure(3.1) it was considered only a diagonal controller $k(s)$ with a unity feedback together the plant matrix $G(s)$. However, control systems may required more complex structures. In this section, some aspects of design are analysed within the ICD.

3.5.1 Weak feedback

As it was shown in Section 3.4, when the system is originally represented by a state space model, fictitious RHPP's and RHPZ's may be introduced. Consider a plant for which all the individual transmittances are stable except for one. When the plant is represented by a state space model of the form of equations(3.39) and (3.40), all the individual transfer functions of the transfer function matrix $G(s)$ are unstable since all the individual transfer functions have the same poles. Ideally, all the individual transfer functions except the originally unstable one should have RHPZ's that exactly cancel with the RHPP's. However, the restriction on $G(s)$ imposed by the state space form, whereby the elements of the numerator matrix are not independent, may prevent these cancellations. Hence, the individual transfer functions will have almost RHPP's and RHPZ's cancellations. In

some sense these almost RHP pole-zero cancellations are fictitious. In these circumstances they may be ignored or cancelled, but in general, it is not advisable to do so.

The solution to these almost RHP pole-zero cancellation is within the state space representation itself. If one individual transfer function is stabilised by a single feedback-loop, then the complete system would be stabilised. Consider a feedback-loop around the individual transfer function $g_{ij}(s)$, with a scalar controller $m(s)$ in the feedback line. The amended system $G'(s)$ has the elements

$$g'_{ij} = \frac{g_{ij}}{(1 + mg_{ij})} \tag{3.52}$$

$$g'_{kj} = \frac{g_{kj}}{(1 + mg_{ij})}, \quad k \neq i \tag{3.53}$$

$$g'_{il} = \frac{g_{il}}{(1 + mg_{ij})}, \quad l \neq j \tag{3.54}$$

$$g'_{il} = g_{il}(1 - \gamma_{kl}h_{ij}), \quad k \neq, i \; l \neq j \tag{3.55}$$

where

$$\gamma_{kl} = \frac{g_{kj}g_{il}}{g_{ij}g_{kl}} \tag{3.56}$$

and

$$h_{ij} = \frac{mg_{ij}}{(1 + mg_{ij})} \tag{3.57}$$

Equation(3.55) can be rewritten as

$$g'_{kl} = \frac{(g_{kl} + m(g_{ij}g_{kl} - g_{kj}g_{il}))}{(1 + mg_{ij})} \tag{3.58}$$

From equations(3.52), (3.53), (3.54) and (3.55), it can be seen that each individual transfer function of the amended system $G'(s)$ possesses the same set of poles. It is convenient to select $m(s)$ in the feedback line with a gain as weak as possible

to minimise the extent to which $G'(s)$ differs from $G(s)$. It is also important not to increase the relative uncertainty of the plant. Hence, it must be checked that the Nyquist plots of the multivariable structure functions $\gamma_{kl}h_{ij}$ in (3.55) do not go near the point (1,0).

3.5.2 Pre-compensation and non-diagonal controllers

In this section, the use of pre-compensation within the ICD is explored for the 2-input 2-output case. Only non-diagonal pre-compensation is investigated but the conclusions apply equally to post-compensation. Consider a transfer function matrix $G(s)$ and a matrix pre-compensator $P(s)$. Then, the precompensated system $G'(s)$ is given by

$$G'(s) = G(s)P(s) \tag{3.59}$$

where the individual transfer functions of of $G'(s)$ are defined by

$$\begin{bmatrix} g'_{11} & g'_{12} \\ g'_{21} & g'_{22} \end{bmatrix} = \begin{bmatrix} (g_{11}p_{11} + g_{12}p_{21}) & (g_{11}p_{12} + g_{12}p_{22}) \\ (g_{21}p_{11} + g_{22}p_{21}) & (g_{21}p_{12} + g_{22}p_{22}) \end{bmatrix} \tag{3.60}$$

and the multivariable structure function

$$\gamma'(s) = \frac{g'_{12}g'_{21}}{g'_{11}g'_{22}} \tag{3.61}$$

When high performance is required, the feedback control might be restricted by the presence of RHP transmission zeros (RHPZ's of $(1-\gamma)$). However, the RHP transmission zeros of the uncompensated plant $G(s)$ are RHP transmission zeros of the pre-compensated plant $G'(s)$ since

$$\left|G'(s)\right| = |G(s)|\,|P(s)|$$

Therefore, pre-compensation can not be used to attain high performance feedback control in the presence of RHP transmission zeros.

It is also important to ascertain the effect of pre-compensation in terms of the plant uncertainty. Assuming that (3.59) describes the relationship between the nominal pre-compensated and uncompensated plants, then

$$P(s) = G^{-1}(s)G'(s) \tag{3.62}$$

considering the plant uncertainty $\Delta G(s)$, the actual precompensated plant is given by

$$G' + \Delta G' = (G + \Delta G)P = (G + \Delta G)^{-1}G^{-1}G' \tag{3.63}$$

$$G' + \Delta G' = G' + \Delta G G^{-1}G' \tag{3.64}$$

Hence, the uncertainty in the actual pre-compensated plant is described by

$$\Delta G' = \Delta G G^{-1}G' \tag{3.65}$$

For the individual transfer functions, the relationship between the precompensated and un-compensated uncertainties, $\Delta g'_{ij}$ and Δg_{ij} $(i, j = 1, 2)$ is, Leithead and O'Reilly [16].

$$\begin{bmatrix} \Delta g'_{11} & \Delta g'_{12} \\ \Delta g'_{21} & \Delta g'_{22} \end{bmatrix} = \frac{1}{g_{11}g_{22}(1-\gamma)} \begin{bmatrix} \Delta g_{11} & \Delta g_{12} \\ \Delta g_{21} & \Delta g_{22} \end{bmatrix} \times \begin{bmatrix} (g_{22}g'_{11} - g_{12}g'_{21}) & (g_{22}g'_{12} - g_{12}g'_{22}) \\ (-g_{21}g'_{11} + g_{11}g'_{21}) & (-g_{21}g'_{12} + g_{11}g'_{22}) \end{bmatrix}$$

Hence,

$$\Delta g'_{11} = \frac{1}{(1-\gamma)}(A_1 \Delta g_{11} + B_1 \Delta g_{12}) \tag{3.66}$$

$$\Delta g'_{12} = \frac{1}{(1-\gamma)}(A_2 \Delta g_{12} + B_2 \Delta g_{11}) \tag{3.67}$$

$$\Delta g'_{21} = \frac{1}{(1-\gamma)}(A_1 \Delta g_{21} + B_1 \Delta g_{22}) \tag{3.68}$$

$$\Delta g'_{22} = \frac{1}{(1-\gamma)}(A_2 \Delta g_{22} + B_2 \Delta g_{21}) \tag{3.69}$$

where

$$A_1 =: g'_{11}/g_{11} - \gamma g'_{21}/g_{21}; \qquad B_1 =: (g_{21}/g_{22})(g'_{21}/g_{21} - g'_{11}/g_{11})$$

$$A_2 =: g'_{22}/g_{22} - \gamma g'_{12}/g_{12}; \qquad B_2 =: (g_{12}/g_{11})(g'_{12}/g_{121} - g'_{22}/g_{22})$$

From equations(3.66)-(3.69) is possible to see that when the multivariable structure function of the un-compensated plant $G(s)$ is close to the point (1,0), the uncertainties of the pre-compensated system are increased by a factor of $(1-\gamma)^{-1}$, which is large. Also, from equations (3.66)-(3.69) is clear that the uncertainty in any element of $G'(s)$ is a linear combination of the uncertainty of two elements of the un-compensated system. Therefore, the uncertainties in the elements of $G'(s)$ can be less than the uncertainties in $G(s)$ if they are appropriately correlated, which in general can not be determined. However, it may be necessary the introduction of a compensator in a control system. Hence, in order to avoid the increment of the uncertainties effects in the compensated system, the compensator must affects the system only at frequencies where the multivariable structure function $\gamma(s)$ of the un-compensated system is far from the point (1,0).

A better way to specify the error of the pre-compensated individual transfer functions is by the relative errors. From (3.66)-(3.69), the relative uncertainty of the elements of the pre-compensated system is related to the relative uncertainty

of the elements of the un-compensated system as follows, Leithead and O'Reilly [16]

$$\frac{\Delta g_{11}'}{g_{11}'} = \frac{1}{(1-\gamma)}[(1-\bar{A}_1)\frac{\Delta g_{11}}{g_{11}} + (\bar{A}_1 - \gamma)\frac{\Delta g_{12}}{g_{12}}] \tag{3.70}$$

$$\frac{\Delta g_{12}'}{g_{12}'} = \frac{1}{(1-\gamma)}[(\bar{B}_1 - \gamma)\frac{\Delta g_{12}}{g_{12}} + (1-\bar{B}_1)\frac{\Delta g_{11}}{g_{11}}] \tag{3.71}$$

$$\frac{\Delta g_{21}'}{g_{21}'} = \frac{1}{(1-\gamma)}[(\bar{B}_2 - \gamma)\frac{\Delta g_{21}}{g_{21}} + (1-\bar{B}_2)\frac{\Delta g_{22}}{g_{22}}] \tag{3.72}$$

$$\frac{\Delta g_{22}'}{g_{22}'} = \frac{1}{(1-\gamma)}[(1-\bar{A}_2)\frac{\Delta g_{22}}{g_{22}} + (\bar{A}_2 - \gamma)\frac{\Delta g_{21}}{g_{21}}] \tag{3.73}$$

where

$$\bar{A}_1 =: \frac{g_{21}' g_{12}}{g_{11}' g_{22}}; \qquad \bar{A}_2 =: \frac{g_{12}' g_{21}}{g_{22}' g_{11}}$$

$$\bar{B}_1 =: \frac{g_{22}' g_{12}}{g_{11}' g_{21}}; \qquad \bar{B}_2 =: \frac{g_{12}' g_{22}}{g_{21}' g_{11}}$$

Each of the relative uncertainty equations(3.70)-(3.73) is of the form

$$\frac{\Delta \alpha'}{\alpha'} = \lambda \frac{\Delta \alpha}{\alpha} + (1-\lambda)\frac{\Delta \beta}{\beta} \tag{3.74}$$

Hence, it follows that the relative error for any individual transfer function $g_{ij}(s)$, is generally increased by system pre-compensation, particularly since λ may have large magnitude.

In the case of non-diagonal controllers, the controller can be treated as a pre-compensator with the controller the identity matrix. Therefore, the results for non-diagonal pre-compensation directly apply to non-diagonal feedback control.

3.5.3 Feedforward control

In Section(3.2.3), it was shown that a multivariable control system may lack stability robustness due to excessive structural sensitivity or excessive phase sensitivity. It was also shown that these adverse characteristics are detected by the

closeness of the multivariable structure functions $\Gamma_i(s)$ to the point (1,0). These problems due to the nature structure of the plant can not be remove by feedback control, Leithead and O'Reilly [13], or by pre/post-compensation as indicated in Section(3.5.2). Also, feedback control is not well suited to cater for non-minimum phase plant characteristics (RHP transmission zeros) as shown in Leithead and O'Reilly [13]. In contrast to other applications for feedforward control (where it is used to anticipate and counteract the effect of some known disturbance before it affects the plant output or to compensate high frequency plant modifications effects in transducers) within the context of the ICD the feedforward control can be used to remove plant RHPZ's, to eliminate the lack of stability robustness due to plant excessive structural sensitivity or excessive phase sensitivity (by shifting the $\Gamma_i(s)$ functions far from the point (1,0)), and as an aid to feedback controller design by decoupling the system at the crossover frequency without adversely affecting stability robustness.

Consider the control system depicted in the block diagram of Figure(3.11), where $K(s)$ is the feedback controller, $G(s)$ is the plant transfer function matrix and $F(s)$ the feedforward controller.

The feedforward control consist in the addition or *feeding forward* of the control signal $u(s)$ to the plant output $y(s)$ via the shaping filter $F(s)$

Because the feedforward term changes the output $y(s)$ to the amended output $z(s)$, the feedforward control term $F(s)$ must be small except when absolutely necessary. The equivalent feedback controller representation for Figure(3.11) is as shown in Figure(3.12) where the equivalent feedback controller $K_e(s)$ is given by

$$K_e(s) = [I + KF]^{-1}K \tag{3.75}$$

It should be noted that the feedback controller is designed on the basis of the amended plant $G'(s) = G(s) + F(s)$. When the difference in output is of import, a pre-filter could aid in achieving the desired response of the closed-loop system.

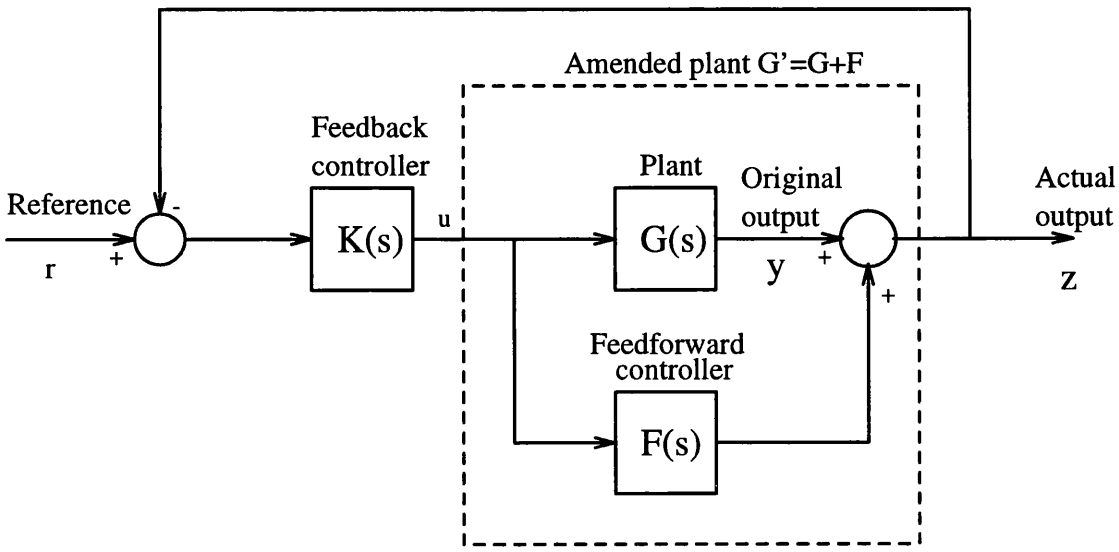

Figure 3.11: Feedforward with feedback control

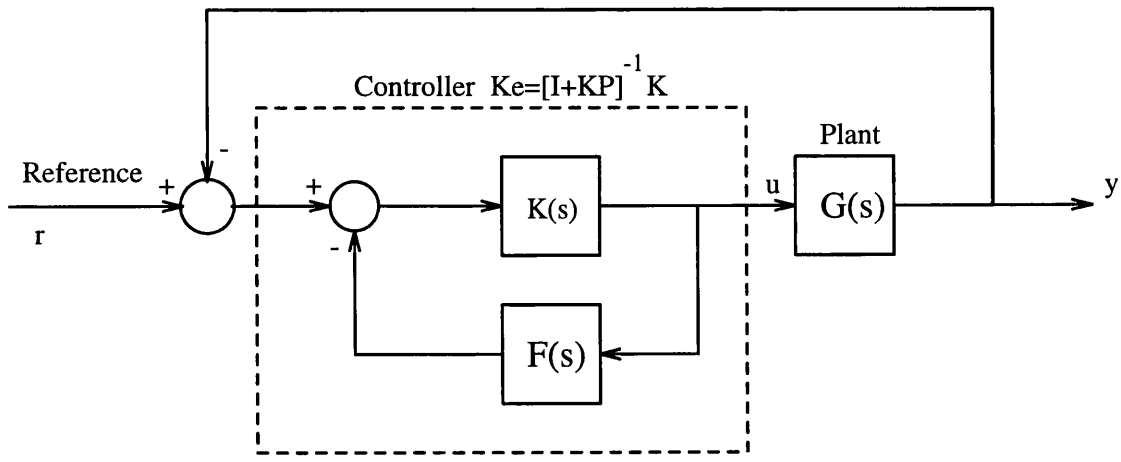

Figure 3.12: Equivalent feedback control

3.6 Conclusions

In this chapter a review of the Individual Channel Design (ICD) framework was presented. It includes the original version for 2-input 2-output systems and the general case for m-input m-output systems. It is shown how a MIMO system can be decomposed into SISO individual channels together with the necessary conditions for the use of the traditional gain and phase margins as a measures for robustness for multivariable systems. Also, an ICD analysis for the use of *weak* feedback, pre/post-compensation and non-diagonal controllers, together with a new application of feedforward control were reviewed. These, technique were analysed for the case of 2-input 2-output systems. However, the conclusions apply directly to the case of m-input m-output systems. It is important to note that only those aspects of the ICD that are used in the design of a control system for the helicopter problem were presented.

Chapter 4

80 Knots Forward Flight ICD Analysis

4.1 Introduction

The purpose of this chapter is to examine in a fundamental way the structural and robustness issues underlying the multivariable helicopter flight control problem. It is understood by structural issues the fundamental potentially performance limiting features of the system such as loop interaction, RHP poles and RHP zeros. As was stated in Chapter 1, a low order rigid body dynamics model represents the prime focus of a flight control system, so the analysis is based on a linear (small signal) rigid body helicopter model without rotor and actuator dynamics. The flight condition selected as starting point of analysis is the forward level flight condition at 80 knots.

Firstly, the linear eighth order rigid body model for the helicopter at 80 knots forward flight is presented, following by a coupling analysis. It is found that after the elimination of an almost RHP pole-zero cancellation via a weak feedback, for design purposes, the helicopter decouples into lateral and longitudinal dynamics. Secondly, it is found by inspection of the multivariable structure function for the lateral dynamics, that the system presents sensitivity problems at frequencies close

to the channel crossover frequencies.

4.2 Helicopter model

The linear rigid body model derived from HELISTAB (Padfield [28]) is a linear eighth order model in state space form

$$\dot{x} = Ax + Bu \tag{4.1}$$

$$y = Cx \tag{4.2}$$

taken from Hughes *et al* [8], and represents the rigid body dynamics of a single main rotor helicopter at 80 knots forward flight. The associated state vector $x(t)$ is described by

$$x(t) = \begin{bmatrix} u \\ w \\ q \\ \theta \\ v \\ p \\ \phi \\ r \end{bmatrix} = \begin{bmatrix} longitudinal\ \ velocity\ \ (m/sec) \\ vertical\ \ velocity\ \ (m/sec) \\ pitch\ \ rate\ \ (rad/sec) \\ pitch\ \ attitude\ \ (rad) \\ lateral\ \ velocity\ \ (m/sec) \\ roll\ \ rate\ \ (rad/sec) \\ roll\ \ attitude\ \ (rad) \\ yaw\ \ rate\ \ (rad/sec) \end{bmatrix} \tag{4.3}$$

The tracking outputs considered for the helicopter flight control problem are as described by the output vector y(t) of equation(4.2) represented by

$$y(t) = \begin{bmatrix} height\ \ rate \\ pitch\ \ attitude \\ turn\ \ rate \\ side-slip\ angle \end{bmatrix} = \begin{bmatrix} c_{11}u + c_{12}w + c_{14}\theta + c_{15}v + c_{17}\phi \\ \theta \\ c_{33}q + c_{38}r \\ c_{45}v \end{bmatrix} \tag{4.4}$$

where the coefficients c_{ij} are as listed in the output matrix C. Also, the four control inputs (pilot inceptors) forming the 4x1 input vector $u = [u_1, u_2, u_3, u_4]^T$ of equation(4.1) are respectively the vertical collective u_1, the longitudinal cyclic u_2, the lateral cyclic u_3, and the tail rotor collective u_4.

In order to abbreviate the notation, the following convention for an n-th order polynomial p(s) in the complex variable s with zeros $-a_1$, $-a_2$, ..., $-a_n$ and gain k is used.

$$p(s) = k(s + a_1)(s + a_2)...(s + a_n) =: [k, -a_1, -a_2, ..., -a_n]^T \tag{4.5}$$

Then, associated with the state-space representation of equations (4.1) and (4.2) is the 4-input 4-output multivariable transfer function matrix model

$$G(s) = C(sI - A)^{-1}B \tag{4.6}$$

described by

$$G(s) = \frac{1}{\Delta}$$

117.8421	30.6525	−0.2618	0.2202
−10.7519	−10.3508	−262.2300	$-5.2552 \pm 5.3272j$
$-0.6711 \pm 2.2565j$	$-1.2201 \pm 5.3007j$	$-2.4637 \pm 7.3586j$	$0.5983 \pm 5.0372j$
$-1.1483 \pm 1.0530j$	$-0.6504 \pm 2.2476j$	$-0.6417 \pm 2.2676j$	−2.4242
−0.1305	$-0.0282 \pm 0.0048j$	$-0.0422 \pm 0.0155j$	−0.0500
−0.0315			−0.0425
14.5286	28.3288	−6.7328	−0.5937
−11.5580	−10.3713	−18.9264	−12.5085
$-0.6577 \pm 2.2916j$	$-0.6586 \pm 2.2367j$	$-0.5992 \pm 2.2592j$	−2.9776
$-0.0334 \pm 0.0032j$	$-0.0283 \pm 0.0011j$	−0.7995	1.4786
−0.5231	−0.7806	−0.0552	−0.5804
		−0.0336	0.1046
			−0.0326
13.4799	−6.8925	−26.6062	−18.0633
$-4.7681 \pm 2.6546j$	−8.2677	$-2.3740 \pm 1.3556j$	−10.2525
$0.3615 \pm 0.6726j$	$0.5797 \pm 2.9000j$	$0.7980 \pm 1.5034j$	−3.2040
−0.5140	−0.9261	−0.4858	−0.3949
$-0.0920 \pm 0.2749j$	0.5769	$0.0691 \pm 0.4054j$	$-0.0608 \pm 0.4124j$
	$-0.0453 \pm 0.1677j$		$0.1337 \pm 0.3608j$
0.0363	−0.0371	−0.2263	0.1627
370.7539	142.9512	100.4791	−111.1415
$-4.6613 \pm 2.7169j$	−7.9616	$-2.0430 \pm 1.2277j$	−10.1948
$0.3116 \pm 0.4023j$	$1.3006 \pm 2.6431j$	2.5186	−3.2044
−0.3937	−0.3475	−0.3750	$0.1300 \pm 0.3747j$
0.0222	0.3010	$0.1213 \pm 0.2633j$	−0.4064
	0.0141		0.0048

(4.7)

with the characteristic polynomial

$$\begin{aligned} \Delta &= [1, -10.5527, -3.1993, -0.6530 \pm 2.2539j, \\ &\quad 0.1339 \pm 0.3765j, -0.4052, -0.0305] \end{aligned} \tag{4.8}$$

and the set of finite multivariable transmission zeros

$$T_z = \{-3.4306 \pm 8.0063j, -0.0236\} \tag{4.9}$$

Also the 2x2 subsystem transfer-function matrix $G_{11}(s)$ of the full system transfer-function matrix $G(s)$ in equation(4.7), associated with the helicopter longitudinal

dynamics (the upper left submatrix in equation(4.7)) possesses the same characteristic polynomial (4.8) and the set of finite transmission zeros given by

$$T_z^{11} = \{-10.4011, -0.6562 \pm 2.2204j, -0.02702, -0.03051\} \quad (4.10)$$

Similarly the 2x2 subsystem transfer-function matrix $G_{22}(s)$ of equation(4.7) associated with the helicopter lateral dynamics (the lower right submatrix in equation(4.7)) possesses the same characteristic polynomial (4.8) and the set of transmission zeros given by

$$T_z^{22} = \{-3.0524 \pm 7.7475j, -2.9032, 0.0741 \pm 0.3881j, -0.5466\} \quad (4.11)$$

Each element $g_{ij}(s)$, i,j=1,2,3,4, of the 4x4 transfer-function matrix $G(s)$ in equation(4.7) represents nominal open-loop signal transmission between the jth pilot inceptor and the ith tracking output. The transfer function matrix model of equation(4.7) for the rigid body dynamics of the helicopter at 80 knots forward level flight, is a nominal small signal model; this model will have both gain and phase uncertainties associated with neglected non-linearities, unmodelled rotor and actuator dynamics, neglected inflow dynamic, etc. It is noted from equation(4.9) that the nominal system possesses only left-hand plane transmission zeros; that is, the nominal system is minimum phase. For analysis of the system, the most important range of frequencies is that close to the channel crossover frequencies. To meet handling quality specifications for the helicopter requires channel crossover frequencies in the region of 2 to 4 rad/sec Tischler [30] and Anonymous [1].

4.3 Potential decoupling of the helicopter control problem

Similar to fixed-wing flight control, McRuer *et al* [24], it is not unreasonable to anticipate that the linearised helicopter longitudinal and lateral dynamics decouple. Firstly, consider that if the helicopter problem decouples into two 2x2 subsystem, $G_{11}(s)$ and $G_{22}(s)$, then

$$\mid G(s) \mid \simeq \mid G_{11}(s) \mid\mid G_{22}(s) \mid \tag{4.12}$$

This is clearly not the case for the following reason. From equations(4.8) and (4.9), $\mid G(s) \mid$ possesses no right half plane zeros (RHPZ's) and two right half plane poles (RHPP's). The RHPP's of $\mid G_{11}(s) \mid$ are the same poles as the RHPP's of $\mid G(s) \mid$ as given by (4.9) while it is observed from equation(4.10) that $\mid G_{11}(s) \mid$ possesses no RHPZ's. However, the RHPP's are the same as the RHPP's of $\mid G(s) \mid$ while it is observed from equation (4.11) that $\mid G_{22}(s) \mid$ possesses 2 RHPZ's. The right hand side of equation(4.12) thus has 4 RHPP's and 2 RHPZ's which does not agree with the number of RHPP's and RHPZ's of the left hand side.

Secondly, examination of the 4-input 4-output multivariable transfer-function matrix model (4.7) of the helicopter suggests that the helicopter longitudinal dynamics (upper left submatrix) and lateral dynamics (lower right submatrix) are strongly coupled. Indeed, this strong cross-coupling is borne out by an inspection of the step responses in Figure 4.1 where, in particular, strong cross-coupling is exhibited by the lateral outputs 3 and 4 in response to the longitudinal inputs 1 and 2 (The original unstable plant (4.7) has been prior stabilised by a *weak* feedback (4.13), weak in the sense that while sufficient to stabilise the plant $G(s)$, the individual transfer-function elements g_{ij} and associated uncertainties of the plant $G(s)$ remain relatively unchanged except at frequencies local to that of the

RHPP's). For this reason, no *a priori* assumption concerning the decoupling of the longitudinal and lateral dynamics can be made and a full 4x4 multivariable treatment of the problem might appear to be necessary as in Yue *et al* [35] and Walker *et al* [34].

Despite the fact that the helicopter longitudinal dynamics and lateral dynamics are strongly coupled, what is shown through the use of the Individual Channel Design (ICD) framework is that *for control design purposes* the helicopter longitudinal dynamics and the lateral dynamics can be considered as decoupled. The keys to this multivariable analysis are the multivariable structure functions $\Gamma_i(s)$, $i = 1, 2, 3, 4$ ($\Gamma_4 = 0$), of equation(3.38) which are indicators of the potential performance of multivariable feedback control before any actual design is attempted. In particular, the Nyquist plot of $\Gamma_2(s)$ for the full system in Figure(4.2) is small in the frequency range of most interest for control, namely, 2-4 rad/sec. In addition, the Nyquist plot of $\Gamma_1(s)$ for the full system (4.7) in Figure(4.2) is very similar to the Nyquist plot of $\Gamma_1(s)$ for the longitudinal dynamics $G_{11}(s)$ in Figure(4.3) and the Nyquist plot of $\Gamma_3(s)$ for the full system (4.7) in Figure(4.2) is very similar to the Nyquist plot of $\Gamma_1(s)$ for the lateral dynamics $G_{22}(s)$ in Figure(4.4). These observations indicate that for control design purposes, the helicopter longitudinal dynamics, as represented by Channel 1 and Channel 2, may very well be decoupled from the lateral dynamics, as represented by Channel 3 and Channel 4, in the region of the crossover frequencies. So as to establish whether or not this is actually the case requires the application of Result 3.7 to the 2-input 2-output Multiple-Channel M_1 representing the longitudinal dynamics and the 2-input 2-output Multiple-Channel M_2 representing the lateral dynamics as follows.

Consider first condition (i) of Result 3.7. From the Bode plots of the diagonal elements of $G_{11}(s)$,$G^*_{11}(s)$, $G_{22}(s)$ and $G^*_{22}(s)$ in Figures(4.5)-(4.8), it is seen that the diagonal elements of $G^*_{11}(s)$ and $G^*_{22}(s)$ do not differ significantly from the respective diagonal elements of $G_{11}(s)$ and $G_{22}(s)$ in the region of the crossover

frequencies, an so condition (i) of Result 3.7 is satisfied. (Observe that the small discrepancies in gain between $g_{22}(s)$ and $g_{22}^*(s)$ in Figure(4.7) of approximately 2dB's may require slightly larger phase and particularly gain margins when designing controllers for Channels $C_1(s)$ and $C_2(s)$). Also, condition (ii) of Result 3.7 is satisfied since from Figures(4.9) and (4.10), it is observed that the multivariable structure function $\Gamma_1^*(s)$ ($\Gamma_2^*(s) = 0$) of the 2-input 2-output system $G_{11}^*(s)$ does not differ significantly from that of $G_{11}(s)$ in the region of the crossover frequencies; likewise, the multivariable structure function $\Gamma_1^*(s)$ ($\Gamma_2^*(s) = 0$) of the 2-input 2-output system $G_{22}^*(s)$ does not differ significantly from that of $G_{22}(s)$.

Lastly, consider condition (iii) of Result 3.7. From Table 4.1, it is seen that the RHPP's and RHPZ's of $G_{11}^*(s)$ do not differ significantly from those of $G_{11}(s)$. Hence, all three conditions of Result 3.7 are satisfied as far as $G_{11}^*(s)$ are concerned; that is, the 2-input 2-output Multiple Channel $M_1(s)$ for the longitudinal dynamics represented by $G_{11}^*(s)$ is weakly coupled to the 2-input 2-output Multiple Channel $M_2(s)$ for the lateral dynamics and can be designed on the basis of the 2-input 2-output system $G_{11}(s)$ alone. However, this does not imply that Multiple Channel $M_2(s)$ can be designed on the basis of the 2-input 2-output system $G_{22}(s)$ alone.

Turning to the 2-input 2-output Multiple-Channel $M_2(s)$, it is seen from Table 4.1 that the RHPP's and RHPZ's of $G_{22}^*(s)$ differ significantly from those of $G_{22}(s)$; indeed, $G_{22}^*(s)$ is minimum phase while $G_{22}(s)$ is non-minimum phase with RHP transmission zeros at $0.0741 \pm 0.3881j$. Hence, condition (iii) of Result 3.7 is not satisfied and it appears that the Multiple-Channel $M_2(s)$, representing the lateral dynamics, is not weakly coupled to the Multiple-Channel $M_1(s)$ representing the longitudinal dynamics. This would mean that after the design for a multivariable controller $K_1(s)$ of (3.15) on the basis of the decoupled system $G_{11}(s)$, the design for controller $K_2(s)$ would have to proceed on the basis of the coupled system $\left(I - G_{21}G_{11}^{-1}H_1G_{12}G_{22}^{-1}\right)G_{22}$ in equation(3.20) where $H_1(s)$ is defined by the diagonal controller $K_1(s)$ as in equation(3.21).

	subsystem RHP transmission Zeros	Subsystem RHP poles		Individual RHPZ's	Individual RHPP's
G_{11}	-	$0.1339 \pm 0.3776j$	g_{11}	-	$0.1339 \pm 0.3766j$
			g_{12}	-	$0.1339 \pm 0.3766j$
			g_{21}	-	$0.1339 \pm 0.3766j$
			g_{22}	-	$0.1339 \pm 0.3766j$
G_{22}	$0.0741 \pm 0.3881j$	$0.1339 \pm 0.3776j$	g_{33}	$0.7980 \pm 1.5034j$	$0.1339 \pm 0.3766j$
				$0.0691 \pm 0.4054j$	
			g_{34}	$0.1337 \pm 0.3608j$	$0.1339 \pm 0.3766j$
			g_{43}	100.4791	$0.1339 \pm 0.3766j$
				2.5186	
				$0.1213 \pm 0.2633j$	
			g_{44}	$0.1300 \pm 0.3747j$	$0.1339 \pm 0.3766j$
				0.0048	
G_{11}^*	-	$0.0741 \pm 0.3881j$	g_{11}^*	-	$0.0741 \pm 0.3881j$
			g_{12}^*	-	$0.0741 \pm 0.3881j$
			g_{21}^*	-	$0.0741 \pm 0.3881j$
			g_{22}^*	-	$0.0741 \pm 0.3881j$
G_{22}^*	-	-	g_{33}^*	$0.6043 \pm 1.7069j$	-
			g_{34}^*	-	-
			g_{43}^*	1.93	-
				105.3	-
			g_{44}^*	0.0044	-

Table 4.1: Subsystem and Multiple Channel RHPP's and RHPZ's for the helicopter model G(s) of eqn.(4.7)

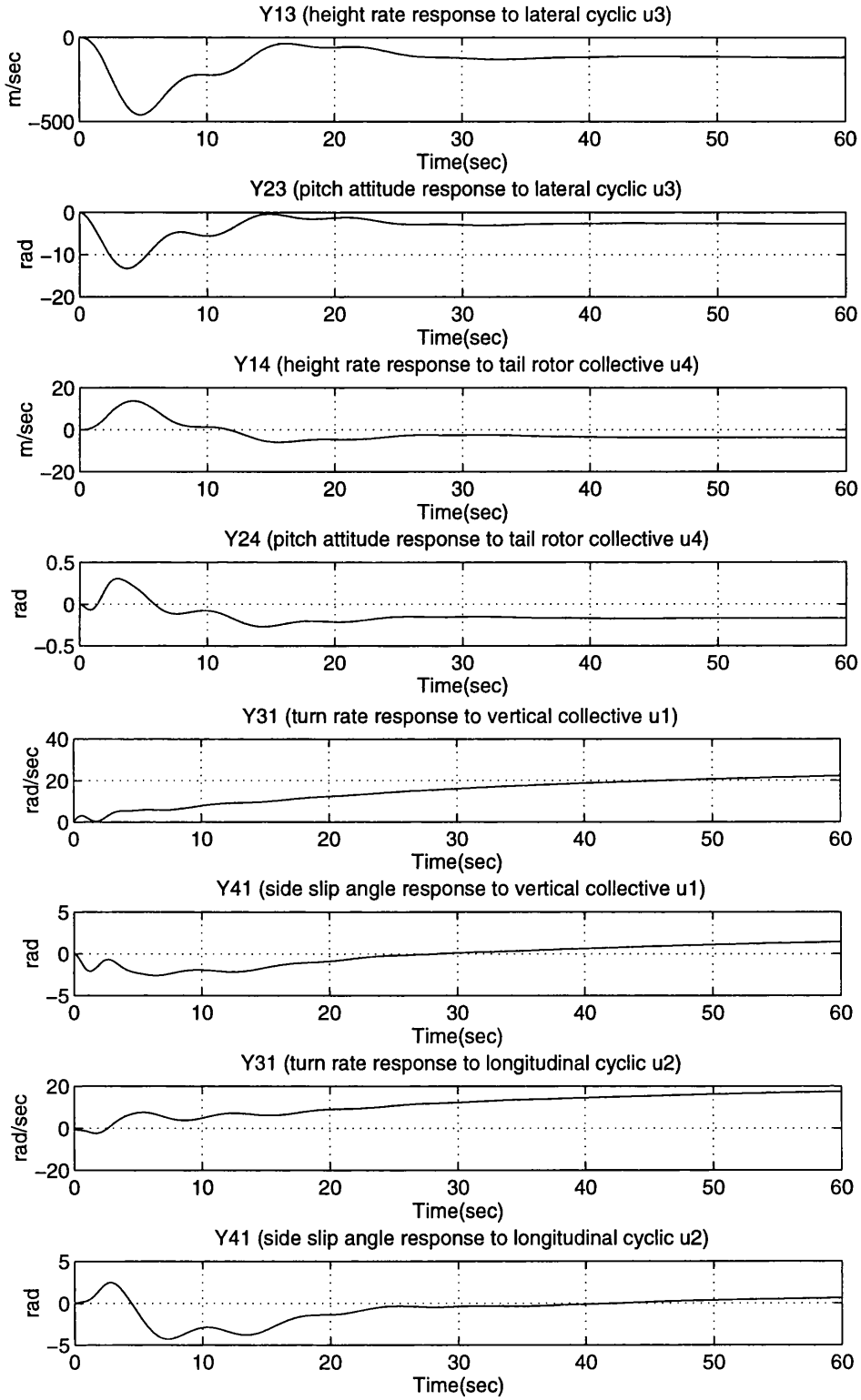

Figure 4.1: Step responses for the full system of eqn.(4.16).

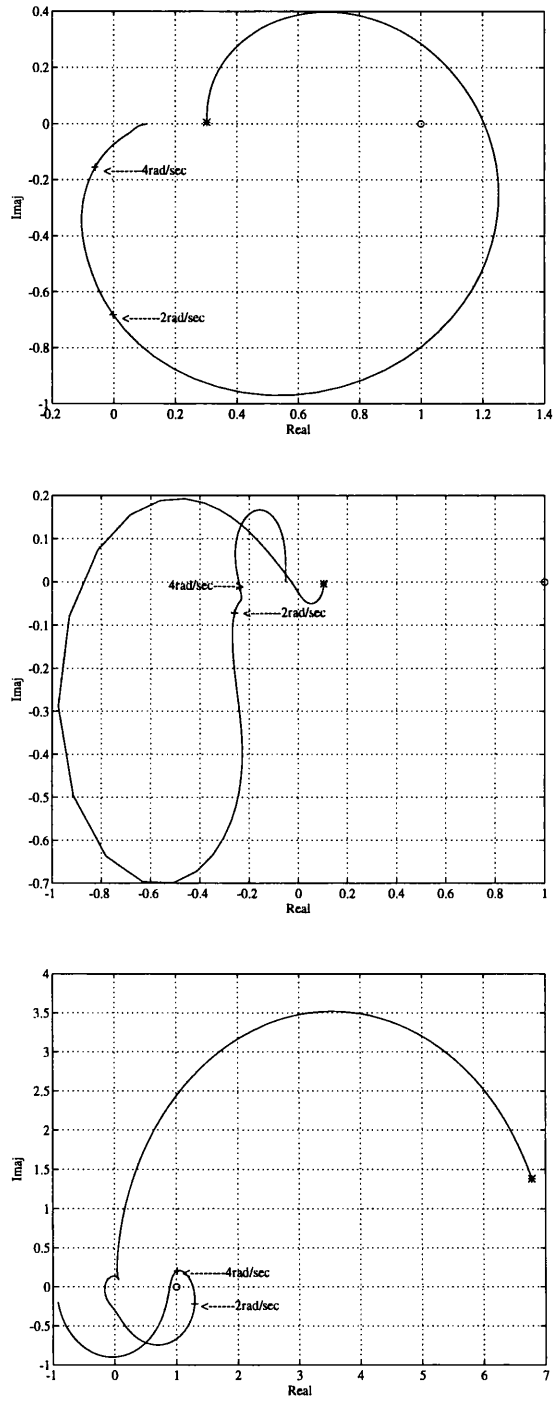

Figure 4.2: Nyquist plots of the multivariable structure functions $\Gamma_1(s)$, $\Gamma_2(s)$ and $\Gamma_3(s)$ for full system $G(s)$ of eqn.(4.16).

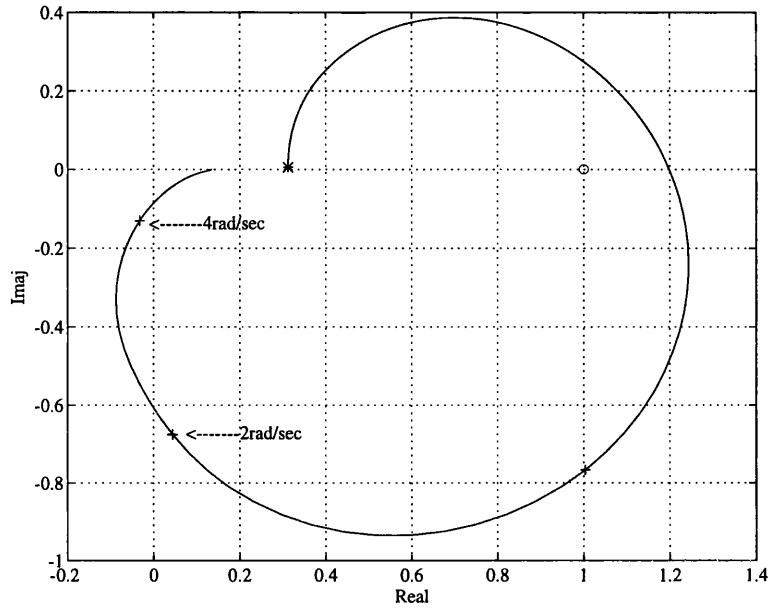

Figure 4.3: Nyquist plot of multivariable structure function $\Gamma_1(s)$ for G_{11}.

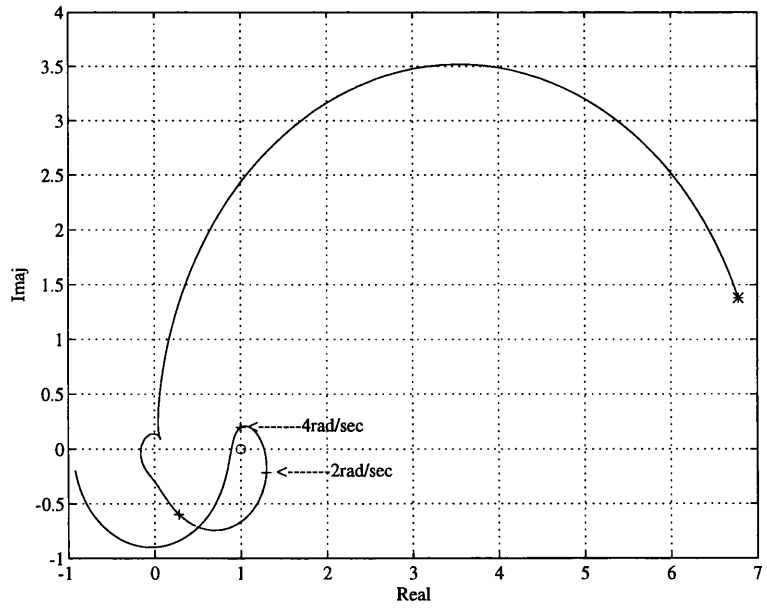

Figure 4.4: Nyquist plot of multivariable structure function $\Gamma_1(s)$ for G_{22}.

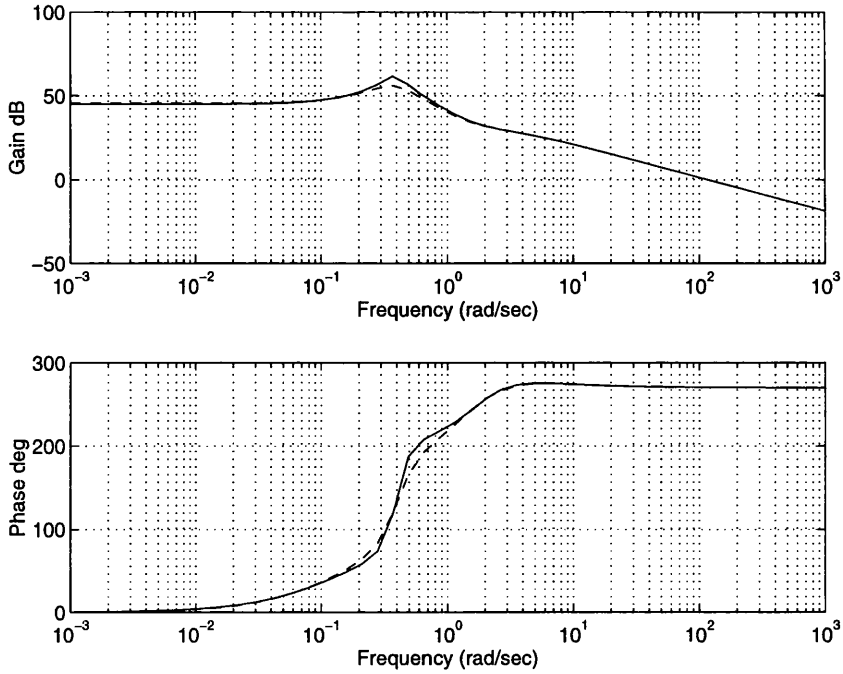

Figure 4.5: Bode plots of diagonal elements g_{11} and g_{11}^* of G_{11} and G_{11}^* respectively.

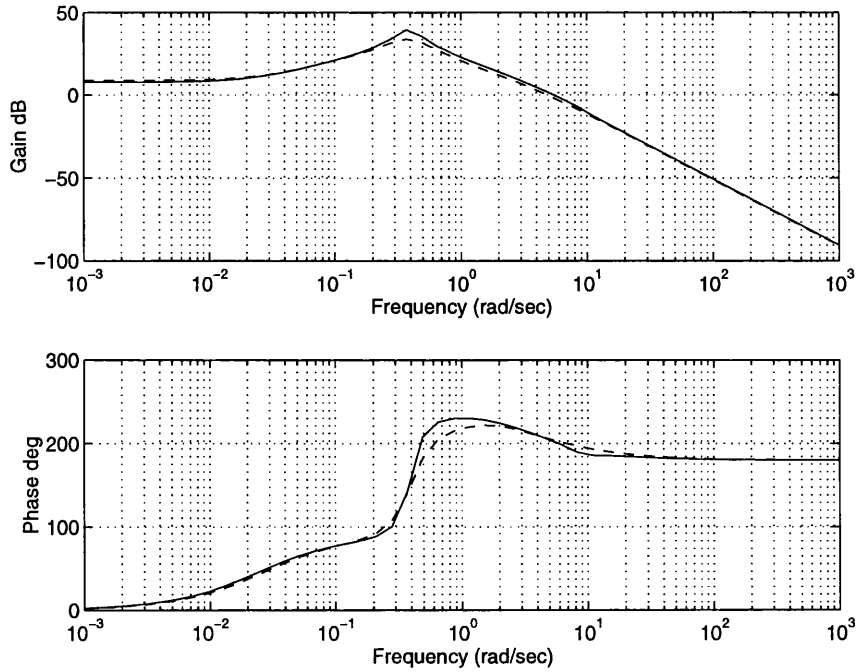

Figure 4.6: Bode plots of diagonal elements g_{22} and g_{22}^* of G_{11} and G_{11}^* respectively.

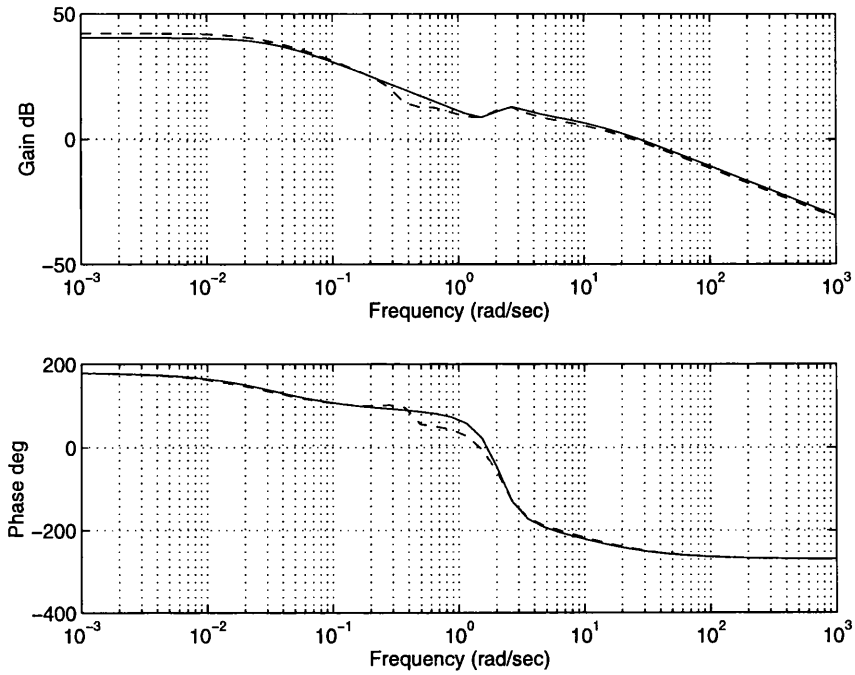

Figure 4.7: Bode plots of diagonal elements g_{11} and g_{11}^* of G_{22} and G_{22}^* respectively.

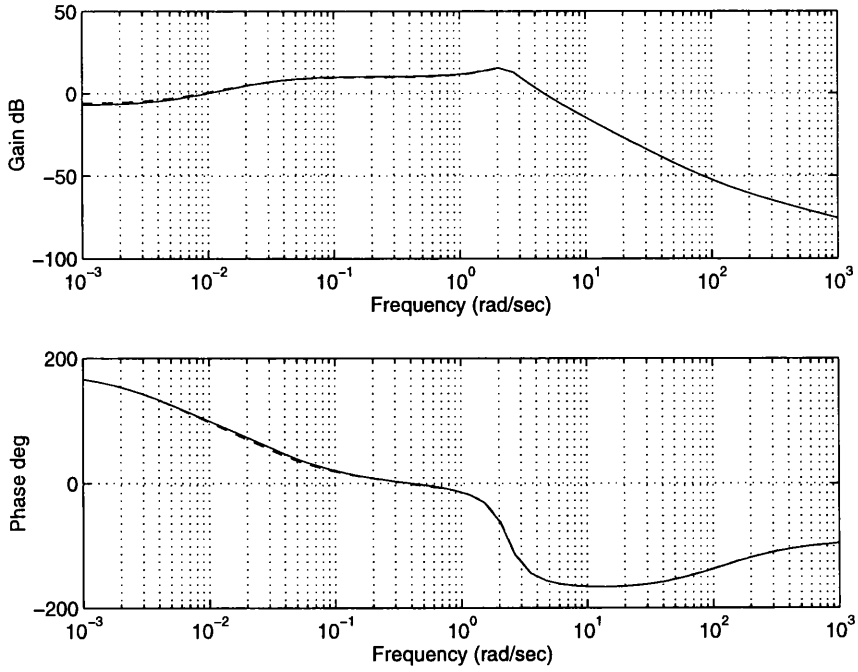

Figure 4.8: Bode plots of diagonal elements g_{22} and g_{22}^* of G_{22} and G_{22}^* respectively.

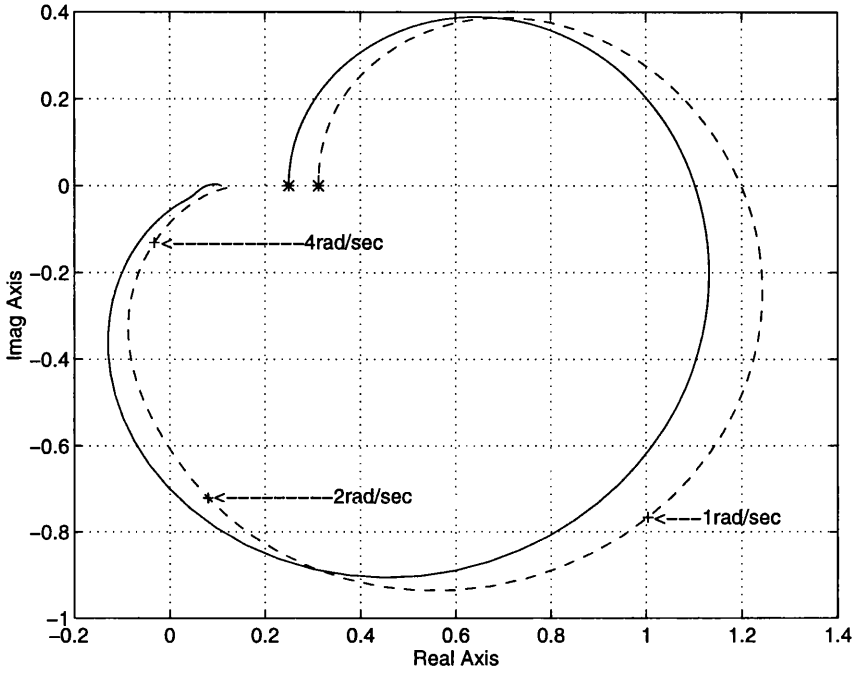

Figure 4.9: Nyquist plots of multivariable structure functions $\Gamma_1(s)$ and $\Gamma_1^*(s)$ for G_{11} and G_{11}^* respectively.

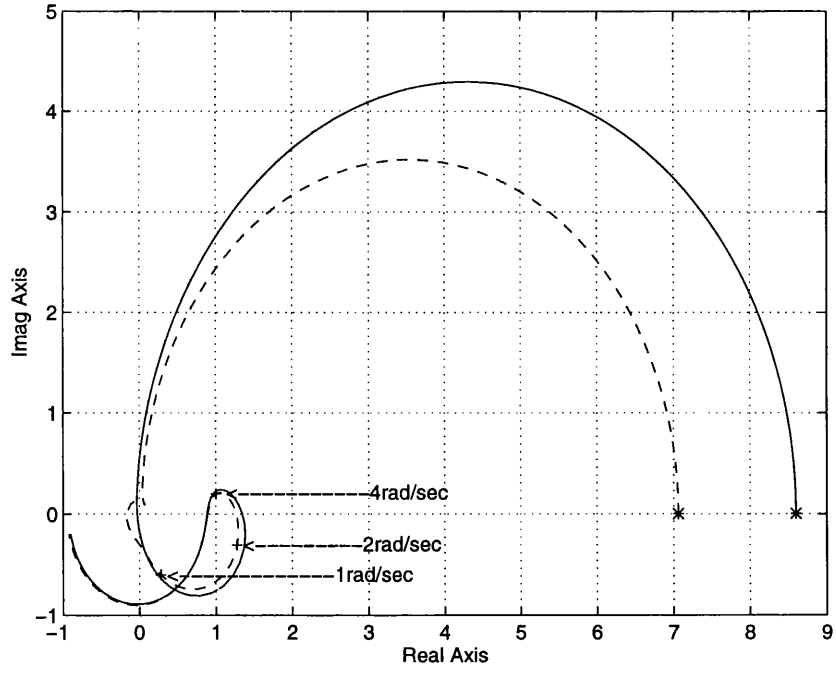

Figure 4.10: Nyquist plots of multivariable structure functions $\Gamma_1(s)$ and $\Gamma_1^*(s)$ for G_{22} and G_{22}^* respectively.

4.4 Complete decoupling of the helicopter control problem

Considering the discussion in Section 3.4 for systems represented in linear state space form, the coupling of the Multiple Channel $M_2(s)$ to Multiple Channel $M_1(s)$ is more apparent than real and can be overcome in the following way. First, observe in Table 4.1 that the RHP transmission zeros of subsystem $G_{22}(s)$, $0.0741 \pm 0.3881j$, almost coincide with the RHPP's of the $G_{22}(s)$ submatrix of the full helicopter transfer-function matrix of equations(4.7) and (4.8). It seems likely that these near-cancelling RHPP's and RPHZ's are a spurious by-product of the highly structured form of the state space representation; that is, these near-cancelling RHPP's and RHPZ's are fictitious and in reality the real physical lateral dynamics represented by $G_{22}(s)$ may be stable and minimum phase. All the elements of a transfer-function matrix obtained from a state space representation are forced to have a common characteristic polynomial denominator thereby requiring additional zeros in some elements of the system transfer-function matrix Leithead and O'Reilly [18]. Hence, it would appear that the lack of decoupling between Multiple Channel $M_1(s)$ and Multiple-Channel $M_2(s)$ for design purposes is artificial and due to the use of a state space model for the system.

If cancellation of these RHPP's and RHPZ's can be achieved, then condition (iii) of Result 3.7 would be satisfied and Multiple-Channel $M_2(s)$ would indeed be weakly coupled to Multiple-Channel $M_1(s)$; nonetheless, it would be unwise to directly do so, Leithead and O'Reilly [18]. As indicated in Section 3.5.1, the solution to this problem is within the state-space property of a common characteristic polynomial denominator whereby if one element of the corresponding transfer-function matrix $G(s)$ in equation(4.7) is stabilised by scalar feedback $m(s)$, then all other elements $g_{ij}(s)$ of $G(s)$ will likewise be stabilised. In effect, the undesirable almost RHP pole-zero cancellation will be replaced by a benign LHP almost pole-zero cancellation. Result 3.7 would then imply that Multiple-Channel $M_2(s)$

is weakly coupled to Multiple-Channel $M_1(s)$.

However, as it was also indicated in Section 3.5.1, stabilisation by a feedback loop has its dangers as well as its benefits. Hence, a satisfactory design of the stabilising feedback function $m(s)$ must result in minimum change to the plant. Two points need to be taken into consideration. Firstly, to minimise structural change requires that the individual transfer-function elements $g_{ij}(s)$ of the plant $G(s)$ in equation(4.7) should remain relatively unchanged except at frequencies local to that of the RHPP's and RHPZ's (at frequencies well below the channel crossover frequencies). Secondly, it should be ensured that the uncertainties of the individual transfer-function elements $g_{ij}(s)$ of $G(s)$ in equation(4.7) should not be increased since this could lead to a lack of robustness in subsequent control design. In order to cater for these two points, a *weak* gain $m(s)$ on the feedback loop is preferable.

A candidate feedback function $m(s)$ round the $g_{12}(s)$ element is

$$m(s) = 0.0085\frac{(s+0.09)}{(s+1.5)^2} \tag{4.13}$$

Application of the feedback function $m(s)$ of equation(4.13) to the full 4-input 4-output helicopter system G(s) of equation(4.7) via the matrix $M(s)$

$$M(s) = \begin{bmatrix} 0 & 0 & 0 & 0 \\ m(s) & 0 & 0 & 0 \\ 0 & 0 & 0 & 0 \\ 0 & 0 & 0 & 0 \end{bmatrix} \tag{4.14}$$

results in the amended system

$$\bar{G}(s) = (I + GM)^{-1} G \tag{4.15}$$

$$\bar{G}(s) = \frac{1}{\bar{\Delta}} \left[\begin{array}{cc|cc} 117.8421 & 30.6525 & -0.2618 & 0.2202 \\ -10.7519 & -10.3509 & -262.2300 & -5.2552 \pm 5.3272j \\ -0.6712 \pm 2.2565j & -1.2202 \pm 5.3008j & -2.4637 \pm 7.3586j & 0.5984 \pm 5.0372j \\ -1.1484 \pm 1.0531j & -0.6504 \pm 2.2476j & -0.6417 \pm 2.2676j & -2.4243 \\ -0.1305 & -0.0283 \pm 0.0049j & -0.0422 \pm 0.0155j & -0.0501 \\ -0.0316 & -1.5 & -1.5 & -0.0426 \\ -1.5 & -1.5 & -1.4999 & -1.5 \\ -1.5 & & & -1.5 \\ \\ 14.5287 & 28.3289 & -6.7329 & -0.5937 \\ -11.5784 & -10.3714 & -18.9181 & -12.5004 \\ -0.6622 \pm 2.1969j & -0.6586 \pm 2.2367j & -0.5986 \pm 2.2666j & -2.7651 \pm 0.8226j \\ -0.3305 \pm 0.5087j & -0.0284 \pm 0.0011j & -1.5597 \pm 0.3999j & -0.4240 \pm 0.5000j \\ -2.8319 & -0.7806 & -0.6899 & 1.2601 \\ -0.0339 \pm 0.0030j & -1.5 & -0.0549 & 0.1354 \\ & -1.5 & -0.0338 & -0.0327 \\ \hline 13.48 & -6.8926 & -26.6062 & -18.0634 \\ -4.5867 \pm 2.7639j & -8.2678 & -2.7055 \pm 1.5761j & -10.2517 \\ 0.2816 \pm 0.9700j & 0.5797 \pm 2.9001j & -0.0959 \pm 0.2249j & -2.9390 \pm 0.8628j \\ -3.0191 & 0.0454 \pm 0.1677j & -1.9433 & -0.1364 \pm 0.8907j \\ -0.3559 \pm 0.5294j & -1.5 & 0.8421 \pm 1.4980j & -0.0398 \pm 0.3823j \\ -0.0852 \pm 0.1978j & -1.5 & -0.3188 \pm 1.0617j & -0.1118 \pm 0.2346j \\ & -0.9262 & & \\ & 0.5769 & & \\ \\ 0.0364 & -0.0371 & -0.2263 & 0.1627 \\ 370.7522 & 142.9512 & 100.4791 & -111.1415 \\ -4.5153 \pm 2.8394j & -7.9616 & 2.5056 & -10.1939 \\ 0.0731 \pm 0.7945j & 1.3006 \pm 2.6431j & -2.6307 \pm 1.4296j & -2.9392 \pm 0.8625j \\ -2.9421 & 0.30101 & -0.0193 \pm 0.2398j & -0.1331 \pm 0.8820j \\ -0.1327 \pm 0.3223j & -1.5 & -0.5703 \pm 0.8566j & -0.1034 \pm 0.2310j \\ 0.0229 & -1.5 & -0.7643 & 0.0048 \\ & -0.3475 & & \\ & 0.0141 & & \end{array}\right] \quad (4.16)$$

with the amended characteristic polynomial

$$\bar{\Delta} = [1, -10.5518, -2.9354 \pm 0.8629j, -0.6522 \pm 2.2540j,$$

$$-0.1289 \pm 0.8763j, -0.1053 \pm 0.22441j, -0.0305] \quad (4.17)$$

and the set of finite multivariable transmission zeros

$$\bar{T}_z = [-3.4306 \pm 8.0063j, -1.5, -1.5, -0.0236] \quad (4.18)$$

Comparing the Bode plots of the amended individual transfer-function elements $\bar{g}_{ij}(s)$ of equation(4.16) with the original $g_{ij}(s)$ of equation(4.7) in Figures(4.11)-(4.14) and their pole-zero structure described by (4.17), (4.18) with (4.8), (4.9), it is confirmed that they are not significantly altered except close to the frequency of the RHPZ's at 0.4 rad/sec. So the first point concerning the choice of feedback function $m(s)$ has been observed. In other words, the choice of stabilising feedback function m(s) in equation(4.13) has not significantly altered the structure of the system in equation(4.7).

Turning to the second point that uncertainties of the individual transfer function elements should not be increased by feedback $m(s)$, recall that the gain $m(s)$ is connected round the $g_{12}(s)$ element of the transfer function matrix $G(s)$ in equation(4.7). Then, it is necessary to check that the Nyquist plots of multivariable structure functions in $\gamma_{ij}h_{12}$ in equation(3.55) do not come close to the point (1,0) in the frequency range of interest, otherwise uncertainty of the individual transfer function elements in equation(4.7) will have been significantly increased by closing the feedback loop $m(s)$ round the plant element $g_{12}(s)$. In total, there are nine such $\gamma_{ij}h_{12}$ for 2x2 subsystems to check in this way as given by Table 4.2

It is observed that the nine Nyquist plots of $\gamma_{ij}h_{12}$ shown in Figures(4.15)-(4.17) do not come close to the point (1,0) in the frequency range of interest, namely 2-4rad/sec, as required for robustness Leithead and O'Reilly [15]. Note that the Nyquist plots of Figures(4.15)-(4.17) are shown for the frequency range of 0.1rad/sec to 2rad/sec only but outside this frequency range the plots tend to the origin.

What has thereby been achieved at this point is a 4-input 4-output amended helicopter system $\bar{G}(s)$ in equations(4.16) and (4.17) which is stable, and has

Input	Output	$\gamma_{ij}h_{12}$
1	2	$\gamma_{12}h_{12}$
1	3	$\gamma_{13}h_{12}$
1	4	$\gamma_{14}h_{12}$
3	2	$\gamma_{32}h_{12}$
3	3	$\gamma_{33}h_{12}$
3	4	$\gamma_{34}h_{12}$
4	2	$\gamma_{42}h_{12}$
4	3	$\gamma_{43}h_{12}$
4	4	$\gamma_{44}h_{12}$

Table 4.2: Multivariable structure functions $\gamma_{ij}h_{12}$

an undesirable RHP almost pole-zero cancellation changed to a benign LHP almost pole-zero cancellation without increasing the system sensitivity; the apparent non-minimum phase characteristic of the lateral dynamics round 0.4 rad/sec, represented by Channel 3 and Channel 4, has been amended without significant change to the system. This is corroborated by Table 4.3 where it is observed that the $\bar{G}_{22}(s)$ submatrix of the amended system $\bar{G}(s)$ in equation(4.16) is stable and minimum phase. With this amended system $\bar{G}(s)$ of equation(4.16), the path is now clear by way of application of Result 3.7 to show that the 2-input 2-output Multiple Channel $M_2(s)$, representing the lateral dynamics, is weakly coupled to the 2-input 2-output Multiple Channel $M_1(s)$, representing the longitudinal dynamics, as follows.

Condition (i) of Result 3.7 is obviously satisfied from inspection of the Bode plots of the diagonal elements of the amended subsystems $\bar{G}_{22}(s)$ and $\bar{G}^*_{22}(s)$ in Figures(4.18) and (4.19). Also, condition (ii) of Result 3.7 is satisfied since from Figure(4.21) the respective multivariable structure function $\bar{\Gamma}_1(s)$ of the amended subsystem $\bar{G}_{22}(s)$ does not differ significantly from that of $\bar{G}^*_{22}(s)$.

From Table 4.3, it is observed that the RHPP's and RHPZ's of $\bar{G}^*_{22}(s)$ do not differ significantly from those of $\bar{G}_{22}(s)$ thereby satisfying condition (iii) of Result 3.7. Hence, all the conditions of Result 3.7 are satisfied as far as $\bar{G}^*_{22}(s)$ and $\bar{G}_{22}(s)$ are concerned; that is, the 2-input 2-output Multiple-Channel $M_2(s)$

		Individual RHPZ's	Individual RHPP's
$\bar{G}_{22}$	g_{33}	$0.8421 \pm 1.4980j$	-
	g_{34}	-	-
	g_{43}	100.4791	-
		2.5056	-
	g_{44}	0.0048	-
$\bar{G}^*_{22}$	g^*_{33}	$0.6039 \pm 1.7071j$	-
	g^*_{34}	-	-
	g^*_{43}	1.9348	-
		105.4427	-
	g^*_{44}	0.0047	-
$\bar{G}_{11}$ and $\bar{G}^*_{11}$ are stable and minimum phase			
G_{22} and G^*_{22} are stable and minimum phase			

Table 4.3: Subsystem and Multiple Channel RHPP's and RHPZ's for the amended helicopter model $\bar{G}(s)$ of eqn.(4.16)

for the lateral dynamics, represented by $\bar{G}^*_{22}(s)$ is weakly coupled to the 2-input 2-output Multiple Channel $M_1(s)$ for the longitudinal dynamics at the channel crossover frequencies. The diagonal controller $K_2(s)$ of equation(3.15) can be designed on the basis of the amended 2-input 2-output system $\bar{G}_{22}(s)$, Finally, it is observed that all conditions of Result 3.7 are satisfied as far as $\bar{G}^*_{11}(s)$ and $\bar{G}_{11}(s)$ are concerned because the feedback $m(s)$ is designed to be weak in the sense that it does not change the structure of the plant and hence does not increased the dependence of $G_{11}(s)$ on $G_{22}(s)$ as confirmed by Figure(4.20); that is, the 2-input 2-output Multiple Channel $M_1(s)$ for the amended system $\bar{G}(s)$ of equation(4.16) remains weakly coupled to the 2-input 2-output Multiple-Channel $M_2(s)$.

4.5 Conclusions

In this chapter an in depth ICD analysis of the helicopter model was presented. It was found that the Multiple-Channels $M_1(s)$ and $M_2(s)$, representing the longitudinal and lateral dynamics respectively, are weakly coupled to each other and the controllers $K_1(s)$ and $K_2(s)$ can be designed independently on the basis of the respective amended 2-input 2-output systems $\bar{G}_{11}(s)$ and $\bar{G}_{22}(s)$. It is emphasised that the system is not decoupled by state feedback; the structure of the amended plant $\bar{G}(s)$ does not differ significantly from that of $G(s)$. Rather, it is making

explicit an implicit property of the system by a weak feedback loop, Verde *et al* [6].

Despite this favourable decoupling of control tasks, structural and robustness problems inherent in the helicopter system (4.7) or (4.16) remain. Examination of the Nyquist plots of the multivariable structure function $\Gamma_1(s)$ for $\bar{G}_{22}(s)$ in Figure(4.18) reveals that it is close to the point (1,0) within the frequency range (0-4rad/sec) of interest. Thus, by Result 3.4, control systems design may suffer from lack of robustness resulting in destabilisation of the system, particularly at low frequency, and loss of performance.

Note that these potential structural and robustness problems are due to the coupled nature of the multivariable system itself within the multivariable system $\bar{G}_{22}(s)$ and are in addition to the familiar robustness problems of unmodelled helicopter rotor and actuator dynamics which affect each channel.

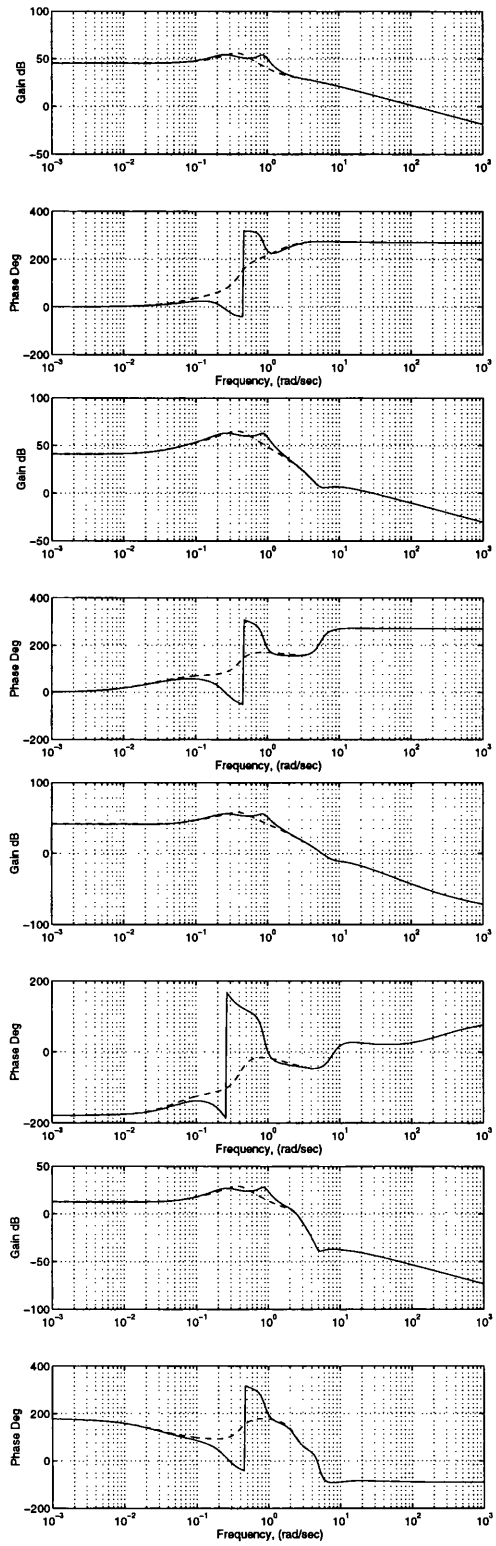

Figure 4.11: Bode plots of $\bar{g}_{1j}(s)$ and $g_{1j}(s)$ for $\bar{G}(s)$ and $G(s)$ respectively.

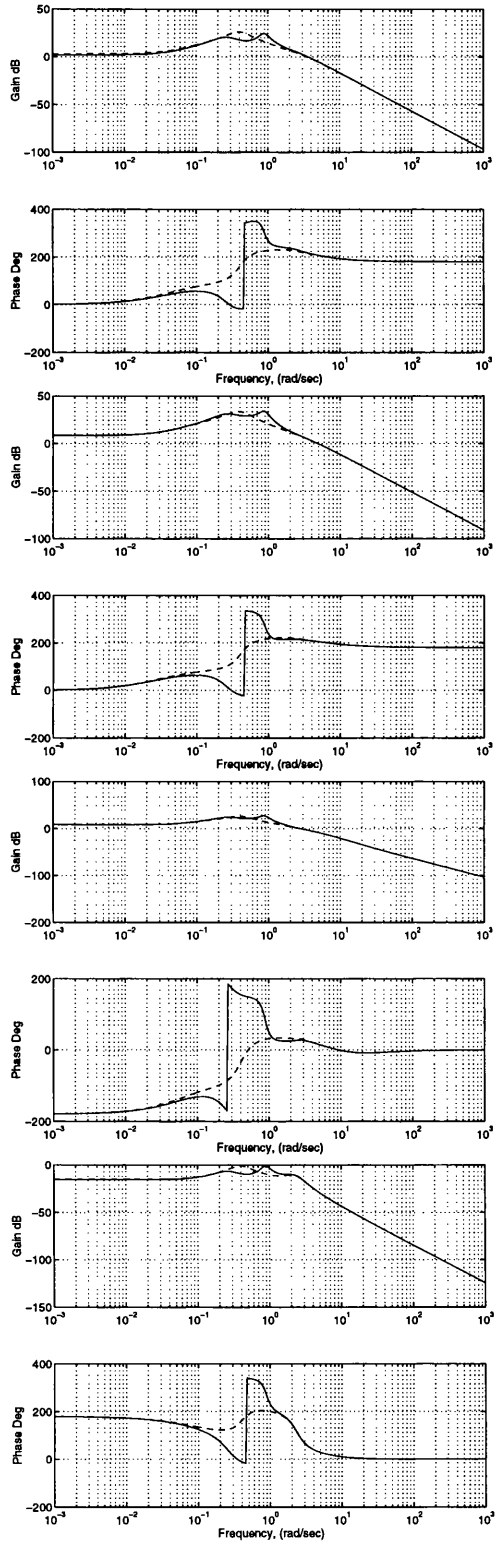

Figure 4.12: Bode plots of $\bar{g}_{2j}(s)$ and $g_{2j}(s)$ for $\bar{G}(s)$ and $G(s)$ respectively.

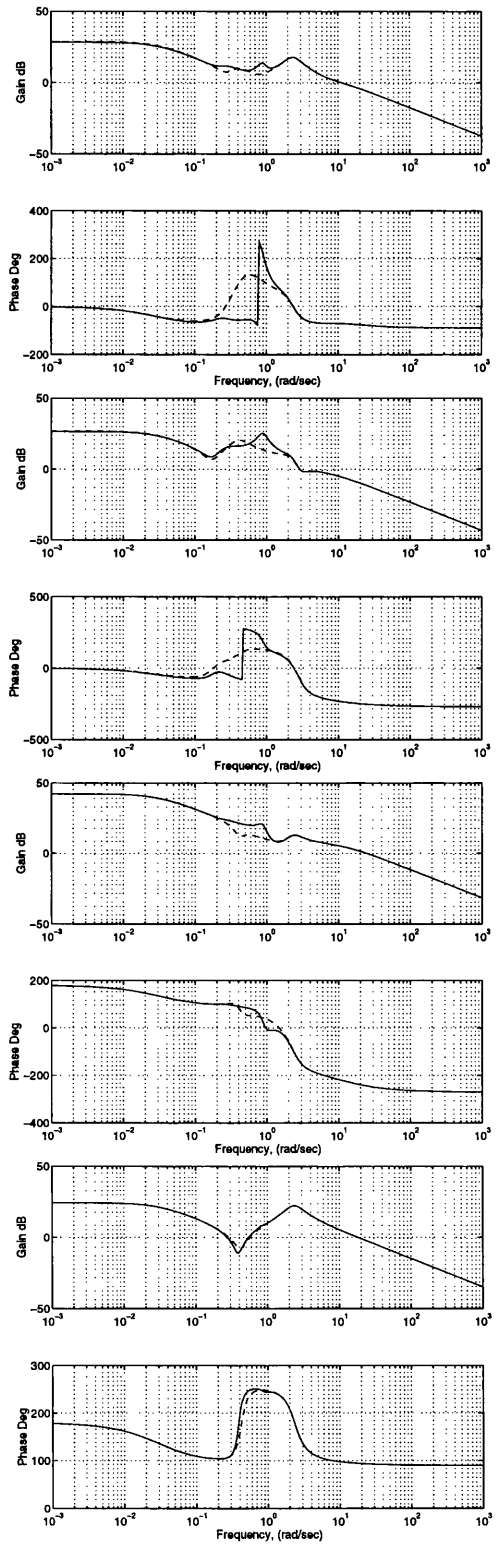

Figure 4.13: Bode plots of $\bar{g}_{3j}(s)$ and $g_{3j}(s)$ for $\bar{G}(s)$ and $G(s)$ respectively.

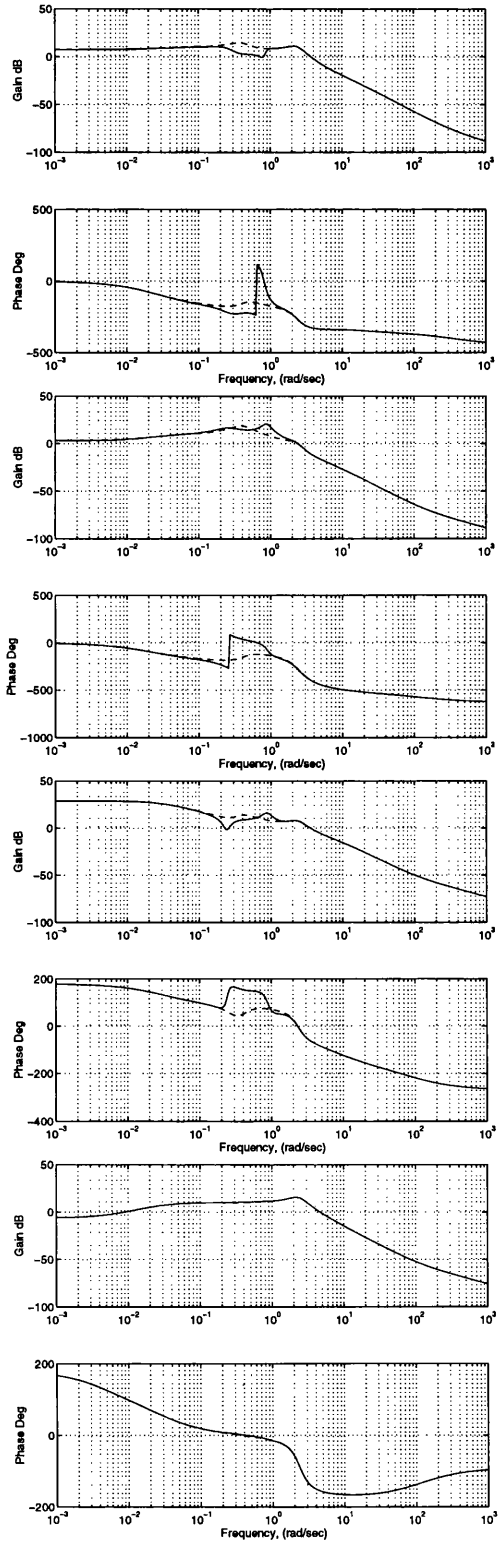

Figure 4.14: Bode plots of $\bar{g}_{4j}(s)$ and $g_{4j}(s)$ for $\bar{G}(s)$ and $G(s)$ respectively.

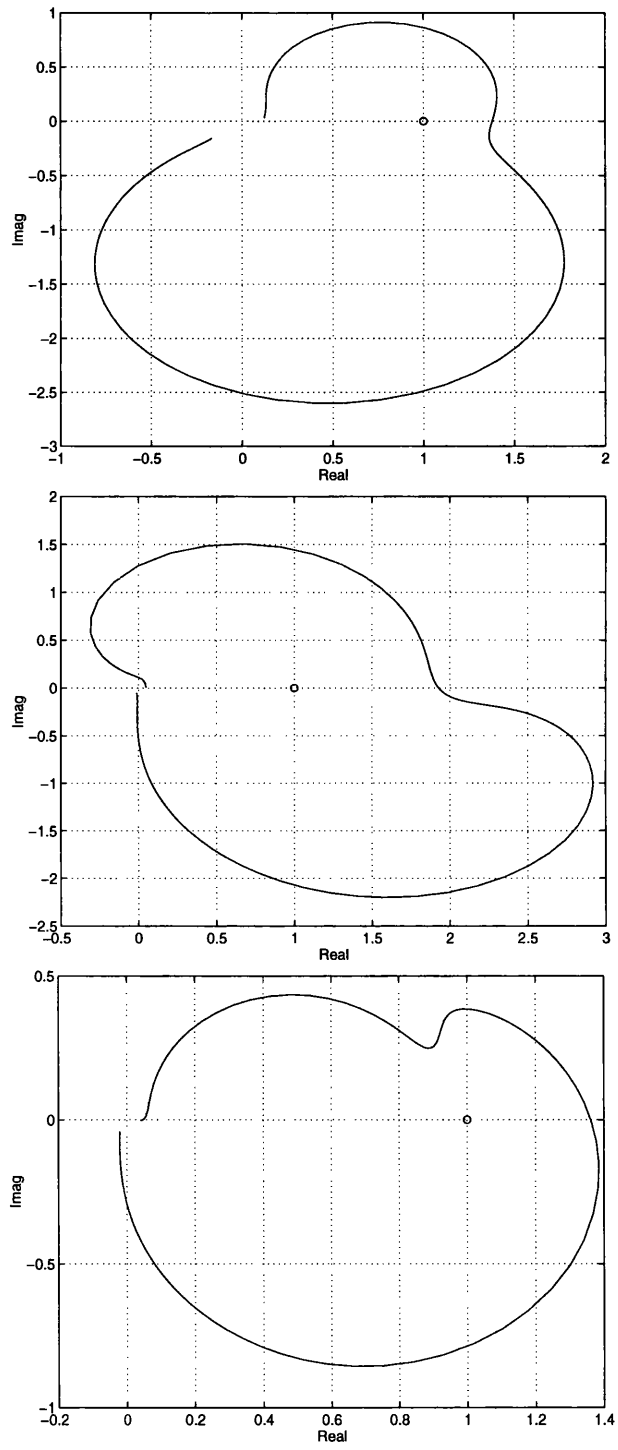

Figure 4.15: Nyquist plots of $\gamma_{ij}h_{12}$ in Table 4.2.

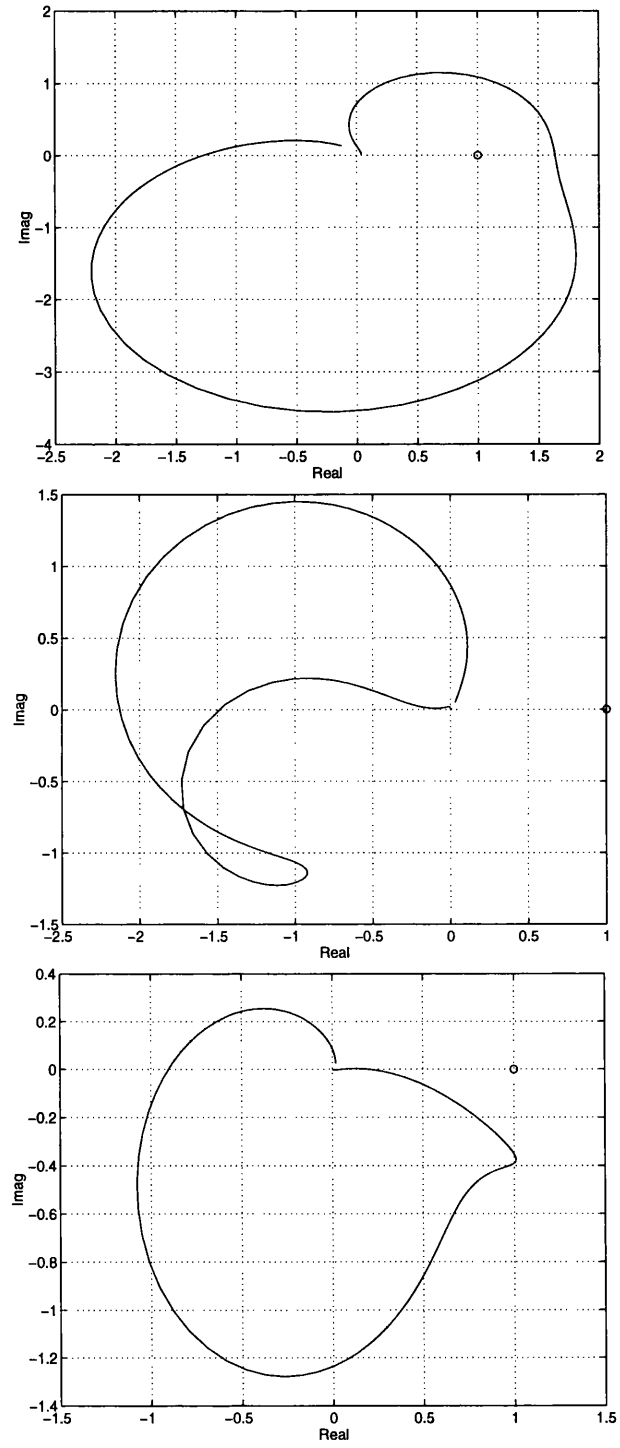

Figure 4.16: Nyquist plots of $\gamma_{ij}h_{12}$ in Table 4.2.

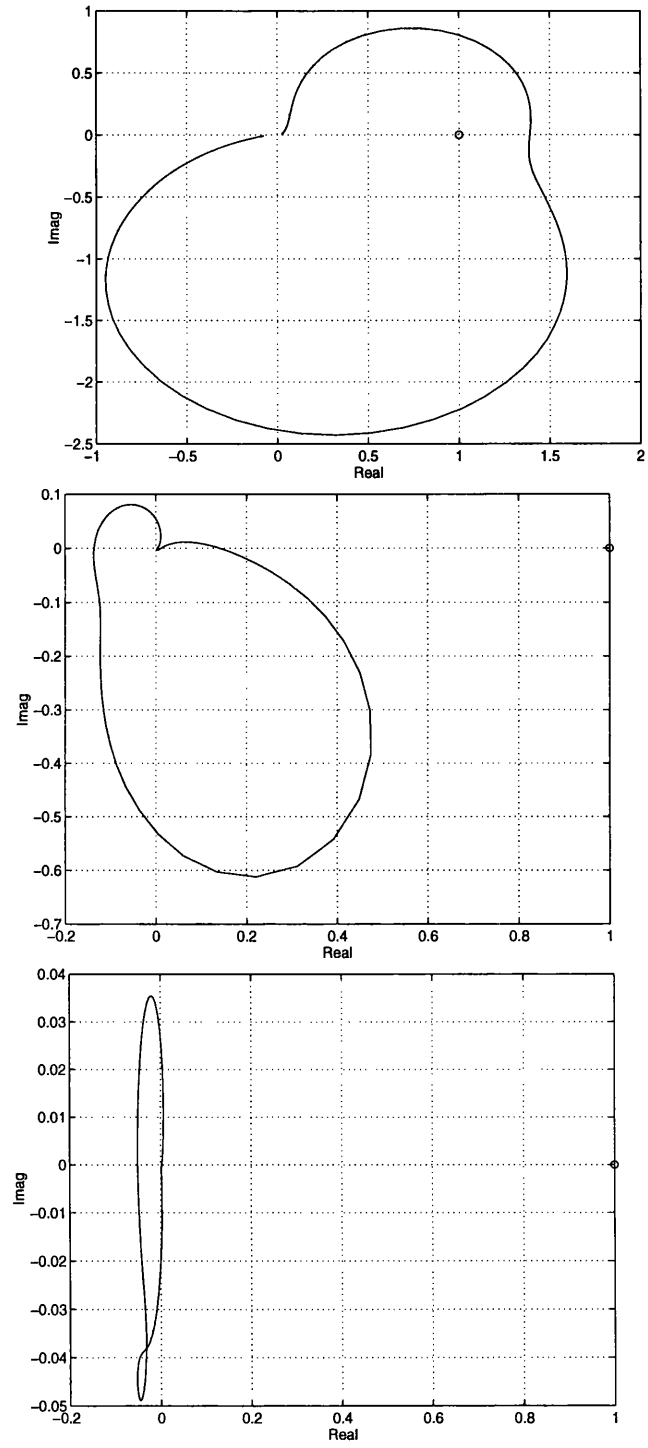

Figure 4.17: Nyquist plots of $\gamma_{ij}h_{12}$ in Table 4.2.

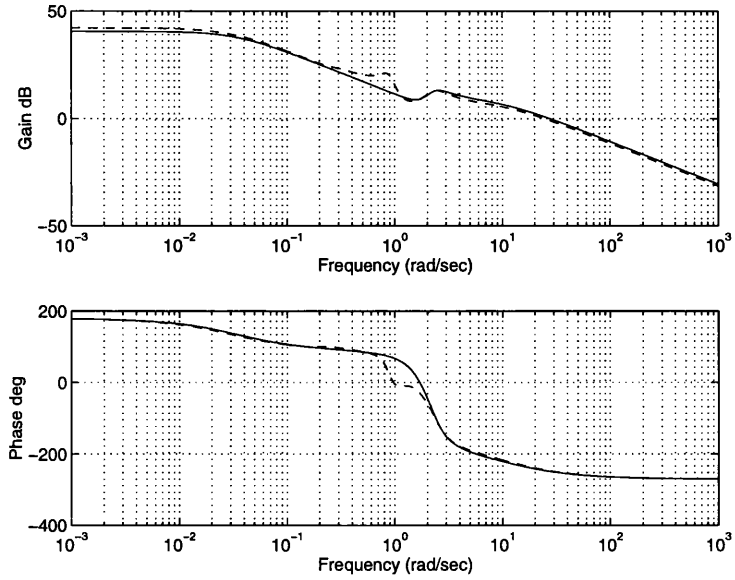

Figure 4.18: Bode plots of diagonal elements $\bar{g}_{11}$ and $\bar{g}_{11}^{*}$ of $\bar{G}_{22}$ and $\bar{G}_{22}^{*}$ respectively.

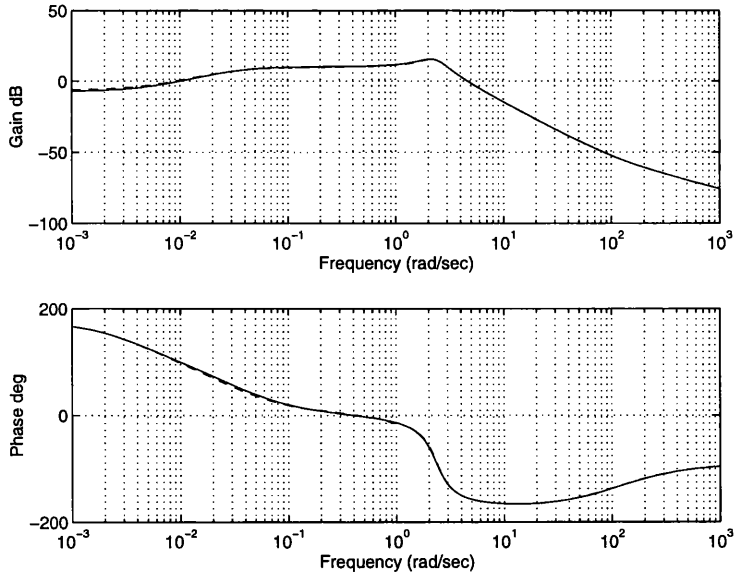

Figure 4.19: Bode plots of diagonal elements $\bar{g}_{22}$ and $\bar{g}_{22}^{*}$ of $\bar{G}_{22}$ and $\bar{G}_{22}^{*}$ respectively.

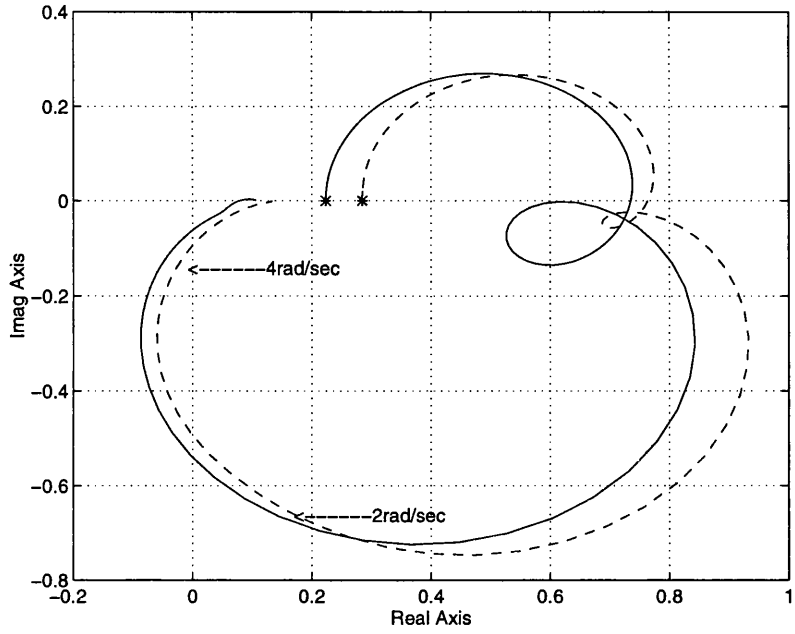

Figure 4.20: Nyquist plots of multivariable structure functions $\bar{\Gamma}_1(s)$ and $\bar{\Gamma}_1^*(s)$ for $\bar{G}_{11}$ and $\bar{G}_{11}^*$ respectively.

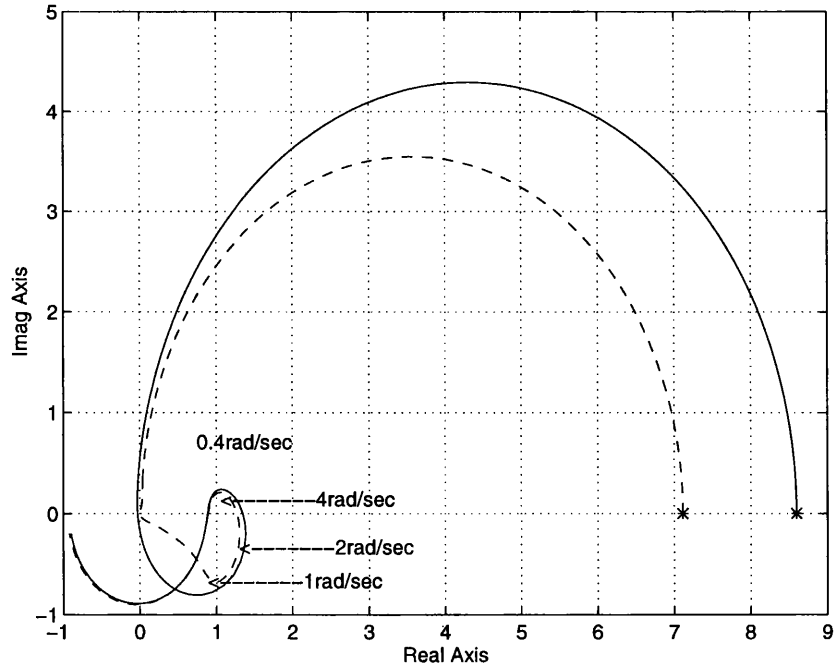

Figure 4.21: Nyquist plots of multivariable structure functions $\bar{\Gamma}_1(s)$ and $\bar{\Gamma}_1^*(s)$ for $\bar{G}_{22}$ and $\bar{G}_{22}^*$ respectively.

Chapter 5

80 Knots Forward Flight Controller Design

5.1 Introduction

In the previous chapter, the ICD structural analysis of the helicopter model at 80 knots forward flight was presented. It was found that the helicopter model, for design purposes, decomposes without significant loss of structural (interaction) information, into two decoupled simpler 2-input 2-output multivariable problems, one for the longitudinal dynamics a one for the lateral dynamics. It was also concluded that due to the closeness to the point (1,0) of the multivariable structure function for the lateral dynamics, the control system design may suffer from lack of robustness. In this chapter, the control system design for the amended helicopter model from Chapter 4 is presented. It is based on the decoupled lateral and longitudinal dynamics of the amended system; i.e, it consists of two separate designs, although both designs are assessed on the basis of the full $4x4$ system. Some additional problems to that of the sensitivity problem in the lateral dynamics are shown. These problems are high cross-coupling at high frequency in the longitudinal dynamics, and the introduction of RHPZ's in the lateral dynamics when the requirements of design are satisfied. All of these problems are solved

via pre-compensation and by the use of a feedforward controller scheme.

5.2 Individual Channel design for the longitudinal dynamics

The helicopter longitudinal dynamics $\bar{G}_{11}(s)$ or the upper left submatrix of equation(4.16), which henceforth will simply be call $G_{11}(s)$ can be described as a 2-input 2-output system. The longitudinal dynamical model relates the vertical collective u_1 and longitudinal cyclic u_2 to height rate h and pitch attitude θ as described by

$$\begin{bmatrix} w(s) \\ \theta(s) \end{bmatrix} = G_{11}(s) \begin{bmatrix} u_1 \\ u_2 \end{bmatrix} \tag{5.1}$$

where

$$G_{11}(s) = \frac{1}{\triangle} \begin{bmatrix} 117.8421 & 30.6525 \\ -10.7519 & -10.3509 \\ -0.6712 \pm 2.2565j & -1.2202 \pm 5.3008j \\ -1.1484 \pm 1.0531j & -0.6504 \pm 2.2476j \\ -0.1305 & -0.0283 \pm 0.0049j \\ -0.0316 & -1.5 \\ -1.5 & -1.5 \\ -1.5 & \\ & \\ 14.5287 & 28.3289 \\ -11.5784 & -10.3714 \\ -0.6622 \pm 2.1969j & -0.6586 \pm 2.2367j \\ -0.3305 \pm 0.5087j & -0.0284 \pm 0.0011j \\ -2.8319 & -0.7806 \\ -0.0339 \pm 0.0030j & -1.5 \\ & -1.5 \end{bmatrix} \tag{5.2}$$

with the characteristic polynomial

$$\begin{aligned} \triangle &= [1, -10.5518, -2.9354 \pm 0.8629j, -0.6522 \pm 2.2540j, \\ &\quad -0.1289 \pm 0.8763j, -0.1053 \pm 0.22441j, -0.0305] \end{aligned} \tag{5.3}$$

5.2.1 Cross Coupling Analysis

As described in Chapter 3, the 2-input 2-output subsystem for the longitudinal dynamics is structurally equivalent to the two SISO individual channels

$$C_1(s) = k_1 g_{11}(1 - \gamma h_2) \tag{5.4}$$

$$C_2(s) = k_2 g_{22}(1 - \gamma h_1) \tag{5.5}$$

where k_1 and k_2 are the controllers and

$$\gamma = \frac{g_{12}g_{21}}{g_{11}g_{22}} \tag{5.6}$$

$$h_1 = \frac{k_1 g_{11}}{1 + k_1 g_{11}} \tag{5.7}$$

$$h_2 = \frac{k_2 g_{22}}{1 + k_2 g_{22}} \tag{5.8}$$

and from equations(3.4) and (3.7), the cross coupling transmittances are given by:

$$C_{12}(s) = \frac{g_{12}}{g_{22}} h_2 \left(\frac{1}{1 + C_1}\right) \tag{5.9}$$

$$C_{21}(s) = \frac{g_{21}}{g_{11}} h_1 \left(\frac{1}{1+C_2}\right) \tag{5.10}$$

As it was shown in Section 3.2.1 these coupling signals can be treated as perturbations over the individual channels $C_1(s)$ and $C_2(s)$ with transfer functions $\frac{g_{12}}{g_{22}} h_2$ and $\frac{g_{21}}{g_{11}} h_1$ respectively.

The Bode plots of $\frac{g_{12}}{g_{22}}$ and $\frac{g_{21}}{g_{11}}$ are shown in Figures(5.1) and (5.2) respectively. From Figure(5.1) it is possible to see that $\frac{g_{12}}{g_{22}}$ is a non-proper transfer function with constant increment of gain of 20 dB/dec from 10rad/sec. Also its gain at this frequency is 18db. On the other hand $\frac{g_{21}}{g_{11}}$ in Figure(5.2) has a maximum gain of -25dB's, thus the cross coupling effect from input 1 to output 2 is not important.

At this point it would be convenient to remark that the design specifications indicate that the bandwidths of the closed loop transfer functions of the individual channels $C_1(s)$ and $C_2(s)$, must be between 2 and 4 rad/sec. In the present work, we adopt the bandwidth definition given in Tischler [30] and Anonymous [1], stated as: the frequency at which the overall augmented-vehicle responds to the input of the pilot, exhibits 45 deg of phase margin or 6 dB's of gain margin, whichever is less. These stability margins refer to the augmented-vehicle as an open-loop element in the pilot/vehicle closed-loop system.

According to the customer requirements and from a classical design standpoint, $k_1(s)$ and $k_2(s)$ must be designed in such way that $C_1(s)$ and $C_2(s)$ have crossover frequencies of roughly the same range (2-4 rad/sec). In order to facilitate this analysis and due to the relatively small gain of $\gamma(s)$ in equation(5.6), at 4 rad/sec (whose Nyquist plot is shown in Figure(5.3) and equations(5.4)-(5.8), $k_1(s)$ and $k_2(s)$ may be designed on the basis of $g_{11}(s)$ and $g_{22}(s)$ alone. Therefore,

the analysis can be carried out on the characteristics of $h_2(s)$ and $h_1(s)$, regardless the exact channels $C_1(s)$ and $C_2(s)$.

Due to the non-proper characteristic of $\frac{g_{12}}{g_{22}}$, $k_2(s)$ must induce a roll-off to h_2 with an slope of at least -40 dB/dec. Nevertheless, this will not be enough to cancel the high gain of $\frac{g_{12}}{g_{22}}$ at frequencies around 10 rad/sec, i.e, if $k_2(s)$ is designed to force $h_2(s)$ to behave like second order system, the gain of $\frac{g_{12}}{g_{22}}h_2$ at 10 rad/sec would be around 1db. Thus unacceptable cross coupling response and high frequency noise measurements are obtained with this design. On the other hand due to the bandwidth of 4rad/sec, the sensitivity function of Channel 1 , $\frac{1}{(1+C_1)}$, will have gain of 0dB from 4 rad/sec to ∞ rad/sec. Then, it does not contribute to the cancellation of $\frac{g_{12}}{g_{22}}$ at high frequency.

There can be followed two approaches in order to solve the shortcomings described above: to increase the bandwidth separation between the channels or to design a pre-compensator to reduce the gain of $g_{12}(s)$ around 10 rad/sec. The first option will require a bandwidth of less than 1 rad/sec in channel 2, in order to obtain adequate cross coupling responses, which is unacceptable. Meanwhile, due to the fact that $\gamma(s)$ is far from the point (1,0) around 10 rad/sec, as required for robustness Leithead and O'Reilly [15], the precompensation is the best option.
As indicated in Section 3.5.2 the design of the pre-compensator must fulfil the following points: 1) To affect the system only around 10 rad/sec, that is, $\gamma(s)$ must remain without changes except around 10 rad/sec; and 2) it must reduce the gain of g_{12} around 10 rad/sec.

The pre-compensated system G'_{11} will be given by:

$$G'_{11} = G_{11}P_{11} \tag{5.11}$$

where

$$P_{11} = \begin{bmatrix} 1 & p_{12} \\ 0 & 1 \end{bmatrix} \tag{5.12}$$

$$G'_{11} = \begin{bmatrix} g'_{11} & g'_{12} \\ g'_{21} & g'_{22} \end{bmatrix} \tag{5.13}$$

where

$$g'_{11} = g_{11} \tag{5.14}$$

$$g'_{21} = g_{21} \tag{5.15}$$

$$g'_{12} = g_{11}p_{12} + g_{12} = g_{12}(1 + \frac{g_{11}}{g_{12}}p_{12}) \tag{5.16}$$

$$g'_{22} = g_{21}p_{12} + g_{22} = g_{22}(1 + \frac{g_{21}}{g_{22}}p_{12}) \tag{5.17}$$

the amended system G'_{11} will have a new γ' given by;

$$\gamma' = \frac{g'_{12}g'_{21}}{g'_{11}g'_{22}} \tag{5.18}$$

An appropriate pre-compensator is given by,

$$P_{11} = \begin{bmatrix} 1 & -4.5\frac{s(s^2+2.5s+31.81)}{(s+5)^2(s+6)^2} \\ 0 & 1 \end{bmatrix} \tag{5.19}$$

The Bode plots of $g'_{12}(s)$ and $g'_{22}(s)$ are shown in Figures(5.4) and (5.5) together with the original $g_{12}(s)$ and $g_{22}(s)$. From these plots it is clear that $g_{12}(s)$ was

affected only around 10 rad/sec whereas $g_{22}(s)$ is kept almost without change. The Nyquist plot of $\gamma'(s)$ and $\gamma(s)$ are shown in Figure(5.6). In this plot it is possible to see that $\gamma'(s)$ differ from $\gamma(s)$ only around 10 rad/sec. Therefore the two points concerning the design of the pre-compensator $P_{11}(s)$ are satisfied.

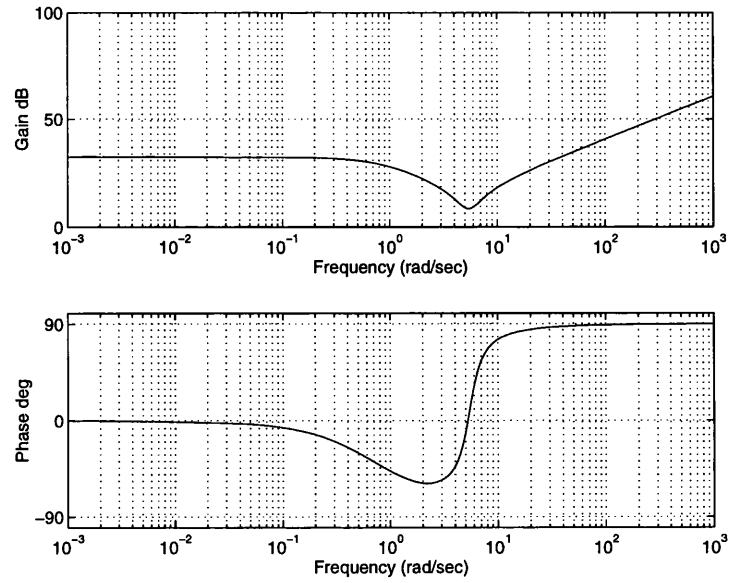

Figure 5.1: Bode plots of $\frac{g_{12}}{g_{22}}$

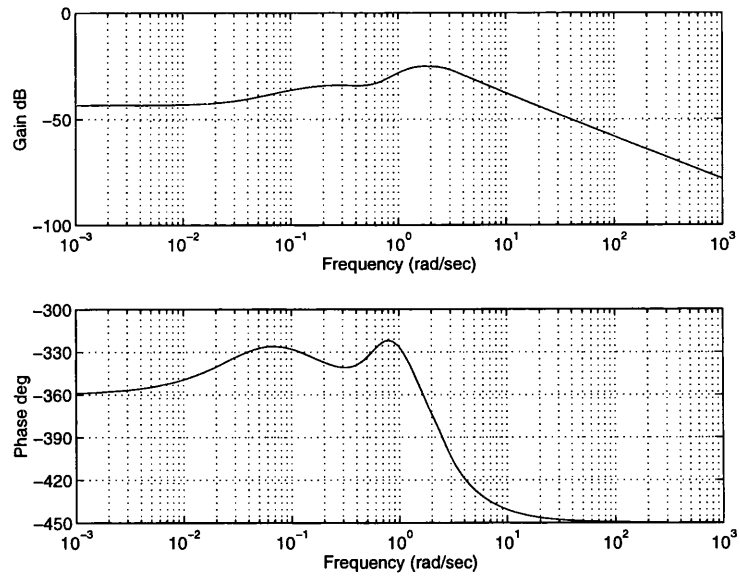

Figure 5.2: Bode plots of $\frac{g_{21}}{g_{11}}$

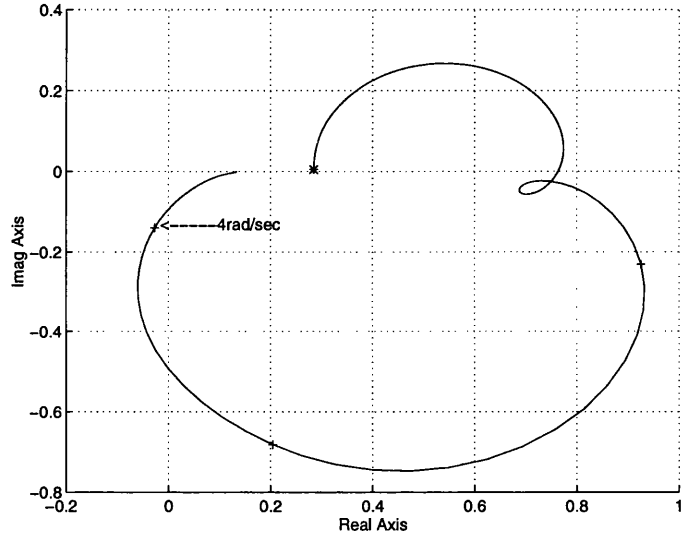

Figure 5.3: Nyquist plot of $\gamma(s)$ of $G_{11}(s)$ (longitudinal dynamics).

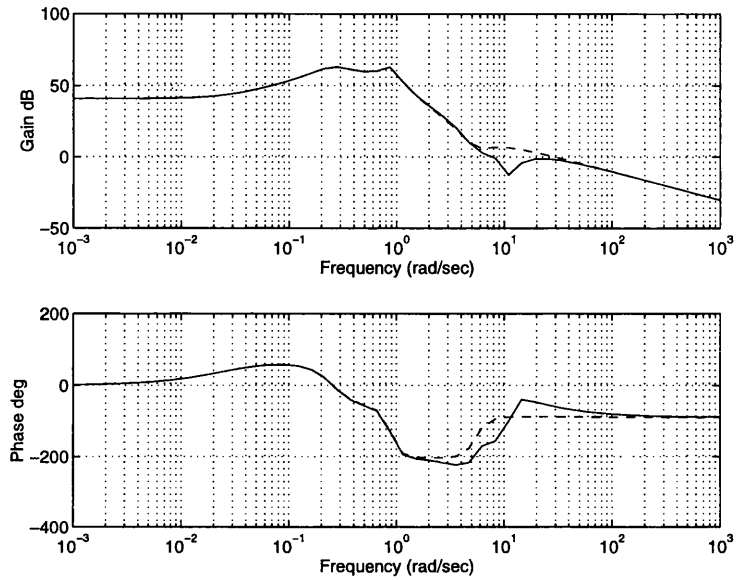

Figure 5.4: Bode plots of $g'_{12}(s)$ and $g_{12}(s)$ respectively

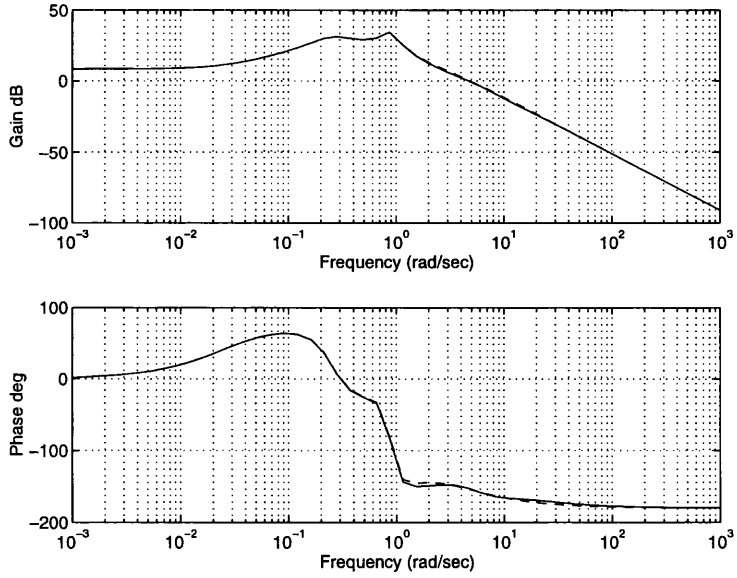

Figure 5.5: Bode plots of $g'_{22}(s)$ and $g_{22}(s)$ respectively

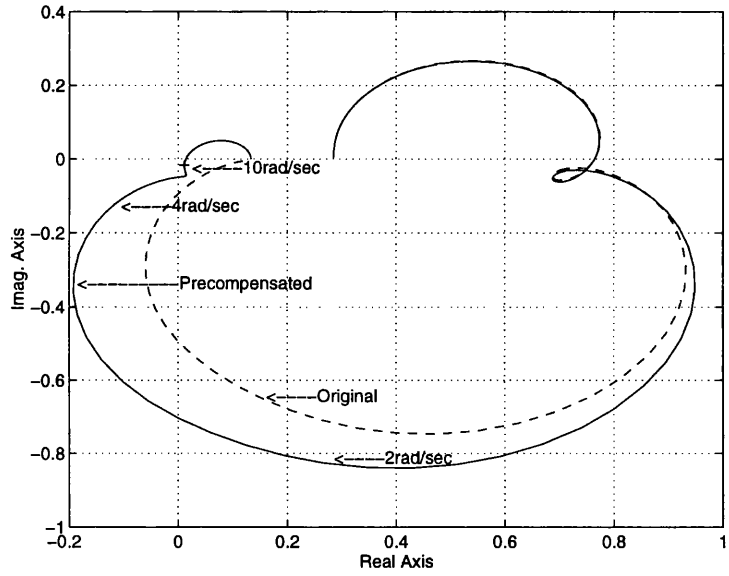

Figure 5.6: Nyquist plot of $\gamma(s)$ and $\gamma'(s)$ of $G_{11}(s)$ and precompensated $G'_{11}(s)$ respectively (longitudinal dynamics).

5.2.2 Feedback controller design

In Chapter 3, it was established that performance of the channels can be assessed by the stability margins of the open-loop channels transmittances. However, in order to guarantee stability robustness two more points have to be accomplished. Therefore, following discussion of Section 3.2.3 and by Results 3.3 and 3.4, in order to guarantee performance and stability robustness the next three points must be satisfied: a) the open-loop transmittances $k_1 g_{11}$ and $k_2 g_{22}$ of subsystems $h_1(s)$ and $h_2(s)$ in equations(5.7) and (5.8) must have adequate gain and phase margins; b) the resulting $\gamma h_1(s)$ and $\gamma h_2(s)$ must not be close to the point (1,0) in the frequency range of interest 0-4 rad/sec; and c) the individual open-loop channels in equations(5.4) and (5.5) must have adequate gain and phase margins within the required channel crossover frequencies of 2-4rad/sec.

The diagonal elements $k_1(s)$ and $k_2(s)$ of $K_1(s)$ designed for the amended longitudinal dynamics system $G'_{11}(s)$ are given by

$$k_1 = 0.47\frac{(s+0.3)(s^2+0.5s+1.62)(s^2+1.6s+7.93)}{s(s+2)(s^2+1.2s+4.36)(s+5)^2} \tag{5.20}$$

$$k_2 = 16\frac{(s+0.127)(s+0.8)(s^2+s+2.35)(s+1)(s^2+1.8s+9.81)}{s(s+0.023)(s^2+s+6.5)(s+2)(s+5)^2(s+10)} \tag{5.21}$$

The designs (5.20) and (5.21) for $k_1(s)$ and $k_2(s)$ result in Bode plots for $k_1 g'_{11}(s)$ and $k_2 g'_{22}(s)$ in Figures(5.7) and (5.8) with crossover frequencies round 2 rad/sec and gain and phase margins respectively of ∞ dB and 79.46 degrees and 15.58 dB and 60.45 degrees. The Bode plots of the actual channel transmittances $C_1(s)$ and $C_2(s)$ in Figures(5.9) and (5.10) confirm that Channel $C_1(s)$ has a gain margin of ∞ dB and a phase margin of 97.14 degrees with crossover frequency

2.9 rad/sec while Channel $C_2(s)$ has a gain margin of 16 dB and a phase margin of 63.96 degrees with crossover frequency 3.09 rad/sec. Lastly, in Figures(5.11) and (5.12) it is shown that the Nyquist plots of the multivariable structure functions $\gamma h_1(s)$ and $\gamma h_2(s)$ are nowhere near the point (1,0). Therefore, the three requirements for performance and robustness are satisfied.

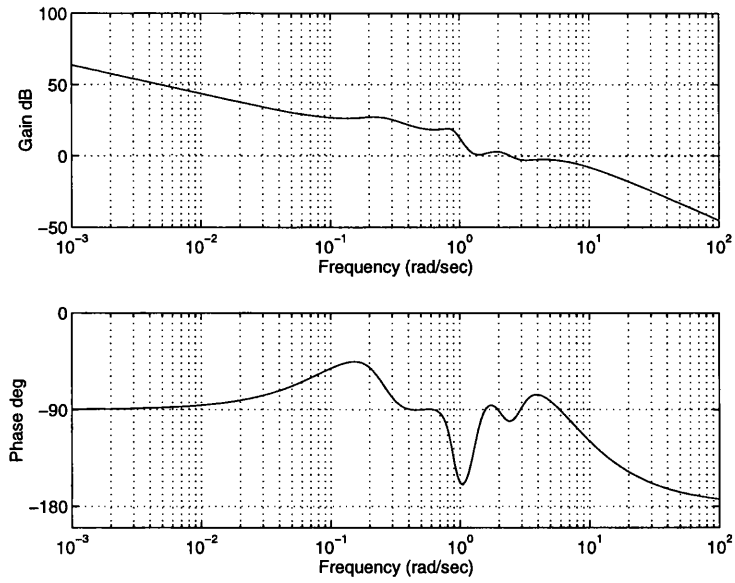

Figure 5.7: Bode plots of $k_1 g'_{11}(s)$ (longitudinal dynamics)

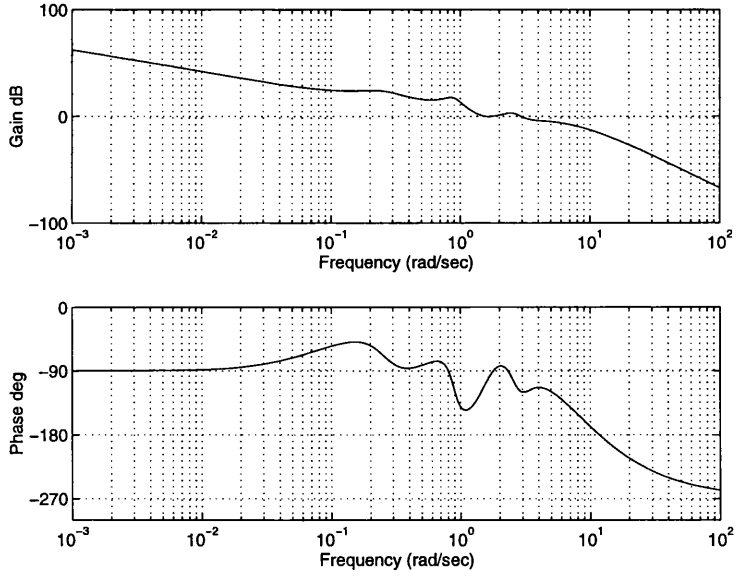

Figure 5.8: Bode plots of $k_2 g'_{22}(s)$ (longitudinal dynamics)

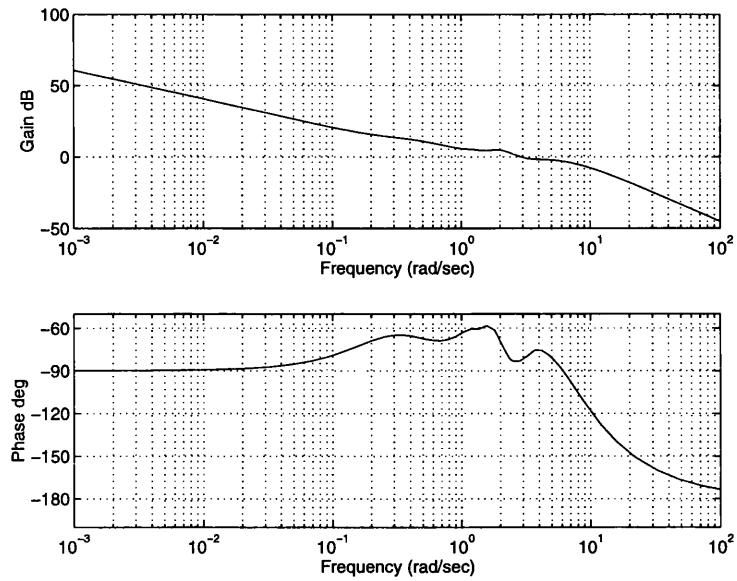

Figure 5.9: Bode plots of $C_1(s)$ (longitudinal dynamics)

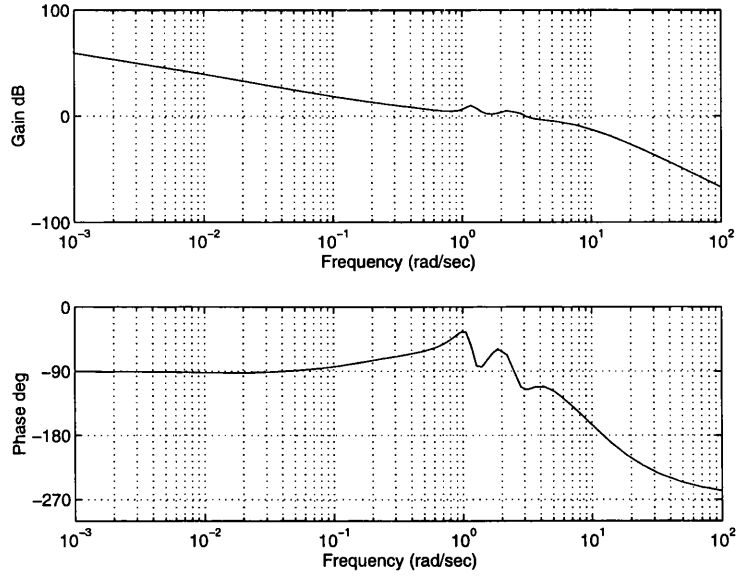

Figure 5.10: Bode plots of $C_2(s)$ (longitudinal dynamics)

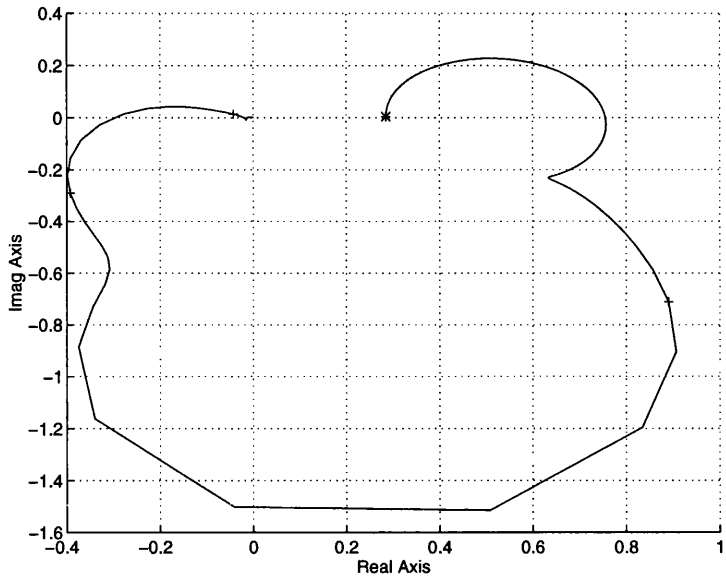

Figure 5.11: Nyquist plot of $\gamma h_1(s)$ (longitudinal dynamics)

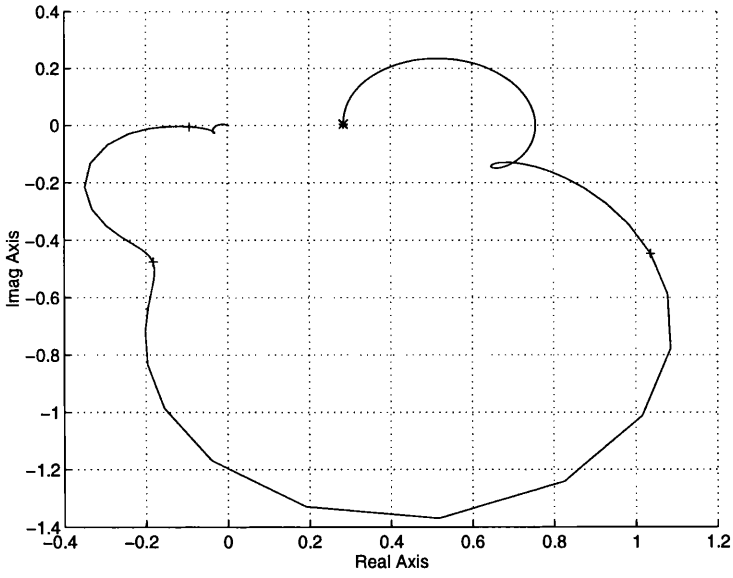

Figure 5.12: Nyquist plot of $\gamma h_2(s)$ (longitudinal dynamics)

5.3 Individual Channel design for the lateral dynamics

Consider the lateral dynamics transfer-function matrix $\bar{G}_{22}(s)$ or the lower right submatrix of equation(4.16) which henceforth will simply be called $G_{22}(s)$. The transfer-function matrix $G_{22}(s)$ represents the small-signal relationship between the lateral cyclic input u_3 and the tail rotor collective input u_4 and the yaw rate output Ψ and side-slip angle output β.

$$\begin{bmatrix} \Psi(s) \\ \beta(s) \end{bmatrix} = G_{22}(s) \begin{bmatrix} u_3 \\ u_4 \end{bmatrix} \tag{5.22}$$

where

$$G_{22}(s) = \frac{1}{\Delta} \begin{bmatrix} -26.6062 & -18.0634 \\ -2.7055 \pm 1.5761j & -10.2517 \\ -0.0959 \pm 0.2249j & -2.9390 \pm 0.8628j \\ -1.9433 & -0.1364 \pm 0.8907j \\ 0.8421 \pm 1.4980j & -0.0398 \pm 0.3823j \\ -0.3188 \pm 1.0617j & -0.1118 \pm 0.2346j \\ \\ -0.2263 & 0.1627 \\ 100.4791 & -111.1415 \\ 2.5056 & -10.1939 \\ -2.6307 \pm 1.4296j & -2.9392 \pm 0.8625j \\ -0.0193 \pm 0.2398j & -0.1331 \pm 0.8820j \\ -0.5703 \pm 0.8566j & -0.1034 \pm 0.2310j \\ -0.7643 & 0.0048 \end{bmatrix} \tag{5.23}$$

with the characteristic polynomial

$$\begin{aligned}\triangle &= [1, -10.5518, -2.9354 \pm 0.8629j, -0.6522 \pm 2.2540j, \\ &\quad -0.1289 \pm 0.8763j, -0.1053 \pm 0.22441j, -0.0305] \end{aligned} \tag{5.24}$$

This 2-input 2-output subsystem $G_{22}(s)$, like that of its longitudinal counterpart $G_{11}(s)$, can be shown to be equivalent to two SISO individual channels of the form of equations(5.4) and (5.5).

5.3.1 Performance limitation

As in the SISO case, the closed-loop performance of the individual channels in equations(5.4) and (5.5) are adversely affected by the presence of channel RHPZ's. From Table(3.1) it is clear that the zeros of the channels depend on $\gamma(s)$ and $h_j(s)$ $j = 1, 2$. In general, it is possible to determine the zeros of the channels by applying the stability criterion of Nyquist to the multivariable structures functions $\gamma h_1(s)$ and $\gamma h_2(s)$ as shown in Result 3.1. From the last statement, it is clear that the channel zeros depend also on the controllers $k_1(s)$ and $k_2(s)$; but, as indicated in Section 3.2.2, when high performance controllers are required, the gain of the controllers $k_i(s)$ are high over a large frequency range, including much of the significant dynamics of the channels, such that $\mid h_i \mid \approx 1$. Thus, any potential restrictions on the performance due to non-minimum phase zeros can be obtained from the characteristics of $(1 - \gamma)$.

The Nyquist plot of the multivariable structure function $\gamma(s)$ of $G_{22}(s)$ is shown in Figure(5.13). From this plot it is possible to see that $\gamma(s)$ encircles the point (1,0) 3 times in an anti-clockwise direction. On the other hand, and by equations(5.6) and (5.23) the number of RHPP's of γ is 3. Hence, following the Nyquist criterion of Result 3.1, the number of RHPZ's of $(1 - \gamma)$ is zero. Apparently there are not potential restrictions due to non-minimum phase behaviour.

Nevertheless, the two unstable complex poles $(0.8421 \pm 1.4980j)$ of $\gamma(s)$ due to the individual transfer function $g_{22}(s)$ of $G_{22}(s)$, are very close to the channel crossover frequency (2 to 4 rad/sec). These RHPP's together with the fact that if $k_2(s)$ is designed such that $h_2(s)$ in equation(5.8) roll-off between 2 and 4 rad/sec, would force $\gamma h_2(s)$ to avoid two of the three required anti-clockwise encirclements to the point (1,0). Therefore, channel $C_1(s)$ of $G_{22}(s)$ will be non-minimum phase with 2 RHPZ's at approximately 1.5 rad/sec, with the consequent limitation in bandwidth and performance.

In order to overcome this performance limitation, a pre-compensator $P_{22}(s)$ can be designed to stabilise the RHPZ's of $g_{22}(s)$ at $(0.8421 \pm 1.4980j)$. This pre-compensator must be designed keeping in mind the robustness properties of the control system. Therefore, the design of the pre-compensator must fulfil the following points: $\gamma(s)$ must remain without changes except around 1.5 rad/sec or at frequencies where $\gamma(s)$ is far from the point (1,0); and second, it must stabilise the 2 RHPZ's of $g_{22}(s)$.

The pre-compensated system $G'_{22}(s)$ will be given by:

$$G'_{22} = G_{22}P_{22} \tag{5.25}$$

where

$$P_{22} = \begin{bmatrix} 1 & 0 \\ p_{21} & 1 \end{bmatrix} \tag{5.26}$$

$$G'_{22} = \begin{bmatrix} g'_{11} & g'_{12} \\ g'_{21} & g'_{22} \end{bmatrix} \tag{5.27}$$

where

$$g'_{11} = g_{12}p_{21} + g_{11} = g_{11}(1 + \frac{g_{12}}{g_{11}}p_{21}) \tag{5.28}$$

$$g'_{21} = g_{22}p_{21} + g_{21} = g_{21}(1 + \frac{g_{22}}{g_{21}}p_{21}) \tag{5.29}$$

$$g'_{12} = g_{12} \tag{5.30}$$

$$g'_{22} = g_{22} \tag{5.31}$$

the amended system G'_{22} will have a new γ' given by;

$$\gamma' = \frac{g'_{12}g'_{21}}{g'_{11}g'_{22}} \tag{5.32}$$

A suitable pre-compensator is given by,

$$P_{22} = \begin{bmatrix} 1 & 0 \\ 6.5\frac{s(s+1.94)(s^2+0.63s+1.11)}{(s^2+0.27s+0.81)(s^2+0.078s+0.146)(s+10)} & 1 \end{bmatrix} \tag{5.33}$$

for which it is observed in Figure(5.14) that $\gamma'(s)$ of $G'_{22}(s)$ is little changed from $\gamma(s)$ of $G_{22}(s)$ except round 1.5 rad/sec. The number of anti-clockwise encirclements of the (1,0) point is reduced from 3 to 1 since the number of RHPP's of $\gamma(s)$ is reduced from 3 to 1. From Figure(5.15) it is possible to see that $g_{11}(s)$ was mainly affected at 1 rad/sec, whereas from Figure(5.16) $g_{21}(s)$ was strongly affected around 0.4 rad/sec. Nevertheless, this does not represent any problem due to $\gamma(s)$ is almost zero at 0.4 rad/sec as shown in Figure(5.13).

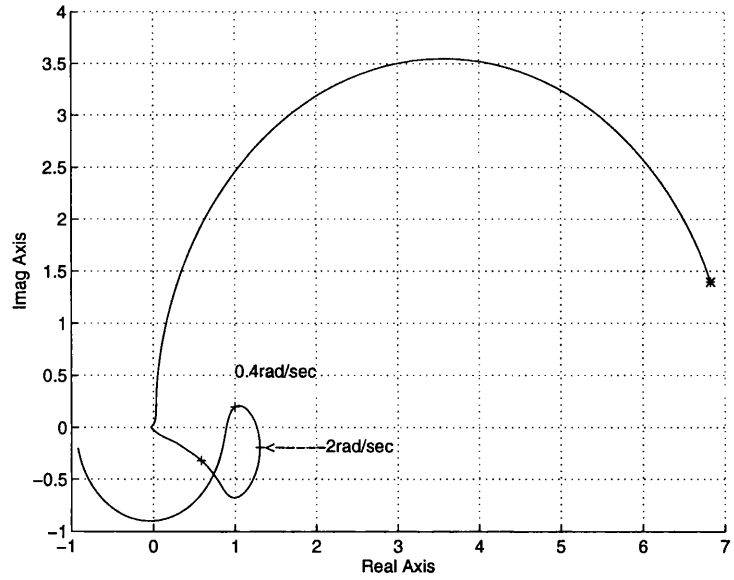

Figure 5.13: Nyquist plot of $\gamma(s)$ for $G_{22}(s)$ (lateral Dynamics)

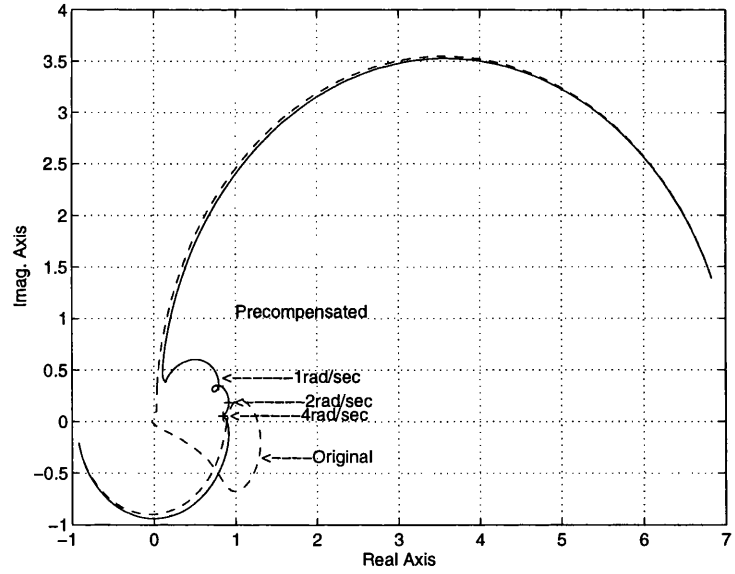

Figure 5.14: Nyquist plot of $\gamma(s)$ and $\gamma'(s)$ of $G_{22}(s)$ and precompensated $G'_{22}(s)$ respectively (lateral dynamics).

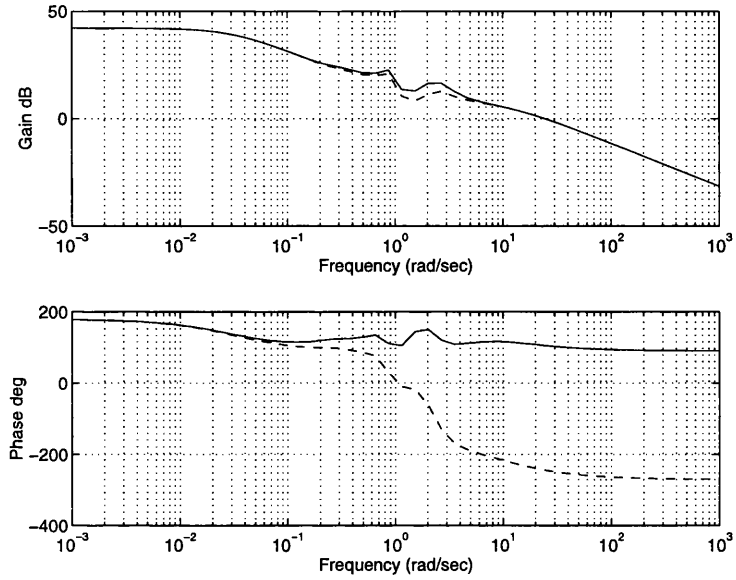

Figure 5.15: Bode plots of $g'_{11}(s)$ and $g_{11}(s)$ respectively

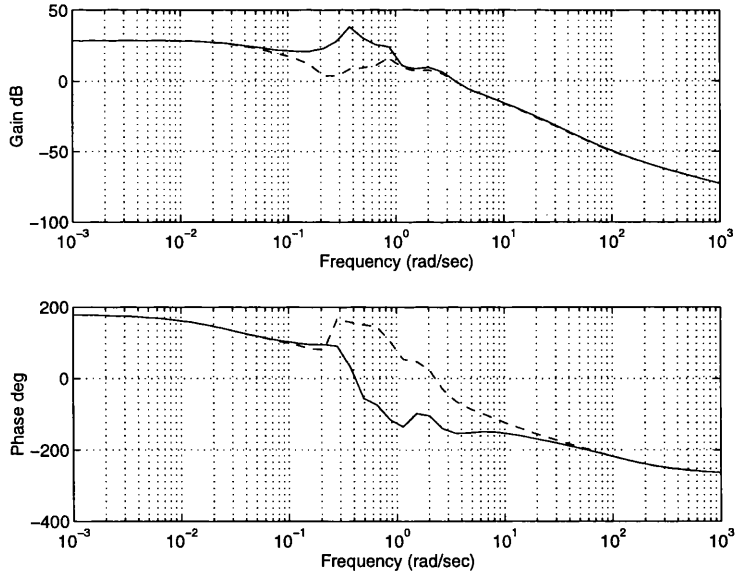

Figure 5.16: Bode plots of $g'_{21}(s)$ and $g_{21}(s)$ respectively

5.3.2 Feedforward controller

For the pre-compensated lateral dynamics $G'_{22}(s)$ which henceforth will be called $G_{22}(s)$ it is observed in Figure(5.14) that $\gamma(s)$ encircles the point (1,0) once in an anti-clockwise direction. On the other hand, $\gamma(s)$ has only one RHPP at 0.0048 (due to $g_{22}(s)$). Thus $(1-\gamma)$ is minimum phase. In order to maintain this characteristic in the actual open-loop channels, it is necessary that $h_1(s)$ and $h_2(s)$ do not change the number of encirclements to the point (1,0) of $\gamma h_1(s)$ and $\gamma h_2(s)$. Also, in order to assure robustness in the control system, neither $\gamma h_1(s)$ nor $\gamma h_2(s)$ must be close the the point (1,0). However, if controllers $k_1(s)$ and $k_2(s)$ are designed such that channels 1 and 2 roll-off between 2 to 4 rad/sec, then $\gamma h_1(s)$ and $\gamma h_2(s)$ will be close to the point (1,0) or they will encircle the point (1,0) once more in clockwise direction than in an anti-clockwise direction.

The former can be explained by the fact that if $k_1(s)$ $(k_2(s))$ is designed such that $h_1(s)$ $(h_2(s))$ rolls-off for instance at 4 rad/sec with a slope of -40 db's/dec. Then, $h_1(s)$ $(h_2(s))$ would introduce a shift of at least -30 degrees at 1 rad/sec in $\gamma h_1(s)$ $(\gamma h_2(s))$ without any significant reduction of gain. Therefore, $\gamma h_1(s)$ $(\gamma h_2(s))$ would be near to the point (1,0) and the control system will present excessive phase and structural sensitivity. On the other hand, if $k_1(s)$ $(k_2(s))$ is designed such that $h_1(s)$ $(h_2(s))$ rolls-off at 2 rad/sec, then $h_1(s)$ $(h_2(s))$ would introduce a shift of -55 degrees in $\gamma h_1(s)$ $(\gamma h_2(s))$ at 1 rad/sec. Therefore, $\gamma h_1(s)$ $(\gamma h_2(s))$ would have two additional encirclements to the point (1,0) in clockwise direction, resulting in the introduction of 2 RHPZ's in channel 1 (channel 2) at frequencies less than the channel crossover frequency. The origin of these problems as was found in Chapter 4, is due to the closeness of $\gamma(s)$ to the point (1,0) at frequencies close to the channel crossover frequency which means that the system suffer from excessive phase sensitivity.

The procedure adopted to solve this problem is by way of a feedforward matrix control, Leithead and O'Reilly [17]. This new application of feedforward can be used not only to shift $\gamma(s)$ far from the point (1,0) without increasing the uncertainty effects, but also to decouple the system at the channel crossover frequency.

The amended plant $G'_{22}(s)$ will be given by:

$$G'_{22} = G_{22} + F_{22} \tag{5.34}$$

where

$$F_{22} = \begin{bmatrix} 0 & f_{12} \\ f_{21} & 0 \end{bmatrix} \tag{5.35}$$

It is clear from equations(5.34) and (5.35) that together with the non-diagonal elements of $G_{22}(s)$ the output of $G_{22}(s)$ will be also changed; that is, the original output y of $G_{22}(s)$ given by

$$y = G_{22}u \tag{5.36}$$

will be changed to the output z of the amended system $G'_{22}(s)$ given by

$$z = (G_{22} + F_{22})u \tag{5.37}$$

Then, it is important to design $F_{22}(s)$ such that z does not differ significantly from y. From equations(5.34) and (5.35) the individual transfer functions of the amended system $G'_{22}(s)$ will be given by

$$g'_{11} = g_{11} \tag{5.38}$$

$$g'_{22} = g_{22} \tag{5.39}$$

$$g'_{12} = g_{12} + f_{12} = g_{12}(1 + \frac{f_{12}}{g_{12}}) \tag{5.40}$$

$$g'_{21} = g_{21} + f_{21} = g_{21}(1 + \frac{f_{21}}{g_{21}}) \tag{5.41}$$

Where $(1 + \frac{f_{21}}{g_{21}})$ and $(1 + \frac{f_{12}}{g_{12}})$ represent the total effect of $F_{22}(s)$ over $g_{12}(s)$ and $g_{21}(s)$ respectively. What we seek to do now is to amend the lateral subsystem $G_{22}(s)$ through the use of feedforward $F_{22}(s)$ in such a way that $G_{22}(s)$ is decoupled round 2 rad/sec and the robustness problem of $\gamma(s)$ being close to the (1,0) point no longer exists. A suitable feedforward matrix $F_{22}(s)$ is given by

$$F_{22} = \begin{bmatrix} 0 & f_{12} \\ f_{21} & 0 \end{bmatrix} \tag{5.42}$$

where the filters

$$f_{12} = 28\frac{s(s^2 + 0.079s + 0.15)}{(s + 0.0305)(s^2 + 1.8s + 9.81)(s^2 + 1.3s + 5.5)} \tag{5.43}$$

$$f_{21} = -30\frac{s^2(s + 0.7)(s + 0.9)(s^2 + 0.5s + 1.27)}{(s^2 + 0.1s + 0.16)(s^2 + 0.26s + 0.77)(s^2 + 0.8s + 5)(s + 6)} \tag{5.44}$$

are designed to affect $g_{12}(s)$ and $g_{21}(s)$ of $G_{22}(s)$ round 3 and 2 rad/sec respectively as depicted in Figures(5.17) and (5.18). The amended plant $G'_{22}(s)$ only differs from $G_{22}(s)$ round 3 rad/sec. This is corroborated by Figure(5.19) where, as required, the amended lateral subsystem $G'_{22}(s)$ is decoupled at 3 rad/sec and $\gamma'(s)$ is far from the (1,0) point at all frequencies.

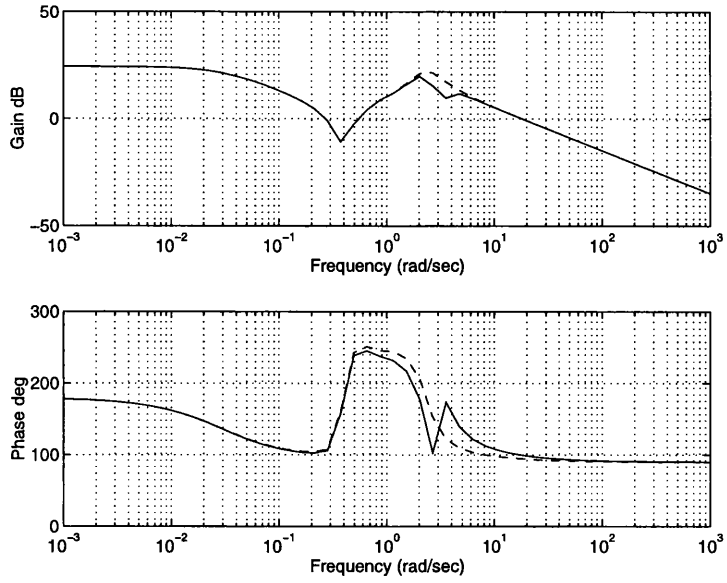

Figure 5.17: Bode plots of $g'_{11}(s)$ amended by feedforward and $g_{11}(s)$ respectively

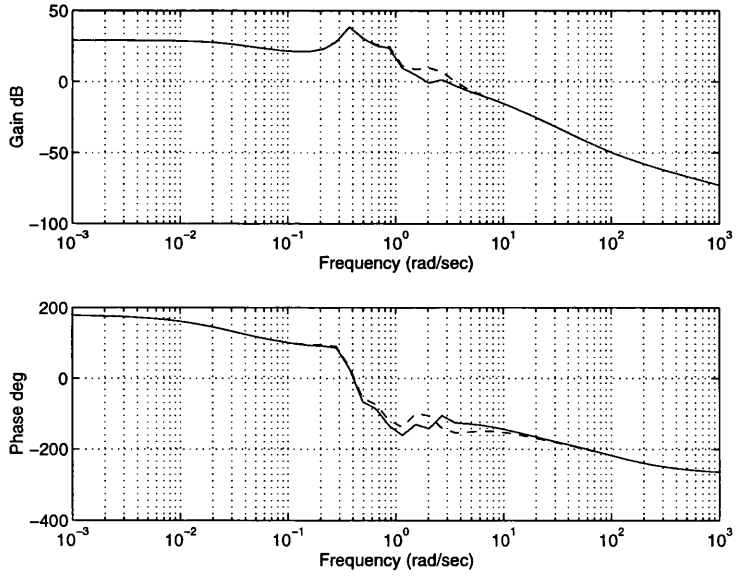

Figure 5.18: Bode plots of $g'_{21}(s)$ amended by feedforward and $g_{21}(s)$ respectively

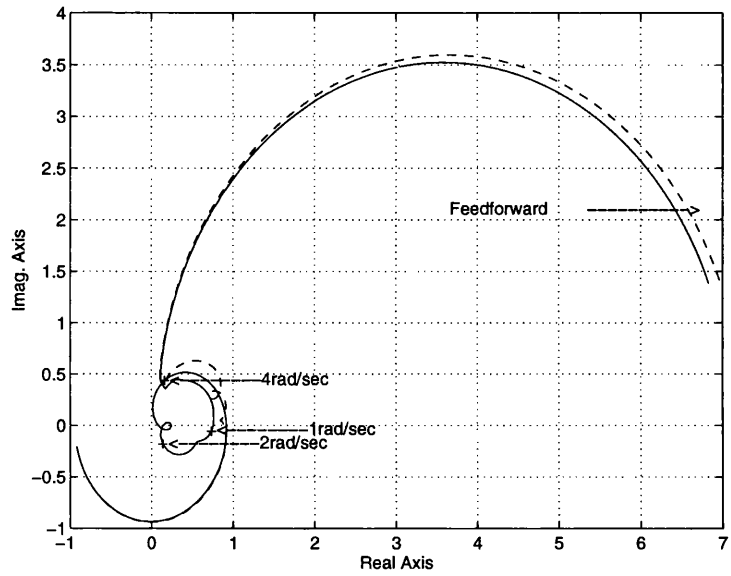

Figure 5.19: Nyquist plot of $\gamma(s)$ and $\gamma'(s)$ of $G_{22}(s)$ and $G'_{22}(s)$ amended by feedforward respectively (lateral dynamics).

5.3.3 Feedback controller design

In the design of the feedback controller for the amended lateral dynamics $G'_{22}(s)$ in equation(5.34), the modifications introduced by the feedforward control have to be considered in the control design process. In Figure(3.11) the block diagram of the system with *explicit* feedforward control and ICD feedback control is shown. Whereas in Figure(3.12), the block diagram of the equivalent system with equivalent controller $K_e(s)$ is presented. Despite the fact that both systems are equivalent, the first one has z as regulated output, but the performance specifications are defined according to the real output y. Therefore, in order to assess the performance of the system on the real output z, the structure of Figure(3.12) will be used, just as a way of performance assessment whereas the robustness will be assessed with the configuration of Figure(3.11). Controller $K_2(s)$ will be designed on the basis of the amended system $G'_{22}(s)$ of equation(5.34). Once this controller has satisfied the robustness requirements, it is used to calculate the equivalent controller $K_e(s)$, in order to assess the performance of the system in the original output y.

The diagonal elements $k_1(s)$ and $k_2(s)$ of $K_2(s)$ designed for the amended system $G'_{22}(s)$ are given by

$$\begin{aligned} k_1 &= -1.2\frac{(s+0.0047)(s^2+s+1.06)(s+1)(s+2)^2}{s(s+0.2)(s^2+0.2s+0.5)(s^2+0.8s+3.05)(s+10)} \\ &\quad \frac{(s^2+2s+9.7)}{(s^2+2s+17)} \end{aligned} \tag{5.45}$$

$$k_2 = 12\frac{(s+0.3)(s+0.5)(s^2+0.6s+2.49)(s^2+1.2s+8.77)}{s(s^2+0.4s+0.6)(s^2+8s+32)(s+2)(s+3)} \tag{5.46}$$

The designs (5.45) and (5.46) for $k_1(s)$ and $k_2(s)$ result in Bode plots for $k_1 g'_{11}$ and $k_2 g'_{22}$ in Figures(5.20) and (5.21) with crossover frequencies round 2 rad/sec and gain and phase margins respectively of ∞ dB and 73.1 degrees and 15.62 dB

and 60.01 degrees. The Bode plots of the actual channel transmittances $C_1(s)$ and $C_2(s)$ for the lateral dynamics in Figures(5.22) and (5.23) confirm that channel $C_1(s)$ has two gain margins of 59 dB and ∞ dB and a phase margin of 65.3 degrees with crossover frequency 3.98 rad/sec while Channel $C_2(s)$ has a gain margin of 15.2 dB and a phase margin of 49 degrees with crossover frequency of 3.6rad/sec. In Figures(5.24) and (5.25) the Nyquist plots of the multivariable structure functions $\gamma' h_1(s)$ and $\gamma' h_2(s)$ show that none of them are close to the point (1,0). Therefore, all the points required for robustness are satisfied.

It just remains to assess the design on the basis of the original output y. In Figures(5.26) and (5.26) the Bode plots of the channels $Ce_1(s)$ and $Ce_2(s)$ for the equivalent system (Figure(3.12)) show that channel $Ce_1(s)$ has two gain margins of 59 dB and ∞ dB and a phase margin of 72.03 degrees with crossover frequency 2.17 rad/sec while Channel $Ce_2(s)$ has a gain margin of 17.3 dB and a phase margin of 62 degrees with crossover frequency of 2.1rad/sec

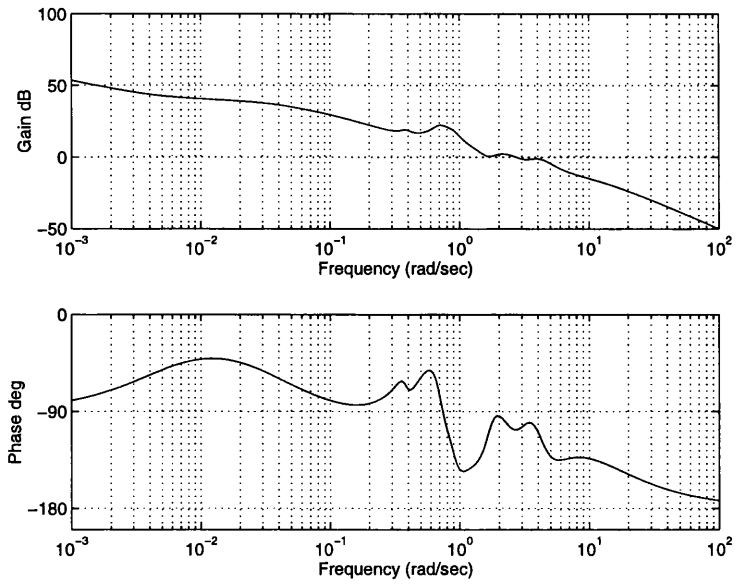

Figure 5.20: Bode plots of $k_1 g'_{11}(s)$ (lateral dynamics)

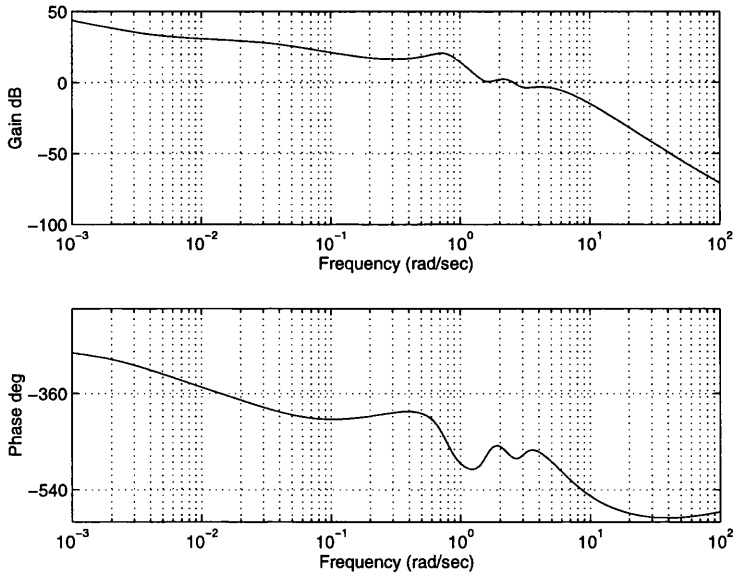

Figure 5.21: Bode plots of $k_2 g'_{22}(s)$ (lateral dynamics)

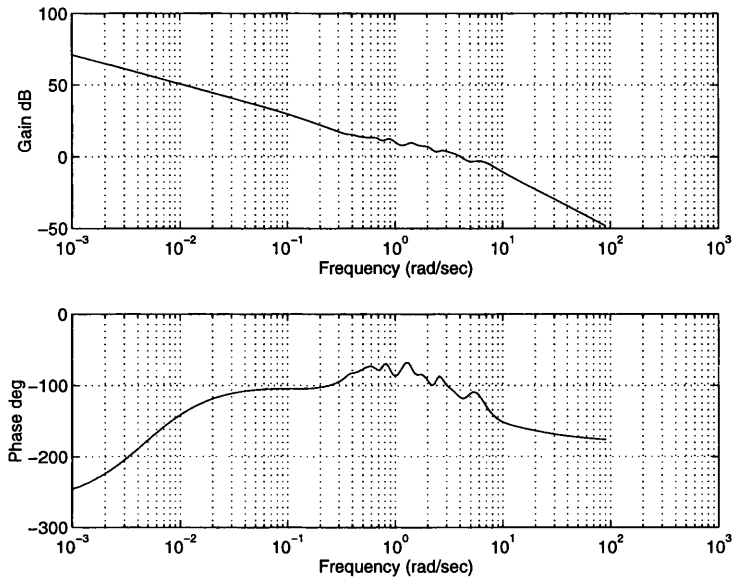

Figure 5.22: Bode plots of $C_1(s)$ (lateral dynamics)

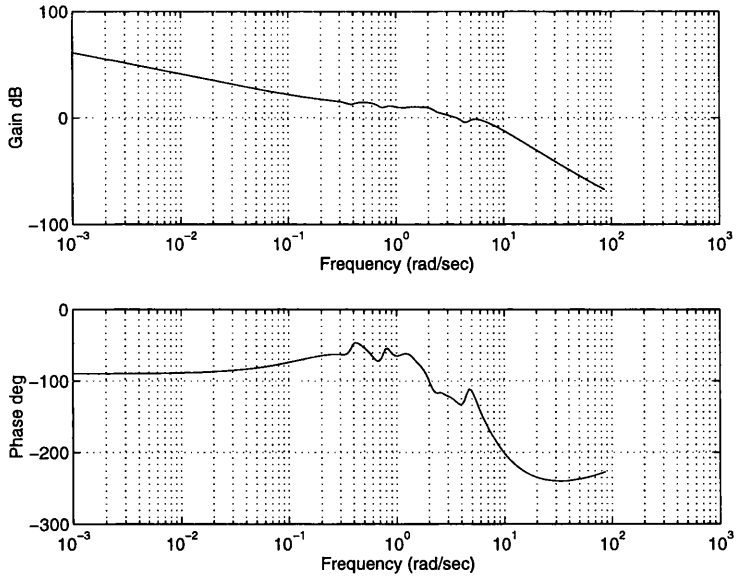

Figure 5.23: Bode plots of $C_2(s)$ (lateral dynamics)

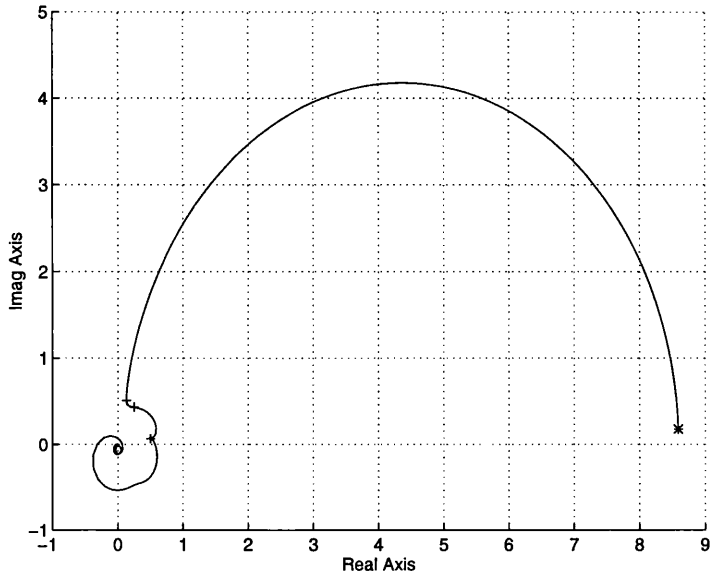

Figure 5.24: Nyquist plot of $\gamma' h_1(s)$ (lateral dynamics)

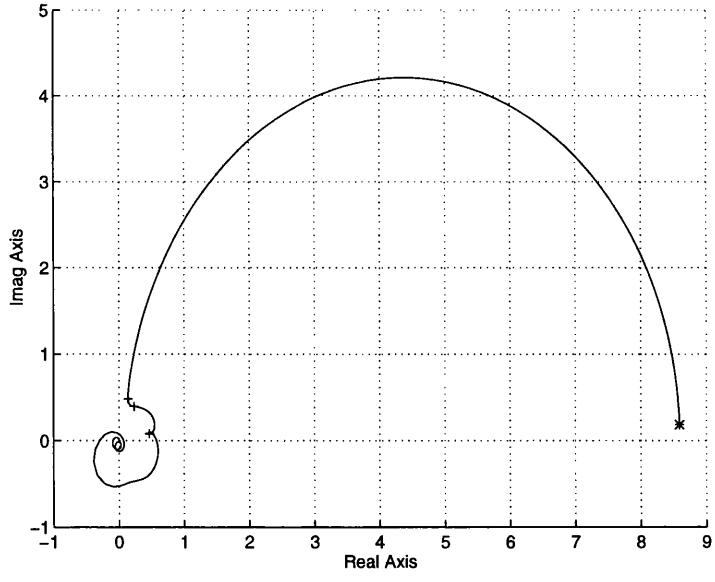

Figure 5.25: Nyquist plot of $\gamma' h_2(s)$ (lateral dynamics)

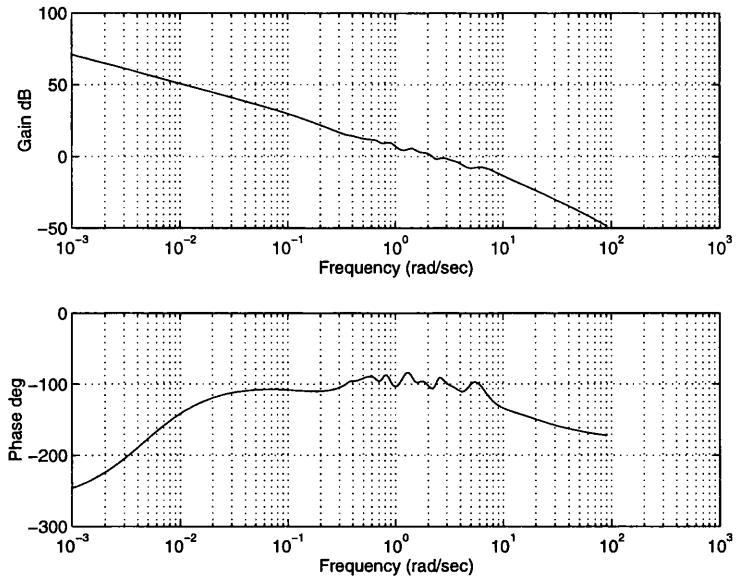

Figure 5.26: Bode plots of Channel $Ce_1(s)$ (lateral dynamics)

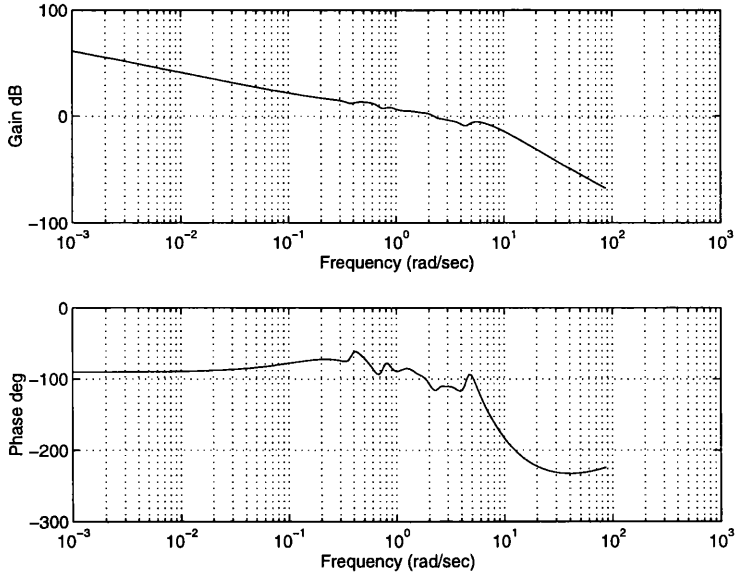

Figure 5.27: Bode plots of Channel $Ce_2(s)$ (lateral dynamics)

5.4 Cross-coupling reduction

Despite the fulfilment of the design requirements of the overall closed-loop system, there remains some cross-coupling, especially between output y_1 (height rate) and input references r_2, r_3 and r_4 for which it is now appropriate to design a pre-filter so as to decouple the overall closed-loop system, Leithead and O'Reilly [16]. A suitable pre-filter $P_r(s)$ is given by,

$$P_r = \begin{bmatrix} 1 & pr_{12} & pr_{13} & pr_{14} \\ 0 & 1 & pr_{23} & 0 \\ 0 & pr_{32} & 1 & pr_{34} \\ 0 & pr_{42} & pr_{43} & 1 \end{bmatrix} \tag{5.47}$$

where

$$pr_{12} = -350\frac{s(s+0.6)(s+0.43)(s^2+1.86s+122)(s^2+2.4s+31.58)}{(s+0.2)(s+0.35)(s^2+s+1.81)(s+10)^2(s+20)^2} \times\frac{(s^2+s+3.86)}{(s^2+2s+6.76)} \tag{5.48}$$

$$pr_{13} = -2\frac{s(s+0.09)(s+0.7)(s+2)}{(s+0.6)(s^2+0.4s+1.48)(s^2+0.16s+0.49)(s+10)} \times\frac{(s^2+4s+40)}{(s^2+2s+17)} \tag{5.49}$$

$$pr_{14} = -190\frac{s(s^2+0.18s+0.23)(s+1)}{(s^2+0.26s+1.58)(s^2+0.14s+0.5)(s+6)(s+8)} \times\frac{(s^2+0.3s+10.26)}{(s^2+2s+17)} \tag{5.50}$$

$$pr_{23} = -0.8\frac{s(s+0.05)(s+1)}{(s^2+0.16s+0.54)(s^2+1.2s+1.57)(s+3)} \tag{5.51}$$

$$pr_{32} = 350\frac{s(s+8)}{(s^2+5s+222.34)(s+110)} \tag{5.52}$$

$$pr_{34} = 400\frac{s(s^2+0.1s+0.16)(s+1)^2(s+2))}{(s+0.01)(s+0.5)(s+0.8)(s^2+s+5.86)(s+7)(s+40)} \times\frac{(s^2+0.3s+9.63)}{(s^2+3s+27.25)} \tag{5.53}$$

$$pr_{42} = -1700\frac{s(s+0.8)}{(s+2)(s^2+0.6s+6.34)(s+3)^2(s+10)(s+20)} \tag{5.54}$$

$$pr_{43} = -0.1\frac{s(s+0.02)}{(s+0.3)(s^2+0.06s+0.15)(s+0.4)(s+0.5)(s+1)(s+2)} \tag{5.55}$$

5.5 Assessment of the multivariable controller design on full helicopter system

The structure of the resulting control system for the full 4-input 4-output helicopter (longitudinal and lateral dynamics) at 80 knots forward flight is summarised in the block diagram of Figure(5.28). The overall control system comprises a number of blocks: a weak feedback M(s) (designed in Chapter 4) sufficient only to stabilise the system thereby avoiding any RHP pole-zero cancellation; a pre-compensator P(s) designed to reduce high-frequency cross-coupling affecting the longitudinal dynamics and to eliminate non-minimum phase behaviour affecting the lateral dynamics; a feedforward controller F(s) designed to overcome a severe lack of robustness as well as decouple the lateral dynamics into two SISO subsystems round crossover frequency (3 rad/sec); a diagonal (4x4) feedback controller matrix K(s), the elements of which are designed on the basis of the decoupled lateral and longitudinal dynamics; a (4x4) pre-filter matrix $P_r(s)$ designed to further

reduce the effects of cross-coupling. All of these blocks are sparse; M(s) has only one entry, P(s) consists of 1's and 0's and two non-unity off diagonal entries, F(s) has only two entries and K(s) has four diagonal entries.

In Figures(5.29)-(5.31), the Bode plots of the closed-loop channels for the $4x4$ control system are shown. In accordance with the bandwidth definition of Tischler [30], namely the frequency at which the overall augmented vehicle exhibits 45 degrees phase margin or 6 dB gain margin whichever is less, the frequency bandwidths of channels 1, 2, 3 and 4 are respectively 4 rad/sec, 4.09 rad/sec, 4.1 rad/sec and 3.9 rad/sec and are all within Level 1 handling quality specifications. Furthermore, the step responses of the overall 4-input 4-output closed-loop system, shown in Figures(5.33)-(5.40), indicate adequate transient behaviour with acceptably low cross-coupling, Liceaga *et al* [19].

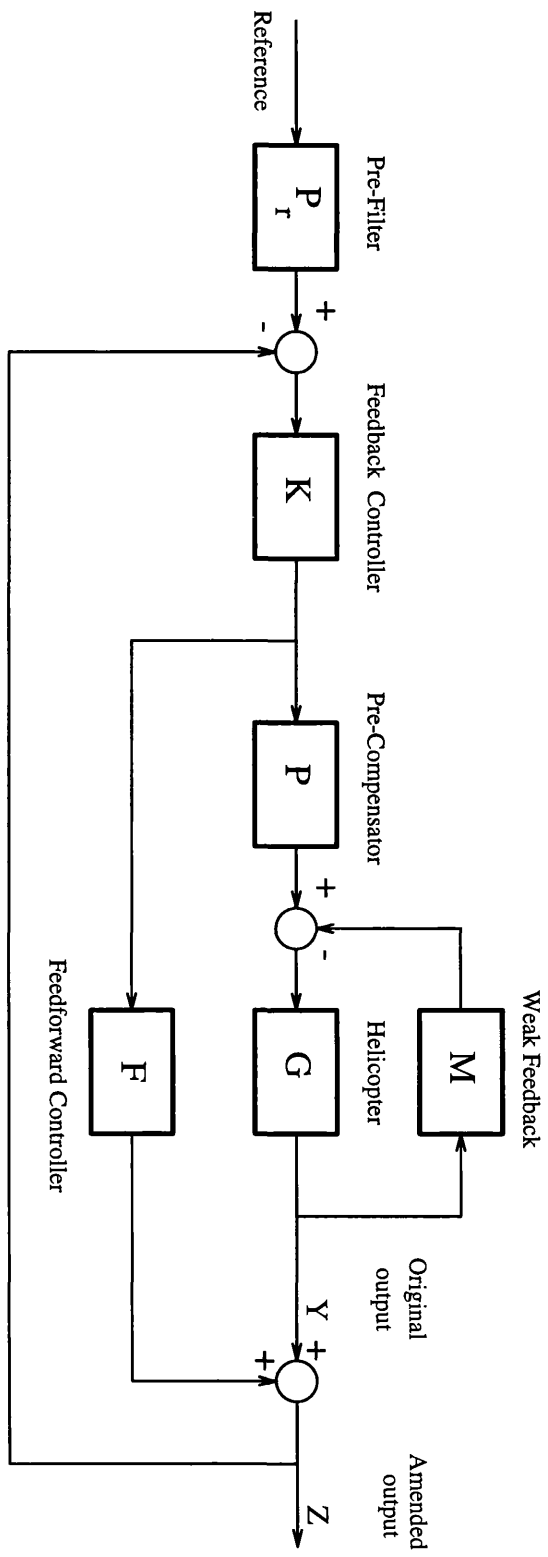

Figure 5.28: ICD Flight control system of the helicopter at 80 knots forward flight.

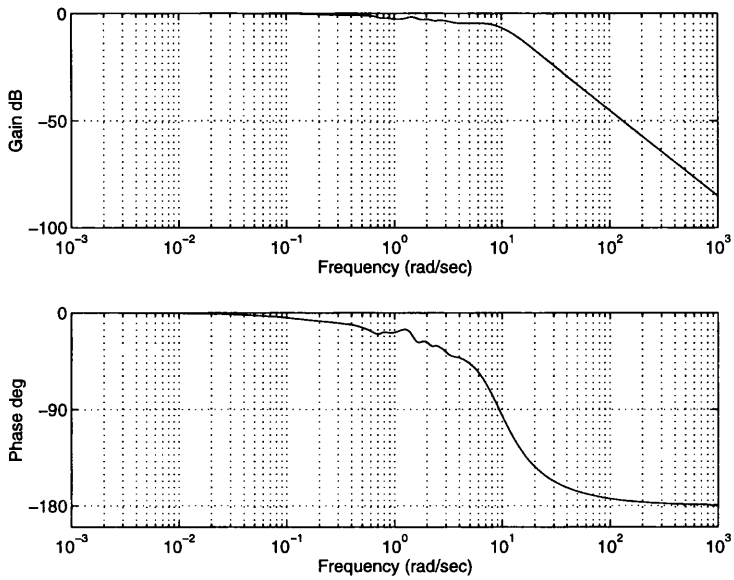

Figure 5.29: Bode plots of closed-loop Channel $C_1(s)$

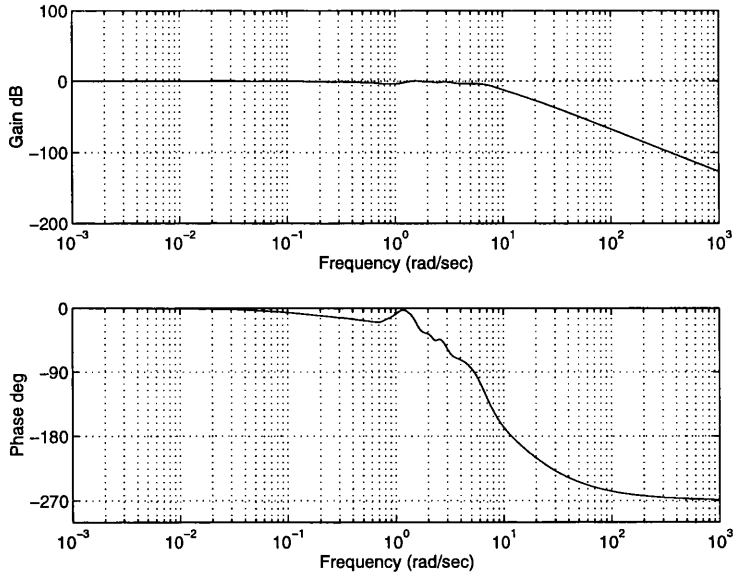

Figure 5.30: Bode plots of closed-loop Channel $C_2(s)$

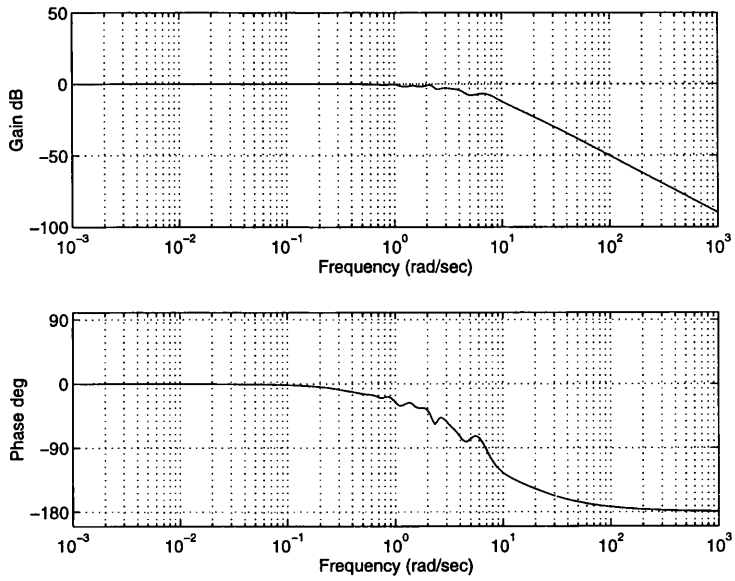

Figure 5.31: Bode plots of closed-loop Channel $C_3(s)$

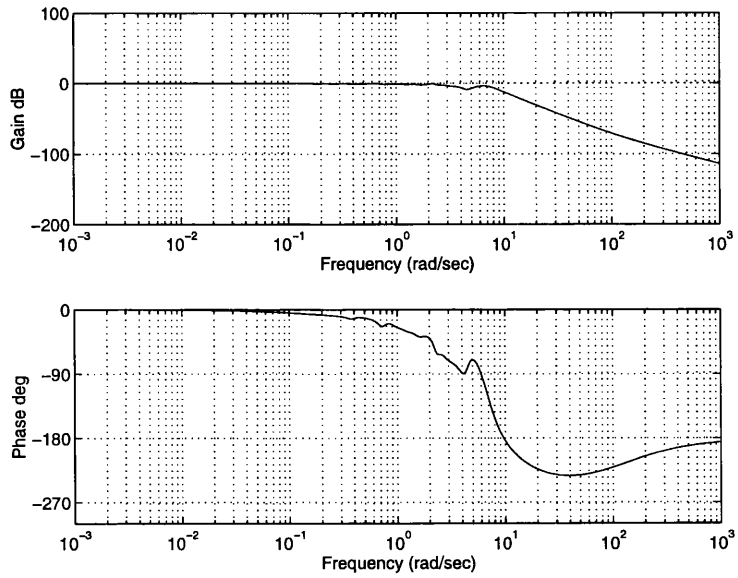

Figure 5.32: Bode plots of closed-loop Channel $C_4(s)$

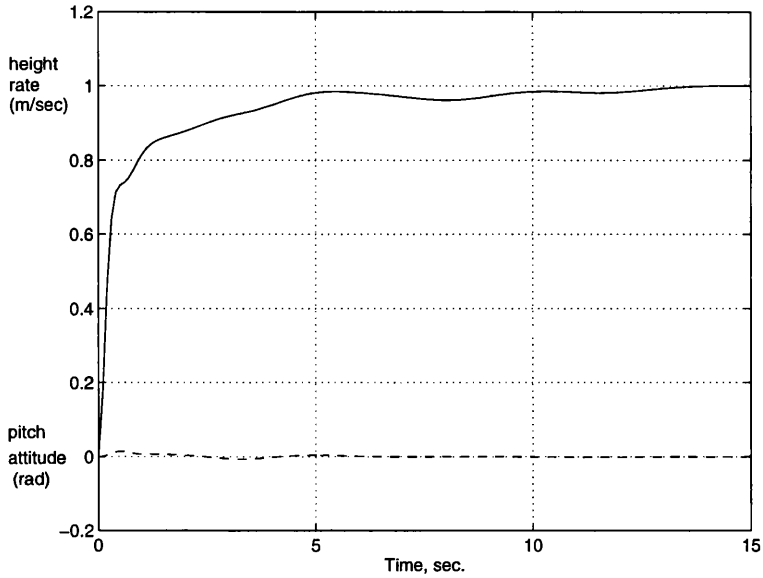

Figure 5.33: Time responses of height rate and pitch attitude to unity step change in input 1

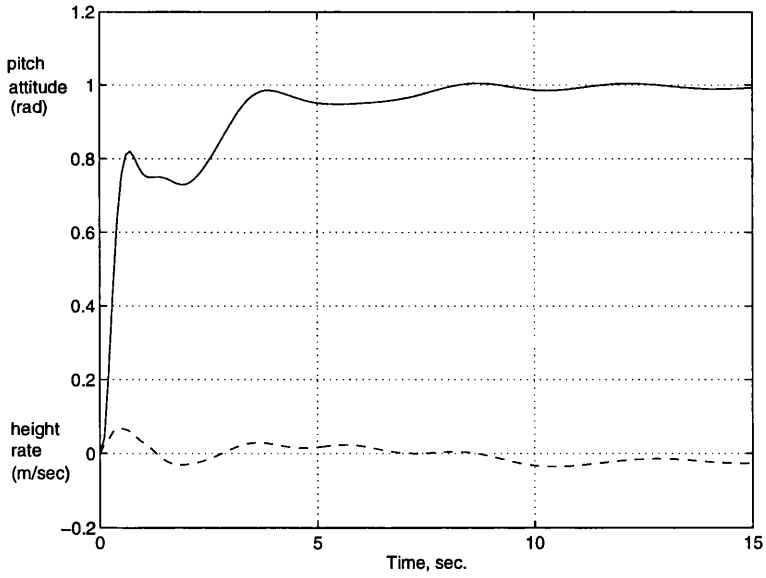

Figure 5.34: Time responses of pitch attitude and height rate to unity step change in input 2

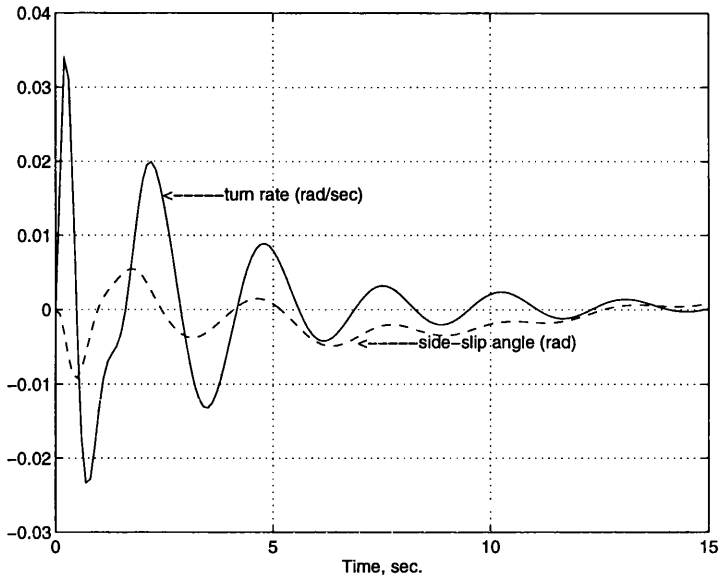

Figure 5.35: Time responses of turn rate and side-slip angle to unity step changes in input 1.

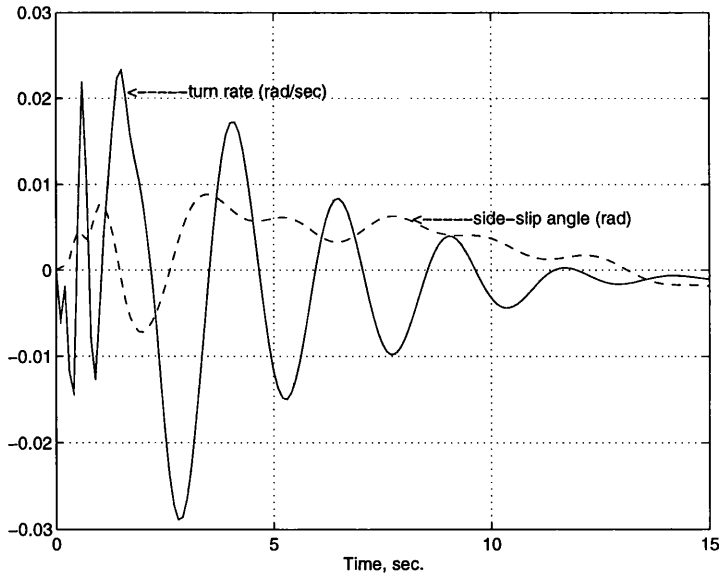

Figure 5.36: Time responses of side-slip angle and turn rate to unity step changes in input 2.

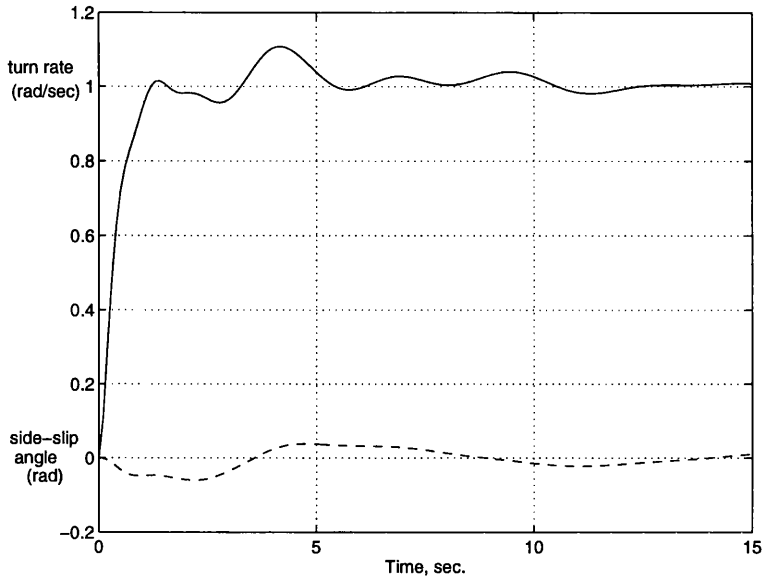

Figure 5.37: Time responses of turn rate and side-slip angle to unity step change in input 3

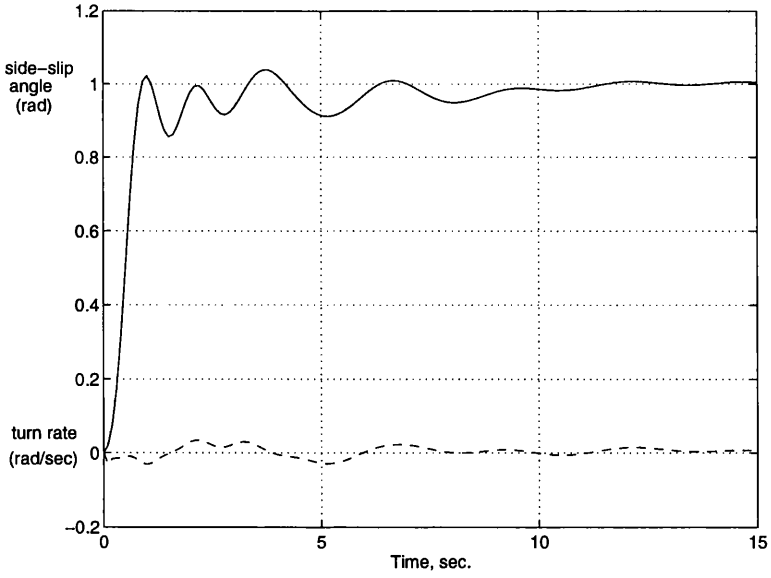

Figure 5.38: Time responses of side-slip angle and turn rate to unity step change in input 4

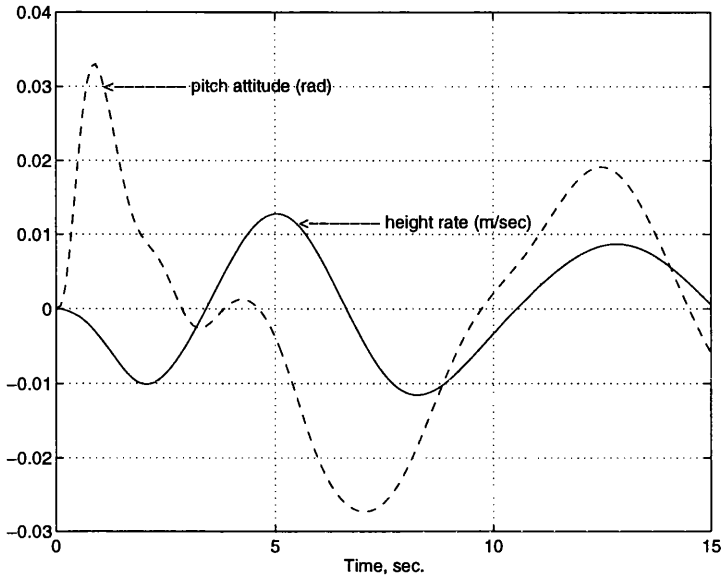

Figure 5.39: Time responses of height rate and pitch attitude to unity step changes in input 3.

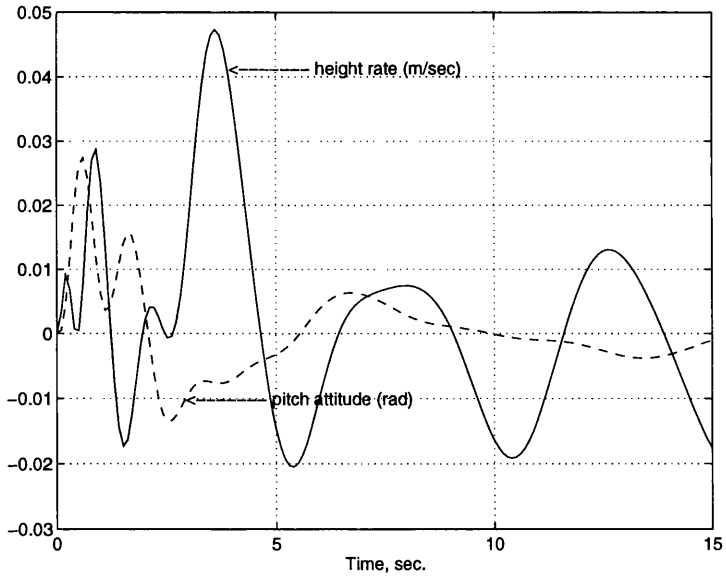

Figure 5.40: Time responses of pitch attitude and height rate to unity step changes in input 4.

5.6 Conclusions

The control system design for the helicopter at 80 knots forward flight is consists of two parts. First, in Chapter 4 a multivariable analysis covering structural and robustness issues was presented. It was shown that for a typical strongly cross-coupled single main rotor helicopter in forward flight at 80 knots, the standard 4-input 4-output multivariable control problem, for design purposes, decomposes, without significant loss of structural (interaction) information, into two decoupled simpler 2-input 2-output multivariable problems, one for the longitudinal dynamics a one for the lateral dynamics. Second, once the major structural attributes of the dynamical system have been elucidated by multivariable analysis, the development of simple effective multivariable control design is carried out in this chapter. This multivariable control system design is built up in systematic fashion using ICD; in particular, a novel type of feedforward control is used to overcome a severe lack of robustness as well as to decouple the lateral dynamics into two SISO subsystems round crossover frequency (3 rad/sec). Unlike multivariable decoupling by feedback, Leithead and O'Reilly [16], this type of decoupling by feedforward, Leithead and O'Reilly [17], is robust to model uncertainty. A diagonal (4x4) feedback controller matrix K(s) is then used, the elements of which are designed on the basis of the decoupled lateral and longitudinal dynamics. The resulting closed-loop bandwidths of the four channels are within Level 1 handling quality specifications, Tischler [30] and Anonymous [1]. Furthermore, the step responses of the overall 4-input 4-output closed-loop system indicate satisfactory transient behaviour with acceptably low cross-coupling, Liceaga *et al* [19, 20]

In summary, it is shown how ICD can provide a thorough multivariable analysis of the helicopter flight control problem leading to effective classical-type control design on each of the four input-output channels for a given flight condition (80

knots forward flight). Clearly, there is scope for further refinement of the multivariable control design in the light of assessment against nonlinear models containing rotor and actuator dynamics, omitted from the original linearised model under study. Also, gain scheduling of controllers between different forward flight conditions should be facilitated by the fact that the 4x4 feedback controller matrix is diagonal.

Chapter 6

30 Knots Forward Flight Analysis and Design

6.1 Introduction

In Chapters 4 and 5 was shown that the ICD is a very powerful tool for analysis and design of high-bandwidth helicopter flight controllers. However, this required an investigation of the dynamical characteristics of the helicopter at different forward flight conditions. In this chapter, the analysis and design of a flight control system for a typical single main rotor helicopter at low speed (30 knots) is presented. This design is carried out following similar procedures of the design of the control system for the helicopter in forward flight at 80 knots. In this way, ICD is used to explore and compare the dynamical characteristics of the helicopter at low speed (30 knots) against the higher speed condition of 80 knots. Therefore, the set of outputs are the same as those considered in the 80 knots design. As the design is carried out on the basis of small-signal low-order rigid body dynamics, it is necessary to evaluate the design on the basis of a model which include a simplified low-order representation of the rotor and actuator dynamics. Also, it is of interest to investigate the robustness and performance of the control system along different forward flight speeds. This can be useful to facilitate the

implementation of a scheduling control scheme for the helicopter.

6.2 Helicopter Model

The linear rigid body dynamics model derived from HELISTAB (Padfield [28]) for a single main rotor helicopter at 30 knots is given by the eighth-order model in state space form

$$\dot{x} = Ax + Bu \tag{6.1}$$

$$y = Cx \tag{6.2}$$

The associated state vector x(t) is described by

$$x(t) = \begin{bmatrix} u \\ w \\ q \\ \theta \\ v \\ p \\ \phi \\ r \end{bmatrix} = \begin{bmatrix} longitudinal\ velocity\ (m/sec) \\ vertical\ velocity\ (m/sec) \\ pitch\ rate\ (rad/sec) \\ pitch\ attitude\ (rad) \\ lateral\ velocity\ (m/sec) \\ roll\ rate\ (rad/sec) \\ roll\ attitude\ (rad) \\ yaw\ rate\ (rad/sec) \end{bmatrix} \tag{6.3}$$

Following the control design of the helicopter at 80 knots in Chapters 4 and 5, the tracking outputs considered for the helicopter flight control problem are as described by the output vector y(t) of equation(6.2), Manness *et al* [21]

$$y(t) = \begin{bmatrix} height\ \ rate \\ pitch\ \ attitude \\ turn\ \ rate \\ side-slip\ angle \end{bmatrix} = \begin{bmatrix} c_{11}u + c_{12}w + c_{14}\theta + c_{15}v + c_{17}\phi \\ \theta \\ c_{33}q + c_{38}r \\ c_{45}v \end{bmatrix} \tag{6.4}$$

where the coefficients c_{ij} are the elements of matrix C in equation(6.2). Also, the four control inputs (pilot inceptors) forming the 4x1 input vector $u = [u_1, u_2, u_3, u_4]^T$ of equation(6.1) are respectively the vertical collective u_1, the longitudinal cyclic u_2, the lateral cyclic u_3, and the tail rotor collective u_4.

Following the notation adopted in Chapter 4, the 4-input 4-output multivariable transfer-function matrix model associated with the state-space representation of equations(6.1) and (6.2) is given by

$$G(s) = C(sI - A)^{-1}B \tag{6.5}$$

described by

$$G(s) = \frac{1}{\triangle}$$

90.8874	8.9088	−0.2631	0.1596
−10.4765	−77.1828	−752.1148	95.6166
−4.1190	−10.4894	−17.0714	−11.5462
$-0.5356 \pm 1.0002i$	$-0.3169 \pm 1.0588i$	$-0.1208 \pm 1.2411i$	−3.6728
$0.0938 \pm 0.3149i$	−0.9222	−0.9235	2.5828
−0.0034	0.0587	−0.2240	−0.8261
	−0.0411	−0.0538	0.0518
6.2012	26.5814	−6.8802	−0.5302
−12.3493	−10.4736	−19.1974	−11.9795
$-0.5314 \pm 0.7523i$	$-0.3195 \pm 1.0592i$	$-0.1777 \pm 1.2305i$	−3.8921
0.2154	−0.5196	−0.5245	2.4663
$-0.0181 \pm 0.0177i$	−0.0375	−0.2300	−0.4980
	−0.0176	−0.0144	0.0911
			−0.0133
−16.1589	−6.732	−27.1877	−13.0550
−7.5342	−6.1183	$-1.8770 \pm 0.7811i$	−10.5939
−2.8707	$0.2028 \pm 1.5708i$	$0.6842 \pm 1.4313i$	−2.5232
$-0.2150 \pm 0.5189i$	1.0035	$0.0416 \pm 0.4847i$	$-0.0965 \pm 0.4960i$
$0.0502 \pm 0.4724i$	−0.9660	−0.4521	$0.0860 \pm 0.3749i$
0.0305	$-0.0035 \pm 0.3138i$		−0.2389
0.0167	−0.0471	−0.2263	0.1177
350.7579	20.4454	19.2826	−41.7621
−6.8055	9.5332	9.1008	−10.4727
−3.0886	−5.4990	−1.6347	−2.5117
$0.0467 \pm 0.4779i$	$0.2232 \pm 0.9314i$	−1.2376	$0.057954 \pm 0.4105i$
−0.2956	−0.4626	−0.4273	−0.3573
−0.0126	0.0595	$0.1231 \pm 0.3157i$	0.05112

(6.6)

with the characteristic polynomial

$$\begin{aligned} \triangle &= [1, -10.7993, -2.5465, -0.3274 \pm 1.1094i, \\ &\quad 0.0898 \pm 0.4604i, -0.3868, -0.0006] \end{aligned} \tag{6.7}$$

and the set of finite multivariable transmission zeros

$$T_z = \{-3.8755 \pm 7.7958i, -0.0098\} \tag{6.8}$$

Each element $g_{ij}(s)$, $i, j = 1, 2, 3, 4$, of the 4x4 transfer-function matrix $G(s)$ in equation(6.6) represents the nominal open-loop signal transmission between

the j-th pilot inceptor and the i-th tracking output. The transfer-function matrix model of equation(6.6) is a nominal-small signal model; it will have both gain and phase uncertainties associated with neglected non-linearities, unmodelled rotor and actuator dynamics. From equation(6.7), it is possible to see that the nominal system is unstable with a pair of right-hand plane (RHP) complex poles at $0.0898 \pm 0.4604i$. Also, from equation(6.8) the system possesses only left-hand plane (LHP) transmission zeros; that is, the nominal system is minimum-phase. However, due to one of the transmission zeros (-0.0098) is very close to the zero, special attention must be put on the structural robustness of the system at low frequencies.

To meet Level 1 handling qualities specifications, it is required that the closed loop transfer functions of the individual channels, must be between 2 and 4 rad/sec. Therefore, for analysis of the system, the most important range of frequencies is approximately 2-4rad/sec. It is important to note that the requirements specified in Tischler [31]-Anonymous [1] are limited to frequencies round 0.5 rad/sec to 4 rad/sec. Moreover, in Anonymous [1]*there is not* a clear indication for stability as a requirement to meet Level 1 handling qualities. However, due to the specifications of design, the possible RHPP's for the closed-loop system can be only at frequencies well below 0.5 rad/sec. This is accepted by the fact that the effects of low frequency RHPP's can be easily compensated by the pilot.

6.3 ICD Analysis

The starting point of analysis following the ICD framework of analysis is given by the so called multivariable structure functions $\Gamma_i(s)$ i=1,...,m, ($\Gamma_m(s) = 0$) of equations(3.38), O'Reilly and Leithead [27, 14]. The Nyquist plots of the multivariable structure functions $\Gamma_1(s)$, $\Gamma_2(s)$ and $\Gamma_3(s)$ are shown in Figure(6.1). From these plots three important points can be detected; a) Due to the large

gain of all the $\Gamma_i(s)$ functions the system is strongly coupled; b) Because $\Gamma_2(s)$ and Γ_3 are very close to the point (1,0) at around 0.0rad/sec, the system lacks robustness due to excessive structural sensitivity or uncertainty in the number of RHPP's and RHPZ's; and c) Similar to the 80 knots forward flight case, due to the small gain of $\Gamma_2(s)$ at the region of the channels cross-over frequencies (2-4rad/sec), for design purposes, the system may decompose, into two 2-input 2-output multivariable problems, one for the longitudinal dynamics and one for the lateral dynamics. Therefore, application of Result 3.7 to the longitudinal dynamics $G_{11}(s)$ (upper left submatrix) and lateral dynamics $G_{22}(s)$ (lower right submatrix) of equation(6.6) is required.

Consider first condition (ii) of Result 3.7. From Figure(6.2), it is seen that the multivariable structure functions $\gamma^*(s)$ and $\gamma(s)$ for $G^*_{11}(s)$ and $G_{11}(s)$ are significantly different at all frequencies. Moreover, condition (iii) is also not satisfied due to $g_{21}(s)$ has a RHPZ at 0.2154 meanwhile $g^*_{21}(s)$ is minimum-phase. Therefore, the Multiple Channel $M_1(s)$ representing the longitudinal dynamics is not weakly coupled to the 2-input 2-output Multiple Channel $M_2(s)$ representing the lateral dynamics. On the other hand, Figure(6.3) shows that the Nyquist plots of $\gamma^*(s)$ and $\gamma(s)$ for $G^*_{22}(s)$ and $G_{22}(s)$ do not differ significantly around the channels cross-over frequencies so condition (ii) of Result 3.7 is satisfied as far of the lateral dynamics are concerned; condition (i) is also satisfied as Figures(6.4) and (6.5) shows no significant differences between $g_{11}(s)$ and $g^*_{11}(s)$, and $g_{22}(s)$ and $g^*_{22}(s)$ around the channels cross-over frequencies (2-4rad/sec). Nonetheless, condition (iii) is not satisfied due to significant differences in the number of RHPP's and RHPZ's between $G^*_{22}(s)$ and $G_{22}(s)$ as is shown in Table 6.1. Moreover, subsystem $G_{22}(s)$ has a pair of RHP transmission zeros at $0.0898 \pm 0.4604i$, whereas multiple channel $G^*_{22}(s)$ is minimum phase. Therefore, Multiple Channel $M_2(s)$ representing the lateral dynamics is not weakly coupled to the 2-input 2-output Multiple Channel $M_1(s)$ representing the longitudinal dynamics.

		Individual RHPZ's	Individual RHPP's
$\bar{G}_{22}$	g_{11}	$0.6842 \pm 1.4313j$	$0.0898 \pm 0.4604j$
		$0.0416 \pm 0.4847j$	-
	g_{12}	$0.0860 \pm 0.3749j$	$0.0898 \pm 0.4604j$
	g_{21}	19.286	$0.0898 \pm 0.4604j$
		9.1008	-
		$0.1232 \pm 0.3157j$	-
	g_{22}	$0.0580 \pm 0.4106j$	$0.0898 \pm 0.4604j$
		0.0511	-
$\bar{G}^*_{22}$	g^*_{11}	$0.5643 \pm 1.4089j$	-
	g^*_{12}	-	-
	g^*_{21}	20.5332	-
		8.4587	-
	g^*_{22}	0.0504	-

Table 6.1: Subsystem G_{22} and Multiple Channel G^*_{22} RHPP's and RHPZ's for the helicopter model $G(s)$ of eqn.(6.6)

Similar to the 80 knots design, the system is affected by an almost RHP pole-zero cancellation, that is, the RHP transmission zeros affecting subsystem $G_{22}(s)$ are very close to the RHP poles of the full system in equation(6.6), so as it was shown in Chapter 4, it is likely that this cancellation is fictitious, Leithead and O'Reilly [18]. Therefore, following the same procedure, a weak feedback is required in order to eliminate this problem. This will result in multiple channel $M_2(s)$ weakly coupled to multiple channel $M_1(s)$. However, by the fact that multiple channel $M_1(s)$ is strongly coupled to multiple channel $M_2(s)$, it is decided to consider the problem as a full 4x4 control problem.

In comparison with the 80 knots design, the system is also affected by the introduction of RHPZ's in some of the channels when the requirements of design are satisfied. That is, as Figure(6.3) shows, in order to keep multiple channel $G^*_{22}(s)$ minimum phase the multivariable structure function $\gamma^*(s)$ required 3 anticlockwise encirclements to the point (1,0), due to the 2 RHPZ's of $g^*_{11}(s)$ at $0.5643 \pm 1.4089j$ and by the RHPZ of $g^*_{22}(s)$ at 0.0504 . Therefore, if any of the channels of $G^*_{22}(s)$

is designed such that it roll-off between 2 and 4 rad/sec, it would force the actual $\gamma_3(s)$ or $\gamma_4(s)$ in equation(3.36), to avoid two of the three required anti-clockwise encirclements to the point (1,0). Therefore, any of the other three channels will be non-minimum phase with 2 RHPZ's at approximately 1.4rad/sec. As concluded in Chapter 4, this is due to the closeness of the RHPZ's of $g^*_{11}(s)$ of $G^*_{22}(s)$ or $g_{33}(s)$ of $G(s)$ to the required channel cross-over frequencies. Therefore, similar to the 80 knots case, it is necessary to design a pre-compensator to stabilise the RHPZ's of $g_{33}(s)$ round 1.4rad/sec.

Despite the fact that the handling quality requirements do not specify any restriction to the control system at low frequency, Anonymous [1], in order to avoid the introduction of RHPZ's at low frequency and guarantee stability robustness, it is necessary to introduce a feedforward control scheme to the control system, Leithead and O'Reilly [17]. Unlike the 80 knots case the feedforward controller will be used only to shift the multivariable structure functions $\Gamma_i(s)$ far from the point (1,0) at low frequency. So, two important changes in the dynamical behaviour of the helicopter between low and high speed are; a) the sensitivity of the system becomes more acute at very low frequency and less problematic at 0.4 rad/sec and 1.5 rad/sec; and b) at low speed the system can not be considered decoupled (for design purposes) around the channels cross-over frequencies.

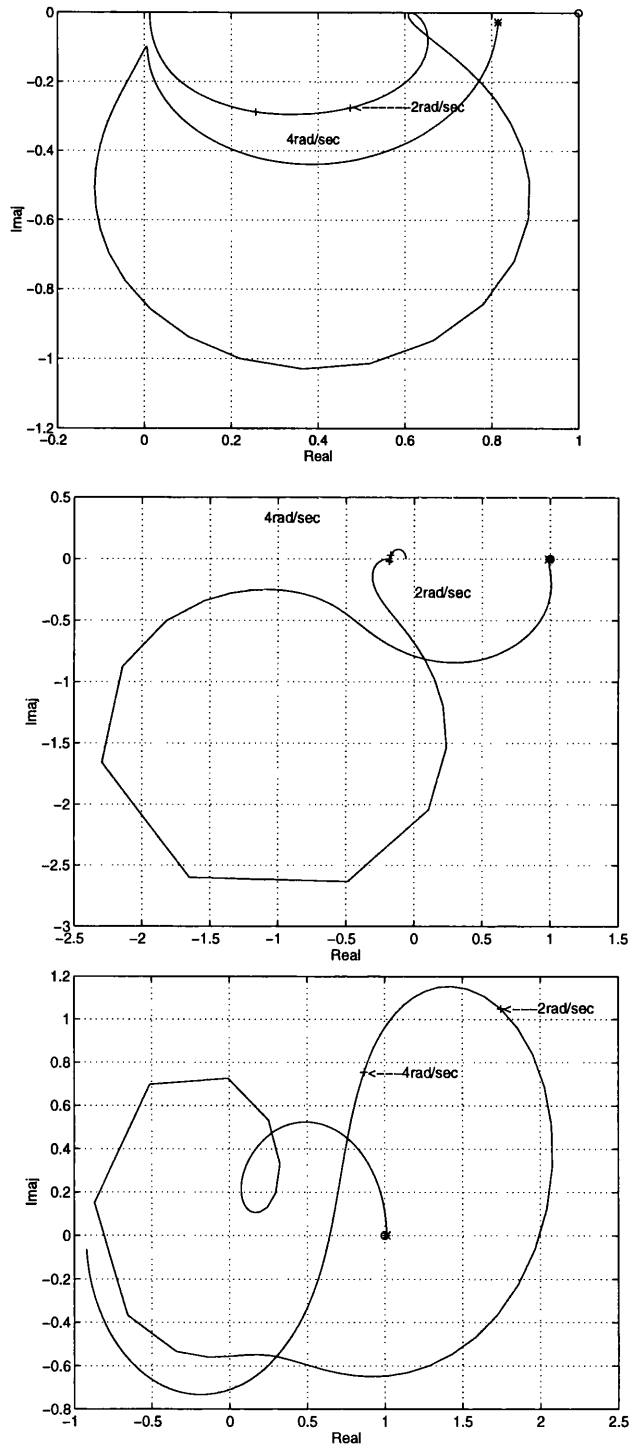

Figure 6.1: Nyquist plots of the multivariable structure functions $\Gamma_1(s)$, $\Gamma_2(s)$ and $\Gamma_3(s)$ for full system G(s) of eqn.(6.6)

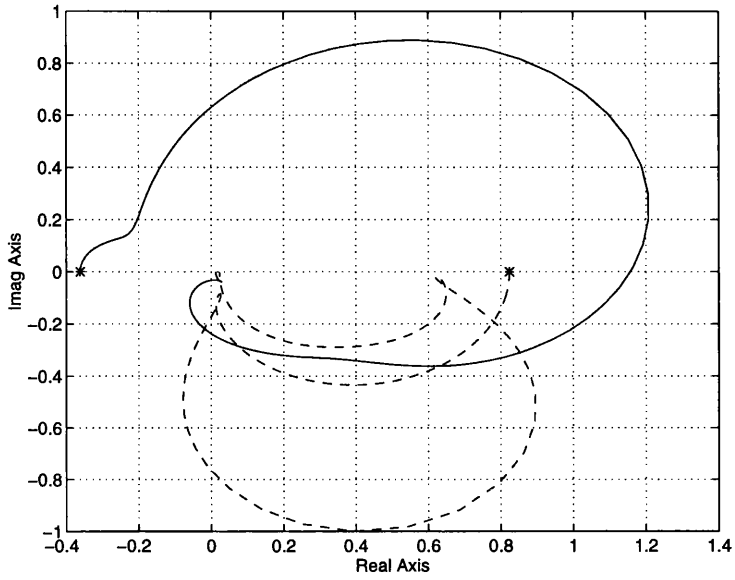

Figure 6.2: Nyquist plots of $\gamma^*(s)$ and γ for $G_{11}^*(s)$ and $G_{11}(s)$ respectively.

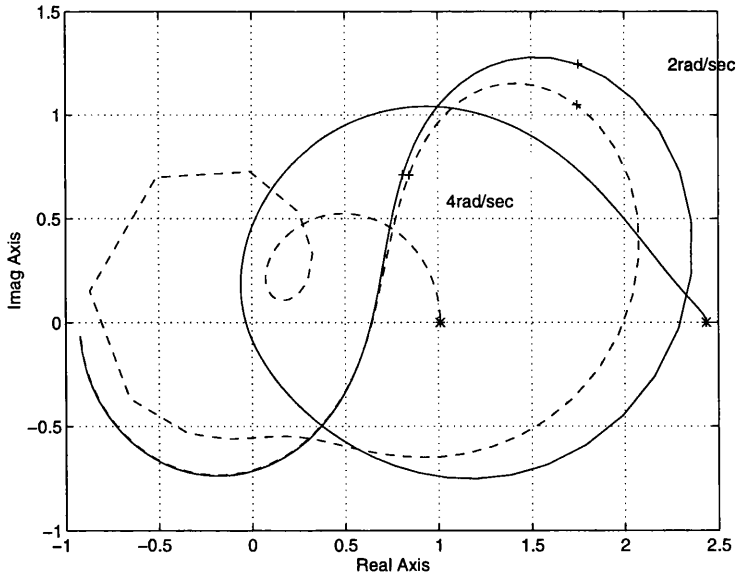

Figure 6.3: Nyquist plots of $\gamma^*(s)$ and γ for $G_{22}^*(s)$ and $G_{22}(s)$ respectively.

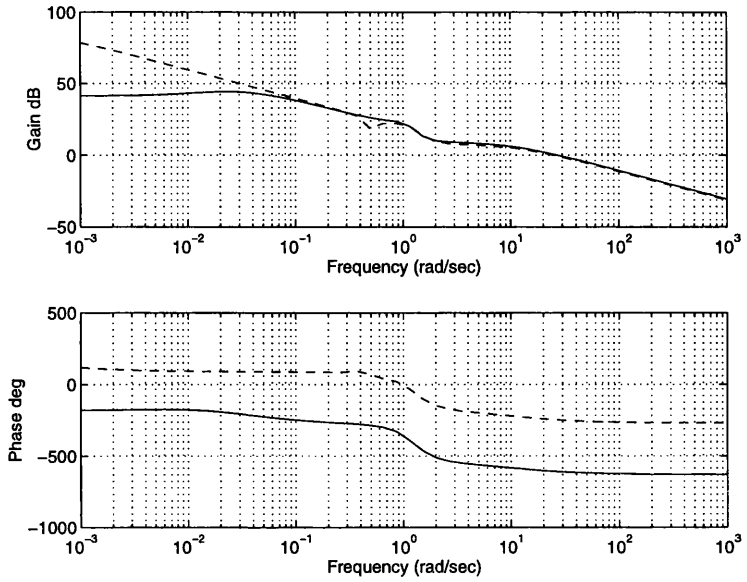

Figure 6.4: Bode plots of $g_{11}^*(s)$ and $g_{11}(s)$ for $G_{22}^*(s)$ and $G_{22}(s)$ respectively.

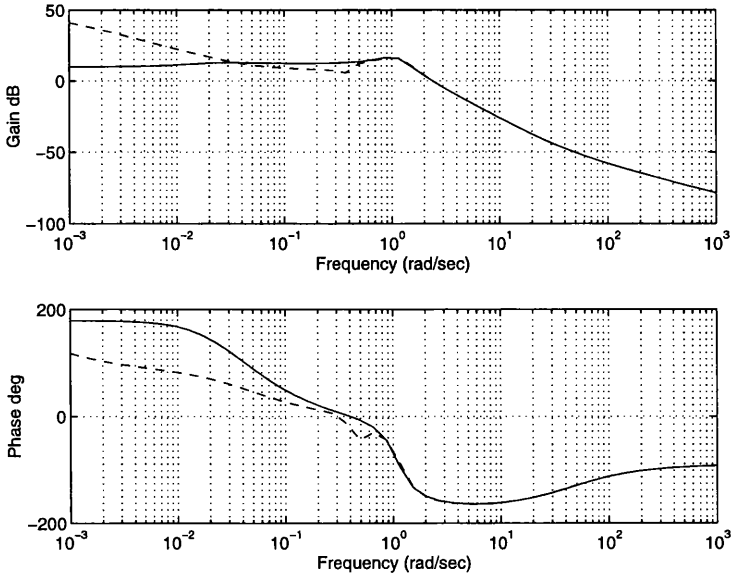

Figure 6.5: Bode plots of $g_{22}^*(s)$ and $g_{22}(s)$ for $G_{22}^*(s)$ and $G_{22}(s)$ respectively.

6.4 Structure Improvement

In the last section, it was found that the helicopter model system at 30 knots presents three important structural problems; a) the requirement of an almost RHP pole zero cancellation to keep minimum phase behaviour; b) a severe limitation in performance due to the introduction of RHPZ's in some of the channels when the requirements of design are satisfied in either channel 3 or channel 4; and c) a high sensitivity problem at very low frequency, detected by the closeness of the $\Gamma_i(s)$ functions to the point (1,0). These problems are solved in a similar way to those presented in Chapter 5, by the use of a weak-feedback, precompensation and feedforward control.

6.4.1 Weak-Feedback Design

As is shown in Chapter 5, the fictitious almost RHP pole zero cancellation may represent a serious robustness problem. Therefore, in order to eliminate this problem the system is stabilised by a *weak feedback*. This is also necessary in order to guarantee internal stability when designing the feedforward controller.

A candidate feedback function round the $g_{22}(s)$ is,

$$m(s) = 1.0157\frac{s(s+0.0006)(s+0.3868)(s+2.5465)}{(s+0.0176)(s+0.0375)(s+0.5196)(s+7)^2} \tag{6.9}$$

Application of the feedback function $m(s)$ of equation(6.9) to the full 4-input 4-output helicopter system $G(s)$ of equation(6.6) via the matrix $M(s)$

$$M(s) = \begin{bmatrix} 0 & 0 & 0 & 0 \\ 0 & m(s) & 0 & 0 \\ 0 & 0 & 0 & 0 \\ 0 & 0 & 0 & 0 \end{bmatrix} \tag{6.10}$$

results in the amended system

$$\bar{G}(s) = (I + GM)^{-1} G = \begin{bmatrix} \bar{G}_1 \\ \dots \\ \bar{G}_2 \end{bmatrix} \tag{6.11}$$

where

$$\bar{G}_1(s) = \frac{1}{\bar{\Delta}} \begin{bmatrix} 90.8874 & 8.9087 & -0.2631 & 0.1591 \\ -10.4715 & -77.1827 & -752.1144 & 95.6114 \\ -9.0177 & -10.4894 & -17.0960 & -11.5916 \\ -4.3723 \pm 0.0156i & -7.0 & -0.6991 \pm 0.1234i & -7.8115 \\ -0.5422 \pm 0.9155i & -0.3169 \pm 1.1058i & -0.1749 \pm 1.2398i & -5.9865 \\ -0.6175 & -0.9221 & -0.9228 & -3.7994 \\ -0.0312 \pm 0.3254i & -0.5195 & -0.5220 & 2.5965 \\ -0.0375 & 0.0586 & -0.2263 & -0.8747 \\ -0.0174 & -0.0375 & 0.0533 & -0.5073 \\ -0.0033 & -0.0410 & -0.0378 & -0.0845 \\ & -0.0175 & -0.0174 & -0.0378 \\ & & & 0.0509 \\ & & & -0.0173 \\ 6.2012 & 26.5813 & -6.8802 & -0.5302 \\ -12.3493 & -10.4736 & -19.1974 & -11.9979 \\ -7.0 & -7.0 & -7.0 & -7.0 \\ -7.0 & -7.0 & -7.0 & -7.0 \\ -0.5314 \pm 0.7523i & -0.3195 \pm 1.0592i & -0.1777 \pm 1.2305i & -3.8921 \\ -0.5196 & -0.5196 & -0.5245 & 2.4663 \\ 0.2154 & -0.5196 & -0.5196 & -0.5196 \\ -0.0375 & -0.0375 & -0.2300 & -0.4980 \\ -0.0181 \pm 0.0177i & -0.0375 & -0.0375 & 0.0911 \\ -0.0176 & -0.0176 & -0.0176 & -0.0375 \\ & -0.0176 & -0.0144 & -0.0133 \\ & & & -0.0176 \end{bmatrix} \tag{6.12}$$

$$\bar{G}_2(s) = \frac{1}{\bar{\Delta}} \begin{bmatrix} 16.1589 & -6.7320 & -27.1877 & -13.0550 \\ -9.0271 & -7.0 & -8.7304 & -10.6765 \\ -7.2072 & -7.0 & -4.8745 & -8.5951 \\ -4.3320 & -6.1183 & -1.7576 \pm 1.1318i & -4.7285 \\ -3.2823 & 0.2028 \pm 1.5708i & 0.6725 \pm 1.4498i & -2.5027 \\ -0.2718 \pm 0.6580i & 1.0035 & -0.2131 \pm 0.3779i & -0.3894 \pm 0.5447i \\ -0.6022 & -0.9660 & -0.5342 \pm 0.0180i & -0.5126 \\ -0.1299 \pm 0.3620i & -0.5196 & -0.0422 & 0.0185 \pm 0.3820i \\ -0.0358 & -0.0035 \pm 0.3138i & -0.0173 & -0.1259 \\ 0.0292 & -0.0375 & & -0.0514 \\ -0.0180 & -0.0176 & & -0.0171 \\ & & & \\ 0.0167 & -0.0471 & -0.2263 & 0.1177 \\ 350.7578 & 20.4454 & 19.2828 & -41.7617 \\ -8.9943 & 9.5333 & 9.1013 & -10.5683 \\ -6.4219 & -7.0 & -8.7417 & -8.5803 \\ -4.0000 \pm 0.2510i & -7.0 & -4.8043 & -4.7292 \\ -0.2435 \pm 0.0053i & -5.4990 & -1.4584 \pm 0.8992i & -2.4798 \\ -0.4939 & 0.2233 \pm 0.9314i & -0.5215 & -0.5231 \\ -0.2157 & -0.5196 & -0.4421 & -0.2824 \pm 0.3586i \\ -0.0408 & -0.4626 & -0.0700 \pm 0.2653i & -0.2911 \\ -0.0146 \pm 0.0013i & 0.0596 & -0.0451 & 0.0510 \\ & -0.0375 & -0.0173 & -0.0470 \\ & -0.0176 & & -0.0171 \end{bmatrix} \quad (6.13)$$

with the amended characteristic polynomial

$$\begin{aligned} \bar{\Delta} \;=\; & [1, -10.8630, -8.6143, -4.7321, -2.5465, -0.3638 \pm 1.1190i, \\ & -0.1687 \pm 0.4750i, -0.5196, -0.3868, -0.0375, -0.0176, -0.0006] \end{aligned} \quad (6.14)$$

and the set of finite multivariable transmission zeros

$$\bar{T}_z \;=\; \{-7.0, -7.0, -3.8755 \pm 7.7958i, -0.0098\} \quad (6.15)$$

As indicated in Chapter 4, to assure that $M(s)$ is really *weak* two points have to be checked; a) the individual transfer functions $g_{ij}(s)$ of the original system of equation(6.6) must not differ significantly from the individual transfer functions $\bar{g}_{ij}(s)$ of the amended system of equation(6.11) except at frequencies local to the

RHPP's; and b) the uncertainties of the individual transfer functions should not be increased by the feedback $m(s)$. In Figures(6.6)-(6.9), the Bode diagrams of the individual transfer functions $g_{ij}(s)$ and $\bar{g}_{ij}(s)$ are shown. From these plots it is possible to see that the individual transfer functions are not significantly altered except at frequencies close to the RHPP's. Therefore, the first point concerning the design of $m(s)$ has been satisfied. To prove if the uncertainties of the individual transfer functions have not been increased by closing the feedback loop $m(s)$ round the $g_{22}(s)$ element, it is necessary to check that the multivariable structure functions $\gamma_{ij}h_{22}$ in Table 6.2 are not close to the point (1,0) in the frequency range of interest Leithead and O'Reilly [15].

$\gamma_{11}h_{22}=\frac{g_{12}g_{21}}{g_{11}g_{22}}h_{22}$
$\gamma_{13}h_{22}=\frac{g_{12}g_{23}}{g_{13}g_{22}}h_{22}$
$\gamma_{14}h_{22}=\frac{g_{12}g_{24}}{g_{14}g_{22}}h_{22}$
$\gamma_{31}h_{22}=\frac{g_{32}g_{21}}{g_{31}g_{22}}h_{22}$
$\gamma_{33}h_{22}=\frac{g_{32}g_{23}}{g_{33}g_{22}}h_{22}$
$\gamma_{34}h_{22}=\frac{g_{32}g_{24}}{g_{34}g_{22}}h_{22}$
$\gamma_{41}h_{22}=\frac{g_{42}g_{21}}{g_{41}g_{22}}h_{22}$
$\gamma_{43}h_{22}=\frac{g_{42}g_{23}}{g_{43}g_{22}}h_{22}$
$\gamma_{44}h_{22}=\frac{g_{42}g_{24}}{g_{44}g_{22}}h_{22}$
where $h_{22}=\frac{mg_{22}}{1+mg_{22}}$

Table 6.2: Multivariable structure functions $\gamma_{ij}h_{22}$

From Figures(6.10)-(6.12) it is observed that the nine Nyquist plots of $\gamma_{ij}h_{22}$ of Table 6.2 do not come close to the (1,0) point in the frequency range of interest, namely 2-4 rad/sec as required for robustness.

At this stage, what has been obtained is an amended helicopter system model $\bar{G}(s)$ in equation(6.11) which is stable, and has the undesirable almost RHP pole zero cancellation removed without increasing the system sensitivity and with minimum changes to the system.

6.4.2 Pre-compensation

As it was noted above, the system has a severe performance limitation due to the introduction of RHPZ's when the specifications of design are meet. It was also concluded, following the discussion of Section 5.3.1, that this is due to the RHPZ's of $\bar{g}_{33}(s)$. That is, they are close to the required channel cross-over frequencies. The solution adopted to eliminate this problem is by way of a pre-compensator. As indicated in Section 3.5.2, the use of any pre-compensator may increase the uncertainty effects. Hence, it must affect the system only at frequencies where the $\Gamma_i(s)$ functions are far from the point (1,0). Inspection of equation(6.11) shows that the RHPZ's of $\bar{g}_{33}(s)$ are around 1.4rad/sec and as is shown in Figure(6.1), all the $\Gamma_i(s)$ are far from the point (1,0) around 1.4 rad/sec. Therefore, if the pre-compensator affects the system at frequencies round the RHPZ's of $\bar{g}_{33}(s)$ or at frequencies where the $\Gamma_i(s)$ functions are far from the point (1,0), then the uncertainties will not have been increased significantly.

A suitable pre-compensator is given by

$$P(s) = \begin{bmatrix} 1 & 0 & 0 & 0 \\ 0 & 1 & 0 & 0 \\ 0 & 0 & 1 & 0 \\ 0 & 0 & p_{43} & 0 \end{bmatrix} \tag{6.16}$$

where

$$p_{43}(s) = 5.0\frac{s^2(s+1.6)(s+1.8)(s+2)}{(s+0.15)(s+0.2)^2(s^2+2.4s+2.65)(s+8)} \tag{6.17}$$

results in the pre-compensated lateral system

$$G' = \bar{G}P \tag{6.18}$$

for which it is observed in Figure(6.13) that the $\Gamma'_i(s)$ of the pre-compensated system $G'(s)$ are little changed from $\bar{\Gamma}_i(s)$ of $\bar{G}(s)$ except round 1.4 rad/sec. The

number of anti-clockwise encirclements of the (1,0) point in $\Gamma_3'(s)$ (dashed line) is reduced from 3 to 1 since its number of RHPP's is reduced from 3 to 1.

In Figure(6.14), the Bode plots of the individual transfer functions $\bar{g}_{3,j}(s)$ and $g_{3,j}'(s)$, $j = 1, .., 4$, for the stabilised system $\bar{G}(s)$ and the pre-compensated system $G(s)'(s)$ shows that the pre-compensator $P(s)$ affects the system mainly at 1.4 rad/sec and 0.5 rad/sec. However, at 0.5 rad/sec the multivariable structure functions of the stabilised system $\bar{G}(s)$ are far from the point (1,0). Moreover, $\bar{\Gamma}_3(s)$ is almost zero at 0.5rad/sec. Therefore, the uncertainty effects are not increased by the use of the pre-compensator $P(s)$.

6.4.3 Feedforward Controller

Similar to the 80 knots case, the system presents a severe sensitivity problem that may result in the introduction of RHPZ's well below the required cross-over frequency in any of the channels. This problem is detected by the closeness of the Nyquist plots of the multivariable structure functions $\Gamma_i(s)$ to the point (1,0) at round 0 rad/sec, Figure(6.1). In order to guarantee stability robustness (but not necessary to meet Level 1 handling qualities), it is necessary to shift the $\Gamma_i(s)$ far from the point (1,0) via the implementation of a feedforward control scheme, Leithead and O'Reilly [17].

A suitable feedforward control is given by,

$$F = \begin{bmatrix} 0 & 0 & 0 & 0 \\ f_{21} & 0 & 0 & 0 \\ 0 & f_{32} & 0 & 0 \\ 0 & 0 & f_{43} & 0 \end{bmatrix} \tag{6.19}$$

where

$$f_{21} = \frac{0.0000052}{(s+0.0004)(s+0.0015)} \tag{6.20}$$

$$f_{32} = \frac{-0.09}{(s+0.00055)(s+0.09)} \tag{6.21}$$

$$f_{43} = \frac{-0.003}{(s+0.00055)(s+0.05)} \tag{6.22}$$

and results in the amended system

$$G'' = G' + F \tag{6.23}$$

In Figure(6.15) the Nyquist plots of the amended system $G''(s)$ are shown. From these plots it is possible to see that none of the $\Gamma_i''(s)$ functions are close to the point (1,0). Therefore, the robustness problem of the Nyquist plots of $\Gamma_i'(s)$ being close to the point (1,0) not longer exist.

Inspection of equations(6.20)-(6.22), shows that the main effect of the feedforward controller $F(s)$ in equation(6.19) is at frequencies less that 0.1rad/sec, well below the frequency range of interest (2-4rad/sec). Therefore, it will not change the original output in the frequency region of interest. That is, the performances of the original and amended outputs will be equal in this range of frequencies, namely 2-4 rad/sec. Hence, it is not necessary to assess the performance of the control system on the basis of the original output. This also indicates that the feedforward controller is introduced in the control system in order to guarantee stability robustness at low frequency, despite the fact that this is not a requirement to meet Level 1 handling qualities.

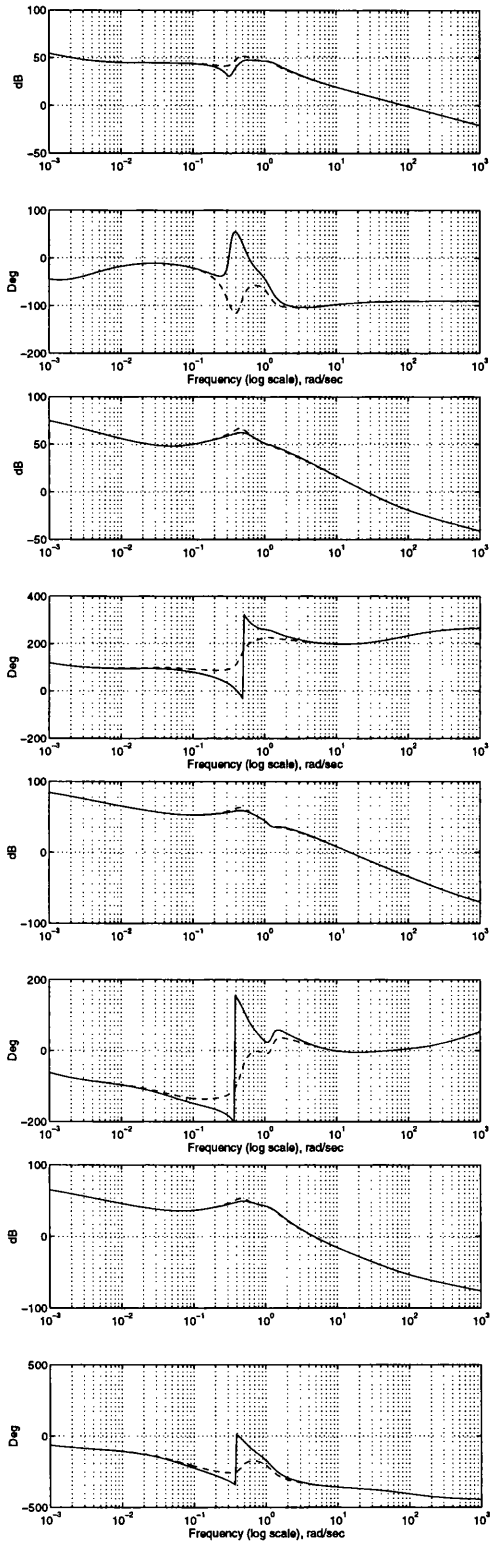

Figure 6.6: Bode plots of $\bar{g}_{1j}(s)$ and $g_{1j}(s)$ for $\bar{G}(s)$ and $G(s)$ respectively.

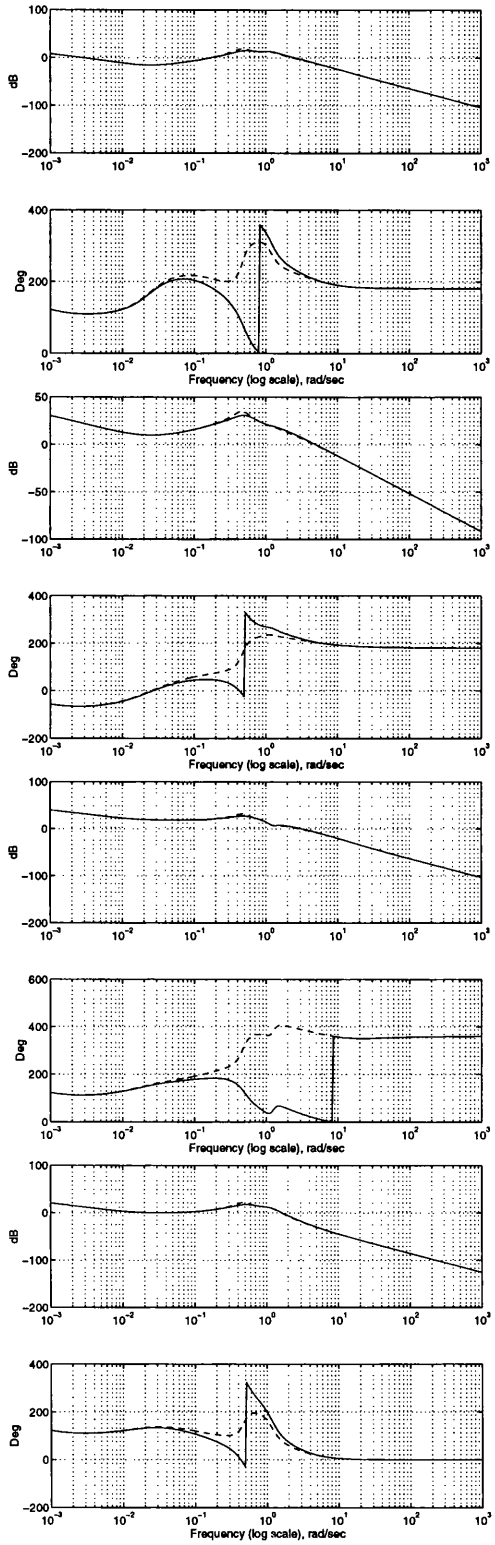

Figure 6.7: Bode plots of $\bar{g}_{2j}(s)$ and $g_{2j}(s)$ for $\bar{G}(s)$ and $G(s)$ respectively.

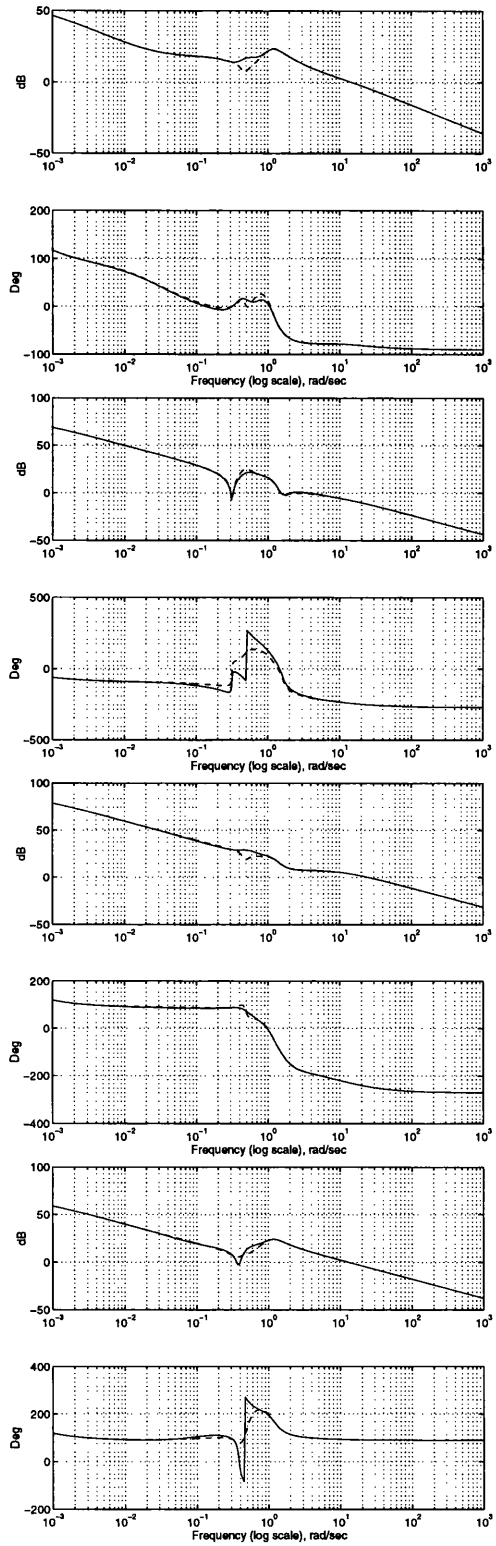

Figure 6.8: Bode plots of $\bar{g}_{3j}(s)$ and $g_{3j}(s)$ for $\bar{G}(s)$ and $G(s)$ respectively.

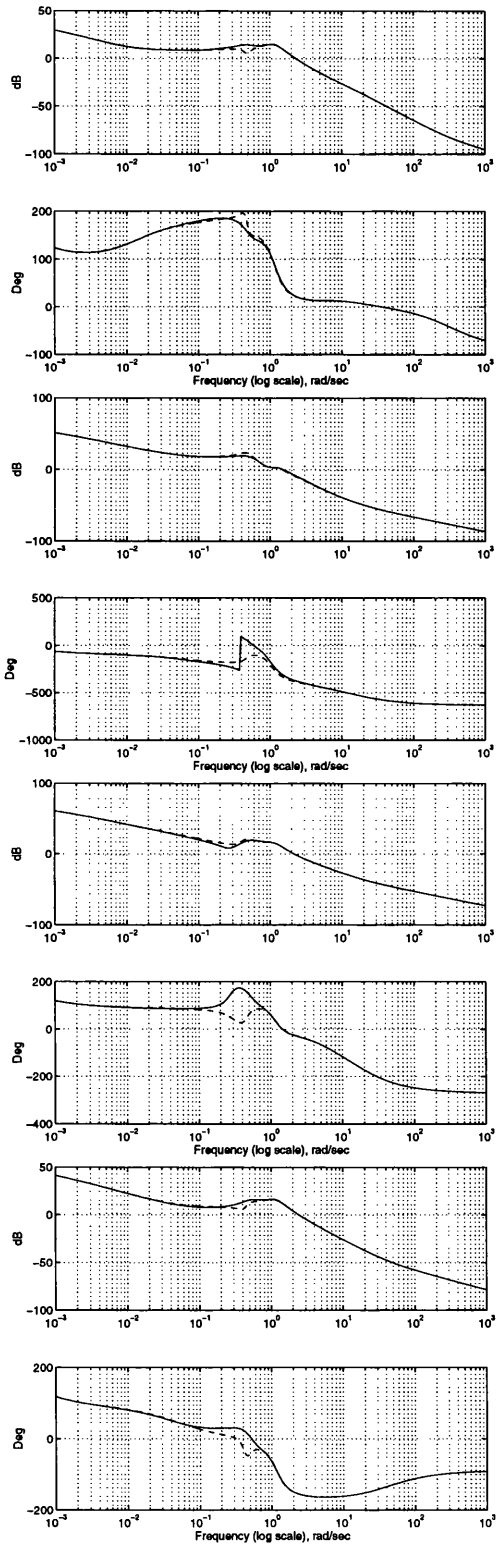

Figure 6.9: Bode plots of $\bar{g}_{4j}(s)$ and $g_{4j}(s)$ for $\bar{G}(s)$ and $G(s)$ respectively.

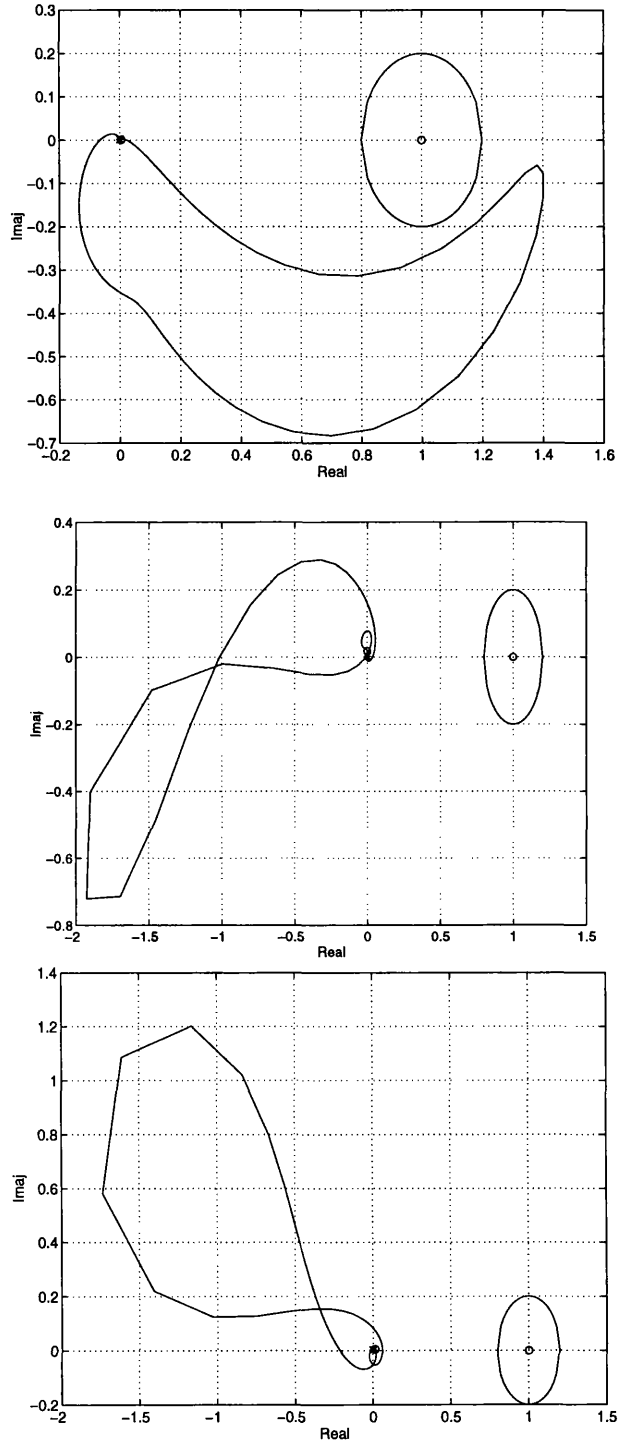

Figure 6.10: Nyquist plots of $\gamma_{ij} h_{22}(s)$ in Table 6.2

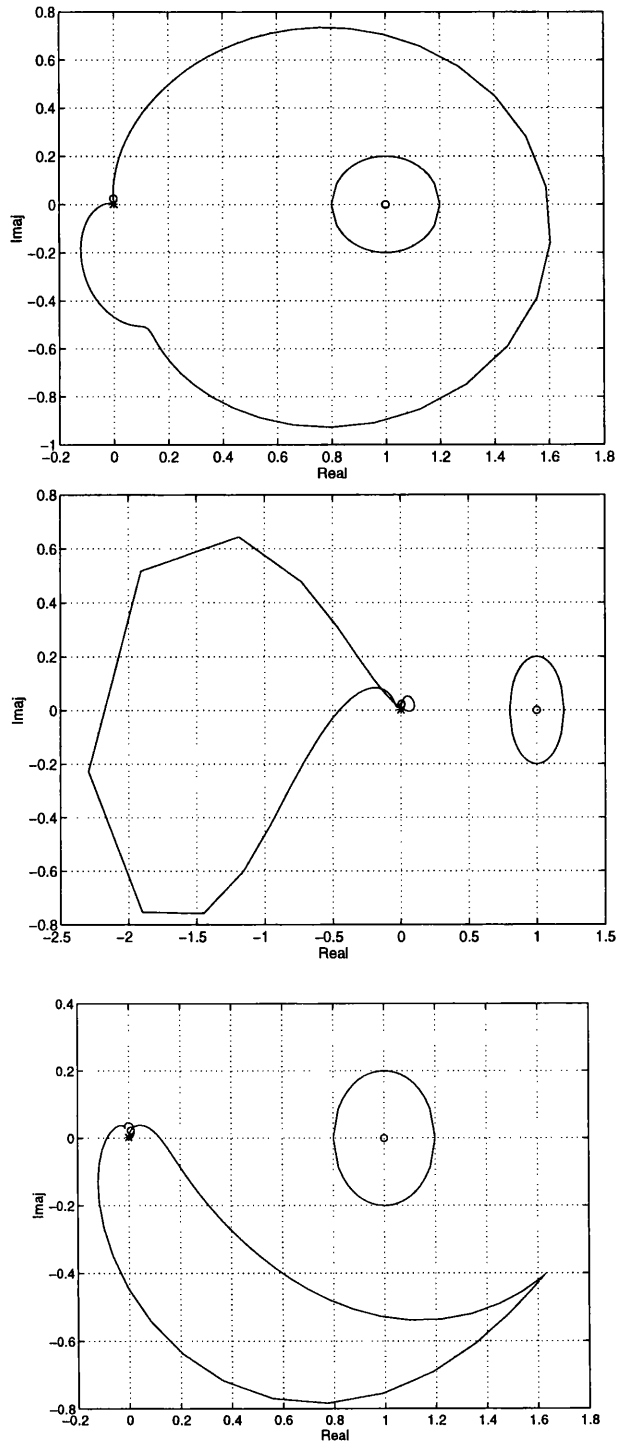

Figure 6.11: Nyquist plots of $\gamma_{ij}h_{22}(s)$ in Table 6.2

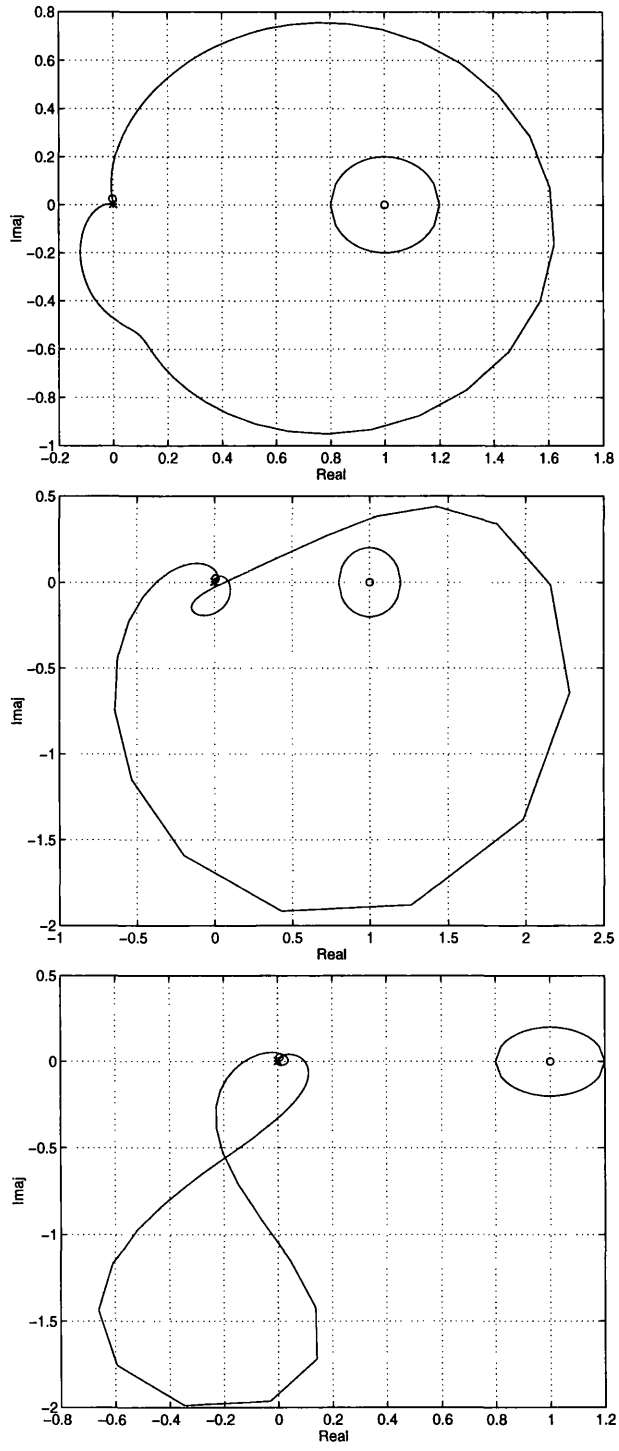

Figure 6.12: Nyquist plots of $\gamma_{ij}h_{22}(s)$ in Table 6.2

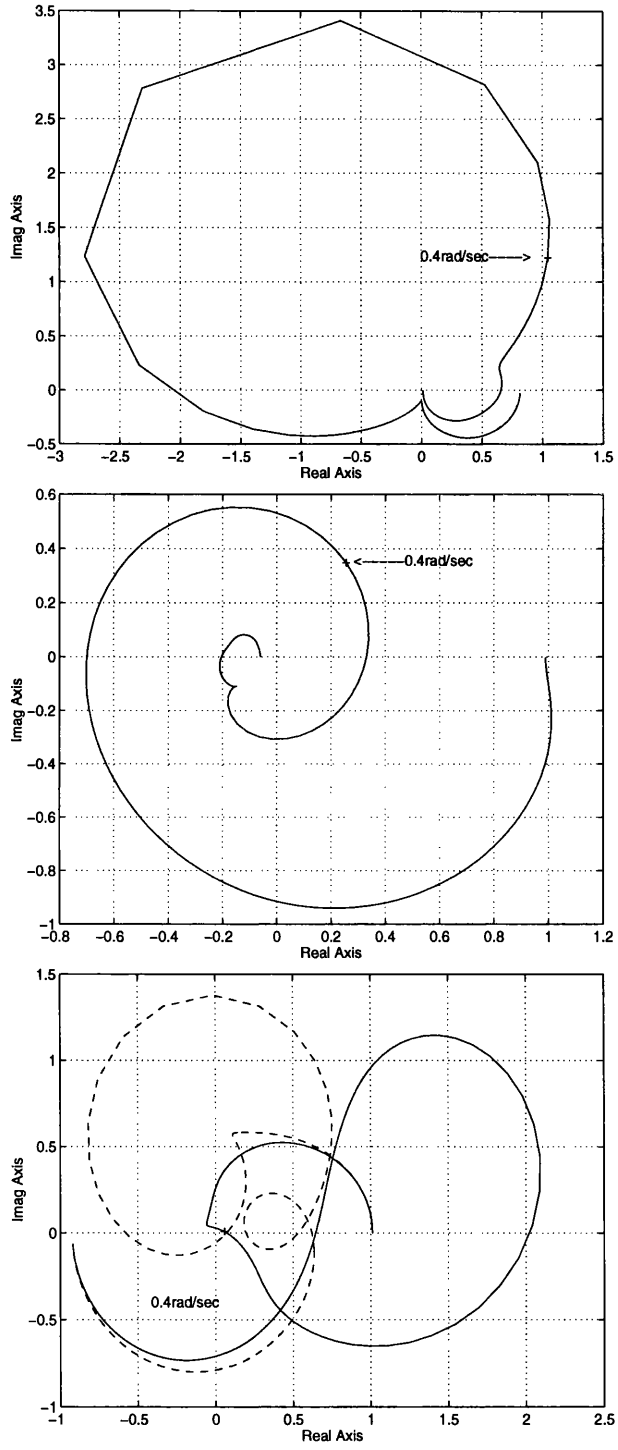

Figure 6.13: Nyquist plots of the multivariable structure functions $\Gamma_1(s)$, $\Gamma_2(s)$ and $\Gamma_3(s)$ for the stabilised system $\bar{G}(s)$ and precompensated system $G'(s)$ respectively

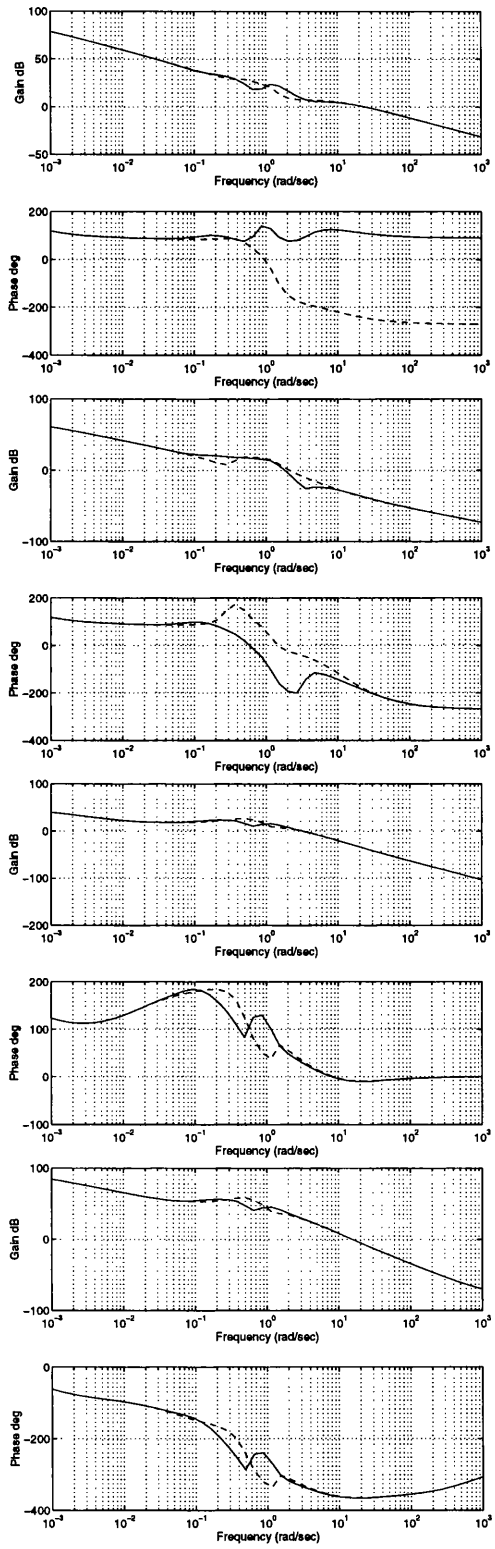

Figure 6.14: Bode plots of the $\bar{g}_{3,j}$ and g'_{3j} for the stabilised system $\bar{G}$ and the precompensated system $G'(s)$ respectively

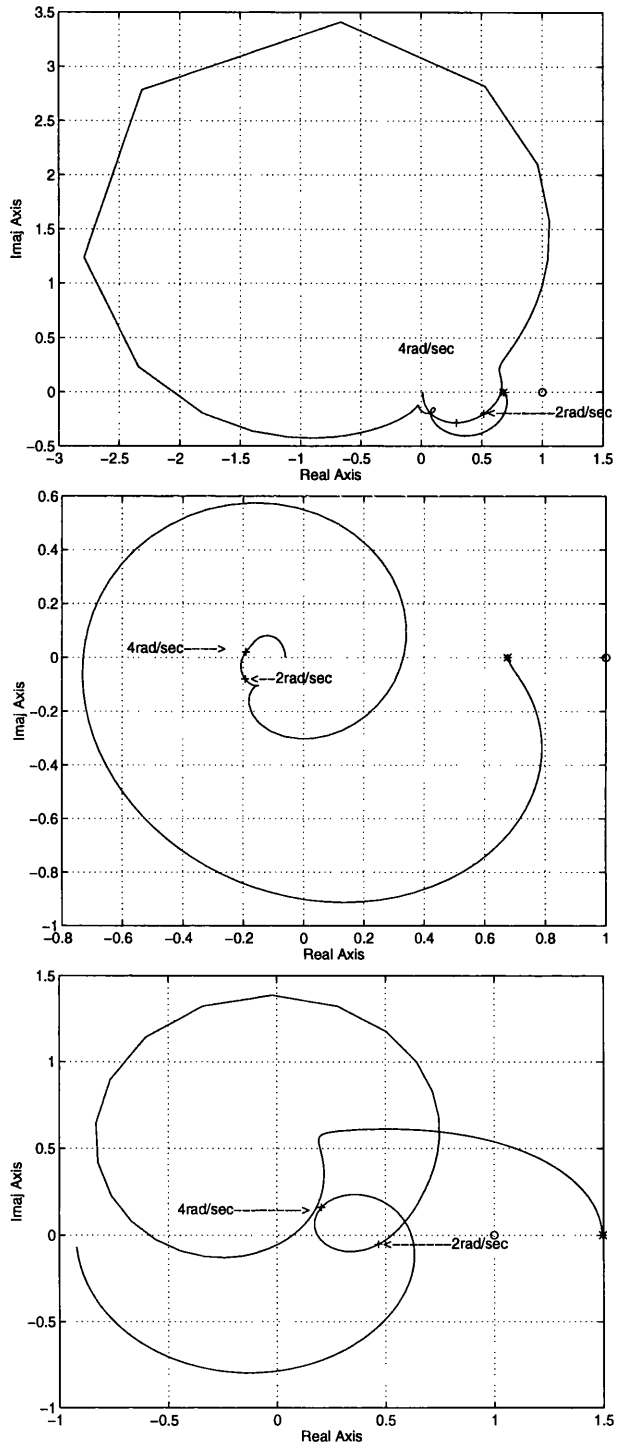

Figure 6.15: Nyquist plots of the multivariable structure functions $\Gamma_1(s)$, $\Gamma_2(s)$ and $\Gamma_3(s)$ for the amended system $G''(s)$

6.5 Feedback Controller

Once the structural problems have been solved, the path is clear for the design of the feedback controller. The amended transfer function matrix $G''(s)$ which henceforth will be called $G(s)$, represents the small signal relationship between the inputs, the vertical collective u_1, the longitudinal cyclic u_2, the lateral cyclic u_3, and the tail rotor collective u_4 to the outputs defined in equation(6.4). The $4x4$ system is structurally equivalent to the 4 SISO individual channels described by Leithead and O'Reilly [14].

$$C_1(s) = k_1 g_{11}(1-\gamma_1) \tag{6.24}$$

$$C_2(s) = k_2 g_{22}(1-\gamma_2) \tag{6.25}$$

$$C_3(s) = k_3 g_{33}(1-\gamma_3) \tag{6.26}$$

$$C_4(s) = k_4 g_{44}(1-\gamma_4) \tag{6.27}$$

where

$$\gamma_i =: \mid G_i \mid / g_{ii} \mid G^i \mid \; ; \quad i = 1,2,3,4 \tag{6.28}$$

where $\gamma_i(s)$ are as in the definition of equation(3.36).

In order to guarantee adequate robustness properties, the following points must be satisfied: a) $k_1 g_{11}(s)$, $k_2 g_{22}(s)$, $k_3 g_{33}(s)$ and $k_4 g_{44}(s)$ must have adequate gain and phase margins; b) the resulting Nyquist plots of $\gamma_1(s)$, $\gamma_2(s)$, $\gamma_3(s)$ and $\gamma_4(s)$ must not be close to the point (1,0) in the frequency range of interest 2-4 rad/sec; and c) the individual open-loop channels must have adequate gain and phase margins within the required channels crossover frequencies of 2-4 rad/sec.

An appropriate set of controllers $k_1(s)$, $k_2(s)$, $k_3(s)$ and $k_4(s)$ are given by,

$$k_1 = 0.037\frac{(s+0.6)(s^2+1.8s+1.64)(s^2+0.7s+11.27)}{s(s+1)(s^2+0.9s+6.96)(s+4)} \tag{6.29}$$

$$k_2 = 25\frac{(s+0.1)(s+0.8)(s^2+0.8s+0.97)(s^2+1s+4.25)}{s(s+0.01)(s^2+1.6s+1.85)(s+5)(s+10)^2} \times\frac{(s^2+s+11.8)}{(s^2+0.6s+9.09)} \tag{6.30}$$

$$k_3 = -2.5\frac{(s+0.02)(s+5)(s^2+0.6s+9.09)}{s(s+3)(s^2+0.8s+7.2)(s+4)} \tag{6.31}$$

$$k_4 = 80\frac{(s+0.65)(s^2+0.3s+0.44)(s^2+1.6s+4.64)}{s(s+0.37)(s+1.5)(s+5)(s+9)(s+10)} \times\frac{(s^2+1.6s+10.88)}{(s^2+0.8s+8)} \tag{6.32}$$

The Bode plots of $k_1g_{11}(s)$, $k_2g_{22}(s)$, $k_3g_{33}(s)$ and $k_4g_{44}(s)$ are shown in Figure(6.16). Inspection of these Bode plots shows that they all have appropriate gain and phase margins within the required crossover frequency. The stability margins of $k_1g_{11}(s)$, $k_2g_{22}(s)$, $k_3g_{33}(s)$ and $k_4g_{44}(s)$ are shown in Table 6.3. Therefore, the first requirement for robustness is satisfied

Transmittance	Phase Margin (deg)	Gain Margin (DB's)	BW's (rad/sec)
k_1g_{11}	78.5	∞	3.126
k_2g_{22}	71.93	18.58	3.165
k_3g_{33}	91.28	∞	2.975
k_4g_{44}	65.0	26.77	2.940

Table 6.3: Gain and phase margins of $k_1g_{11}(s)$, $k_2g_{22}(s)$, $k_3g_{33}(s)$ and $k_4g_{44}(s)$

In Figure(6.17), the Nyquist plots of the multivariable structure functions $\gamma_1(s)$, $\gamma_2(s)$, $\gamma_3(s)$ and $\gamma_4(s)$ are shown. From these figures it is possible to see that none of these plots are close to the point (1,0). Thus, point (b) is satisfied.

In Figure(6.18), the Bode plots of the open-loop channels transmittances $C_1(s)$, $C_2(s)$, $C_3(s)$ and $C_4(s)$ are shown. From these plots and their stability margins shown in Table 6.4, point (c) is also satisfied.

Transmittance	Phase Margin (deg)	Gain Margin (DB's)	BW's (rad/sec)
C_1	86.1	∞	2.066
C_2	80.62	18.65	2.0
C_3	74.77	∞, -28.67	2.29
C_4	65.93	19.92	2.028

Table 6.4: Gain and phase margins for channels $C_1(s)$, $C_2(s)$, $C_3(s)$ and $C_4(s)$

It just remains to check if the closed-loop single channels transmittances satisfy the requirements of design. The Bode plots of the closed-loop individual channels transmittances $Cl_1(s)$, $Cl_2(s)$, $Cl_3(s)$ and $Cl_4(s)$ are shown in Figures(6.19) and (6.20). Following the definition of bandwidth, Tischler [31], the resulting bandwidths for the closed-loop channels $Cl_1(s)$, $Cl_2(s)$, $Cl_3(s)$ and $Cl_4(s)$ are 3rad/sec, 2.91rad/se., 2.7rad/sec and 2.8rad/sec respectively. Therefore, the design specifications are satisfied.

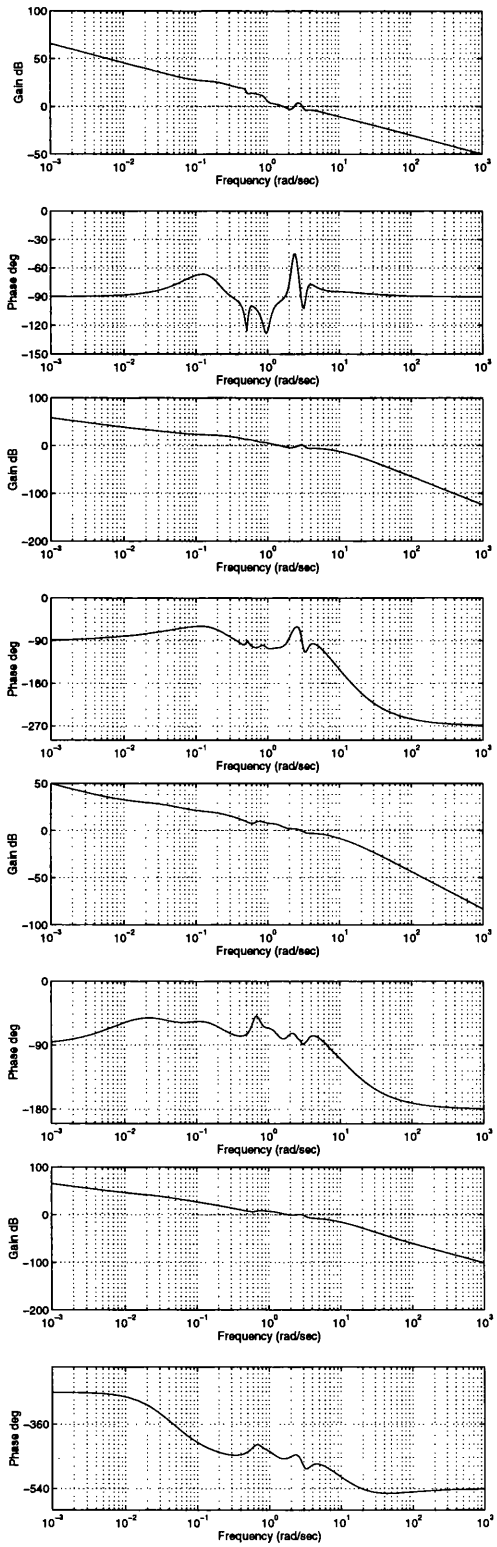

Figure 6.16: Bode plots of $k_1 g_{11}(s)$, $k_2 g_{22}(s)$, $k_3 g_{33}(s)$ and $k_4 g_{44}(s)$respectively.

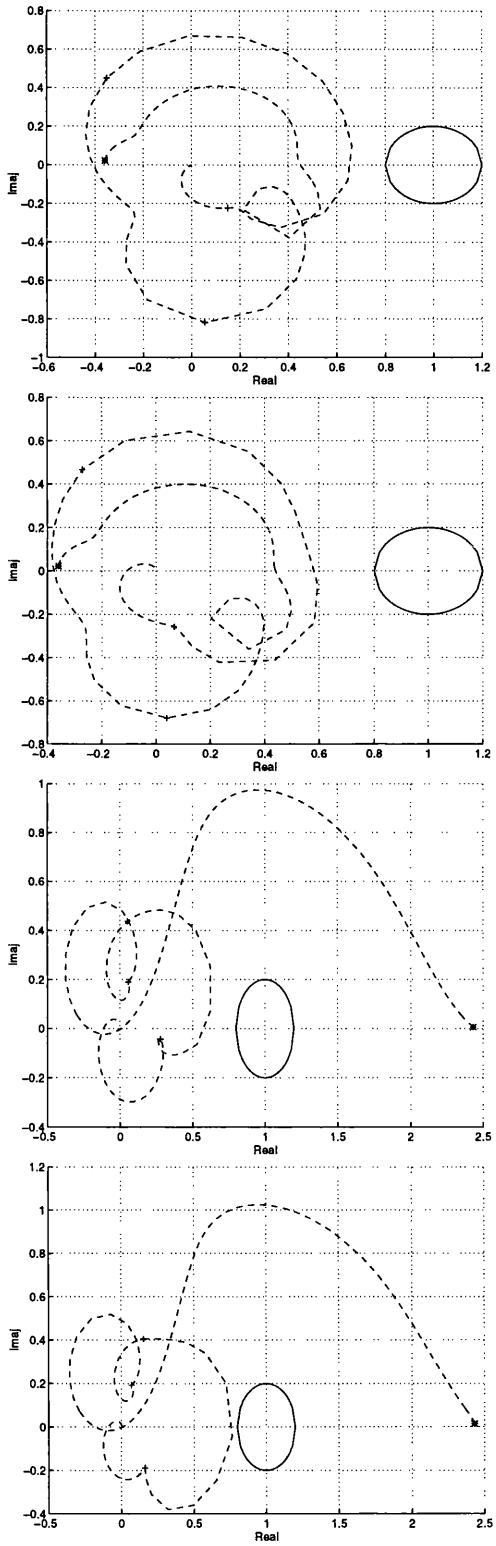

Figure 6.17: Nyquist plots of the multivariable structure functions $\gamma_1(s)$, $\gamma_2(s)$, $\gamma_3(s)$ and $\gamma_4(s)$

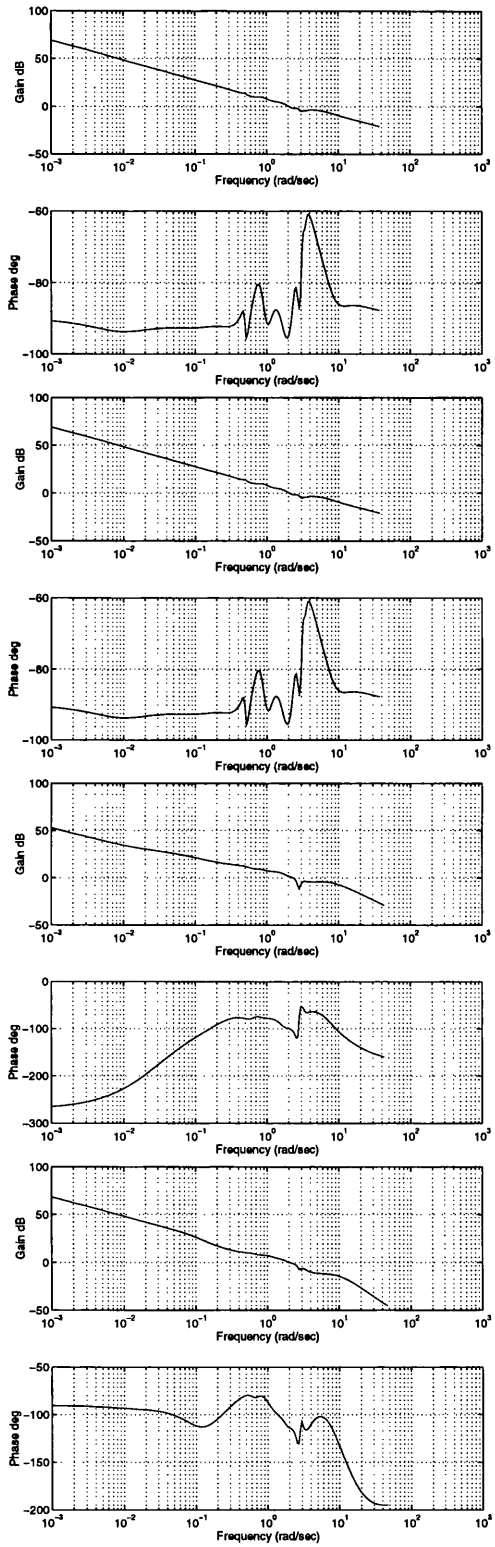

Figure 6.18: Bode plots of $C_1(s)$, $C_2(s)$, $C_3(s)$ and $C_4(s)$ respectively.

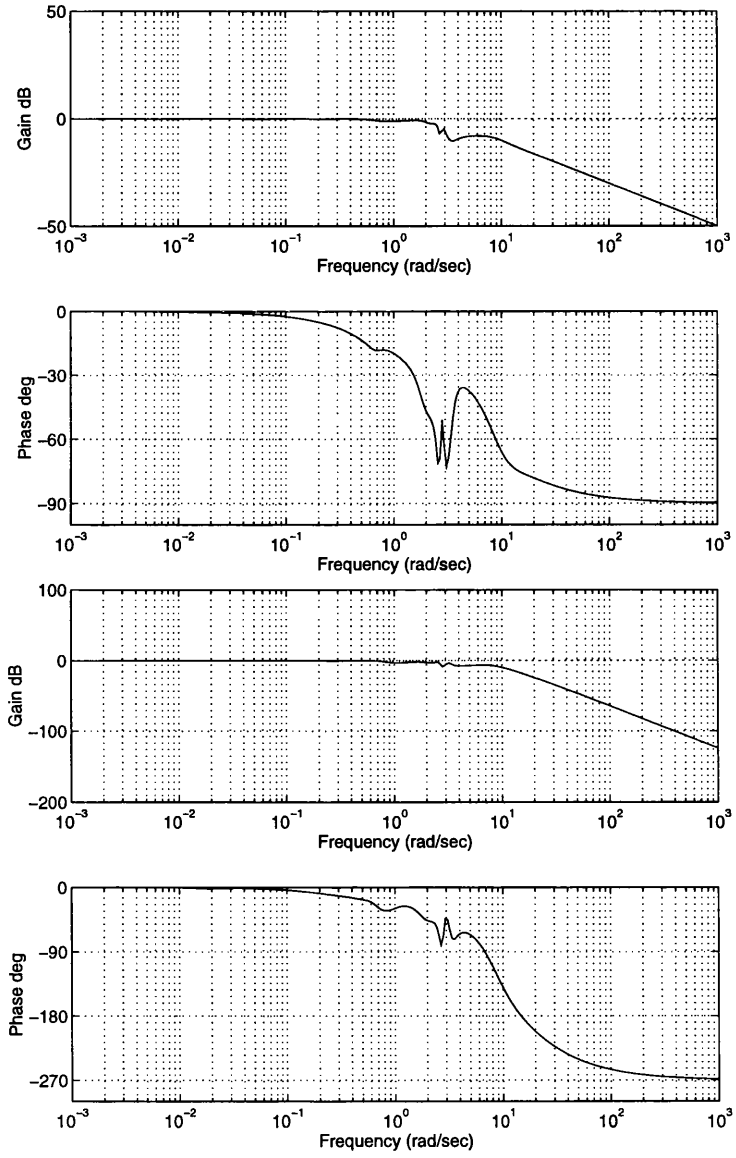

Figure 6.19: Bode plots of $Cl_1(s)$ and $Cl_2(s)$ respectively.

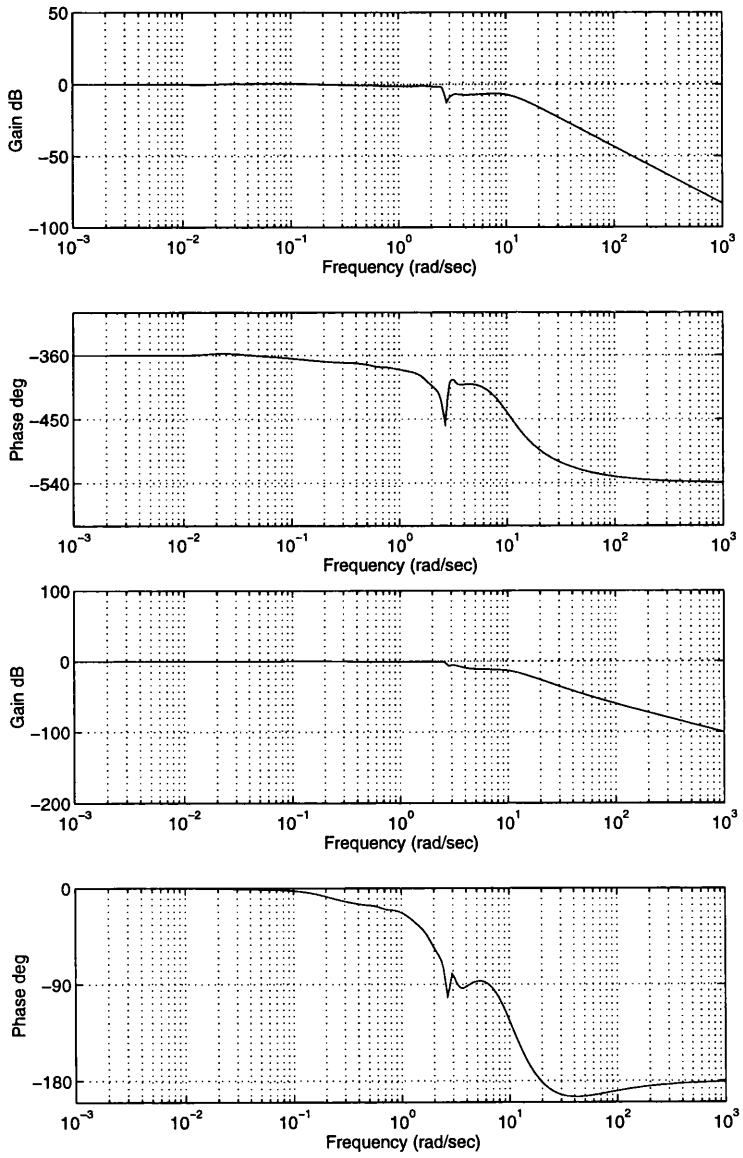

Figure 6.20: Bode plots of $Cl_3(s)$ and $Cl_4(s)$ respectively.

6.6 Cross-coupling Reduction

In this section, a pre-filter to the overall closed loop system is introduced in order to satisfy Level 1 handling quality specifications, Anonymous [1]. Despite the fulfilment of the design requirements for the individual channels, there remains some cross-coupling in the overall closed-loop system, specifically between the output y_1 (height rate) and the input references r_2, r_3 and r_4 for which it is now appropriate to design a pre-filter so as to decouple the overall closed-loop system, Leithead and O'Reilly [16]. A suitable pre-filter $Pr(s)$ is given by,

$$P_r = \begin{bmatrix} 1 & pr_{12} & pr_{13} & pr_{14} \\ 0 & 1 & 0 & pr_{24} \\ 0 & pr_{32} & 1 & pr_{34} \\ 0 & 0 & 0 & 1 \end{bmatrix} \tag{6.33}$$

where

$$\begin{aligned} pr_{12} &= -3500 \frac{s^2(s+1.5)(s^2+1.1s+4.925)}{(s+0.1)(s+0.4)(s^2+s0.2+7.57)(s+3)} \\ &\quad \times \frac{1}{(s+10)(s+15)} \end{aligned} \tag{6.34}$$

$$\begin{aligned} pr_{13} &= -2 \frac{s(s+0.01)^2(s+3)(s+5)(s^2+0.3s+8.43)}{(s+0.3)(s+0.4)(s^2+0.3s+7.58)(s^2+0.0.9s+10.44)} \\ &\quad \times \frac{1}{(s+1)(s+10)^2} \end{aligned} \tag{6.35}$$

$$\begin{aligned} pr_{14} &= -90000 \frac{s(s+0.01)(s^2+0.02s+0.49)}{(s+0.3)(s+1)^2(s^2+0.2s+7.57)(s+5)} \\ &\quad \times \frac{(s^2+0.7s+4.53)}{(s+7)(s+8)(s+15)} \end{aligned} \tag{6.36}$$

$$pr_{24} = -80\frac{s(s+0.01)(s^2+0.2s+0.57)(s+8)}{(s+3)(s+1)(s+1.5)(s+2.5)(s^2+3s+4.5)(s+20)} \quad (6.37)$$

$$pr_{32} = 350\frac{s(s+0.1)(s^2+1.4s+5.78)(s^2+s+9.25)}{(s+1.5)(s+2)(s+2.5)(s^2+0.2s+7.57)(s+3)} \quad (6.38)$$

$$pr_{34} = 500\frac{s(s+0.0006)(s^2+0.08s+0.16)}{(s^2+0.03s+0.0004)(s+0.5)(s^2+0.4s+7.6)} \times\frac{(s^2+0.8s+5.45)(s^2+4.2s+6.97)}{(s+4)(s+5)(s^2+21.4s+141.53)} \quad (6.39)$$

In Figures(6.21)-(6.28), the step responses of the overall control system indicate adequate transient behaviour with acceptably low cross-coupling.

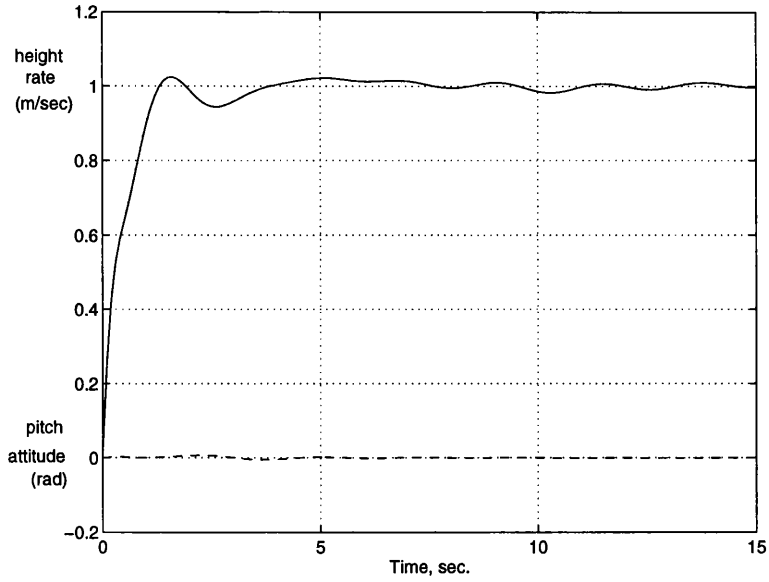

Figure 6.21: Time responses of height rate and pitch attitude to unity step change in input 1.

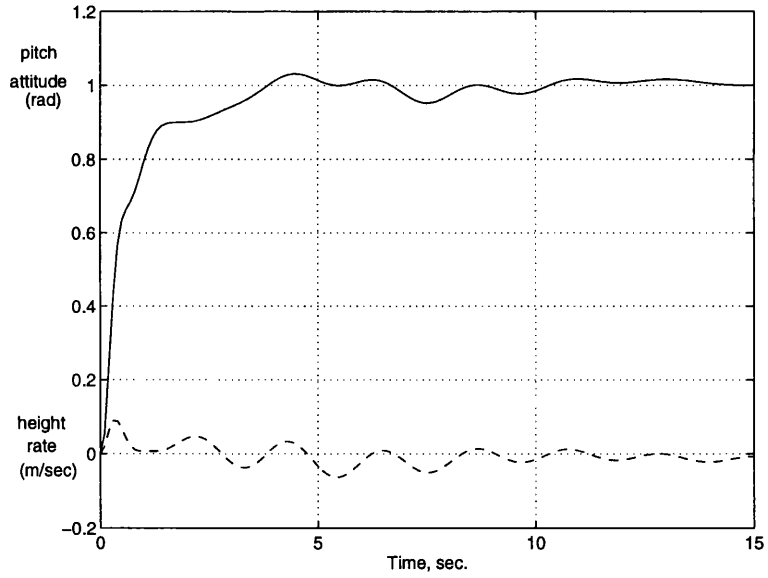

Figure 6.22: Time responses of height rate and pitch attitude to unity step change in input 2.

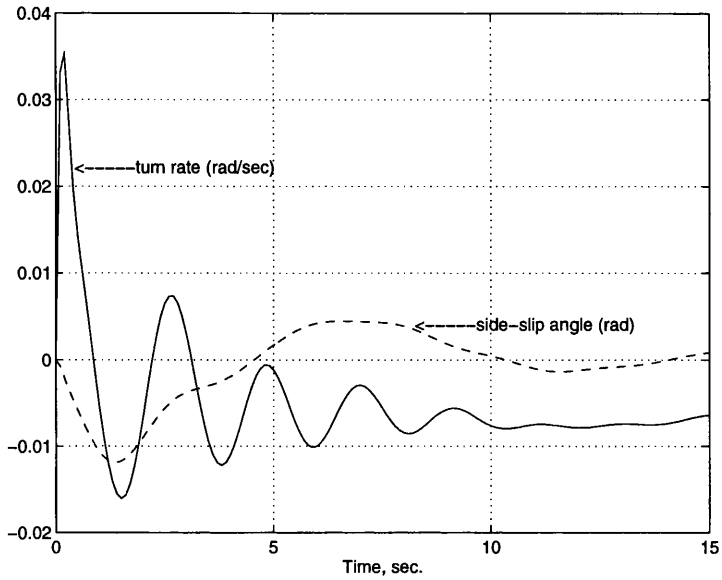

Figure 6.23: Time responses of turn rate and side-slip angle to unity step change in input 1.

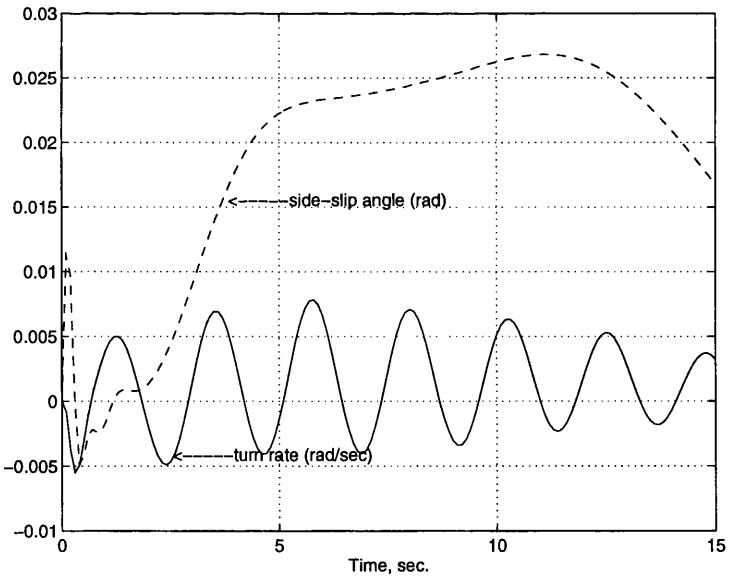

Figure 6.24: Time responses of turn rate and side-slip angle to unity step change in input 2.

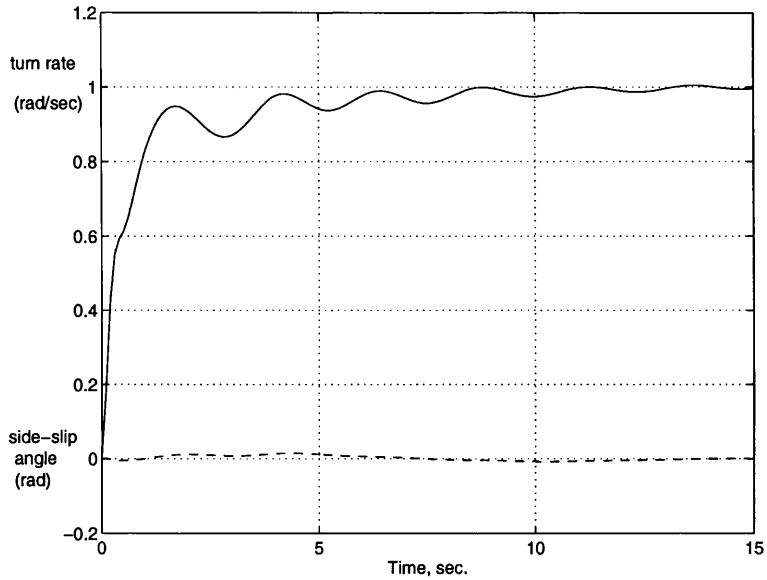

Figure 6.25: Time responses of turn rate and side-slip angle to unity step change in input 3.

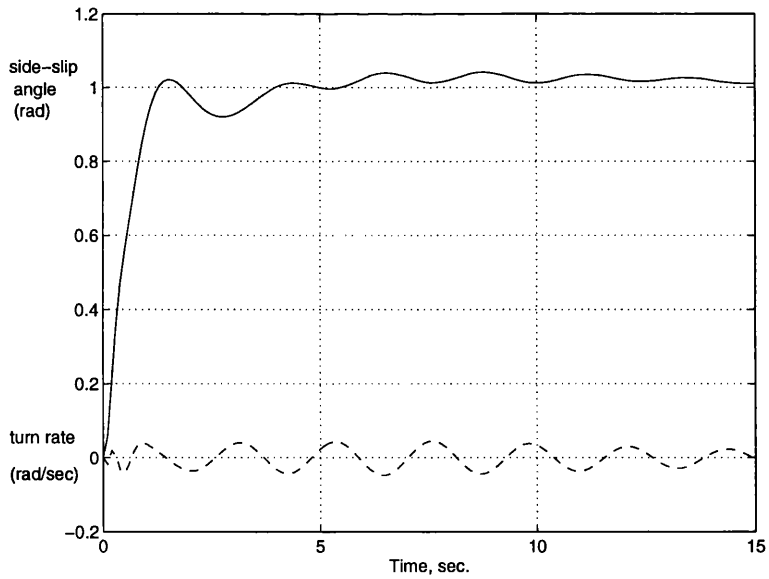

Figure 6.26: Time responses of turn rate and side-slip angle to unity step change in input 4.

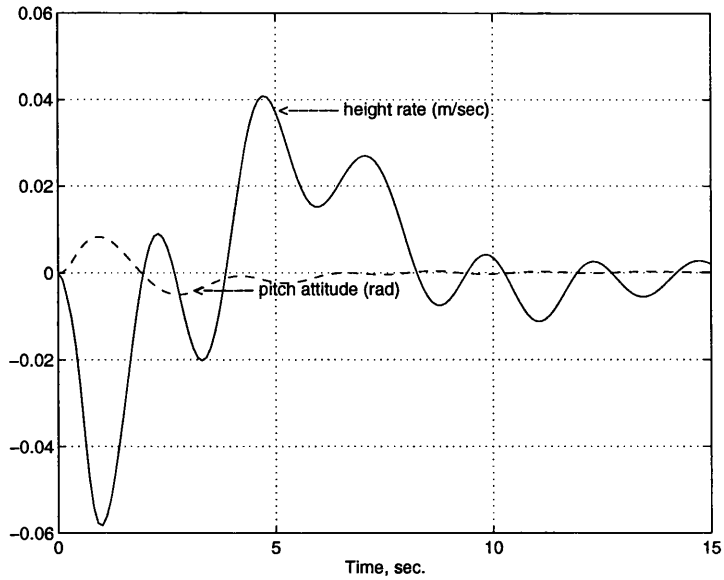

Figure 6.27: Time responses of height rate and pitch attitude to unity step change in input 3.

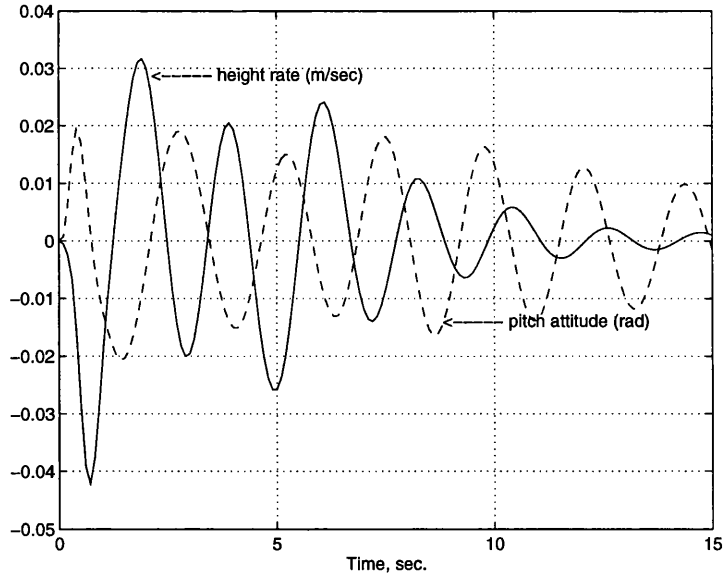

Figure 6.28: Time responses of height rate and pitch attitude to unity step change in input 4.

6.7 Higher-order Model Evaluation

As it was mentioned in Manness *et al* [21], low-order rigid body dynamics models are the prime focus of a flight control system. This is made possible by the assumption that the unmodelled dynamics are at frequencies higher than the required channel cross-over frequencies. Therefore, channel roll-off must be able to cope with the problems introduced by the unmodelled dynamics. However, problems may turn up specifically with the unmodelled dynamics relatively close to the channel cross-over frequencies. Hence, any control system must be evaluated on the basis of a higher order model. In order to perform this evaluation, the control system designed in Sections 6.4 and 6.5 are applied to a higher-order model which include a simplified low-order representation of the actuators and rotor dynamics.

The higher-order model derived from Padfield [28] is a linear model in state space representation of the helicopter at 30 knots that includes eight rigid-body states, four actuators states and six rotor flapping states. The six rotor states correspond to the coning, advancing flap and regressing flap modes with poles at about $-15.5112 \pm 69.6627i$, $-15.8541 \pm 35.5185i$ and $-8.4847 \pm 10.4052i$. The actuators are represented as first order lags of the form:

$$Ac(s) = \frac{a}{(s+a)} \tag{6.40}$$

with poles at -12.6rad/sec except for the tail rotor collective pitch whose pole is at -25rad/sec.

The resulting matrix transfer function for the higher order model associate to the state space representations is given by:

$$G(s) = \begin{bmatrix} G_1(s) \\ \dots \\ G_2(s) \end{bmatrix} \tag{6.41}$$

where

$$G_1(s) = \frac{1}{\triangle} \begin{bmatrix} 1145.23 & 115.5937 & -0.00794 & 3.9791 \\ -15.4489 \pm 69.5153i & -23.5287 \pm 58.7970i & -1216.7228 & 95.4733 \\ -15.9267 \pm 35.4863i & -0.0836 \pm 39.6417i & 595.61 \pm 849.76i & -15.7013 \pm 69.5022i \\ -25.0000 & -15.8418 \pm 35.6449i & -15.804 \pm 35.510i & -15.8541 \pm 35.5192i \\ -8.8793 \pm 9.9846i & -25.0 & -32.1697 & -8.2840 \pm 11.3456i \\ -12.6 & -8.0174 \pm 10.0828i & -25.0 & -12.8540 \\ -7.5398 \pm 2.7269i & -12.6000 & -2.5024 \pm 12.793i & -12.6023 \\ -0.5368 \pm 0.9993i & -12.6000 & -12.6 & -12.5989 \pm 0.0019i \\ 0.0934 \pm 0.3141i & -0.3166 \pm 1.0603i & -0.1810 \pm 1.2443i & -4.7094 \\ -0.0033 & -0.9215 & -0.923 & 2.4299 \\ -12.6 & -0.0409 & -0.224 & -0.8251 \\ & 0.0586 & 0.0538 & 0.0852 \\ & & -12.6 & 0.0519 \\ & & & \\ 18.5648 & 1.8737 & 0.0001 & 13.2451 \\ -2.4577 \pm 86.1169i & -265.6346 & -62759.48 & -16.8739 \pm 69.5898i \\ -50.3353 & 109.0109 \pm 211.19i & 62731.04 & -15.8538 \pm 35.5193i \\ -13.0645 \pm 35.669i & -15.8064 \pm 35.5508i & -15.8054 \pm 35.5057i & -8.2240 \pm 11.643i \\ -25.0000 & -25.0000 & -31.1753 & -12.8429 \\ -7.1097 \pm 12.0593i & -8.0231 \pm 10.1181i & -25.0000 & -12.6030 \pm 0.0053i \\ -12.6000 & -12.6000 & -1.9011 \pm 13.2977i & -12.5940 \\ -12.6000 & -0.3192 \pm 1.0606i & -12.6000 & -5.0102 \\ -0.5308 \pm 0.7579i & -0.5196 & -12.6000 & 2.3184 \\ 0.2131 & -0.0371 & -0.1777 \pm 1.2341i & -0.4980 \\ -0.0184 \pm 0.0176i & -0.0177 & -0.5245 & 0.0910 \\ & -12.6000 & -0.2299 & -0.0133 \\ & & -0.0144 & \end{bmatrix} \quad (6.42)$$

$$G_2(s) = \frac{1}{\triangle}\begin{bmatrix}
173.3742 & 17.4962 & -0.000633 & -326.3738 \\
-13.6689 \pm 67.2367i & -148.4661 & -7939.047 & -15.5136 \pm 69.6784i \\
-15.0975 \pm 35.3255i & 123.9914 & 7079.453 & -15.8541 \pm 35.5184i \\
-25.0000 & -15.9447 \pm 35.5677i & 812.4028 & -8.4484 \pm 10.2696i \\
-13.2353 \pm 8.0829i & -30.4083 & -15.8565 \pm 35.5423i & -12.8944 \\
-12.6000 & -25.0000 & -25.0000 & -12.6005 \pm 0.0008i \\
-7.7095 & -12.6000 \pm 0.0000i & -14.2377 & -12.5991 \\
-3.9813 & -4.8189 \pm 6.7611i & -12.6000 & -3.0724 \\
-0.2150 \pm 0.5206i & 0.2036 \pm 1.6044i & -1.9660 \pm 0.8656i & -0.0968 \pm 0.4977i \\
0.0515 \pm 0.4736i & 0.9876 & 0.6836 \pm 1.4258i & 0.0868 \pm 0.3747i \\
0.0308 & -0.9682 & 0.0428 \pm 0.4859i & -0.2381 \\
-12.6000 & -0.0035 \pm 0.3131i & -0.4516 & \\
 & & -12.6000 & \\
-0.0799 & -0.0081 & 0.0002 & 2.9413 \\
-770.9186 & -415.109 \pm 540.7946i & -33262.7493 & -15.496 \pm 69.6564i \\
-17.28368 \pm 64.007i & -15.9358 \pm 35.57285i & 33188.3518 & -15.854 \pm 35.5184i \\
-15.1456 \pm 34.4829i & -26.1320 & -15.8548 \pm 35.5433i & -41.3346 \\
-25.0000 & -25.0000 & -25.0000 & -8.4941 \pm 10.2405i \\
-14.2733 \pm 7.9997i & 10.3279 \pm 6.4722i & 18.6408 & -12.8945 \\
-12.6000 & -12.6000 & -13.9689 & -12.6017 \pm 0.0030i \\
-12.6000 & -4.6579 \pm 6.0829i & -12.6000 & -12.5966 \\
-6.3932 & 0.2356 \pm 0.9260i & 9.0647 & -3.0608 \\
-4.7604 & -0.4632 & -1.9575 & 0.0592 \pm 0.4110i \\
0.0485 \pm 0.4791i & 0.0593 & -1.1754 & -0.3566 \\
-0.2939 & -12.6000 & -0.4274 & 0.0511 \\
-0.0127 & & 0.1238 \pm 0.3156i &
\end{bmatrix} \quad (6.43)$$

with the characteristic polynomial

$$\begin{aligned}\triangle \;=\; & [1, -15.5112 \pm 69.6627i, -15.8541 \pm 35.5185i, -25, -8.4847 \pm 10.4052i, \\ & -12.8939, -12.6010 \pm 0.0018i, -12.5980, -3.1026, -0.3280 \pm 1.1120i, \\ & 0.0916 \pm 0.4605i, -0.3864, -0.0005] \end{aligned} \quad (6.44)$$

and the set of finite multivariable transmission zeros

$$T_z \;=\; \{-15.8696 \pm 35.5381i, -3.8754 \pm 7.7958i, -0.0098\} \quad (6.45)$$

Inspection of equations(6.6), (6.7), (6.41) and (6.44) shows that the dynamics of the actuator and rotor dynamics introduce changes at frequencies far from

the region of interest for analysis and design purposes (0-4 rad/sec). This is also corroborated by the multivariable structure functions of the higher-order model. In Figure(6.29), the Nyquist plots of the multivariable structure functions $\Gamma_{1h}(s)$, $\Gamma_{2h}(s)$ and $\Gamma_{3h}(s)$ ($\Gamma_{4h}(s) = 0$) for the higher-order model are shown. Comparison with those of the low order model in Figure(6.1), shows that there are not any differences between these plots in the frequency range of interest, namely 0-4rad/sec. Therefore, there are not significant changes in the control system when this is applied to the higher-order model. However, as the actuators are approximated by first order lags with poles at -12.6 rad/sec except for the tail rotor collective pitch whose pole is at -25 rad/sec, a phase lag of approximately -10 to -15 degrees in each channel may affect the performance of the system around 2 to 4 rad/sec. Hence, performance evaluation is required in order to guarantee Level 1 handling qualities by the control system with the higher-order model. This evaluation is performed in both the frequency and the time domain by analysing the Bode diagrams and the unity step responses of the overall closed-loop channels.

In Figures(6.30) and (6.31), the Bode plots of the closed-loop channels for the higher-order model are shown. The resulting bandwidths for the higher-order closed-loop channels $Cl_{1h}(s)$, Cl_{2h}(s), Cl_{3h}(s) and Cl_{4h}(s) are 2.7rad/sec, 2.7rad/sec, 2.5rad/sec and 2.8rad/sec respectively. In Figures(6.32)-(6.39), the time responses of the control system with the higher-order model are shown. Comparison of the step responses of Figures(6.32)-(6.39) and Figures(6.21)-(6.28) together with the resulting channels bandwidths of the higher-order model, shows that the design specifications are not significantly altered by the introduction of the unmodelled rotor and actuators dynamics.

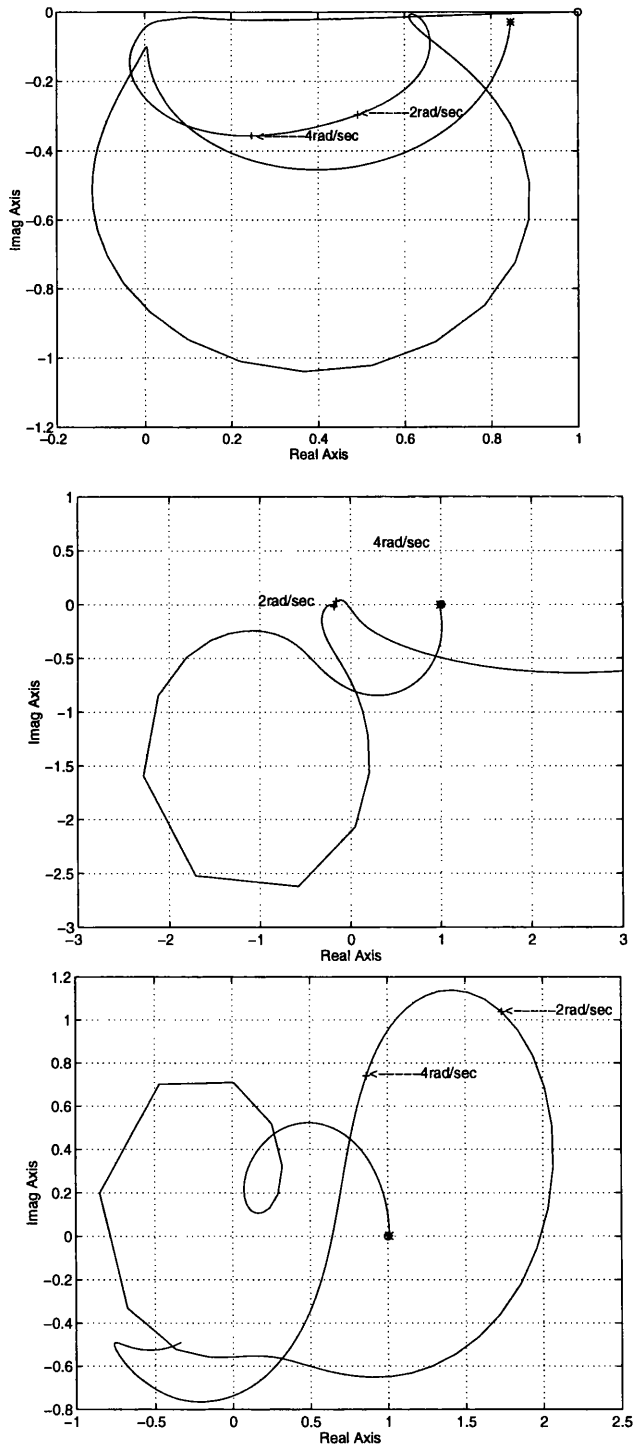

Figure 6.29: Nyquist plots of the multivariable structure functions $\Gamma_{1h}(s)$, $\Gamma_{2h}(s)$ and $\Gamma_{3h}(s)$

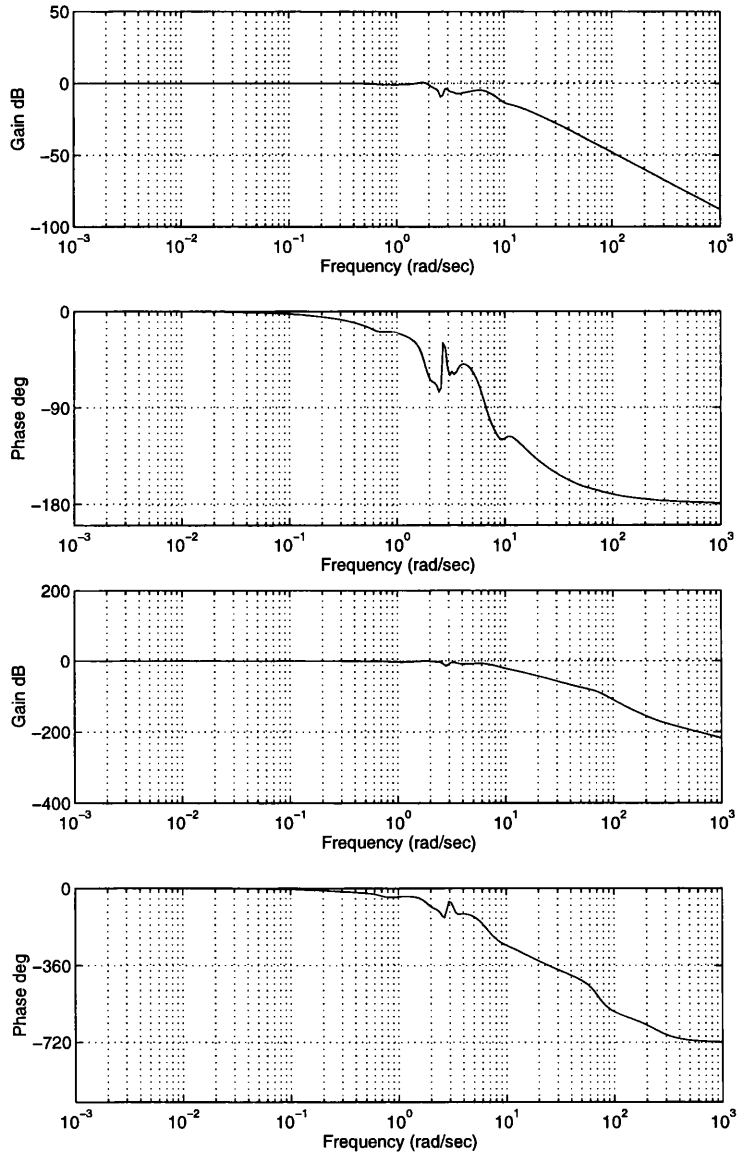

Figure 6.30: Bode plots of $Cl_{1h}(s)$ and $Cl_{2h}(s)$ respectively.

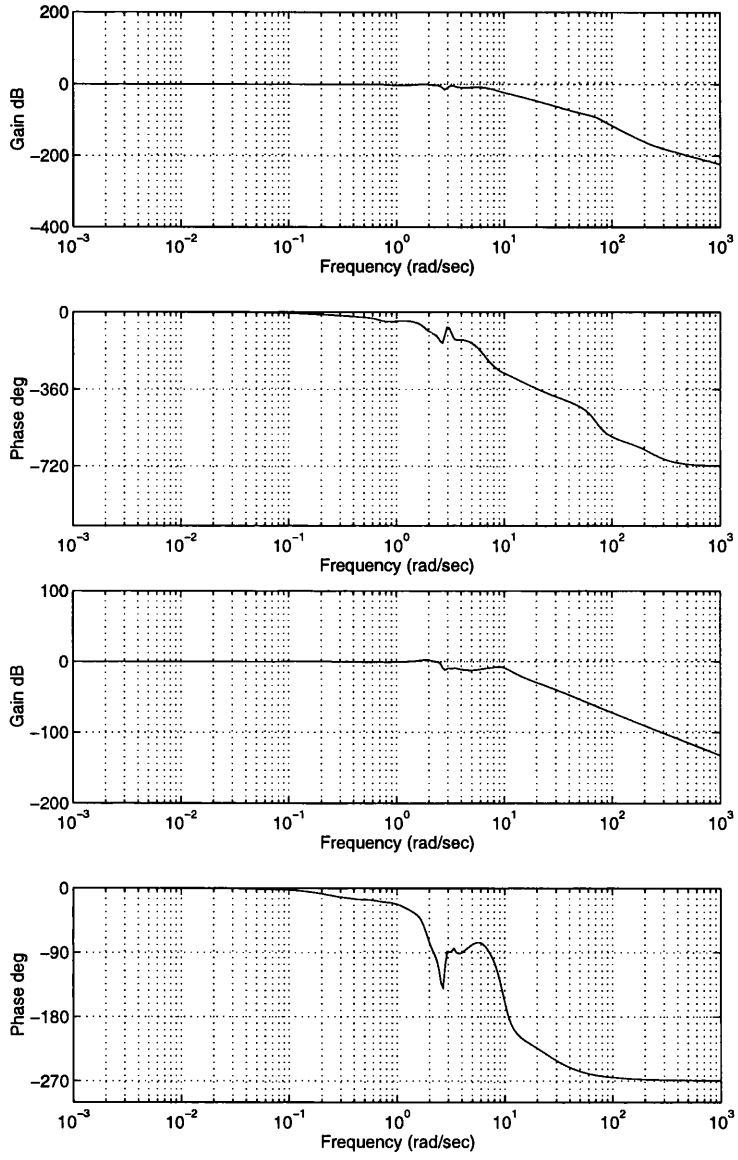

Figure 6.31: Bode plots of $Cl_{3h}(s)$ and $Cl_{4h}(s)$ respectively.

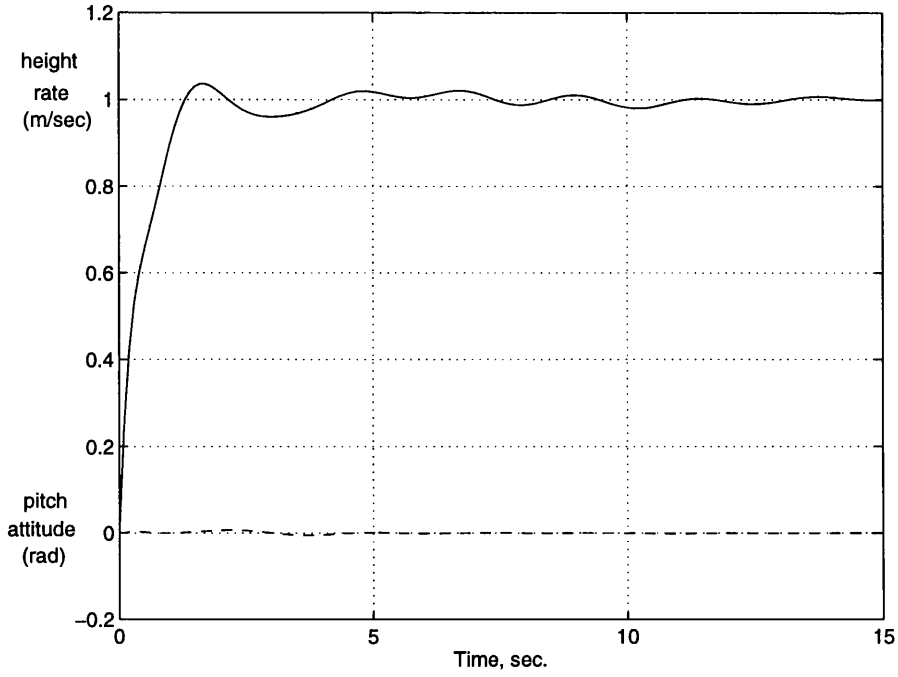

Figure 6.32: Time responses of height rate and pitch attitude to unity step change in input 1 (higher order model).

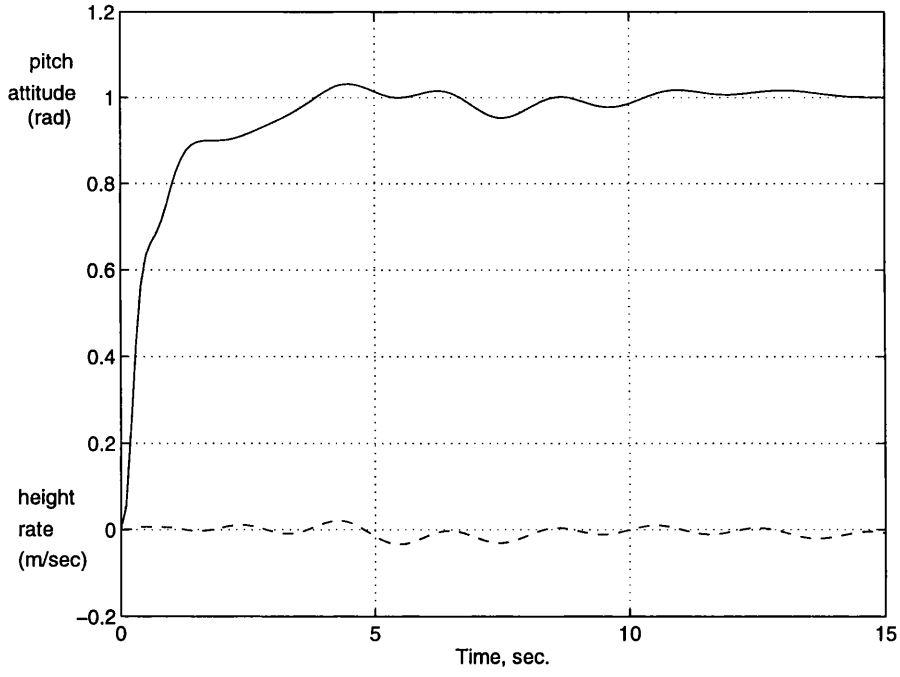

Figure 6.33: Time responses of height rate and pitch attitude to unity step change in input 2 (higher order model).

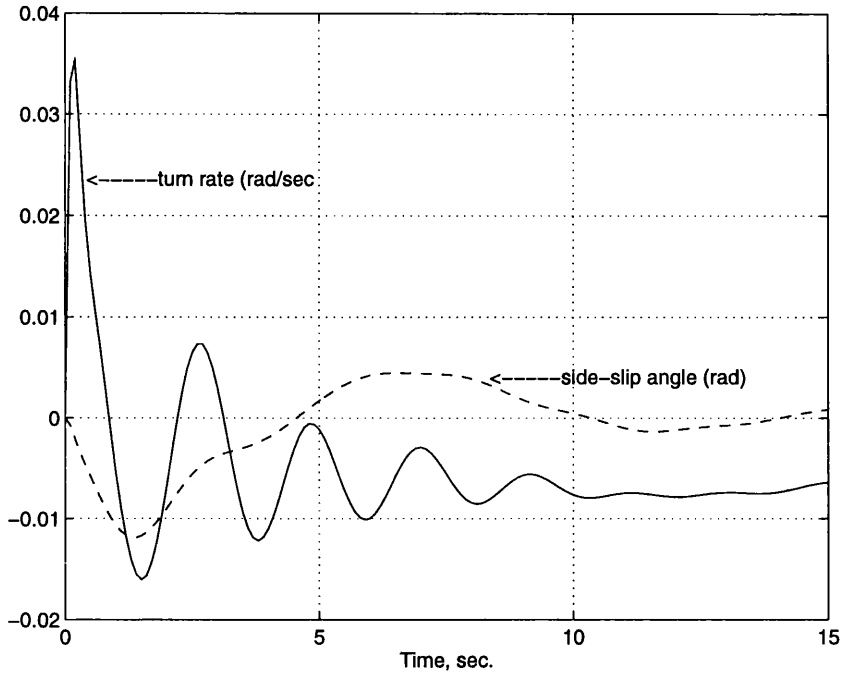

Figure 6.34: Time responses of turn rate and side-slip angle to unity step change in input 1 (higher order model).

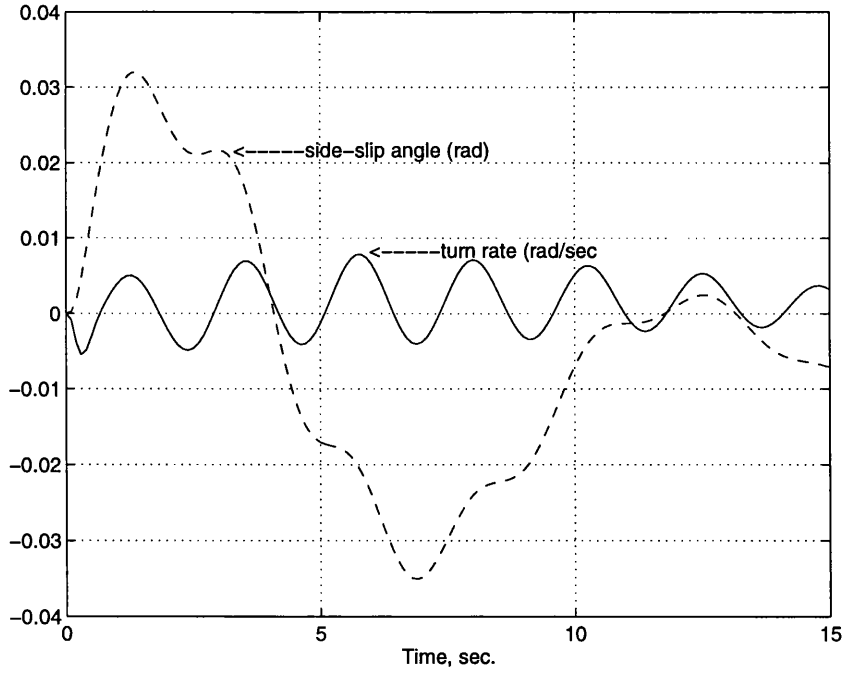

Figure 6.35: Time responses of turn rate and side-slip angle to unity step change in input 2 (higher order model).

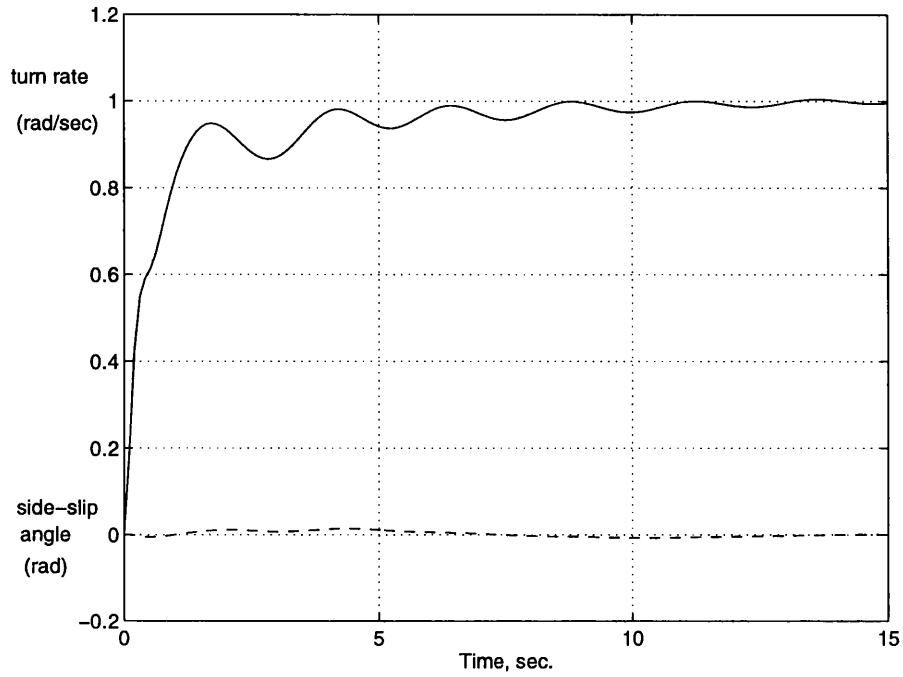

Figure 6.36: Time responses of turn rate and side-slip angle to unity step change in input 3 (higher order model).

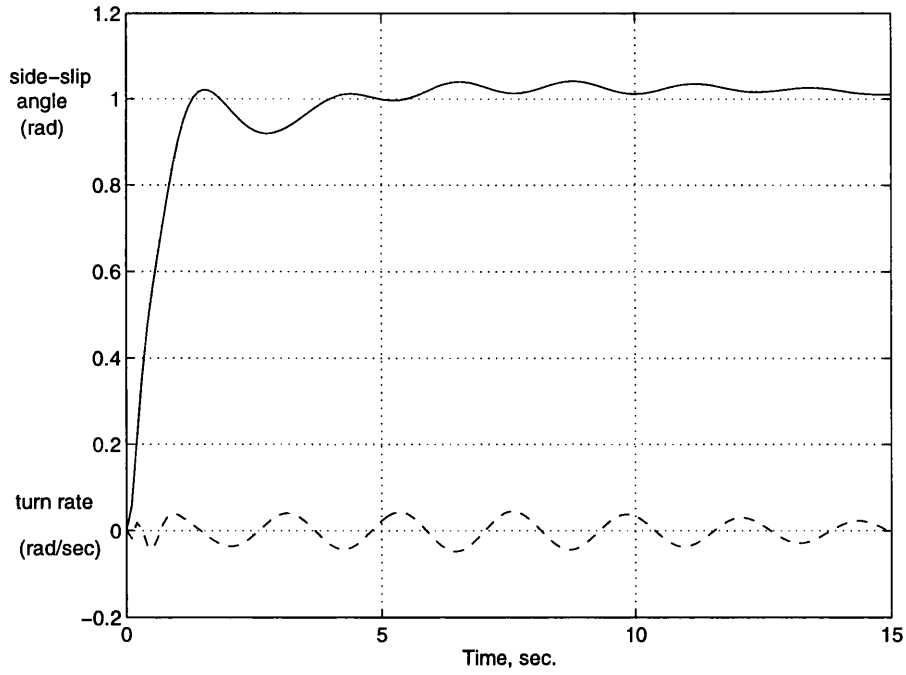

Figure 6.37: Time responses of turn rate and side-slip angle to unity step change in input 4 (higher order model).

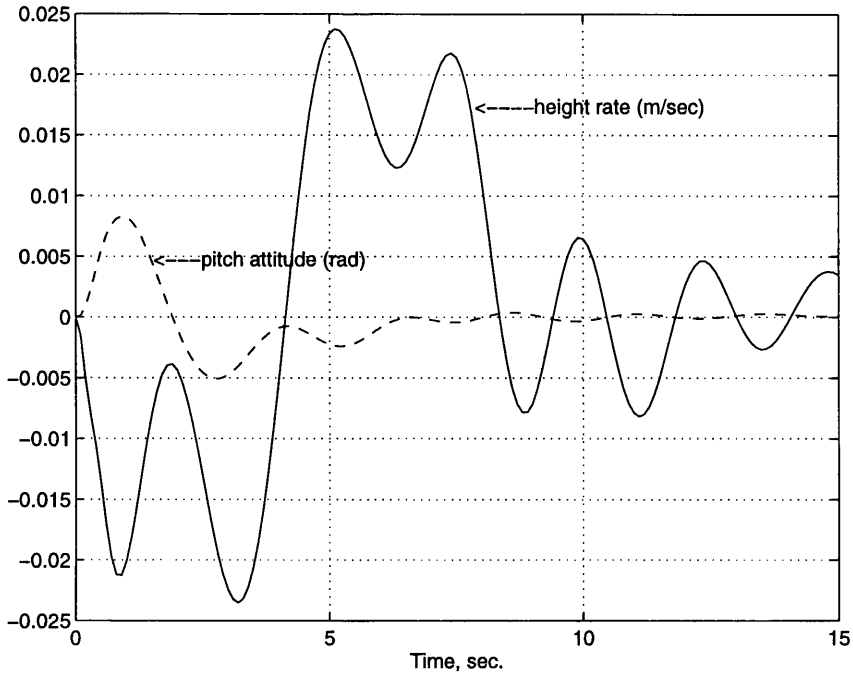

Figure 6.38: Time responses of height rate and pitch attitude to unity step change in input 3 (higher order model).

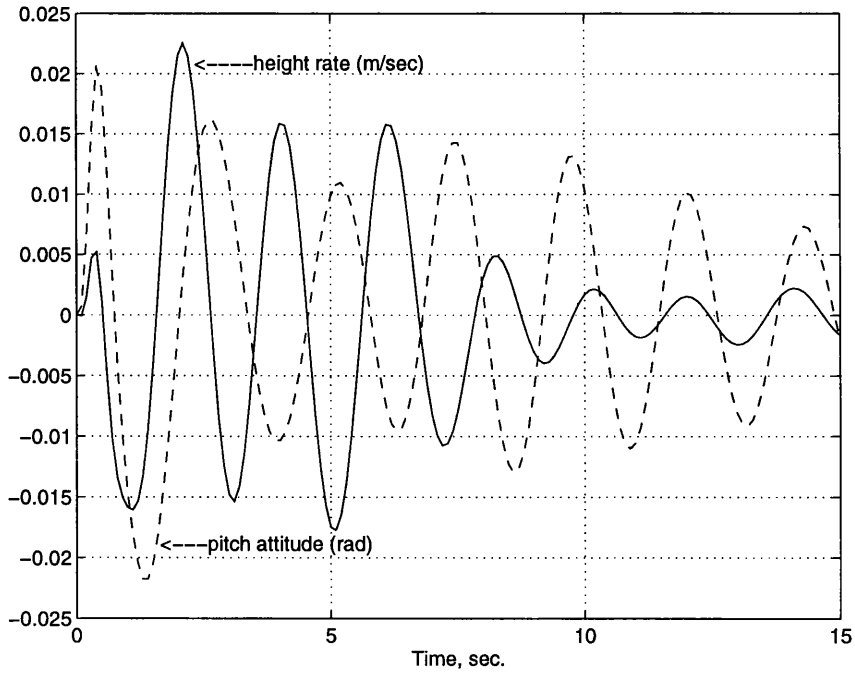

Figure 6.39: Time responses of height rate and pitch attitude to unity step change in input 4 (higher order model).

6.8 Assessment at Different Speeds

As it was mentioned in O'Reilly and Leithead [27], the ICD approach is more a framework of analysis than design. However, throughout this Chapter and in the previous design in Chapters 4 and 5, it was also established that it can be a powerful tool for design where a multivariable control system can be designed in a very transparent way using simple classical control theory tools. In Figure(6.40), the block diagram of the control system for the helicopter at 30 knots is shown. This control system may appear complicated, but similar to the 80 knots control system it should be noted that all the matrices are sparse; $M(s)$ has only one entry, $P(s)$ consists of 1's and 0's with only 2 non-unity off diagonal entries, $F(s)$ has only 3 entries and $K(s)$ has 4 diagonal entries. Also, the resulting control system is very similar to that at 80 knots. Therefore, in this section interest is focused on the robustness of the control system over a range of different speeds. This could be useful, in order to use the ICD approach as a way of designing a scheduled control system for the helicopter.

To assess the performance and robustness of the control system in a region of operation, it is applied to the linear models of the helicopter at 20 knots, 25 knots, 35 knots and 40 knots forward flight. These models include the approximations of the rotor and actuator dynamics. The matrix transfer functions of these systems are shown in Appendix A. All the steps of the design were repeated to verify that the design requirements are satisfied along this range of speeds. In order to reduce the number of figures, and because most of the plots do not change significantly from those of the 30 knots design, these plots are not shown except for those which are necessary. It was found that the control system can be applied with adequate robustness and performance properties in the range of 25 to 35 knots despite the fact of good step responses from 20 to 40 knots. That is, at 20 and 40 knots the control system presents robustness problems.

In Figure(6.41) the Nyquist plot of $\gamma_{34}h_{22}(s)$ Table 6.2 for the system at 40 knots is shown. This plot shows that the matrix $M(s)$ in equation(6.10) is not a weak-feedback for the model at 40 knots due to its closeness to the point (1,0). That is, application of matrix $M(s)$ to the model at 40 knots increases the uncertainty effects on the individual transfer function $g_{34}(s)$. Also, the structure of the system (number of RHPP'z and RHPZ's) is uncertain. Therefore, the robustness of the control system *can not* be guaranteed.

In Figure(6.42), the Nyquist plots of the multivariable structure function $\gamma_2(s)$ for channel 2 in equation(6.25) for the model at 20 knots is shown. From this plot, it is possible to see that $\gamma_2(s)$ is close to the point (1,0) at round 3 rad/sec. Therefore, channel 2 for the model at 20 knots suffers from structural sensitivity at frequencies close to the channel cross-over frequency that can introduce a pair of RHPZ's at round 3rad/sec Leithead and O'Reilly [15].

However, the modifications required in the control system to improve the robustness of the control system at 20 and 40 knots are very simple. For instance, if the gain of the feedback function $m(s)$ in equation(6.9) is increased to 1.7 then, matrix $M(s)$ in equation(6.10) would satisfy the *weak feedback* requirements to the model at 40 knots. Also, if controller $k_1(s)$ in equation(6.29) is updated to

$$k_1 = 0.037\frac{(s+0.6)(s^2+1.8s+1.64)(s^2+0.7s+11.27)}{s(s+1)(s^2+0.9s+6.96)(s+8)} \qquad (6.46)$$

the Nyquist plot of $\gamma_2(s)$ in equation(6.25) will not be close to the point (1,0), resulting in the elimination of the structural sensitivity problem in channel 2 for the model at 20 knots.

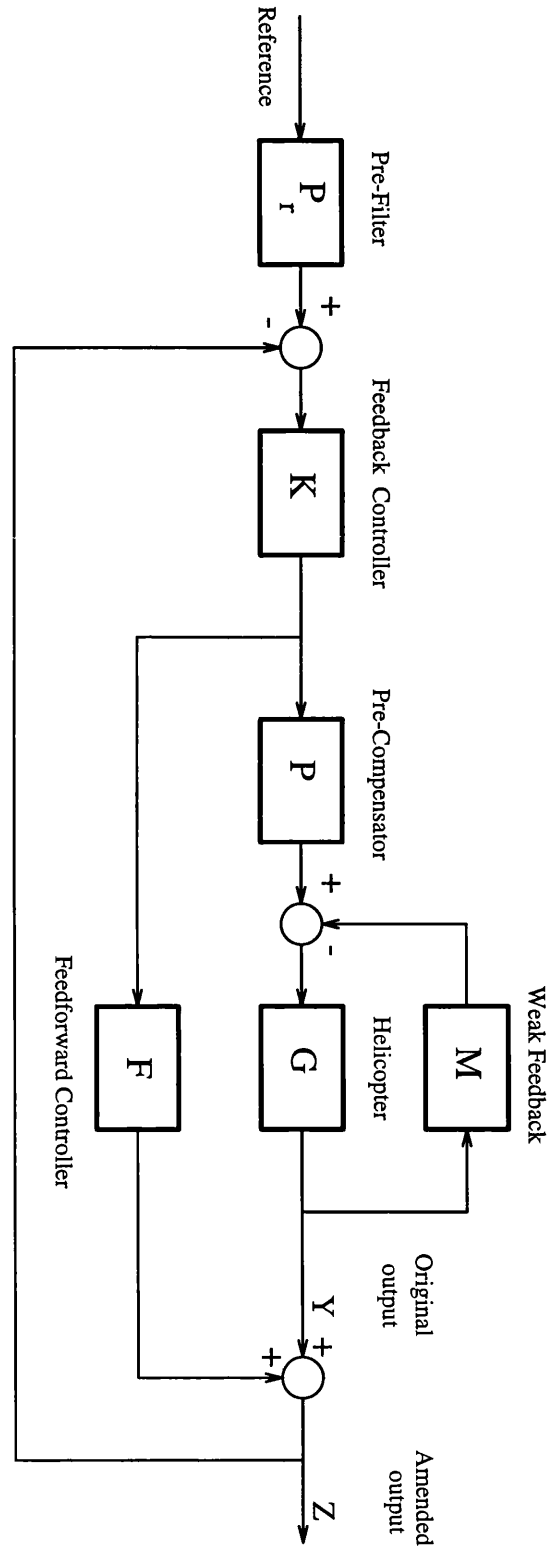

Figure 6.40: ICD Flight control system of the helicopter at 30 knots forward flight

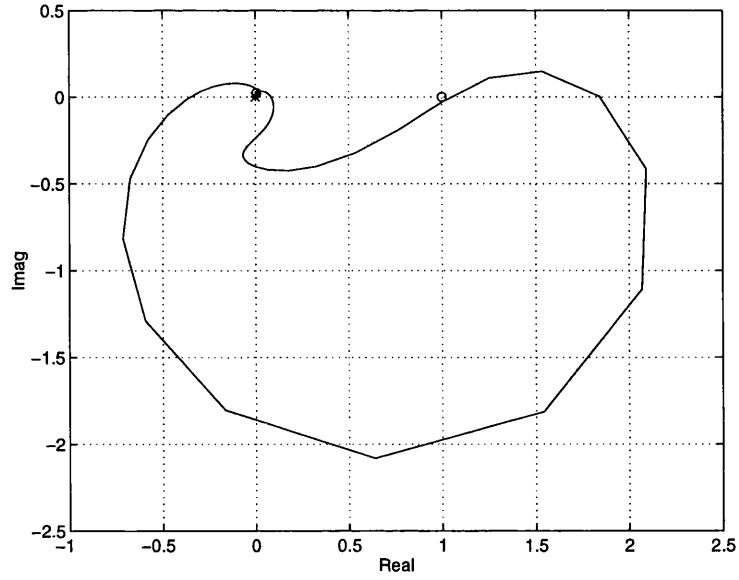

Figure 6.41: Nyquist plot of $\gamma_{34}h_{22}$ for the 40 knots model

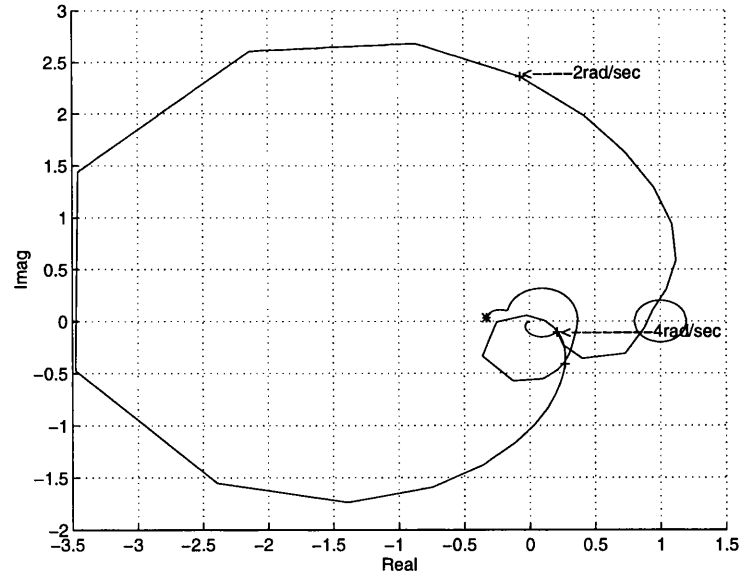

Figure 6.42: Nyquist plots of γ_2 for the 20 knots model

6.9 Conclusions

The objective of this chapter is to continue the design of a control system for a typical single main rotor helicopter. In Chapters 4 and 5 the potential of the ICD as a framework of analysis and design for the helicopter was explored. This analysis and design were developed on the basis of a standard flight condition, namely 80 knots forward flight. In this Chapter, the analysis and design of a control system for the helicopter at 30 knots forward flight following the results obtained in Chapters 4 and 5 is presented. It was found that the helicopter presented two important differences between high and low speed conditions: a) at high speed 60 to 90 knots, the helicopter decouples *for design purposes* into lateral and longitudinal dynamics, whereas at low speed, 20 to 60 knots the system can not be decomposed into lateral and longitudinal dynamics; b) at low speed the sensitivity problems of the system are more acute and severe at low frequency while at high speed the sensitivity problems arise at frequencies close to the channel cross-over frequencies. Due to the system not decoupling into lateral and longitudinal dynamics, the design was carried out on the basis of the full $4x4$ system. Following the results of Chapter 5, a feedforward controller is used to overcome the sensitivity problem that introduces a lack of stability robustness. The resulting closed-loop bandwidths of the four channels are within Level 1 handling quality specifications. Furthermore, the step responses of the overall $4x4$ closed-loop system indicates satisfactory transient behaviour with acceptably low cross-coupling.

Also, the control system was evaluated against a higher-order model which includes approximations of the rotor and actuator dynamics. It was found that the control system satisfies the design specifications in Level 1 handling quality when this is applied to the higher-order model.

A second evaluation of the control system was carried out by the application of the control system to the linearised models of the helicopter from 20 to 40 knots forward flight. It was found that despite acceptable step responses from

20 to 40 knots, the robustness of the system can be guaranteed only from 25 to 35 knots. However, it was also found that in order to get appropriate robustness characteristics at 20 and 40 knots, the control system requires simple modifications. Therefore, a gain scheduling control system between different forward flight conditions should be facilitated by the former and by fact that the elements of the control system are sparse.

Chapter 7

Analysis and Design for Hover

7.1 Introduction

Following the results obtained in Chapters 4, 5 and 6 for the control system designs of the helicopter at 80 and 30 knots forward flight, the control system design for the helicopter in hover is presented. Similar to the two previous designs, it consists of an ICD analysis of the model system followed by an improvement of the structure of the model via *weak* feedback and post-compensation. Once the structural problems have been solved, the feedback control design is carried out. Also, because the design in based on a linearised low-order rigid body dynamics model, the control system is assessed against a higher-order model which includes a simplified low order representation of the actuator and rotor dynamics.

It is well known that the dynamical characteristics of the helicopter change substantially from one flight condition to another, Prouty [33]. Therefore, significant differences are found between this analysis and design from those of Chapters 4-6. For instance, it is found that the model system in hover decouples at the channels crossover frequencies. This represents an important conclusion which resolves an apparent contradiction about this dynamical behaviour of the helicopter, i.e, McRuer *et al* [24] suggest that the helicopter in hover is highly coupled whereas

Prouty [33] indicates the contrary. A second significant difference between hover and forward flight is that in hover the helicopter does not present sensitivity problems.

7.2 The Helicopter Model in Hover

The model of the helicopter in hover, obtained from Manness *et al* [22], is an eighth order model based on a linearised state-space representation of the HELISTAB flight mechanics software package Padfield [28].

$$\dot{x} = Ax + Bu \tag{7.1}$$

$$y = Cx \tag{7.2}$$

This model represent the linearised rigid body dynamics of a single main-rotor helicopter in hover, with the system matrix A assuming quasi-static rotor flapping. The associated state vector $x(t)$ is described by

$$x(t) = \begin{bmatrix} u \\ w \\ q \\ \theta \\ v \\ p \\ \phi \\ r \end{bmatrix} = \begin{bmatrix} longitudinal\ velocity\ (m/sec) \\ vertical\ velocity\ (m/sed) \\ pitch\ rate\ (rad/sec) \\ pitch\ attitude\ (rad) \\ lateral\ velocity\ (m/sec) \\ roll\ rate\ (rad/sec) \\ roll\ attitude\ (rad) \\ yaw\ rate\ (rad/sec) \end{bmatrix} \tag{7.3}$$

Following Manness *et al* [22], the tracking outputs considered for the helicopter in hover/low speed flight regime, in an attitude command/attitude hold (ACAH) response, are described by the output vector $y(t)$ of equation(7.2) represented by

$$y(t) = \begin{bmatrix} height\ rate \\ pitch\ attitude \\ roll\ attitude \\ yaw\ rate \end{bmatrix} = \begin{bmatrix} c_{11}u + c_{12}w + c_{15}v \\ \theta \\ \phi \\ r \end{bmatrix} \tag{7.4}$$

where the coefficients c_{ij} are the elements of the output matrix C. The four control inputs (pilots inceptors) forming the $4x1$ input vector $u = [u_1, u_2, u_3, u_4]^T$ of equation(7.1) are respectively the vertical collective u_1, the longitudinal cyclic u_2, the lateral cyclic u_3 and the tail rotor collective u_4.

Following notation defined in Chapter 4 (equation(4.5)) for polynomials in s, the 4-input 4-output multivariable transfer-function matrix model associated with the state-space representation of equations(7.1) and (7.2) is given by

$$G(s) = C(sI - A)^{-1}B \tag{7.5}$$

$$G(s) = \frac{1}{\triangle} \begin{bmatrix} 94 & -0.7884 & -0.3444 & 0.2982 \\ -10.8711 & -9.7637 & 4.7785 \pm 2.9774j & -11.0169 \\ -2.2232 & -1.4072 & -2.0565 \pm 1.1668j & -2.1972 \\ -0.1786 \pm 0.6027j & -0.1702 \pm 1.1156j & 0.0525 \pm 0.5037j & -0.5401 \pm 0.8972j \\ 0.2390 \pm 0.5337j & 0.6572 \pm 0.8734j & -0.3783 & 0.6888 \\ -0.3357 & -0.4248 & & 0.1019 \pm 0.4534j \\ \\ 1.8765 & 26.0447 & -7.1953 & -0.8067 \\ -12.4298 & -10.5131 & -19.2664 & -11.4188 \\ -1.0744 & -0.1210 \pm 0.3622j & 0.0155 \pm 0.8987j & -1.8056 \\ 0.0554 \pm 0.7383j & -0.3111 & -0.3738 & 0.1056 \pm 0.8054j \\ -0.2896 & -0.1389 & -0.3138 & -0.3138 \\ -0.0070 & -0.0067 & -0.0062 & -0.0061 \\ \\ 8.3194 & -33.7565 & -161.9611 & -2.2391 \\ -1.8504 \pm 0.9509j & -4.2888 & -1.9084 & -5.7872 \\ 0.0302 \pm 0.3513j & 0.0815 \pm 0.8483j & 0.0472 \pm 0.4279j & -2.3863 \\ -0.2938 & -0.3870 & -0.3803 & 0.0734 \pm 0.4054j \\ 0.1256 & -0.3147 & -0.3141 & -0.3142 \\ & -0.0072 & -0.0120 & -0.0069 \\ \\ 17.3060 & -5.9910 & -27.5910 & -15.1350 \\ -10.0598 & -4.2783 & -2.0088 & -10.7436 \\ -2.2300 & -1.5302 & 0.7481 \pm 1.1949j & -2.2238 \\ 0.2240 \pm 0.5521j & 0.5856 \pm 1.2047j & -1.2605 & 0.2341 \pm 0.5497j \\ -0.1421 \pm 0.5920j & 0.0820 \pm 0.8498j & 0.0446 \pm 0.4130j & -0.1471 \pm 0.5892j \\ -0.2903 & -0.3126 & 0.3114 & -0.3139 \end{bmatrix} \tag{7.6}$$

with the characteristic polynomial

$$\begin{aligned} \triangle &= [1, -10.8743, -2.2226, 0.2395 \pm 0.5322j, \\ &\quad -0.1811 \pm 0.6026j, -0.3224 \pm 0.0066j] \end{aligned} \tag{7.7}$$

and the set of finite multivariable transmission zeros

$$T_z = \{-0.0094, -0.0063\} \tag{7.8}$$

7.3 ICD Analysis

Similar to the two previous designs in Chapters 4-6, the starting point of analysis are the Nyquist plots of the multivariable structure functions $\Gamma_i(s)$, $i = 1,2,3$. ($\Gamma_4(s) =: 0$), for the plant matrix $G(s)$ of equation(7.6). These plots are shown in Figure(7.1). Due to all of the Nyquist plots of $\Gamma_i(s)$ are mainly in the left half plane, far from the point (1,0), it is concluded that the system has a robust structure, O'Reilly and Leithead [27, 15]. An important aspect that can also be detected from the Nyquist plots of $\Gamma_i(s)$ is that due to the low gain at all frequencies of $\Gamma_1(s)$ and $\Gamma_3(s)$, some channels may be decoupled. In order to determine which channel may decoupled, the system $G(s)$ of equation(7.6) is re-arranged as follows

$$G(s) = \frac{1}{\triangle} \begin{bmatrix} g_{33} & g_{32} & g_{31} & g_{34} \\ g_{23} & g_{22} & g_{21} & g_{24} \\ g_{13} & g_{12} & g_{11} & g_{14} \\ g_{43} & g_{42} & g_{41} & g_{44} \end{bmatrix} \tag{7.9}$$

In Figure(7.2), the Nyquist plots of $\Gamma_1(s)$, $\Gamma_2(s)$ and $\Gamma_3(s)$ of the re-arranged system $G(s)$ of equation(7.9) are shown. From these plots, the following points can be detected. First, due to the large gain of Γ_3, channels 2 and 3 are together coupled; second, due to the low gain of Γ_2, channels 1 and 4 may be decoupled from channels 2 and 3; and third, due to the low gain of $\Gamma_1(s)$, channel 1 may be decoupled from all the other channels.

As it was mentioned above, channels 1 and 4 may be decoupled from the other channels. In order to verify if this is the case, Result 3.7 will be applied. Firstly, assume a partitioning of the re-arranged system $G(s)$, as in equation(3.15), with $G_{11}(s) = g_{11}(s)$, i.e., the system is partitioned into one single channel and one 3-input 3-output multiple channel $M_2(s)$.

The Bode plots of $g_{11}(s)$ and $G_{11}^*(s) = g_{11}^*(s)$ are shown in Figure(7.3). From these plots is possible to see that $g_{11}(s)$ and $g_{11}^*(s)$ are almost equal.

In Table 7.1, the RHPP's and RHPP's of $g_{11}(s)$ and $g_{11}^*(s)$ are shown. From this table, it is clear that the structures of $g_{11}(s)$ and $g_{11}^*(s)$ differ significantly, i.e., $g_{11}^*(s)$ is stable and minimum phase meanwhile $g_{11}(s)$ is unstable and non-minimum phase. Therefore, channel 1 is not weakly coupled to multiple channel $M_2(s)$.

transmittance	RHP Zeros	RHP Poles
g_{11}	$0.2390 \pm 0.5337j$	$0.2395 \pm 0.5322j$
g_{11}^*	-	-

Table 7.1: RHPZ's and RHPP's of $g_{11}(s)$ and $g_{11}^*(s)$

Secondly, consider a partitioning of $G(s)$, with $G_{11}(s) = g_{44}(s)$. The Bode plots of $G_{11}(s) = g_{44}(s)$ and $G_{11}^*(s) = g_{44}^*$, are shown in Figure(7.4). Similar to the previous case, both Bode plots present almost no differences, but again the structures of $G_{11}(s) = g_{44}(s)$ and $G_{11}^*(s) = g_{44}^*$ differ significantly, i.e., $G_{11}^*(s) = g_{44}^*$ is stable and minimum phase whereas $G_{11}(s) = g_{44}(s)$ is unstable and non-minimum phase as it is shown in Table 7.2. Therefore, channel 4 is also coupled. It must be noted that condition (ii) of Result 3.7 is not required to be checked from the fact that with these particular partitions, $G_{11}(s)$ and $G_{11}(s)^*$, are SISO transmittances.

transmittance	RHP Zeros	RHP Poles
g_{44}	$0.2341 \pm 0.5497j$	$0.2395 \pm 0.5322j$
g_{44}^*	-	-

Table 7.2: RHPZ's and RHPP's of $g_{44}(s)$ and $g_{44}^*(s)$

It just remains to check if channels 2 and 3 decouple from channels 1 and 4. In order to verify if this is the case, the re-arranged system $G(s)$ of equation(7.9) is partitioned as follows

$$G(s) = \frac{1}{\Delta}\begin{bmatrix} g_{33} & g_{32} & \vdots & g_{31} & g_{34} \\ g_{23} & g_{22} & \vdots & g_{21} & g_{24} \\ \dots & \dots & \dots & \dots & \dots \\ g_{13} & g_{12} & \vdots & g_{11} & g_{14} \\ g_{43} & g_{42} & \vdots & g_{41} & g_{44} \end{bmatrix} = \begin{bmatrix} Gr_{11}(s) & \vdots & Gr_{12}(s) \\ \dots & \dots & \dots \\ Gr_{21}(s) & \vdots & Gr_{22}(s) \end{bmatrix} \quad (7.10)$$

It must be noted that with this re-arrangement the system can not be split in the traditional lateral and longitudinal dynamics.

In Figures(7.5) and (7.6), the Bode Plots of the diagonal elements of $Gr_{11}(s)$ and $Gr_{11}^*(s)$ are shown. From these plots, it is seen that the diagonal elements $Gr_{11}^*(s)$ do not differ significantly from the respective diagonal elements of $Gr_{11}(s)$ in the region of the crossover frequencies (3 to 4 rad/sec). Therefore, condition (i) of Result 3.7 is satisfied. Also, condition (ii) is satisfied as Figures(7.7) and (7.8) show that the multivariable structure function $\Gamma r_1(s)$ of the 2-input 2-output system $Gr_{11}^*(s)$ does not differ significantly from that of $Gr_{11}(s)$. It must be noted that the differences do not include the channel crossover frequency of 3 to 4 rad/sec. as expected from the very low gain of the original $\Gamma_i(s)$ $i = 1, 2, 3$ (Figures(7.2)); that is, $\Gamma r_1(s)$ and $\Gamma r_1^*(s)$ are practically equal from 0.7 to ∞ rad/sec.

Lastly, consider condition (iii). From Table 7.3 it is seen that the RHPP's and RHPZ's of $Gr_{11}(s)$ are significantly different from those of $Gr_{11}^*(s)$, i.e., the individual transfer function $g_{22}(s)$ of $Gr_{11}(s)$ is minimum phase, whereas the individual transfer function $g_{22}^*(s)$ of $Gr_{11}^*(s)$ is non-minimum phase with 2 RHPZ's at $0.0050 \pm 0.4319j$. Therefore, multiple channel $M_1(s)$ (associated with channels 2 and 3) is coupled to Multiple channel $M_2(s)$ (representing channels 1 and 4).

Also, from Table 7.3 is possible to see that $Gr_{11}(s)$ and $Gr_{11}^*(s)$ are both non-minimum phase, with transmission zeros at $0.2395 \pm 0.5322j$ and $0.2335 \pm 0.5500j$ respectively. Nevertheless, this transmission zeros coincide exactly with the RHPP's of both subsystems. This means that in order to keep channels 2

	subsystem RHP transmission Zeros	Subsystem RHP poles		Individual RHPZ's	Individual RHPP's
Gr_{11}	$0.2395 \pm 0.5322j$	$0.2395 \pm 0.5322j$	g_{22}	-	$0.2395 \pm 0.5322j$
			g_{23}	$0.0155 \pm 0.8987j$	$0.2395 \pm 0.5322j$
			g_{32}	$0.0815 \pm 0.8483j$	$0.2395 \pm 0.5322j$
			g_{33}	$0.2341 \pm 0.5497j$	$0.2395 \pm 0.5322j$
Gr_{11}^*	$0.2335 \pm 0.5500j$	$0.2335 \pm 0.5500j$	g_{22}^*	$0.0050 \pm 0.4319j$	$0.2335 \pm 0.5500j$
			g_{23}^*	$0.0141 \pm 0.8835j$	$0.2335 \pm 0.5500j$
			g_{32}^*	$0.0815 \pm 0.8488j$	$0.2335 \pm 0.5500j$
			g_{33}^*	$0.0474 \pm 0.4276j$	$0.2335 \pm 0.5500j$

Table 7.3: Subsystem $Gr_{11}(s)$ and Multiple Channel $Gr_{11}^*(s)$ RHPP's and RHPZ's for the helicopter model $G(s)$

and 3 minimum phase, an exact RHP pole-zero cancellation is required. However, similar to the cases analysed in Chapters 4 and 6, due to the almost RHP pole-zero cancellations in Tables 7.1 and 7.2 and the exact RHP cancellation in Tables 7.3 almost coinciding with the RHP poles of the system (equation(7.7)), it seems that the required exact cancellation for channels 2 and 3 together with the almost RHP pole-zero cancellation affecting channels 1 and 4 are fictitious and are due to the highly structured form of the state-space representation of the system.

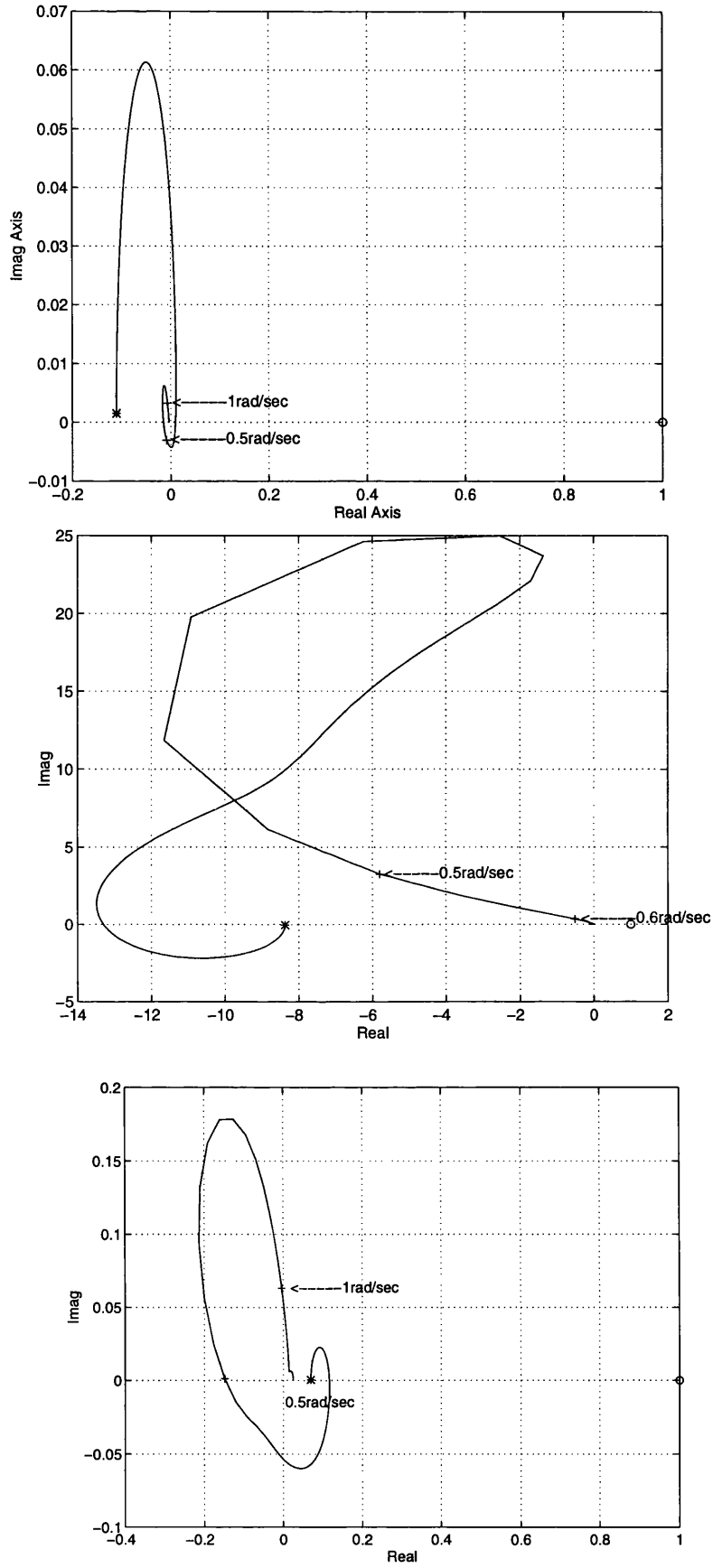

Figure 7.1: Nyquist Plot of $\Gamma_1(s)$, $\Gamma_2(s)$ and $\Gamma_3(s)$ of the system $G(s)$ respectively

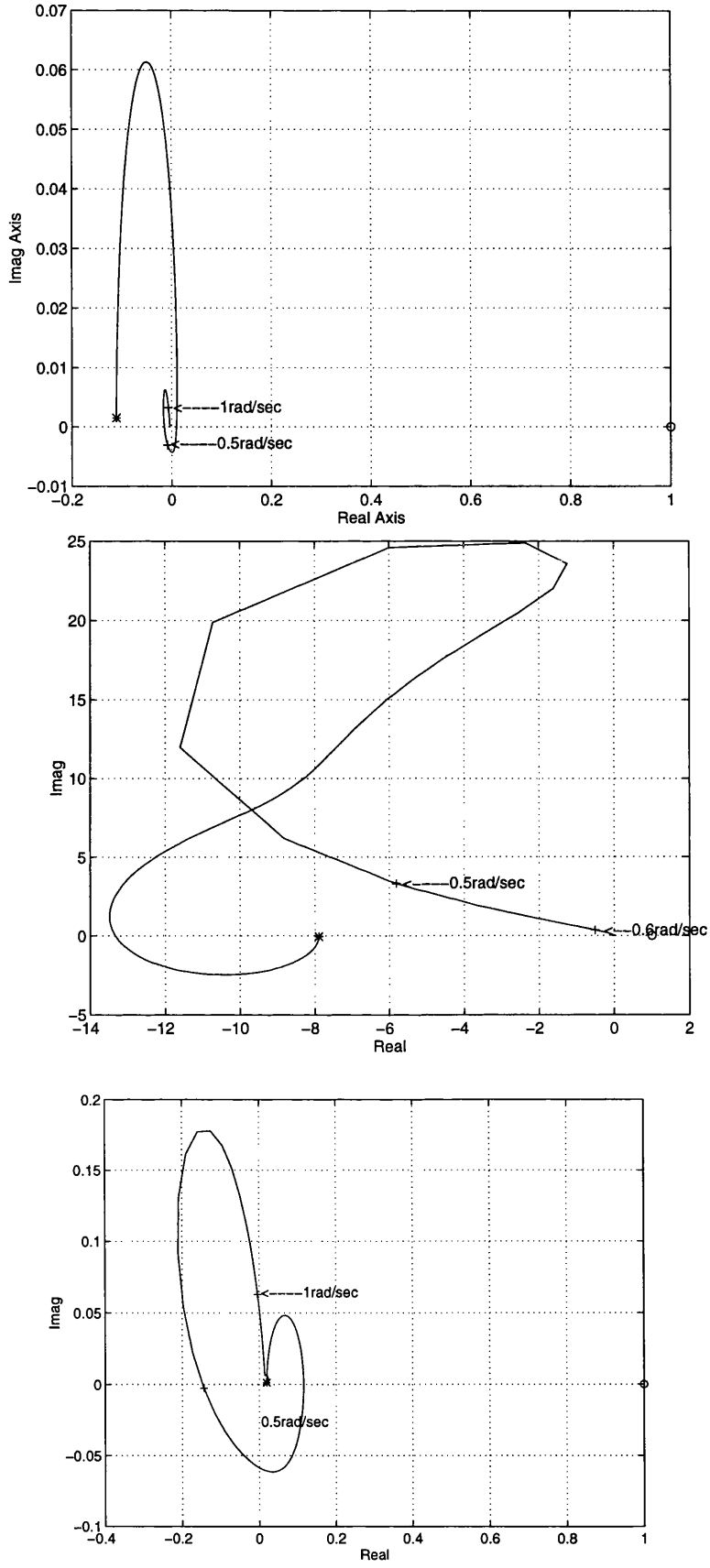

Figure 7.2: Nyquist Plot of $\Gamma_1(s)$, $\Gamma_2(s)$ and $\Gamma_3(s)$ of the re-arranged system $G(s)$ respectively

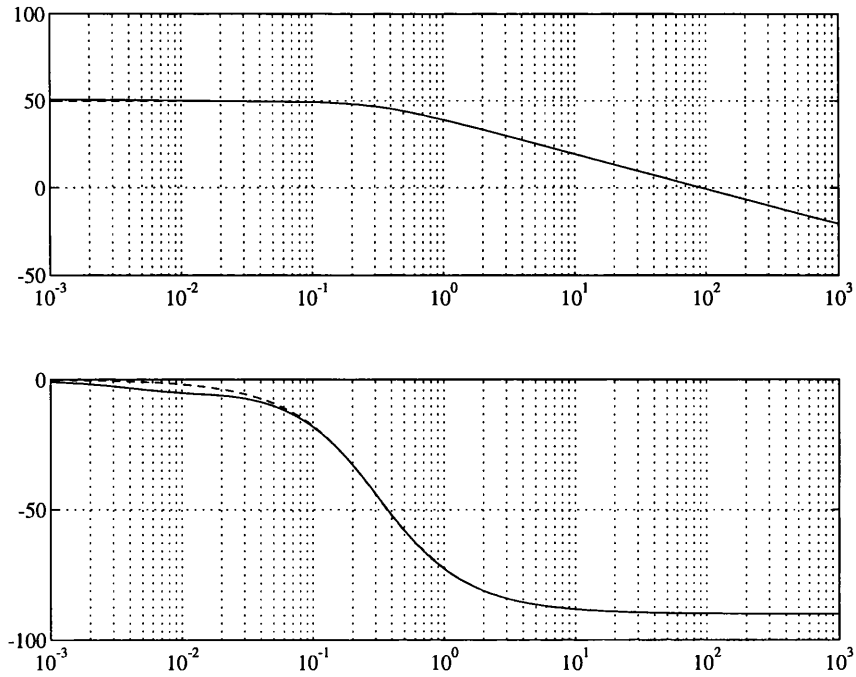

Figure 7.3: Bode Plots of $G_{11}(s) = g_{11}(s)$ and $G_{11}^*(s) = g_{11}^*(s)$ respectively

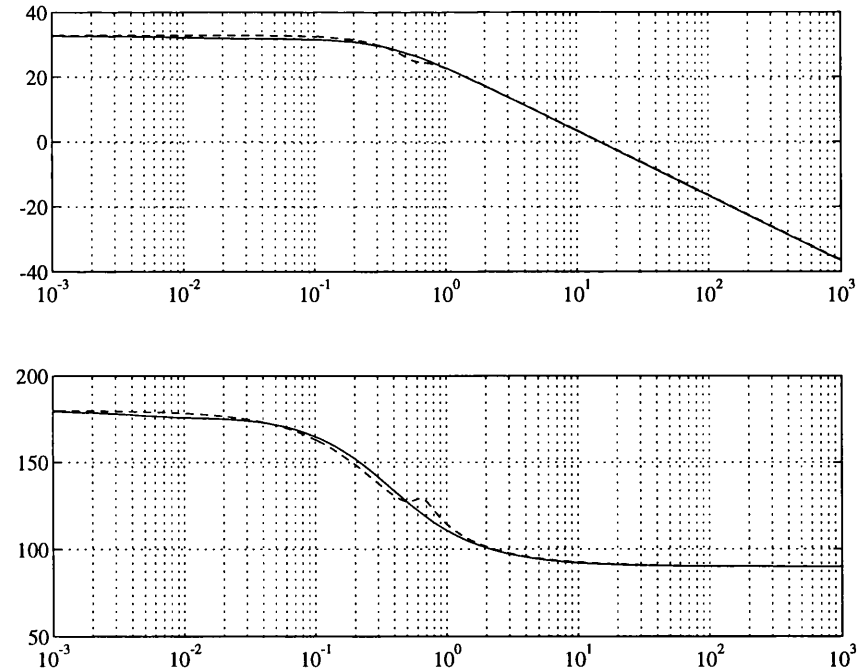

Figure 7.4: Bode Plots of $G_{11}(s) = g_{44}(s)$ and $G_{11}^*(s) = g_{44}^*(s)$ respectively

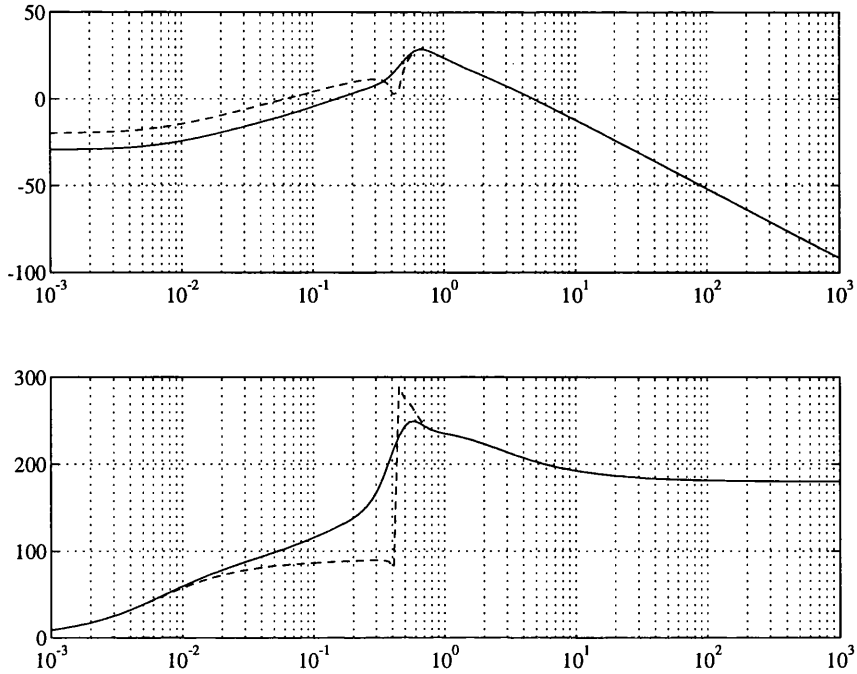

Figure 7.5: Bode Plots of $g_{22}(s)$ and $g_{22}^*(s)$ of $Gr_{11}(s)$ and $Gr_{11}^*(s)$ respectively

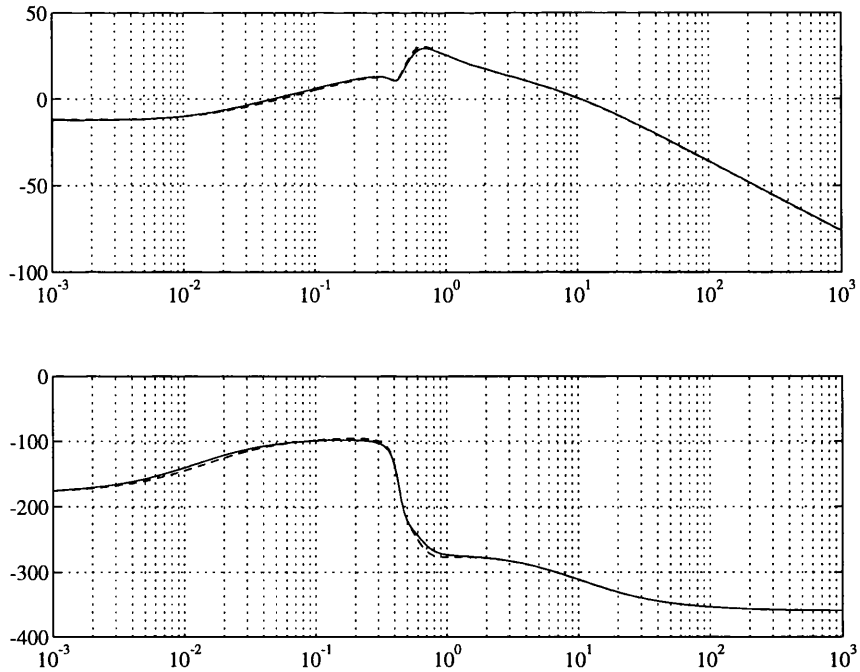

Figure 7.6: Bode Plots of $g_{33}(s)$ and $g_{33}^*(s)$ of $Gr_{11}(s)$ and $Gr_{11}^*(s)$ respectively

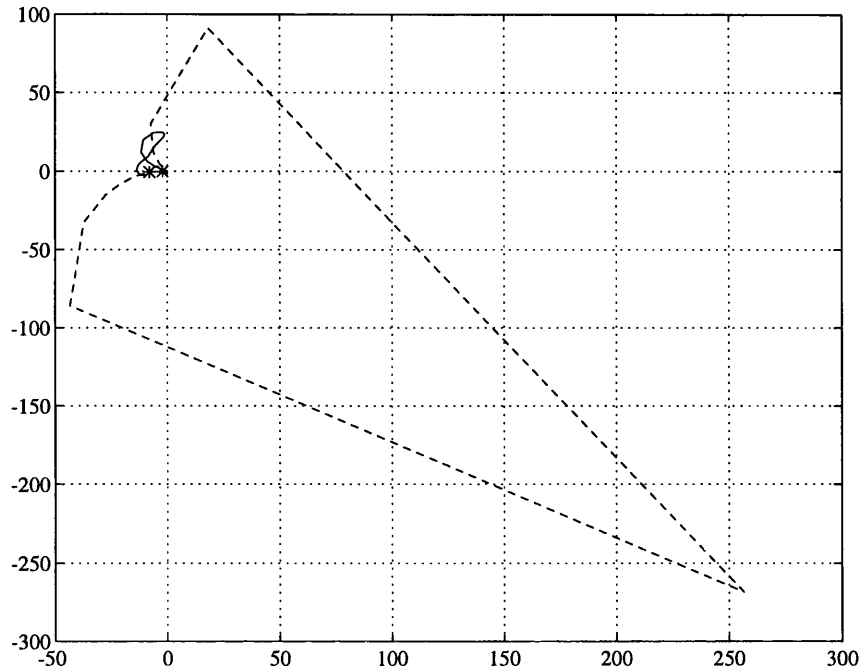

Figure 7.7: Nyquist plots of $\Gamma r_1(s)$ and $\Gamma r_1^*(s)$ of $Gr_{11}(s)$ and $Gr_{11}^*(s)$ respectively

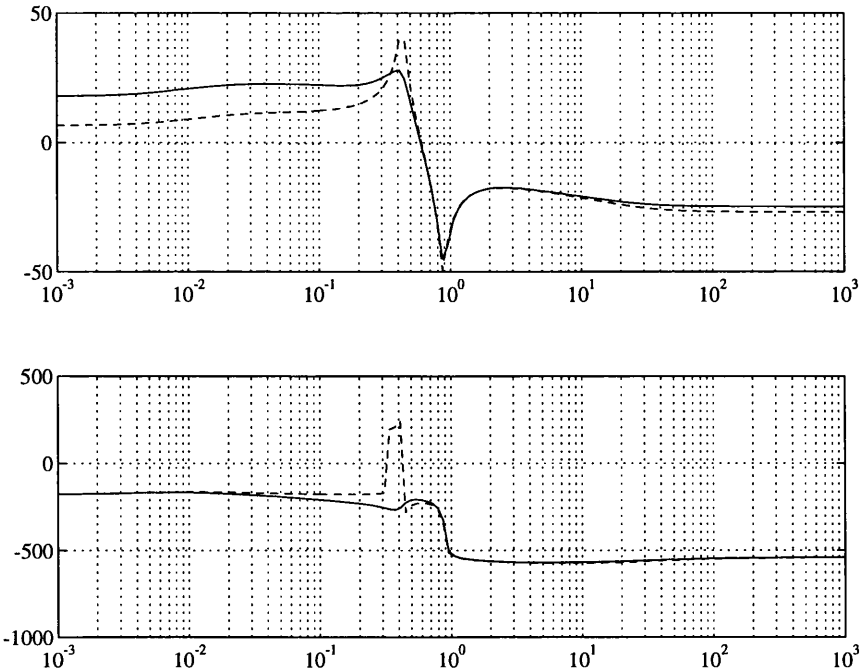

Figure 7.8: Bode Plots of $\Gamma r_1(s)$ and $\Gamma r_1^*(s)$ of $Gr_{11}(s)$ and $Gr_{11}^*(s)$ respectively

7.4 Structure improvement

In the last section, it was shown that due to an almost RHP pole-zero cancellation, channels 1 and 4 are strongly coupled. Moreover, it was also shown that the minimum-phase characteristic of channels 2 and 3 depend on an exact RHP pole-zero cancellation. Nevertheless, the almost RHP pole-zero cancellation affecting channels 1 and 4, and the exact RHP pole-zero cancellation affecting channels 2 and 3, almost coincide with the RHPP's of the full helicopter transfer-function matrix. Therefore, it seems that these near-cancelling RHPP's and RHPZ's together with the exact RHP cancellation are fictitious. That is, they are due to the highly structured form of the state-space representation of the system. However, due to its unstable characteristics, it would be unwise to ignore it or to directly eliminate them. Following the procedure adopted in Chapters 4 and 6, a *weak* feedback is the best solution to solve these problems. In this way, the inherently decoupled channels 1 and 4 will decouple, and the minimum phase characteristic of channels 2 and 3 will not longer depend on an exact RHP cancellation. In other words, by stabilising the system with the *weak* feedback, the undesirable almost exact RHP pole-zero cancellations will be changed to a benign almost exact LHP pole-zero cancellations.

7.4.1 Weak feedback

From equation(7.6), is possible to see that the only minimum phase individual transfer function of the transfer-function matrix $G(s)$ is $g_{22}(s)$. Therefore, the weak feedback should be closed round this element.

A candidate feedback function $m(s)$ around the $g_{22}(s)$ element is given by,

$$\begin{aligned} m(s) &= 0.7125\frac{s(s+0.05)(s+2.22)}{(s+0.1)(s+0.14)(s+0.31)(s+0.5)(s+1)(s+2.5)} \\ &\quad \times\frac{(s^2+0.365s+0.3924)(s^2+0.645s+0.1024)}{(s+8)(s^2+0.24s+0.144)} \end{aligned} \tag{7.11}$$

Application of the feedback function $m(s)$ to the full 4-input 4-output helicopter system $G(s)$ via the matrix $M(s)$

$$M(s) = \begin{bmatrix} 0 & 0 & 0 & 0 \\ 0 & m(s) & 0 & 0 \\ 0 & 0 & 0 & 0 \\ 0 & 0 & 0 & 0 \end{bmatrix} \tag{7.12}$$

results in the amended system

$$\bar{G}(s) = (I + GM)^{-1} G = \begin{bmatrix} \bar{G}_1 \\ \dots \\ \bar{G}_2 \end{bmatrix} \tag{7.13}$$

where

$$\bar{G}_1(s) = \frac{1}{\bar{\Delta}} \begin{bmatrix} 94.0249 & -0.7884 & -0.3444 & 0.2982 \\ -10.8685 & -9.7637 & -7.9669 & -11.0150 \\ -7.8454 & -8.0 & 4.8047 \pm 3.0075j & -7.9493 \\ -3.0757 & -2.5 & -2.4788 \pm 1.2057j & -3.0296 \\ -2.2206 & -1.4072 & -2.3570 & -2.2153 \\ -0.1435 \pm 0.1266j & 0.6572 \pm 0.874j & -0.3507 \pm 0.7637j & -0.6252 \pm 0.7560j \\ -0.2079 \pm 0.5789j & -0.1702 \pm 1.1156j & -0.0402 \pm 0.7645j & -0.3439 \pm 0.8541j \\ -0.0719 \pm 0.5407j & -1.0 & -0.3802 & 0.7437 \\ -0.1298 \pm 0.3380j & -0.1200 \pm 0.3600j & -0.3068 \pm 0.0119j & -0.0161 \pm 0.7371j \\ -0.3269 & -0.5000 & -0.0461 \pm 0.1333j & -0.3065 \pm 0.0116j \\ -0.3149 & -0.4248 & -0.794 & -0.0324 \pm 0.1277j \\ -0.1451 & -0.3100 & & -0.0780 \\ -0.0962 & -0.1400 & & \\ & -0.1000 & & \\ 1.8765 & 26.0447 & -7.1953 & -0.8067 \\ -12.4298 & -10.5131 & -19.2664 & -11.4188 \\ -8.0000 & -8.0000 & -8.0000 & -8.0000 \\ -2.5000 & -2.5000 & -2.5000 & -2.5000 \\ 0.0554 \pm 0.7383j & -1.0000 & 0.0155 \pm 0.8987j & -1.8056 \\ -1.0744 & -0.5000 & -1.0000 & -01056 \pm 0.8054j \\ -1.0000 & -0.1210 \pm 0.3622j & -0.1200 \pm 0.3600j & -1.0000 \\ -0.1200 \pm 0.3600j & -0.1200 \pm 0.3600j & -0.5000 & -0.1200 \pm 0.3600j \\ -0.5000 & -0.3111 & -0.3738 & -0.5000 \\ -0.3100 & -0.3100 & -0.3138 & -0.3100 \\ -0.2896 & -0.1400 & -0.3100 & -0.3138 \\ -0.1400 & -0.1389 & -0.1400 & -0.1400 \\ -0.1000 & -0.1000 & -0.1000 & -0.1000 \\ -0.0070 & -0.0067 & -0.0062 & -0.0061 \end{bmatrix} \tag{7.14}$$

$$\bar{G}_2(s) = \frac{1}{\bar{\triangle}} \begin{bmatrix}
8.3194 & -33.7565 & -161.9611 & -2.2391 \\
-7.9260 & -8.0000 & -7.9365 & -7.8732 \\
-2.7702 & -4.2988 & -2.9994 & -5.8890 \\
-2.0364 \pm 0.4954j & -2.5000 & -2.1623 & -3.2428 \\
-0.3808 \pm 0.8876j & 0.0815 \pm 0.8483j & -0.3349 \pm 0.8081j & -2.2441 \\
-0.0312 \pm 0.7053j & -1.0000 & -0.0406 \pm 0.7350j & -0.3830 \pm 0.8297j \\
-0.3115 \pm 0.0108j & -0.1200 \pm 0.3600j & -0.3808 & -0.0267 \pm 0.7236j \\
-0.2820 & -0.5000 & -0.3140 & -0.3142 \\
0.0896 & -0.3870 & -0.3108 \pm 0.0119j & -0.3100 \pm 0.0119j \\
-0.0547 \pm 0.1045j & -0.3147 & -0.0286 \pm 0.1156j & -0.0262 \pm 0.1136j \\
-0.0810 & -0.3100 & -0.0755 & -0.0758 \\
 & -0.1400 & -0.0120 & -0.0069 \\
 & -0.1000 & & \\
 & -0.0072 & & \\
 & & & \\
17.3060 & -5.9910 & -27.5910 & -15.1350 \\
-10.0535 & -8.0000 & -7.9367 & -10.7401 \\
-7.9506 & -4.2783 & -3.0094 & -7.9468 \\
-3.0804 & -2.5000 & -2.1771 & -3.0765 \\
-2.2219 & 0.5856 \pm 1.2047j & 0.7536 \pm 1.1971j & -2.2207 \\
-0.1001 \pm 0.7332j & -1.5302 & -1.3690 & -0.1043 \pm 0.7338j \\
-0.2931 \pm 0.6718j & 0.0820 \pm 0.8498j & -0.3260 \pm 0.8072j & -0.2799 \pm 0.6693j \\
0.0375 \pm 0.5739j & -1.0000 & -0.0420 \pm 0.7334j & 0.0443 \pm 0.5570j \\
-0.1213 \pm 0.1865j & -0.1200 \pm 0.3600j & -0.3118 \pm 0.0125j & -0.1334 \pm 0.1896j \\
-0.3053 & -0.5000 & -0.3120 & -0.3139 \\
-0.2945 & -0.3126 & -0.0269 \pm 0.1095j & -0.3064 \\
-0.2593 & -0.3100 & -0.0750 & -0.2582 \\
-0.0873 & -0.1400 & & -0.0878 \\
 & -0.1000 & &
\end{bmatrix} \tag{7.15}$$

with the characteristic polynomial

$$\begin{aligned}
\bar{\triangle} \;=\; & [1, -10.8717, -7.9454, -3.0751, -0.1484 \pm 0.7251j, \\
& -0.1071 \pm 0.5528j, -0.1846 \pm 0.5504j, -0.1160 \pm 0.3570j, \\
& -0.3209 \pm 0.0063j, -0.3106, -0.1398, -0.0974]
\end{aligned} \tag{7.16}$$

and the set of finite multivariable transmission zeros

$$\begin{aligned}
\bar{T}_z \;=\; & \{-8.0, -2.5, -1.0, -0.12 \pm 0.36j, -0.5, -0.31, \\
& -0.14, -0.1, -0.0094, -0.0063\}
\end{aligned} \tag{7.17}$$

To assure that uncertainties of the individual transfer functions are not increased by $m(s)$, it is necessary to check that the Nyquist plots of the multivariable structure functions $\gamma_{ii}h_{22}$ (equation(3.55)) do not come close to the point (1,0) in the frequency range of interest, otherwise uncertainty of the individual transfer-function elements will have been significantly increased. The nine $\gamma_{ij}h_{22}$ for 2x2 subsystems to check in this way are given in Table 7.4

Input	Output	$\gamma_{ij}h_{22}$
1	1	$\gamma_{11}h_{22}$
1	3	$\gamma_{13}h_{22}$
1	4	$\gamma_{14}h_{22}$
3	1	$\gamma_{31}h_{22}$
3	3	$\gamma_{33}h_{22}$
3	4	$\gamma_{34}h_{22}$
4	1	$\gamma_{41}h_{22}$
4	3	$\gamma_{43}h_{22}$
4	4	$\gamma_{44}h_{22}$

Table 7.4: Multivariable structure functions $\gamma_{ij}h_{22}$

Comparing the Bode plots of the amended individual transfer functions $\bar{g}_{ij}(s)$ (equation(7.13)) with the original $g_{ij}(s)$ (equation(7.6)) in Figures(7.9)-(7.12) and their pole-zero structure described by equations(7.6)-(7.7) and equations(7.13)-(7.16), it is observed that they are not significantly altered except close to the frequency of the RHPP's. So the first requirement to the feedback function $m(s)$ has been satisfied, i.e, the stabilisation of $G(s)$ by the feedback function $m(s)$ has not significantly altered the structure of the system. It remains to check if the uncertainties of the individual transfer functions have not been increased. In Figures(7.13) to (7.15), the Nyquist plots of the nine $\gamma_{ij}h_{22}(s)$ of Table 7.4 are shown. From these figures, it is observed that none of nine Nyquist plots come close to the point (1,0) in the frequency range of interest of 3-4 rad/sec as the second requirement on $m(s)$ dictates.

In order to prove that after the stabilisation of the system $G(s)$ by the weak

feedback $M(s)$ the amended channel 1 decoupled, Result 3.7 is applied to the amended system $\bar{G}(s)$ of equations(7.13)-(7.16), following the same procedure of Section 7.3, i.e, with $\bar{G}_{11}(s) = \bar{g}_{11}(s)$.

The Bode plots of $\bar{G}_{11}(s) = \bar{g}_{11}(s)$ and $\bar{G}^*_{11}(s) = \bar{g}^*_{11}(s)$ are shown in Figure(7.16). From these plots it is clear that both Bode plots are practically the same. Also, due to the fact that $\bar{g}^*_{11}(s)$ and $\bar{g}_{11}(s)$ are stable and minimum phase both have similar pole-zero structure. Therefore, channel 1 decouples and controller $k_1(s)$ can be designed on the basis of $\bar{G}_{11}(s) = \bar{g}_{11}(s)$ alone.

Inspection of equation(7.13) shows that after the application of the the weak feedback $M(s)$, the amended individual transfer function $\bar{g}_{44}(s)$ is still non-minimum phase. Therefore, channel 4 remains coupled. The reason for this non-minimum phase characteristic can be explained by the Nyquist plot of $\gamma_{44}h_{22}$ in Figure(7.15). This figure shows that the Nyquist path of $\gamma_{44}h_{22}(s)$ encircles the point (1,0) twice in an anti-clockwise sense. Thus, by Result 3.1 $\bar{g}_{44}(s)$ has 2 RHPZ's at $0.0443 \pm 0.5570j$.

It remains to check if channels 2 and 3 are not longer affected by the exact RHP cancellation. Repeating the same procedure of Section 7.3, the amended system $\bar{G}(s)$ is partitioned as follows.

$$\bar{G}(s) = \frac{1}{\bar{\Delta}} \begin{bmatrix} \bar{g}_{33} & \bar{g}_{32} & \vdots & \bar{g}_{31} & \bar{g}_{34} \\ \bar{g}_{23} & \bar{g}_{22} & \vdots & \bar{g}_{21} & \bar{g}_{24} \\ \dots & \dots & \dots & \dots & \dots \\ \bar{g}_{13} & \bar{g}_{12} & \vdots & \bar{g}_{11} & \bar{g}_{14} \\ \bar{g}_{43} & \bar{g}_{42} & \vdots & \bar{g}_{41} & \bar{g}_{44} \end{bmatrix} = \begin{bmatrix} \bar{G}r_{11}(s) & \vdots & \bar{G}r_{12}(s) \\ \dots & \dots & \dots \\ \bar{G}r_{21}(s) & \vdots & \bar{G}r_{22}(s) \end{bmatrix} \tag{7.18}$$

From condition (iii) of Result 3.7, the pole-zero structure of the resulting $\bar{G}r^*_{11}$ is as given in Table 7.5

From Table 7.5, is clear that despite the stabilisation by the weak-feedback,

	subsystem RHP transmission Zeros	Subsystem RHP poles		Individual RHPZ's	Individual RHPP's
$\bar{G}r^*_{11}$	$0.0436 \pm 0.5383j$	$0.0436 \pm 0.5383j$	$\bar{g}^*_{22}$	$0.0022 \pm 0.4360j$	$0.0436 \pm 0.5383j$
			$\bar{g}^*_{23}$	$0.0142 \pm 0.8837j$	$0.0436 \pm 0.5383j$
			$\bar{g}^*_{32}$	$0.0815 \pm 0.8488j$	$0.0436 \pm 0.5383j$
			$\bar{g}^*_{33}$	-	$0.0436 \pm 0.5383j$

Table 7.5: Multiple Channel RHPP's and RHPZ's for $\bar{G}r^*_{11}(s)$

the minimum phase characteristics of channels 2 and 3 still depends on an exact RHP pole-zero cancellation. That is, because the Nyquist plot of the multivariable structure function $\bar{\Gamma}^*(s)$ of $\bar{G}r^*_{11}(s)$ (Figure(7.17) does not encircle the point (1,0) and by the two RHPZ's of $\bar{g}^*_{22}(s)$ then, multiple channel $\bar{G}r^*_{11}(s)$ has 2 RHPZ at $0.0436 \pm 0.5383j$. Therefore, 2 RHPP's are required (Table 7.5), in order to keep channels 2 and 3 minimum phase. Similar to the case of channel 4, this problem can be also explained by the Nyquist plots of $\gamma_{41}h_{22}(s)$ and $\gamma_{44}h_{22}(s)$ in Figure(7.15). These plots encircle the point (1,0) twice in an anti-clockwise sense. Therefore, the amended individual transfer functions $\bar{g}_{41}(s)$ and $\bar{g}_{43}(s)$ remain non-minimum phase with RHPZ's similar to those of the original $g_{41}(s)$ and $g_{43}(s)$.

A possible solution to these problems is to design the weak feedback loop round a different individual transfer function. However, due to the fact that *all* of the other transfer functions (equation(7.6)), have almost RHP pole-zero cancellations, the resulting inner loop will not be weak. The solution proposed is therefore to design a post-compensator to stabilise the RHPZ's of $\bar{g}_{44}(s)$.

7.4.2 Post-Compensator

In the previous section was found that despite the design of a weak feedback, channel 4 remains coupled and channels 2 and 3 are still affected by an exact RHP pole-zero cancellation. The solution adopted to eliminate these problems is post-compensation. With the use of the post-compensator, it is intended to stabilise the RHPZ's of the amended individual transfer function $\bar{g}_{44}(s)$. The design of the post-compensator $P(s)$ must satisfy the requirements described in Section 3.5.2,

i.e, it must not increase the uncertainty effects, otherwise the robustness of the control system would be put at risk. Therefore, the post-compensator must affect the system at frequencies where the multivariable structure functions $\Gamma_1(s)$, $\Gamma_2(s)$ and $\Gamma_3(s)$ are far from the point (1,0). In Figures(7.18), the Nyquist plots of the multivariable structure functions $\bar{\Gamma}_1(s)$, $\bar{\Gamma}_2(s)$ and $\bar{\Gamma}_3(s)$ of the amended helicopter system $\bar{G}(s)$ are shown. From these figures, it is clear that none of them are close to the point (1,0). Hence, the post-compensator does not represent a robustness problem. Nevertheless, it is convenient to design the post-compensator in such a way that it affects the system only around the RHPZ's of $\bar{g}_{44}(s)$. An appropriate post-compensator $P(s)$ to the amended system $\bar{G}(s)$ of equation(7.13) is given by

$$P(s) = \begin{bmatrix} 1 & 0 & 0 & 0 \\ 0 & 1 & 0 & 0 \\ 0 & 0 & 1 & 0 \\ 0 & 0 & p_{43} & 1 \end{bmatrix} \tag{7.19}$$

where

$$p_{43} = \frac{1.4s}{s^2 + 1.65s + 0.64} \tag{7.20}$$

Application of the post-compensator $P(s)$ to the system $\bar{G}(s)$ will result in the post-compensated system $\bar{G}'(s)$

$$\bar{G}'(s) = P(s)\bar{G}(s) \tag{7.21}$$

From equation(7.19) it is clear that only the fourth row of the amended system $\bar{G}(s)$ will be affected by the post-compensator. Hence, all the other elements remain equal except $\bar{g}_{41}(s)$, $\bar{g}_{42}(s)$, $\bar{g}_{43}(s)$ and $\bar{g}_{44}(s)$. Then, the resulting post-compensated elements are given by

$$\bar{g}'_{41} = \bar{g}_{41} + p_{43}\bar{g}_{31} = \bar{g}_{41}(1 + p_{43}\frac{\bar{g}_{31}}{\bar{g}_{41}}) \tag{7.22}$$

$$\bar{g}'_{42} = \bar{g}_{42} + p_{43}\bar{g}_{32} = \bar{g}_{42}(1 + p_{43}\frac{\bar{g}_{32}}{\bar{g}_{42}}) \tag{7.23}$$

$$\bar{g}'_{43} = \bar{g}_{43} + p_{43}\bar{g}_{33} = \bar{g}_{43}(1 + p_{43}\frac{\bar{g}_{33}}{\bar{g}_{43}}) \tag{7.24}$$

$$\bar{g}'_{44} = \bar{g}_{44} + p_{43}\bar{g}_{34} = \bar{g}_{44}(1 + p_{43}\frac{\bar{g}_{34}}{\bar{g}_{44}}) \tag{7.25}$$

From equations(7.22)-(7.25), it is clear that the effect of the post-compensator over the system is given by the functions $p_{43}\frac{\bar{g}_{31}}{\bar{g}_{41}}$, $p_{43}\frac{\bar{g}_{32}}{\bar{g}_{42}}$, $p_{43}\frac{\bar{g}_{33}}{\bar{g}_{43}}$ and $p_{43}\frac{\bar{g}_{34}}{\bar{g}_{44}}$. From Figures(7.19) and (7.20), it is shown that the main effect of the post-compensator over $\bar{g}_{41}(s)$ and $\bar{g}_{44}(s)$ is at around 0.55rad/sec. Whereas, $\bar{g}_{42}(s)$ and $\bar{g}_{43}(s)$ are mainly affected around 1.5rad/sec as Figures(7.21) and (7.22) shown. It is necessary to note, that despite the large influence of the post-compensator over $\bar{g}_{42}(s)$ and $\bar{g}_{43}(s)$ of approximately 10dB's at around 1.5rad/sec, it does not represent any problem, because all the multivariable structure functions are almost zero from 0.8 to ∞rad/sec.

The resulting RHP pole-zero structures of $\bar{g}'_{41}(s)$, $\bar{g}'_{42}(s)$, $\bar{g}'_{43}(s)$ and $\bar{g}'_{44}(s)$ are shown in Table 7.6

	$\bar{g}'_{41}$	$\bar{g}'_{42}$	$\bar{g}'_{43}$	$\bar{g}'_{44}$
RHP-zeros	-	$0.0828 \pm 0.8468j$	-	-
RHP-poles	-	-	-	-

Table 7.6: Pole-zero structure of $\bar{g}'_{41}(s)$, $\bar{g}'_{42}(s)$, $\bar{g}'_{43}(s)$ and $\bar{g}'_{44}(s)$

From Table 7.6, it is clear that the post-compensated individual transfer function $\bar{g}'_{44}(s)$ is stable and minimum phase. Thus, the almost RHP pole-zero cancellation affecting channel 4 has been removed and all the conditions of Result 3.7 are satisfied. That is, consider a partition of the post-compensated system $\bar{G}'(s)$ with $\bar{G}r'_{11}(s) = \bar{g}'_{44}(s)$. The Bode plots of $\bar{G}r'_{11}(s) = \bar{g}'_{44}(s)$ and $\bar{G}r'^{*}_{11}(s) = \bar{g}'^{*}_{44}(s)$ are shown in Figure(7.23). From these plots it is possible to see that both Bode plots do not differ significantly. From the last fact and due to both $\bar{G}r'_{11}(s) = \bar{g}'_{44}(s)$ and $\bar{G}r'^{*}_{11}(s) = \bar{g}'^{*}_{44}(s)$ being stable and minimum phase, it is conclude that channel

4 is decoupled. Therefore, controller $k_4(s)$ can be designed on the basis of $\bar{g}'_{44}(s)$ alone.

It remains to check if channels 2 and 3 are not longer affected by the exact RHP cancellation. Repeating the procedure of Section 7.3 (and applying Result 3.7) the post-compensated system is partitioned as follows

$$\bar{G}'(s) = \frac{1}{\bar{\Delta}'} \begin{bmatrix} \bar{g}'_{33} & \bar{g}'_{32} & \vdots & \bar{g}'_{31} & \bar{g}'_{34} \\ \bar{g}'_{23} & \bar{g}'_{22} & \vdots & \bar{g}'_{21} & \bar{g}'_{24} \\ \dots & \dots & \dots & \dots & \dots \\ \bar{g}'_{13} & \bar{g}'_{12} & \vdots & \bar{g}'_{11} & \bar{g}'_{14} \\ \bar{g}'_{43} & \bar{g}'_{42} & \vdots & \bar{g}'_{41} & \bar{g}'_{44} \end{bmatrix} = \begin{bmatrix} \bar{G}r'_{11} & \vdots & \bar{G}r'_{12} \\ \dots & \dots & \dots \\ \bar{G}r'_{21} & \vdots & \bar{G}r'_{22} \end{bmatrix} \tag{7.26}$$

The pole-zero structure of the resulting $\bar{G}r'^{*}_{11}(s)$ is given in Table 7.7

	subsystem RHP transmission Zeros	Subsystem RHP poles		Individual RHPZ's	Individual RHPP's
$\bar{G}r'^{*}_{11}$	-	-	$\bar{g}'^{*}_{22}$	-	-
			$\bar{g}'^{*}_{23}$	$0.0223 \pm 0.9038j$	-
			$\bar{g}'^{*}_{32}$	$0.0815 \pm 0.8488j$	-
			$\bar{g}'^{*}_{33}$	-	-

Table 7.7: Multiple Channel RHPP's and RHPZ's for $\bar{G}r'^{*}_{11}$

From Table 7.7, is clear that the minimum phase characteristic of channels 2 and 3 no longer depend on an exact RHP pole-zero cancellation. Moreover, due to the Bode plots of the diagonal elements of $\bar{G}r'^{*}_{11}(s)$ and $\bar{G}r^{*}_{11}(s)$ in Figures(7.24) and (7.25) not differing significantly, as well as the Nyquist and Bode plots of $\bar{\Gamma}'(s)$ and $\bar{\Gamma}'^{*}(s)$ of $\bar{G}r^{*}_{11}(s)$ and $\bar{G}r'^{*}_{11}(s)$ (Figures(7.26) and (7.27)), the three points of Result 3.7 are satisfied. Therefore, multiple channel $\bar{G}r'^{*}_{11}(s)$ decouples and controllers $k_2(s)$ and $k_3(s)$ can be designed on the basis of $\bar{G}r'_{11}(s)$ alone.

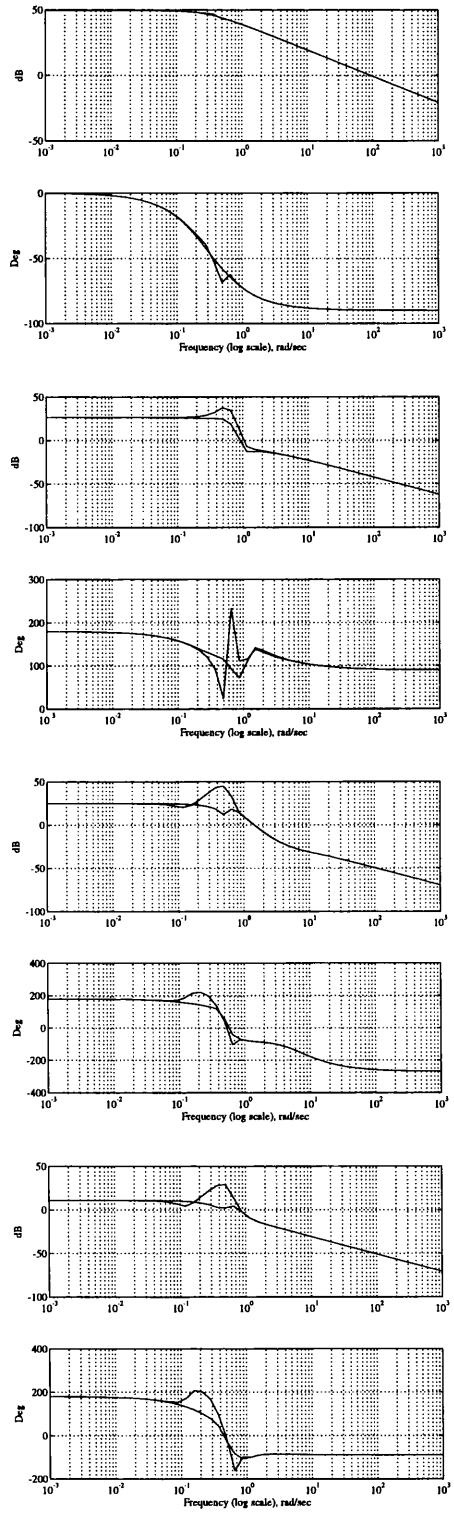

Figure 7.9: Bode plots of $\bar{g}_{1j}(s)$ and $g_{1j}(s)$ for $\bar{G}(s)$ and $G(s)$ respectively.

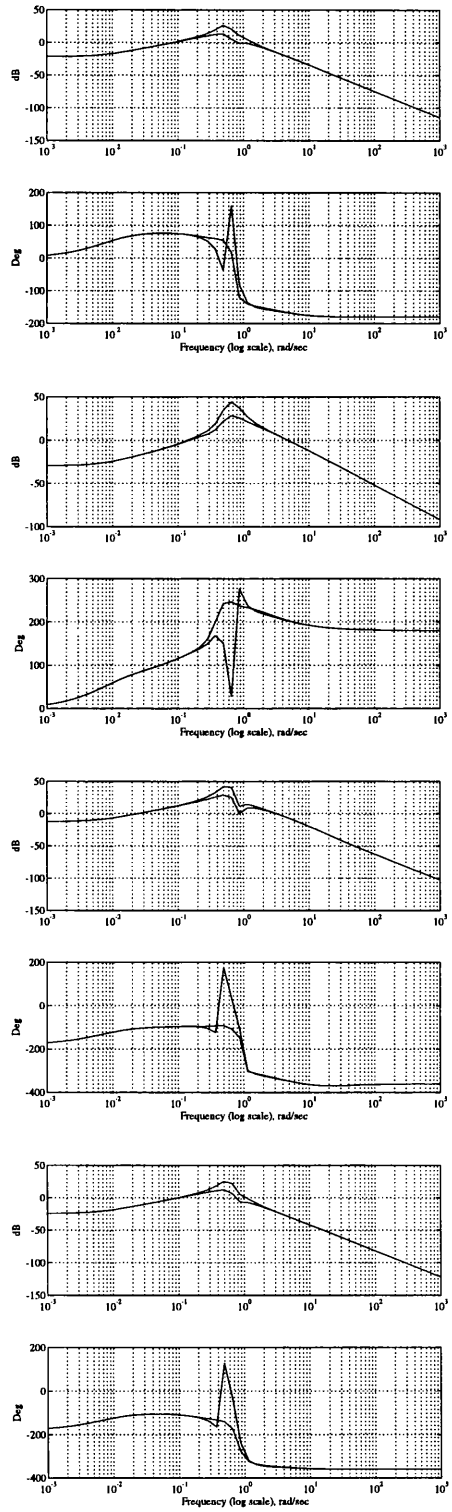

Figure 7.10: Bode plots of $\bar{g}_{2j}(s)$ and $g_{2j}(s)$ for $\bar{G}(s)$ and $G(s)$ respectively.

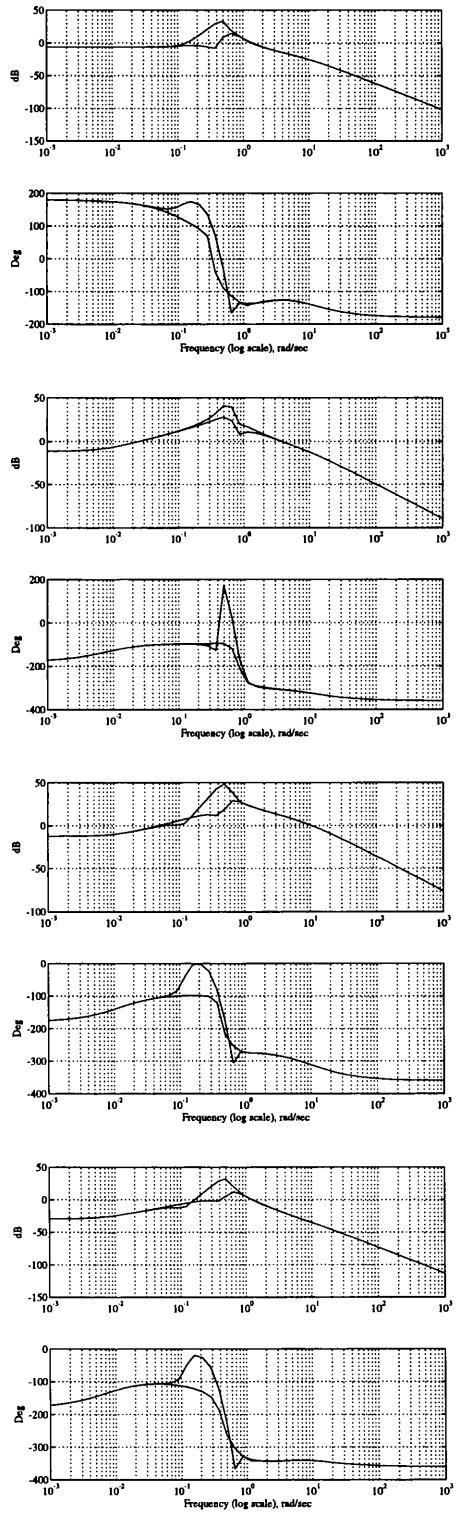

Figure 7.11: Bode plots of $\bar{g}_{3j}(s)$ and $g_{3j}(s)$ for $\bar{G}(s)$ and $G(s)$ respectively.

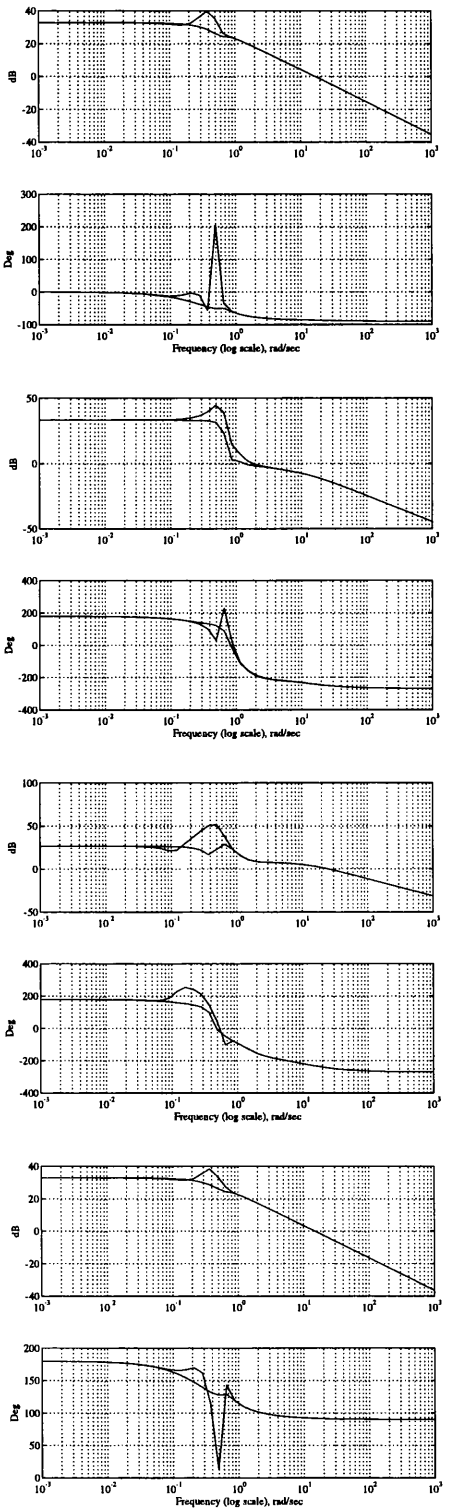

Figure 7.12: Bode plots of $\bar{g}_{4j}(s)$ and $g_{4j}(s)$ for $\bar{G}(s)$ and $G(s)$ respectively.

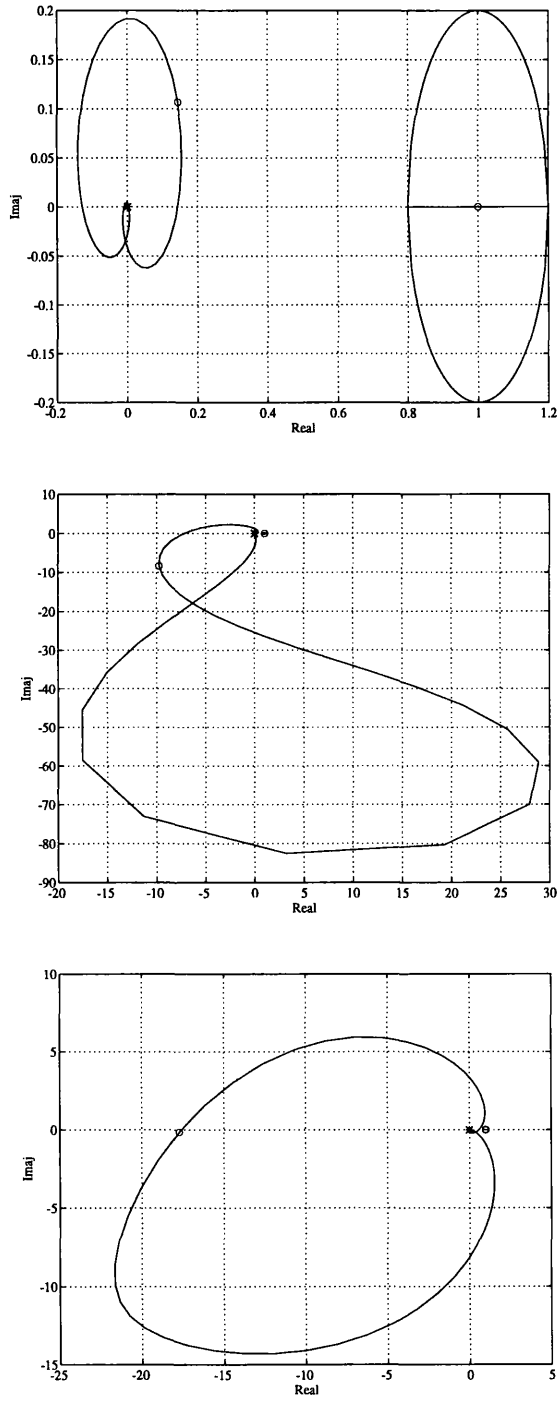

Figure 7.13: Nyquist Plots of $\gamma_{1j}h_{22}(s)$

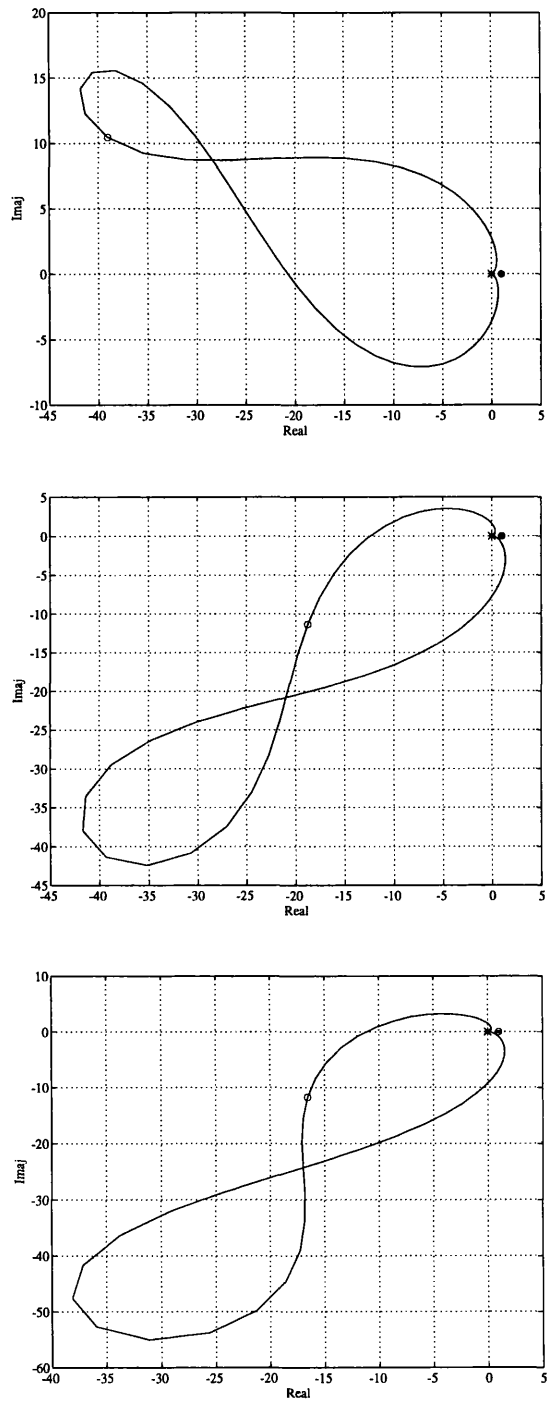

Figure 7.14: Nyquist Plots of $\gamma_{3j} h_{22}(s)$

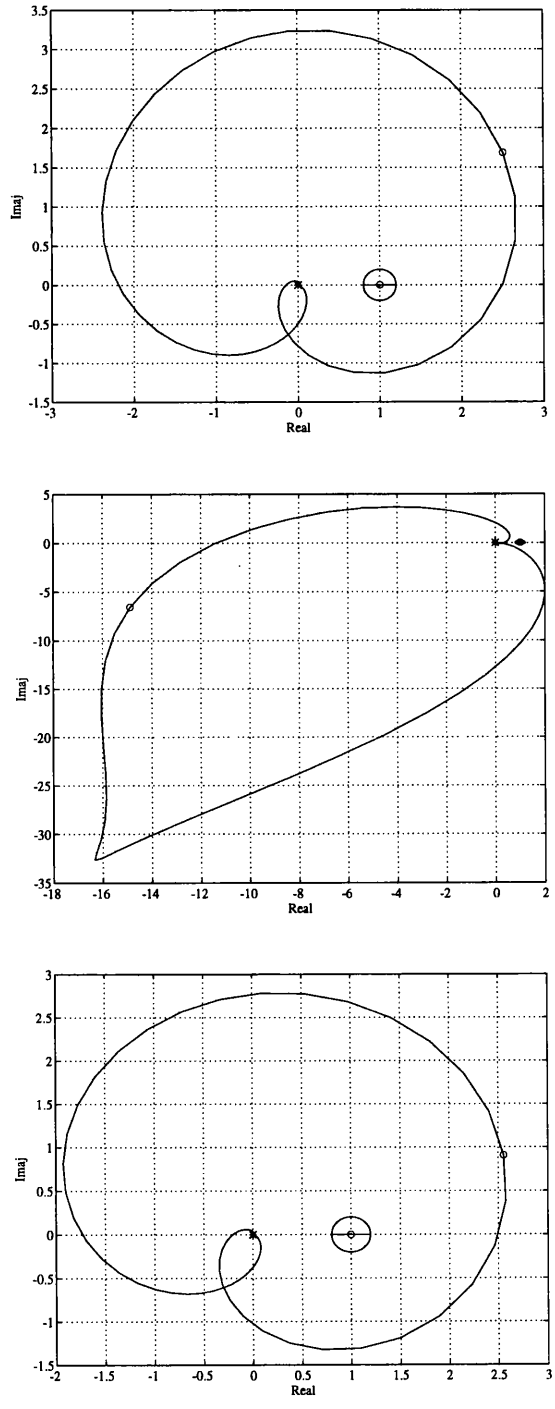

Figure 7.15: Nyquist Plots of $\gamma_{4j} h_{22}(s)$

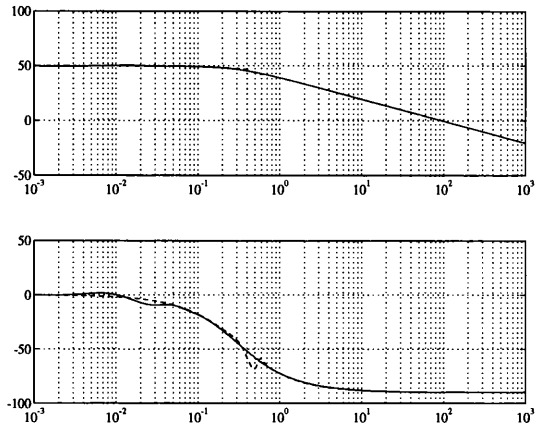

Figure 7.16: Bode Plots of $\bar{g}^*_{11}(s)$ and $\bar{g}^*_{11}(s)$ respectively

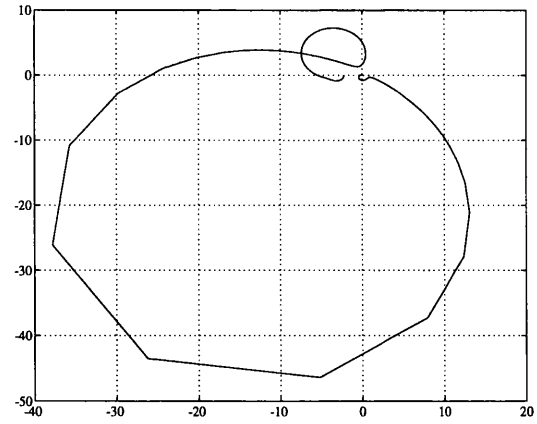

Figure 7.17: Nyquist Plot of $\bar{\Gamma}^*(s)$ of $\bar{G}r^*_{11}(s)$

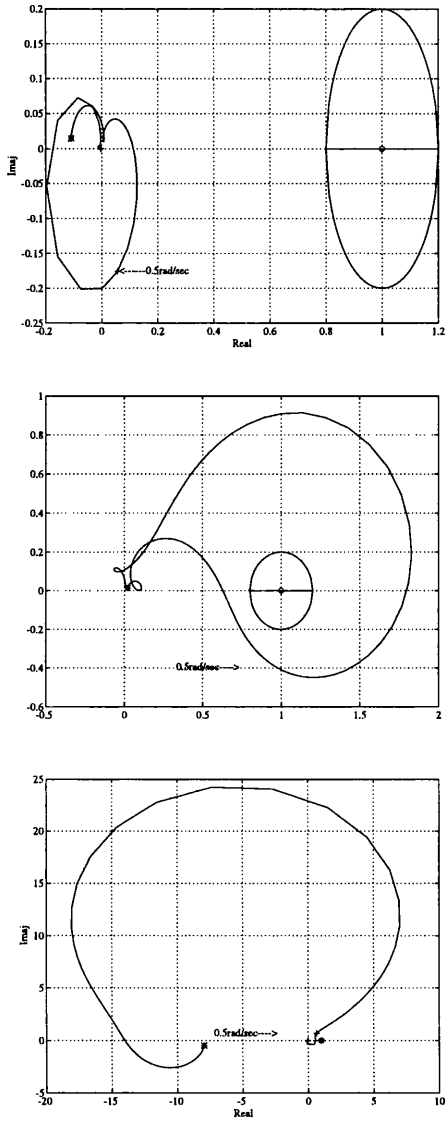

Figure 7.18: Nyquist plots of $\bar{\Gamma}_1(s)$, $\bar{\Gamma}_2(s)$ and $\bar{\Gamma}_3(s)$ of the amended system $\bar{G}(s)$

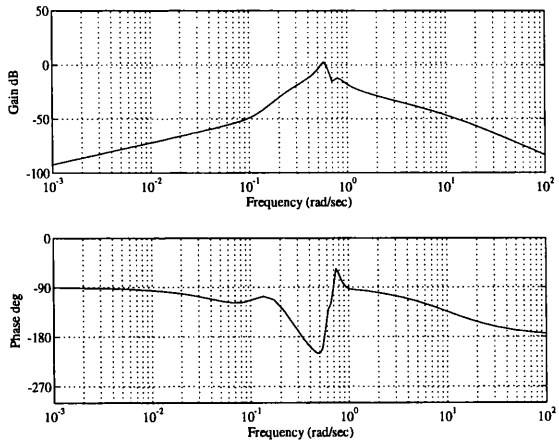

Figure 7.19: Bode plots of $p_{43}\frac{\bar{g}_{31}}{\bar{g}_{41}}$

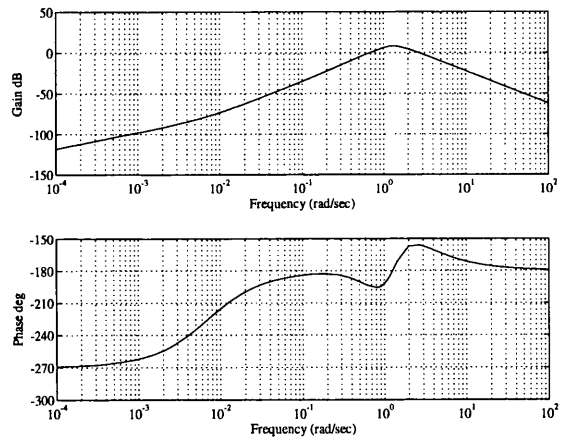

Figure 7.20: Bode plots of $p_{43}\frac{\bar{g}_{32}}{\bar{g}_{42}}$

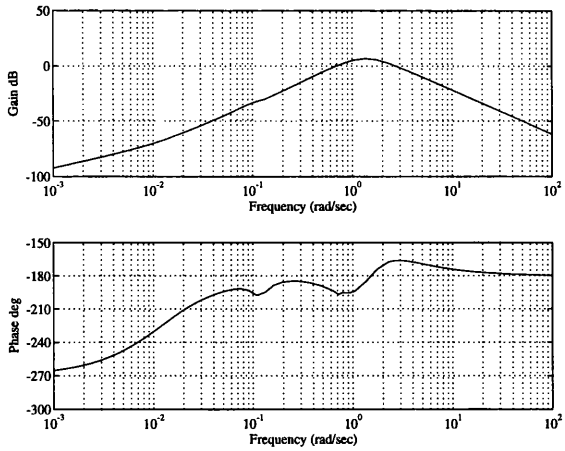

Figure 7.21: Bode plots of $p_{43}\frac{\bar{g}_{33}}{\bar{g}_{43}}$

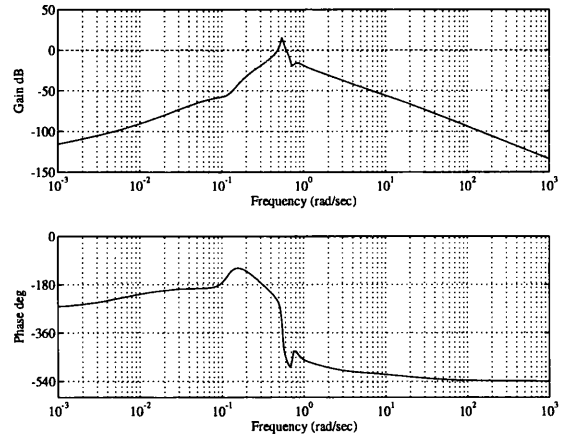

Figure 7.22: Bode plots of $p_{43}\frac{\bar{g}_{34}}{\bar{g}_{44}}$

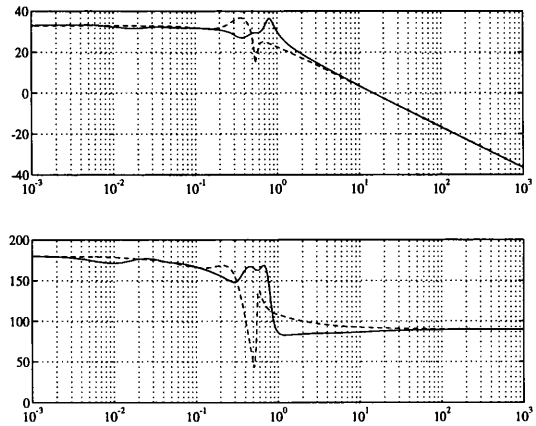

Figure 7.23: Bode plots of $\bar{g}^{*}_{44}(s)$ and $\bar{g}'^{*}_{44}(s)$

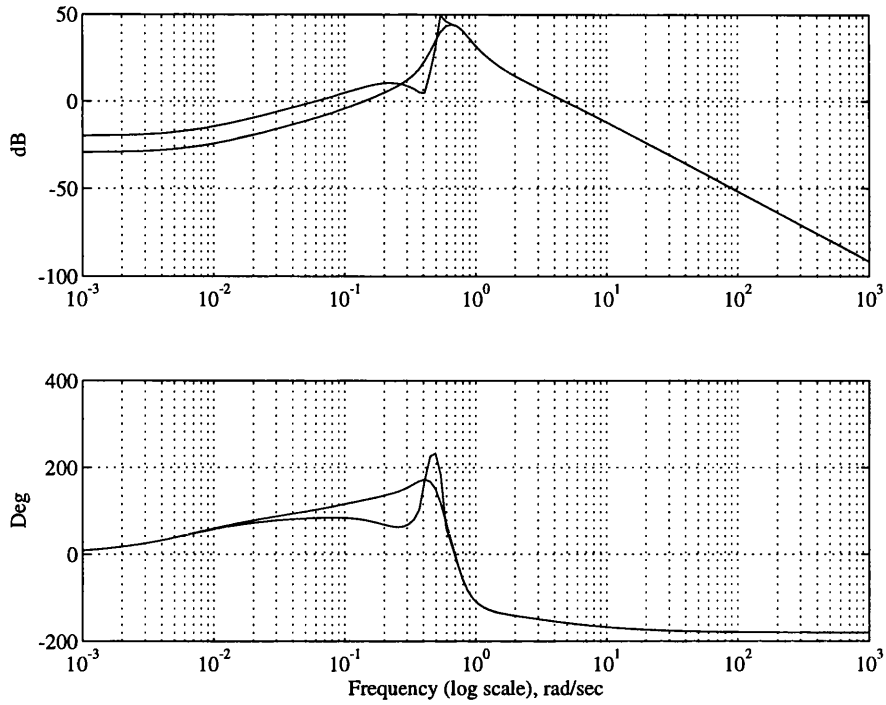

Figure 7.24: Bode plots of $\bar{g}^*_{22}(s)$ and $\bar{g}'^*_{22}(s)$

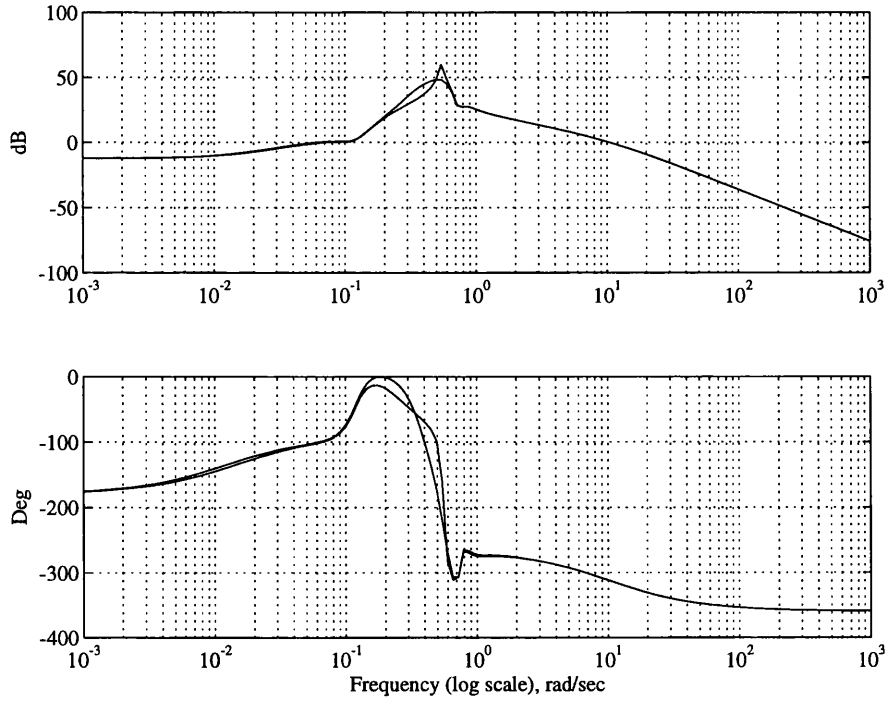

Figure 7.25: Bode plots of $\bar{g}^*_{33}(s)$ and $\bar{g}'^*_{33}(s)$

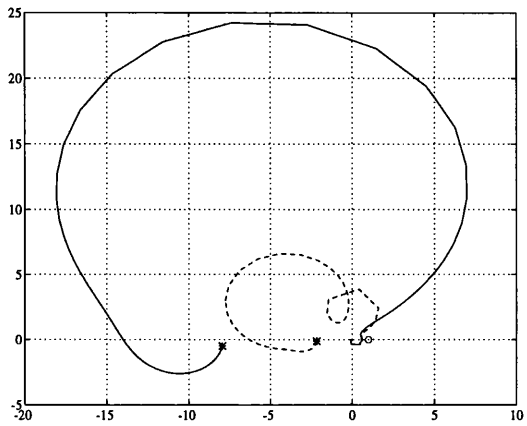

Figure 7.26: Nyquist plots of $\bar{\Gamma}'(s)$ and $\bar{\Gamma}'^{*}(s)$ of $\bar{G}r_{11}^{*}(s)$ and $\bar{G}r_{11}'^{*}(s)$

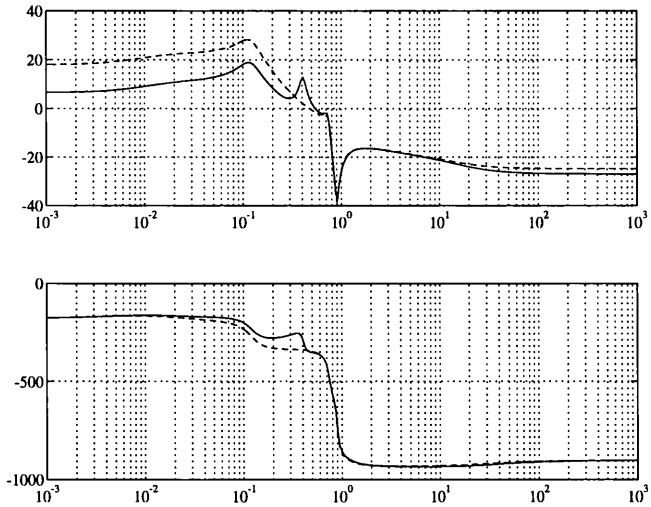

Figure 7.27: Bode plots of $\bar{\Gamma}'(s)$ and $\bar{\Gamma}'^{*}(s)$ of $\bar{G}r_{11}^{*}(s)$ and $\bar{G}r_{11}'^{*}(s)$

7.5 Feedback Controller

In the previous sections, some structural characteristics of the linearised model for the helicopter in hover were analyzed. It was found that despite an apparent decoupled characteristic, due to an almost RHP pole-zero cancellation (close to the system RHPP's) the system is strongly coupled. Moreover, in order to keep channels 2 and 3 minimum phase an exact RHP pole-zero cancellation at roughly the same frequency of the almost RHP pole-zero cancellation is required. It was also concluded that these almost exact cancellations are apparently fictitious. In order to eliminate these problems the system was stabilised via weak-feedback $M(s)$, such that the almost and exact RHP cancellations are changed by a benign LHP almost and exact pole-zero cancellation. Unfortunately, despite the stabilisation by the weak-feedback, channels 2 and 3 are still affected by an exact RHP pole-zero cancellation. Thus, a post-compensator $P(s)$ was designed in order to eliminate this exact RHP pole-zero cancellation. In must be noted that the dangers associated with these procedures were avoided with minimum changes to the system. After the post-compensation the resulting amended system $\bar{G}'(s)$, which henceforth will be called $G(s)$ has the individual channels 1 and 4, and the subsystem $G_{23}(s)$ associated with channels 2 and 3 decoupled. Therefore, controllers $k_1(s)$ and $k_4(s)$ can be designed on the basis of the amended diagonal elements $g_{11}(s)$ and $g_{44}(s)$, respectively. Also, as the multivariable structure function of $\Gamma_{23}(s)$ associated with channels 2 and 3 is almost zero from 0.8 to ∞ rad/sec (Figure(7.28)), controllers $k_2(s)$ and $k_3(s)$ can be designed on the basis of $g_{22}(s)$ and $g_{33}(s)$, respectively. In other words, the system can be considered decoupled for design purposes at the required channel crossover frequencies in the range 2-4 rad/sec.

As was shown in Section 3.3.1, the system $4x4$ transfer-function matrix $G(s)$ is structurally equivalent to the 4 individual channels

$$C_1(s) = k_1 g_{11}(1-\gamma_1) \tag{7.27}$$

$$C_2(s) = k_2 g_{22}(1-\gamma_2) \tag{7.28}$$

$$C_3(s) = k_3 g_{33}(1-\gamma_3) \tag{7.29}$$

$$C_4(s) = k_4 g_{44}(1-\gamma_4) \tag{7.30}$$

where $\gamma_i(s)$ are as defined in equation(3.36)

As it was mentioned above, the controller design can be carried out on the basis of the amended diagonal elements. Nevertheless, in order to guarantee adequate robustness properties, the following points must be satisfied: a) $k_1 g_{11}(s)$, $k_2 g_{22}(s)$, $k_3 g_{33}(s)$ and $k_4 g_{44}(s)$ must have adequate gain and phase margins; b) the resulting Nyquist plots of $\gamma_1(s)$, $\gamma_2(s)$, $\gamma_3(s)$ and $\gamma_4(s)$ must not be close to the point (1,0) in the frequency range of interest 0-4 rad/sec.; and c) the individual open-loop channels must have adequate gain and phase margins within the required channels crossover frequencies of 2-4 rad/sec. For this particular flight condition, the requirements for the control system requires that the bandwidth of the closed-loop channels must be between 3.5 to 5.3 rad/sec, Manness *et al* [22] and Anonymous [1]

An appropriate set of controllers $k_1(s)$, $k_2(s)$, $k_3(s)$ and $k_4(s)$ are given by,

$$k_1(s) = 1.62\frac{s^2+0.6441s+0.1040}{s(s+0.3362)(s+50)} \tag{7.31}$$

$$\begin{aligned} k_2(s) = {} & 0.52\frac{(s^2+0.6s+0.3925)(s^2+0.2972s+0.5479)}{s(s+3)(s+1)(s+0.2)(s+0.0067)} \\ & \times\frac{(s+0.7)(s+0.5)}{(s^2+0.4s+0.1696)} \end{aligned} \tag{7.32}$$

$$k_3(s) = -0.2\frac{(s+11)(s+2.2)(s^2+0.48s+0.3385)(s^2+0.4s+0.4)}{s(s+0.12)(s+0.3)(s+0.4)(s+2)(s+10)} \times\frac{(s^2+0.64s+0.1024)}{(s^2+0.4s+0.2249)} \tag{7.33}$$

$$k_4(s) = -8.06\frac{(s^2+0.6447s+0.1040)}{s(s+0.3139)(s+50)} \tag{7.34}$$

The Bode plots of $k_1g_{11}(s)$, $k_2g_{22}(s)$, $k_3g_{33}(s)$ and $k_4g_{44}(s)$ are shown in Figures (7.29)-(7.32). From these plots it is possible to see that all the Bode plots have appropriate gain and phase margins within the required crossover frequencies WB's. The stability margins of $k_1g_{11}(s)$, $k_2g_{22}(s)$, $k_3g_{33}(s)$ and $k_4g_{44}(s)$ are shown in Table 7.8. Therefore, the first requirement for robustness is satisfied.

transmittance	Phase Margin (deg)	Gain Margin (DB's)	WB's (rad/sec)
k_1g_{11}	86.62	∞	3.039
k_2g_{22}	76.28	34.92	2.607
k_3g_{33}	82.89	∞	2.14
k_4g_{44}	83.0	∞	2.363

Table 7.8: Stability margins of $k_1g_{11}(s)$, $k_2g_{22}(s)$, $k_3g_{33}(s)$ and $k_4g_{44}(s)$

In Figures(7.33)-(7.36), the Nyquist plots of the multivariable structure functions $\gamma_1(s)$, $\gamma_2(s)$, $\gamma_3(s)$ and $\gamma_4(s)$ are shown. From these figures, it is possible to see that none of these plots are close to the point (1,0). Thus, point (b) is satisfied.

In Figures(7.37)-(7.40), the Bode plots of the open-loop channel transmittances $C_1(s)$, $C_2(s)$, $C_3(s)$ and $C_4(s)$ are shown. From these plots and their stability margins shown in Table 7.9, point (c) is also satisfied.

It just remains to check if the closed-loop single channel transmittances satisfy the requirements of design. The Bode plots of the closed-loop individual channels transmittances $Cl_1(s)$, $Cl_2(s)$, $Cl_3(s)$ and $Cl_4(s)$ are shown in Figures(7.41)-(7.44). Following the definition of bandwidth adopted in Chapters 5 and 6, the

resulting bandwidths for the closed-loop $Cl_1(s)$, $Cl_2(s)$, $Cl_3(s)$ and $Cl_4(s)$ are 5.3rad/sec., 5.0rad/sec., 5.1rad/sec. and 5.05 rad/sec. respectively. Therefore, the design specifications are satisfied.

transmittance	Phase Margin (deg)	Gain Margin (DB's)	WB's (rad/sec)
C_1	86.62	∞	3.0
C_2	76.28	34.9	2.6
C_3	82.89	∞	2.1
C_4	83.0	∞	2.3

Table 7.9: stability margins of $C_1(s)$, $C_2(s)$, $C_3(s)$ and $C_4(s)$

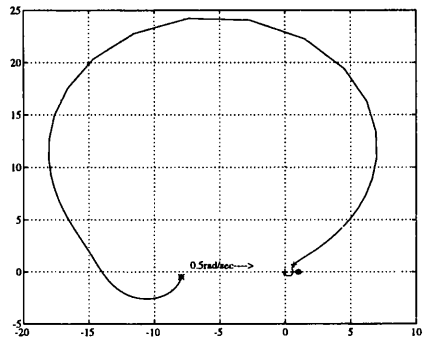

Figure 7.28: Nyquist plot of $\Gamma_{23}(s)$

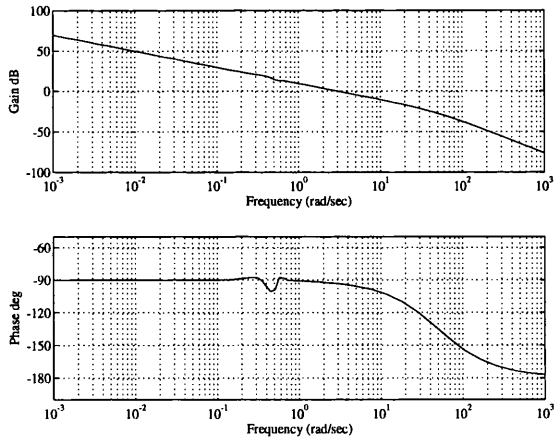

Figure 7.29: Bode plots of $k_1 g_{11}(s)$

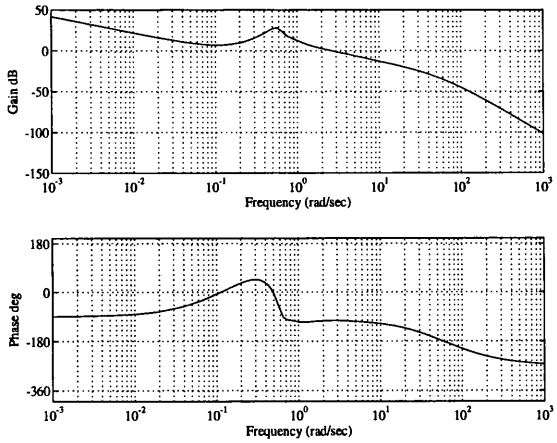

Figure 7.30: Bode plots of $k_2 g_{22}(s)$

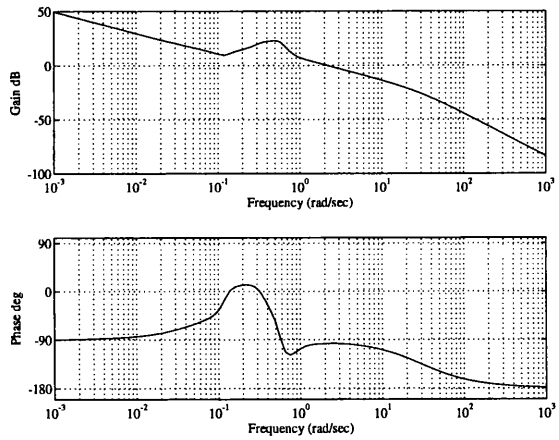

Figure 7.31: Bode plots of $k_3 g_{33}(s)$

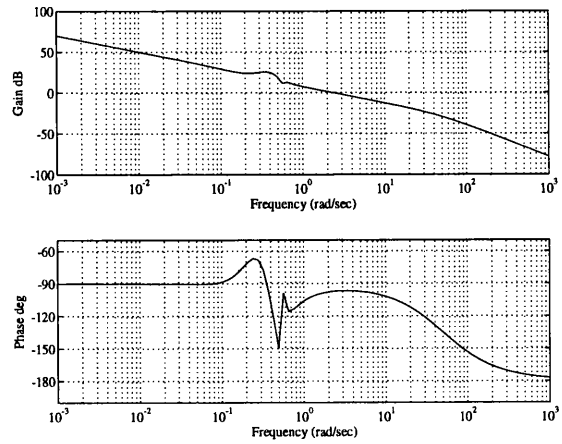

Figure 7.32: Bode plots of $k_4 g_{44}(s)$

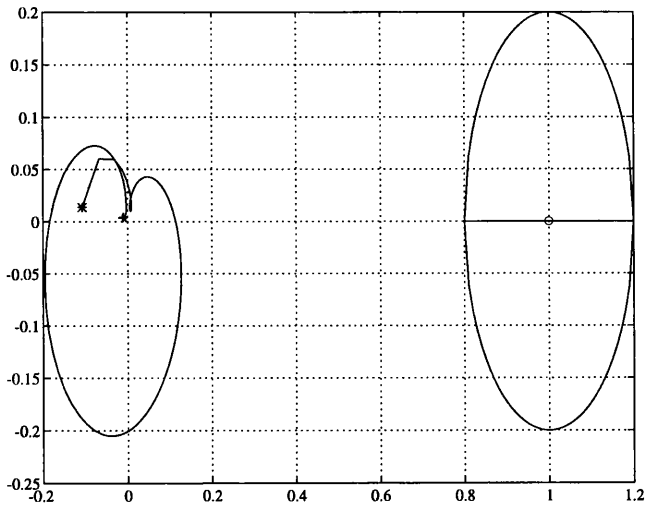

Figure 7.33: Nyquist Plot of $\gamma_1(s)$

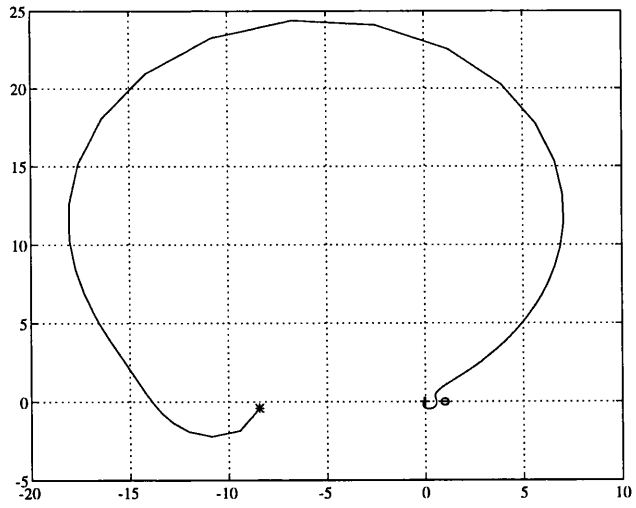

Figure 7.34: Nyquist Plot of $\gamma_2(s)$

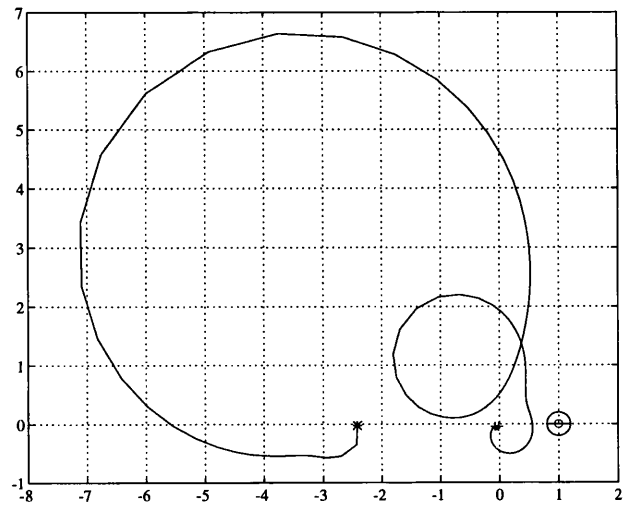

Figure 7.35: Nyquist Plot of $\gamma_3(s)$

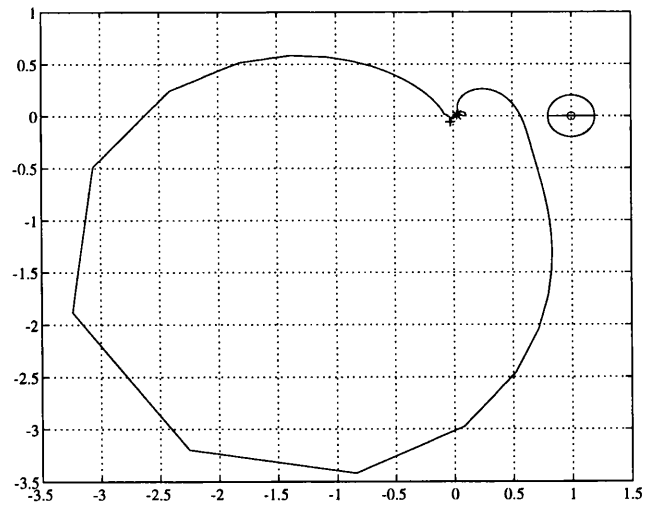

Figure 7.36: Nyquist Plot of $\gamma_4(s)$

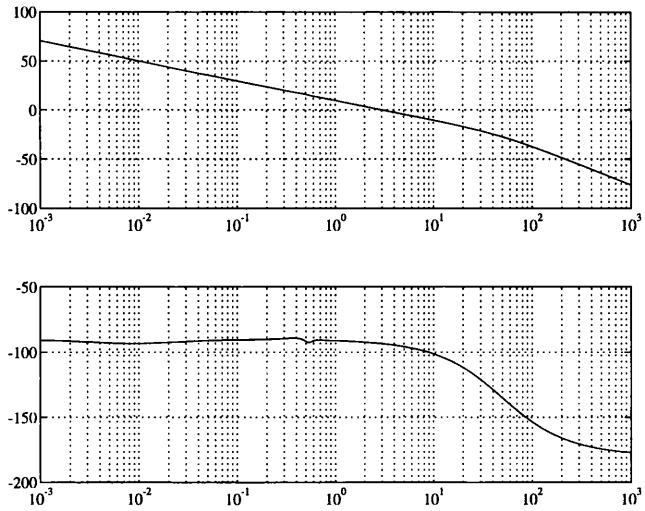

Figure 7.37: Bode Plots of the open-loop single channel $C_1(s)$

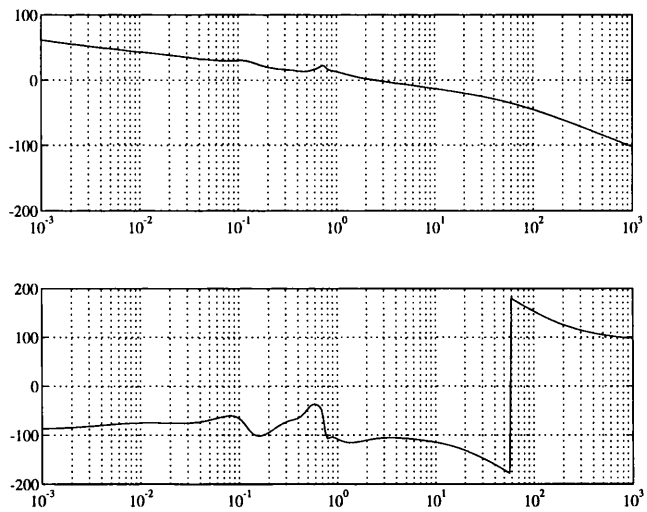

Figure 7.38: Bode Plots of the open-loop single channel $C_2(s)$

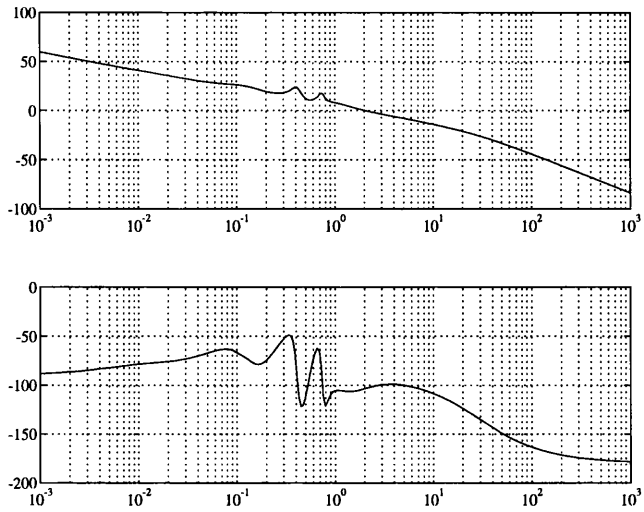

Figure 7.39: Bode Plots of the open-loop single channel $C_3(s)$

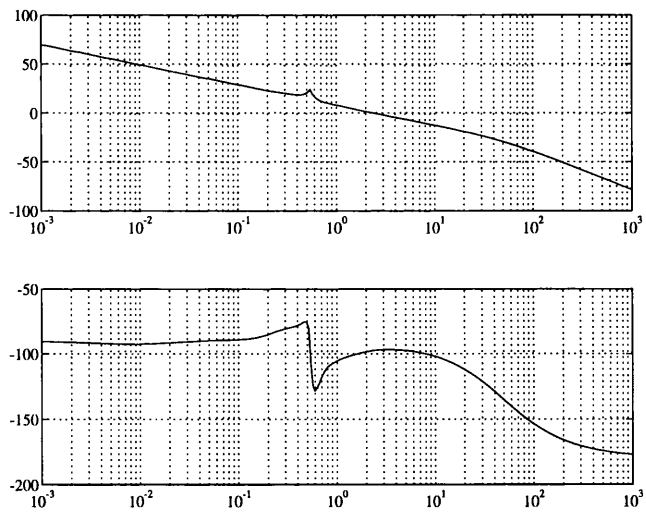

Figure 7.40: Bode Plots of the open-loop single channel $C_4(s)$

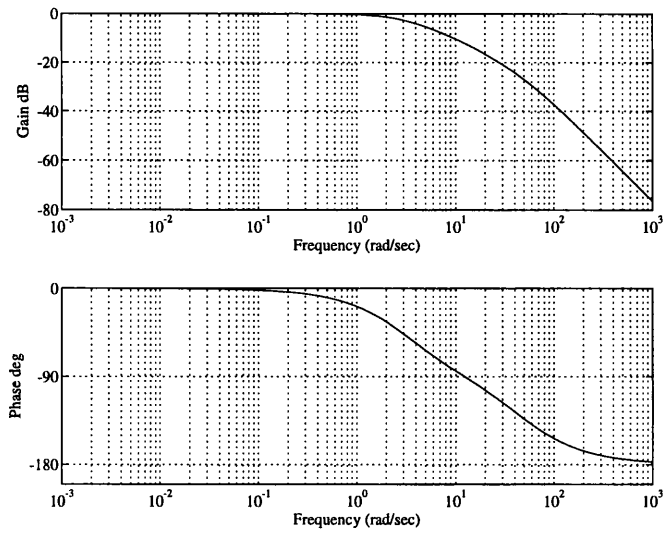

Figure 7.41: Bode Plots of the closed-loop single channel $Cl_1(s)$

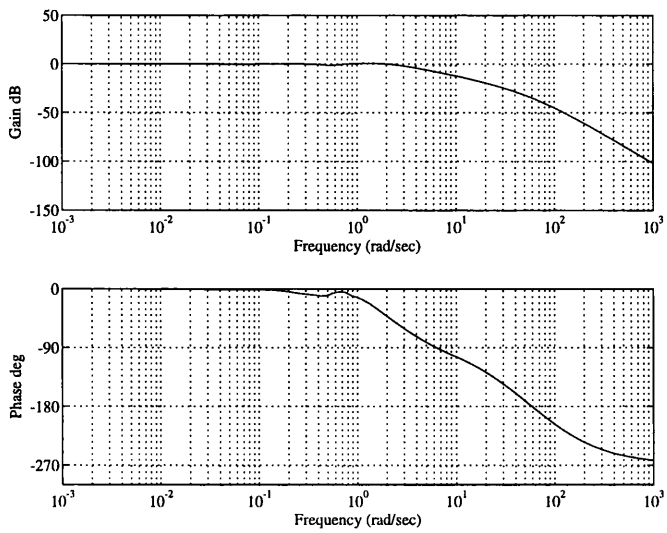

Figure 7.42: Bode Plots of the closed-loop single channel $Cl_2(s)$

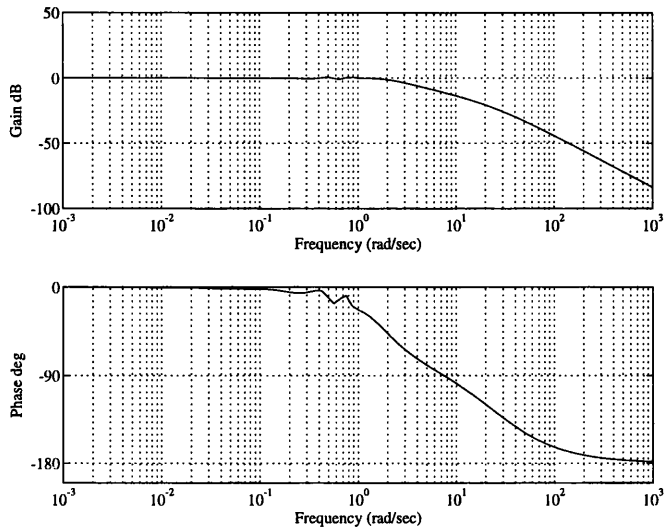

Figure 7.43: Bode Plots of the closed-loop single channel $Cl_3(s)$

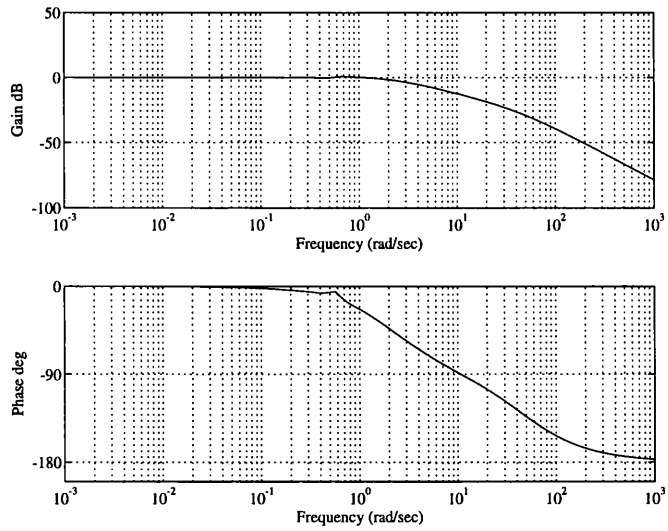

Figure 7.44: Bode Plots of the closed-loop single channel $Cl_4(s)$

7.6 Cross-coupling Reduction

In order to assess the design in terms of the time responses, a unity step variation in the inputs commands is applied. It results in excellent responses to height rate and yaw rate commands as expected from the coupling analysis. Nevertheless, despite the relatively small responses of the off-diagonal elements to the pitch attitude and roll attitude commands, it is necessary to improve these responses. In particular, the effects of the roll attitude command over the height rate and yaw rate responses must be reduced.

In order to reduce the effects of the off-diagonal elements in the closed-loop system, a pre-filter $Pr(s)$ is designed, such that the closed-loop system decouples.

An appropriate pre-filter $Pr(s)$ is given by

$$Pr = \begin{bmatrix} 1 & pr_{12} & pr_{13} & 0 \\ 0 & 1 & pr_{23} & 0 \\ 0 & pr_{32} & 1 & 0 \\ 0 & pr_{42} & pr_{43} & 1 \end{bmatrix} \tag{7.35}$$

where

$$pr_{12} = -\frac{1000s^2 + 1s}{68000s^3 + 40680s^2 + 402s + 1} \tag{7.36}$$

$$pr_{13} = -19\frac{s}{(100s+1)(3.333s+1)} \tag{7.37}$$

$$pr_{23} = -0.4\frac{s(s^2 + 0.2s + 0.19)}{(s+0.08)(s^2+1.6s+1.2)(s+1)(s^2+0.6s+0.6)} \tag{7.38}$$

$$pr_{32} = 0.08\frac{s^2}{(0.33s+1)(0.33s+1)} \tag{7.39}$$

$$pr_{42} = 0.01\frac{s(s+0.05)(s+0.06)}{(s+0.007)^2(s+0.1)(s+0.2)(S+0.8)(s+1)} \tag{7.40}$$

$$pr_{43} = -50\frac{s(s^2+0.7802s+7.4524)}{(s+0.01)(s+0.2)(s+1)^2(s+2)^2} \tag{7.41}$$

The time responses of the system with prefilter are shown in Figures(7.45)-(7.52). From these plots, it is possible to see that the effects of the off-diagonal elements of the closed-loop system have been reduced, obtaining almost completely decoupled responses. Thus, the system peforms within Level 1 handling quality specifications.

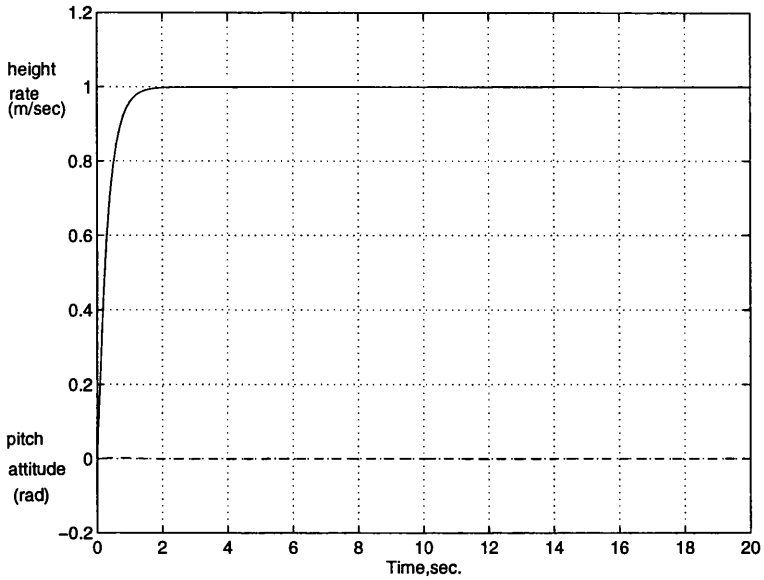

Figure 7.45: Time responses of height rate and pitch attitude to unity step change in input 1

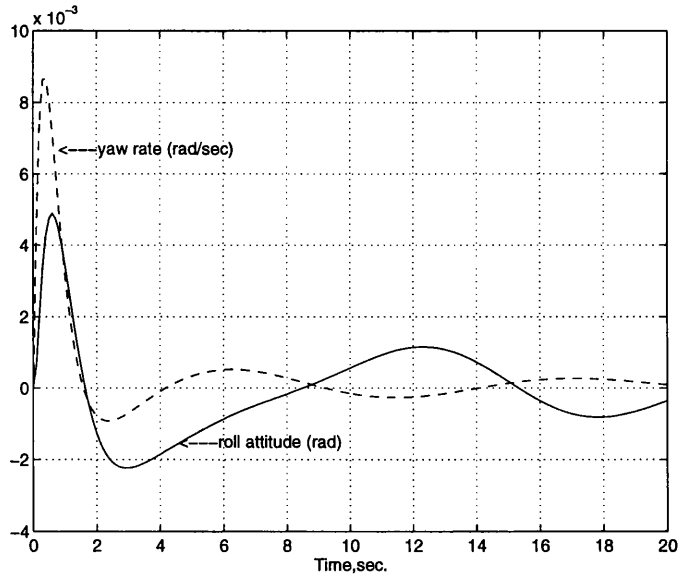

Figure 7.46: Time responses of roll attitude and yaw rate to unity step changes in input 1.

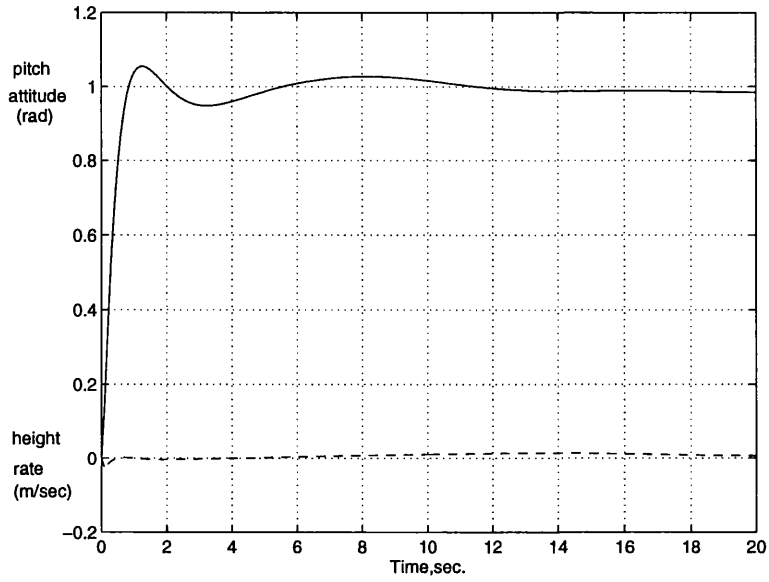

Figure 7.47: Time responses of pitch attitude and height rate to unity step change in input 2

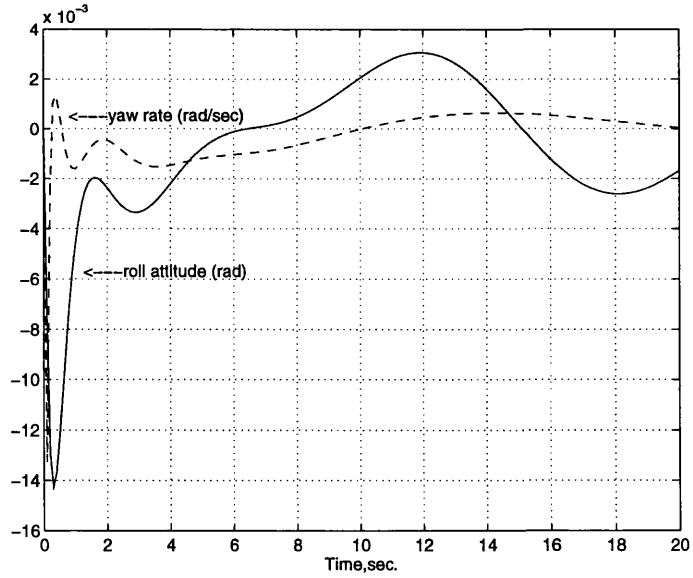

Figure 7.48: Time responses of roll attitude and yaw rate to unity step changes in input 2.

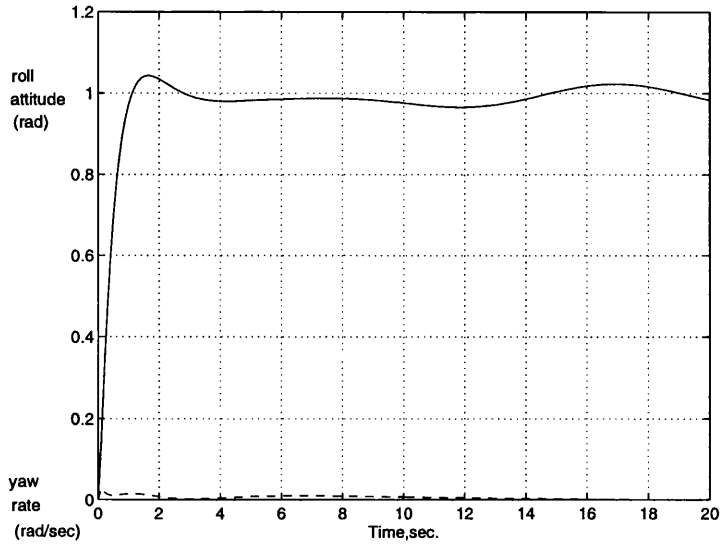

Figure 7.49: Time responses of roll attitude and yaw rate to unity step change in input 3

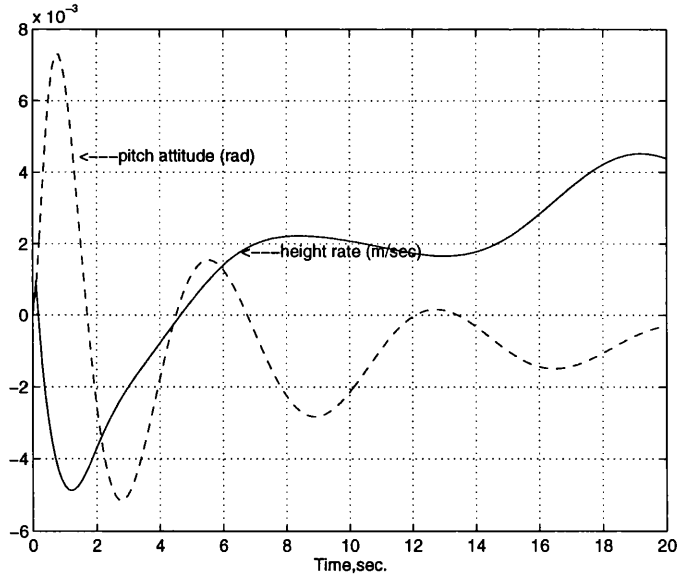

Figure 7.50: Time responses of height rate and pitch attitude to unity step change in input 3

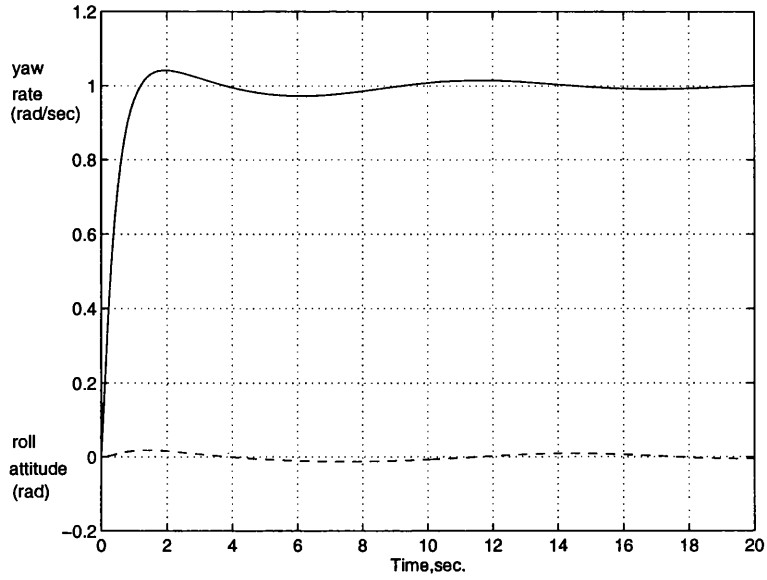

Figure 7.51: Time responses of roll attitude and yaw rate to unity step changes in input 4.

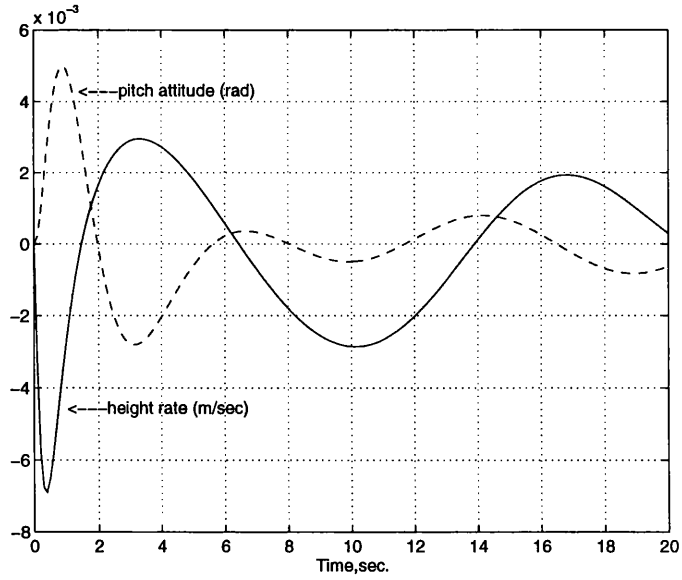

Figure 7.52: Time responses of height rate and pitch attitude to unity step changes in input 4.

7.7 Higher-order Model Evaluation

The helicopter model in hover on which the design is based is a low-order rigid body dynamical linear system model. Thus, similar to the 30 knots forward flight design of Chapter 6, the control system is evaluated in terms of a higher-order model which includes eight rigid-body states, four actuators states and six rotor flapping states. The actuator were represented as first order lags with poles at -12.6 rad/sec except for the tail rotor collective pitch whose pole is at -25rad/sec. The six rotor states correspond to the coning, advancing flap and regressing flap modes with poles at about $-9 \pm 10j$, $-16 \pm 36j$ and $-16 \pm 70j$.

The higher-order model of the helicopter in hover derived from Padfield [28] is a linear state-space representation. The resulting transfer-function matrix for the higher-order model associated with the state-space representation is given by:

$$G(s) = \begin{bmatrix} G_1(s) \\ \dots \\ G_2(s) \end{bmatrix} \tag{7.42}$$

$$G_1(s) = \frac{1}{\Delta} \begin{bmatrix} 1184.7098 & 0.0262 & 0.00453 & 7.4540 \\ -15.4907 \pm 69.6664i & 555.34 & -41.2 \pm 1.5042i & -15.5099 + 69.6495i \\ -15.8536 \pm 35.5453i & -479.93 & -15.85 \pm 35.54i & -15.8535 + 35.5453i \\ -25.0000 & -1238.3 & 35.5754 & -8.4491 + 10.5957i \\ -8.4909 \pm 10.4448i & -15.8535 \pm 35.55i & -25.0 & -13.0549 \\ -12.9762 & -25.00 & -20.1984 & -12.6011 + 0.0019i \\ -12.6000 & -7.23 \pm 9.82i & -12.6 & -12.5979 \\ -12.6000 & -12.60 & -12.6 & -2.6267 \\ -2.6719 & -1.43 & 3.666 \pm 3.4505i & -0.5395 + 0.8981i \\ 0.2407 \pm 0.5338i & -0.1921 \pm 1.123i & -1.879 \pm 1.314i & 0.6912 \\ -0.1792 \pm 0.6043i & 0.65 \pm 0.86i & 0.05 \pm 0.503i & 0.1032 + 0.4550 \\ -0.3357 & -0.43 & -0.3859 & \\ & -12.6 & & \\ & & & \\ 23.6138 & 0.0047 & 0.0000335 & -20.1633 \\ -16.3860 \pm 69.6398i & -7355.479 & -108464.8 & -15.7743 \pm 69.6540i \\ -15.8530 \pm 35.5447i & 5994.993 & 108437.7 & -15.8535 \pm 35.5453i \\ -25.0000 & 1313.333 & -15.8535 \pm 35.5453i & -8.0985 \pm 11.1091i \\ -7.3801 \pm 12.2201i & -15.8535 \pm 35.5453i & -31.7511 & -13.8536 \\ -15.0146 & -25.0000 & -25.0000 & -12.6016 \pm 0.0027i \\ -12.6000 & -8.0058 \pm 10.1206i & -1.9883 \pm 13.3715i & -12.5969 \\ -1.1368 & -12.6000 & -12.6000 & -2.0483 \\ 0.0570 \pm 0.7393i & -12.6000 & 0.0129 \pm 0.8922i & 0.1098 \pm 0.8077i \\ -0.2899 & -0.1210 \pm 0.3628i & -0.3802 & -0.3138 \\ -0.0069 & -0.3112 & -0.3139 & -0.0061 \\ -12.6000 & -0.1387 & -0.0062 & \\ & -0.0064 & -12.6000 & \end{bmatrix} \tag{7.43}$$

$$G_2(s) = \frac{1}{\triangle} \begin{bmatrix} 104.7291 & 0.0021 & 0.0003 & -55.9975 \\ -15.6091 \pm 70.8116i & -33432.34 & -4016.88 \pm 7297.74i & -15.5489 \pm 70.2569i \\ -15.8527 \pm 35.5449i & 33400.78 & 7986.32 & -15.8535 \pm 35.5453i \\ -25.0000 & -15.8536 \pm 35.545i & -15.8536 \pm 35.545i & -8.6562 \pm 4.7490i \\ -14.4463 \pm 1.6563i & -25.0000 & -25.0000 & -12.6056 \\ -12.6000 & -22.9707 & -13.7752 & -12.5972 \pm 0.0049i \\ -12.6000 & -12.6000 \pm 0.0000i & -12.6000 & -12.1952 \\ -1.9047 \pm 1.2475i & -4.4824 \pm 5.0069i & -2.1774 & -2.9772 \\ 0.0307 \pm 0.3524i & 0.0863 \pm 0.8559i & 0.0456 \pm 0.4257i & 0.0743 \pm 0.4066i \\ -0.2939 & -0.3870 & -0.3880 & -0.3142 \\ 0.1255 & -0.3148 & -0.3141 & -0.0067 \\ & -0.0072 & -0.0073 & \\ & & -12.6000 & \\ 218.0341 & 0.0043 & 0.0006 & -378.3695 \\ -15.5010 \pm 69.7676i & -9837.34 & -1816.41 \pm 3120.53i & -15.4927 \pm 69.6819i \\ -15.8535 \pm 35.5453i & 9805.97 & 3585.610 & -15.8535 \pm 35.5453i \\ -25.0000 & -15.8535 \pm 35.5453i & -15.8535 \pm 35.5453i & -8.4900 \pm 10.3404i \\ -8.5059 \pm .7457i & -25.0000 & -25.0000 & -12.9715 \\ -12.9330 & -22.9281 & -13.7704 & -12.6006 \pm 0.0010i \\ -12.6000 & -12.6000 & -12.6000 & -12.5989 \\ -12.6000 & -4.4790 \pm 4.9825i & -2.1847 & -2.6733 \\ -2.6868 & -1.5302 & -1.5251 & 0.2359 \pm 0.5496i \\ 0.2255 \pm 0.5519i & 0.5858 \pm 1.2051i & 0.5857 \pm .2034i & -0.1479 \pm 0.5908i \\ -0.1431 \pm 0.5940i & 0.0869 \pm 0.8572i & 0.0455 \pm 0.4262i & -0.3139 \\ -0.2905 & -0.3127 & -0.3118 & \\ & -12.6000 & -12.6000 & \end{bmatrix} \quad (7.44)$$

with the characteristic polynomial

$$\begin{aligned} \triangle \;=\; & [1, -15.4912 \pm 69.6660i, -15.8535 \pm 35.5453i, -8.4899 \pm 10.4482i, \\ & -12.9780, -2.6708, 0.2412 \pm 0.5322i, -0.1817 \pm 0.6042i, \\ & -0.3224 \pm 0.0066i, -12.60, -12.60, -12.60, -25.0] \end{aligned} \quad (7.45)$$

and the set of finite multivariable transmission zeros

$$T_z \;=\; \{-0.0083, -0.0062\} \quad (7.46)$$

In Figure(7.53), the Nyquist plots of the multivariable structure functions $\Gamma_{1h}(s)$, $\Gamma_{2h}(s)$ and $\Gamma_{3h}(s)$ of the higher-order model of equation(7.42) are shown.

Comparison with those of the low-order model in Figure(7.1), shows that the higher-order system model differs from the low-order system model at low frequency (0-0.02rad/sec) and at high frequency (20-∞rad/sec). However, the differences at low frequency are very small and those at high frequency occur at frequencies above the channel crossover frequencies. Hence, there are not significant changes in the control system when this is applied to the higher-order model. Nevertheless, as indicated in Chapter 6, the actuators may introduce a phase lag of approximately -10 to -15 degrees in each channel. Therefore. it is necessary to assess the performance of the control system with the higher-order model in order to guarantee Level 1 handling qualities. This evaluation is performed in both the frequency and time domain by analysing the Bode diagrams and the unity step responses of the overall closed-loop channels.

In Figures(7.54) and (7.55), the Bode plots of the closed-loop channels for the higher-order model are shown. The resulting bandwidths for the higher-order closed-loop channels $Cl_{1h}(s)$, Cl_{2h}(s), Cl_{3h}(s) and Cl_{4h}(s) according to the definition of Tischler [30], are 5.1rad/sec, 4.9rad/sec, 5rad/sec and 4.8rad/sec respectively. In Figures(7.56)-(7.63), the time responses of the control system with the higher-order model are shown. From these plots and the resulting closed-loop channel bandwidths, it is clear that the control system is capable of maintaining stability and performance despite the unmodelled high frequency dynamics.

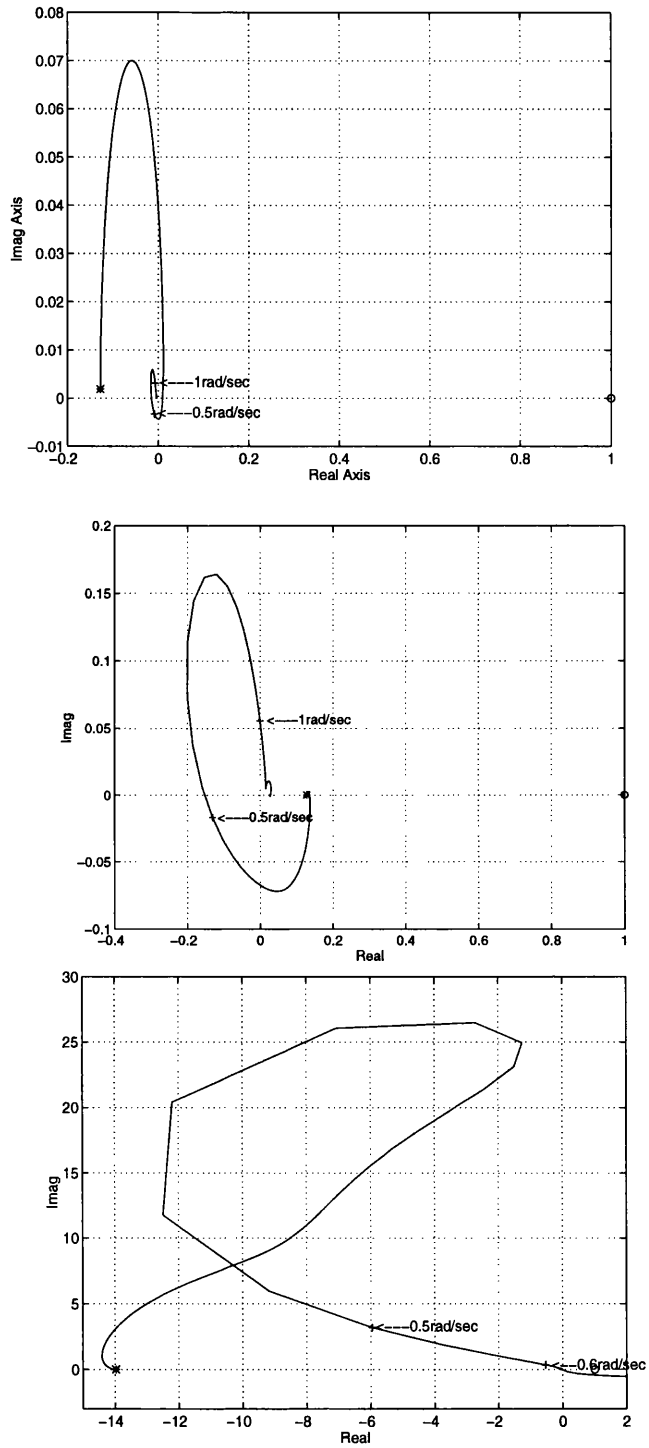

Figure 7.53: Nyquist plots of the multivariable structure functions $\Gamma_{1h}(s)$, $\Gamma_{2h}(s)$ and $\Gamma_{3h}(s)$

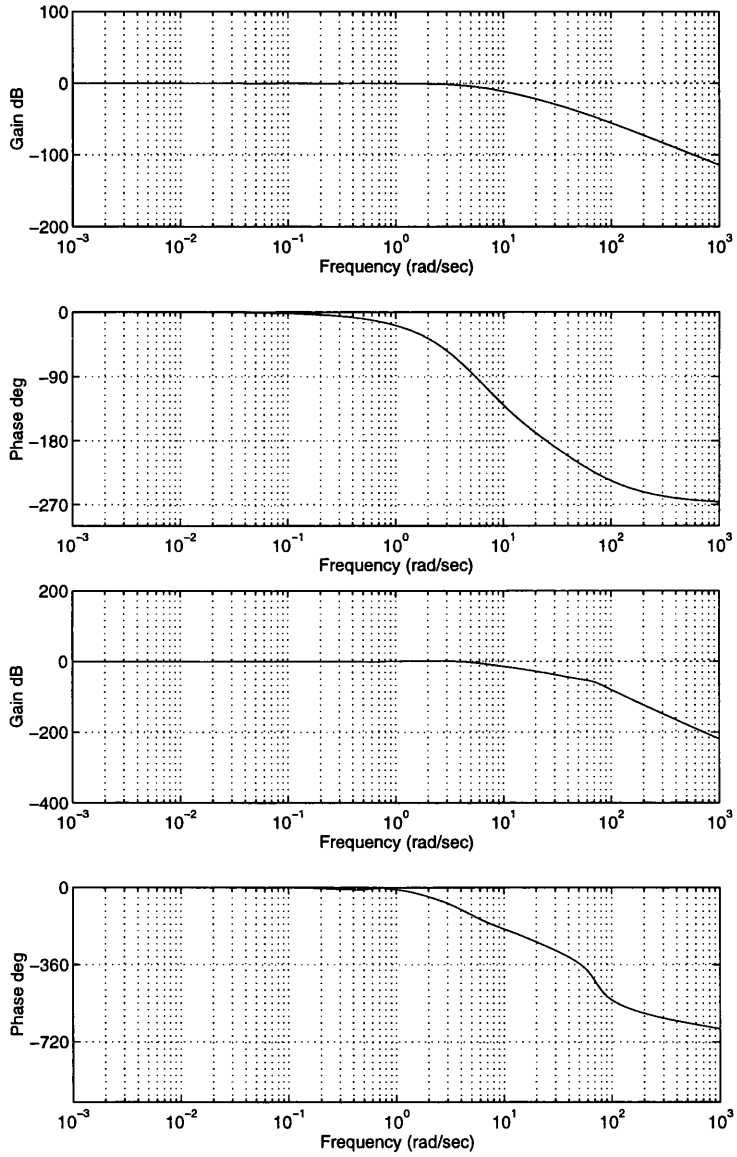

Figure 7.54: Bode plots of $Cl_{1h}(s)$ and $Cl_{2h}(s)$ respectively.

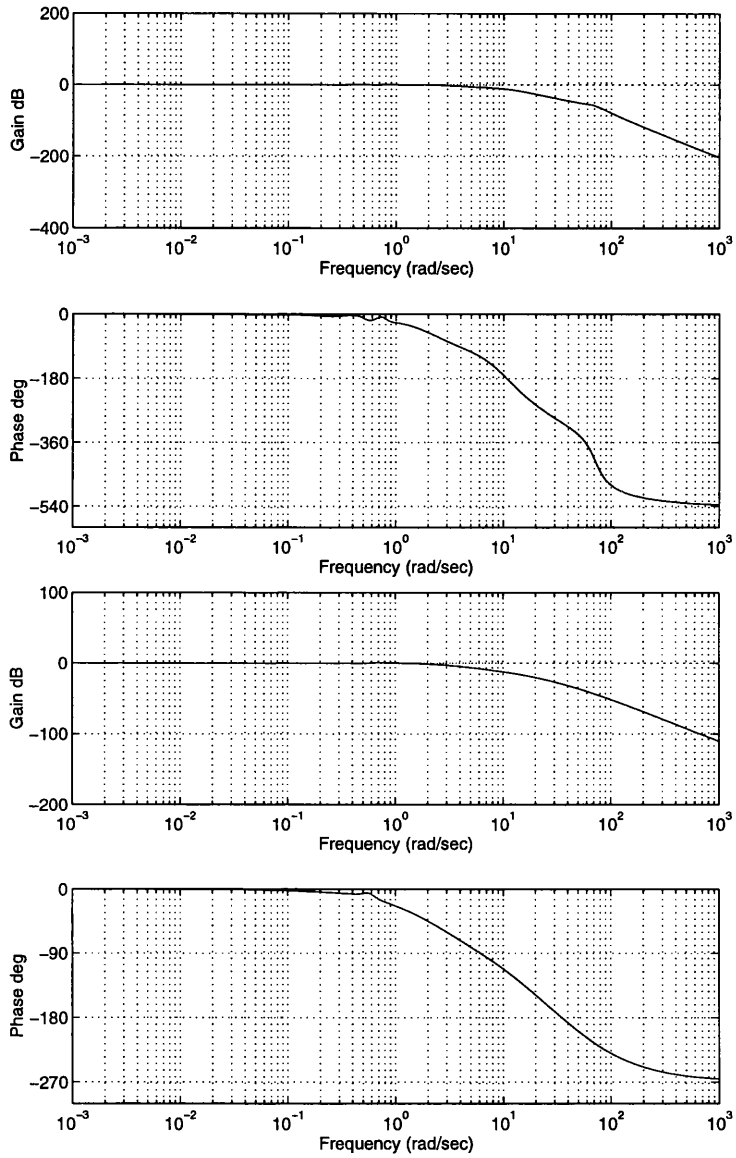

Figure 7.55: Bode plots of $Cl_{3h}(s)$ and $Cl_{4h}(s)$ respectively.

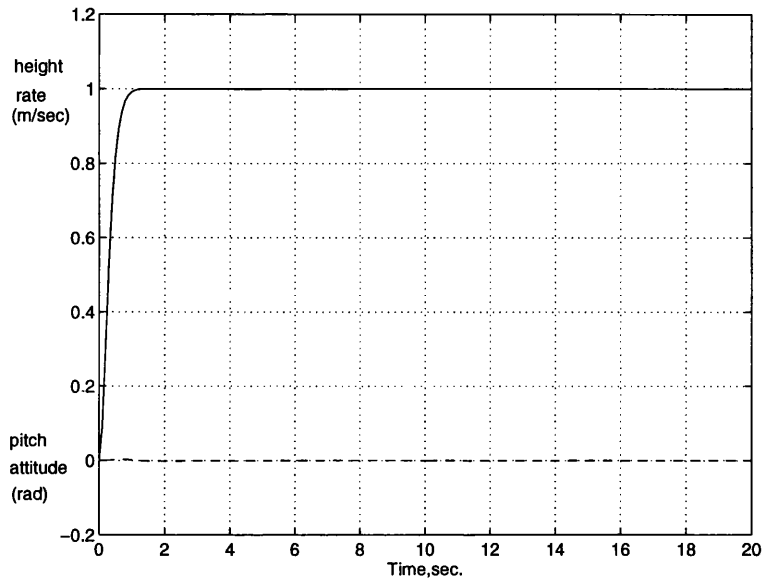

Figure 7.56: Time responses of height rate and pitch attitude to unity step change in input 1 (higher order model)

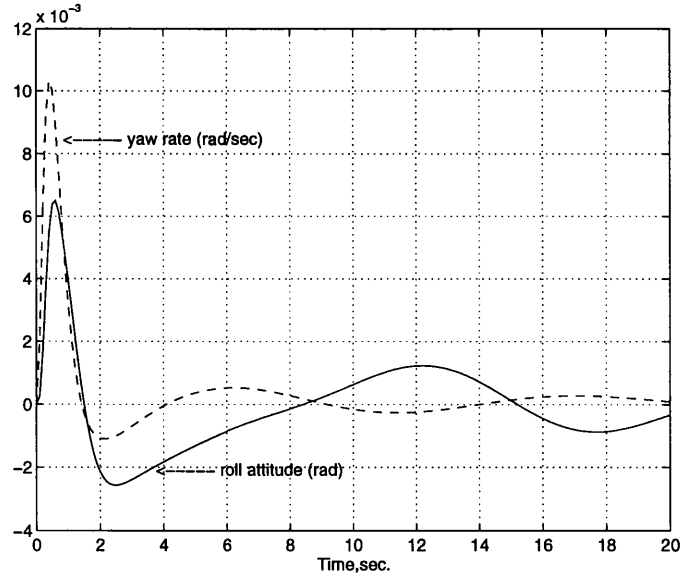

Figure 7.57: Time responses of roll attitude and yaw rate to unity step changes in input 1 (higher order model)

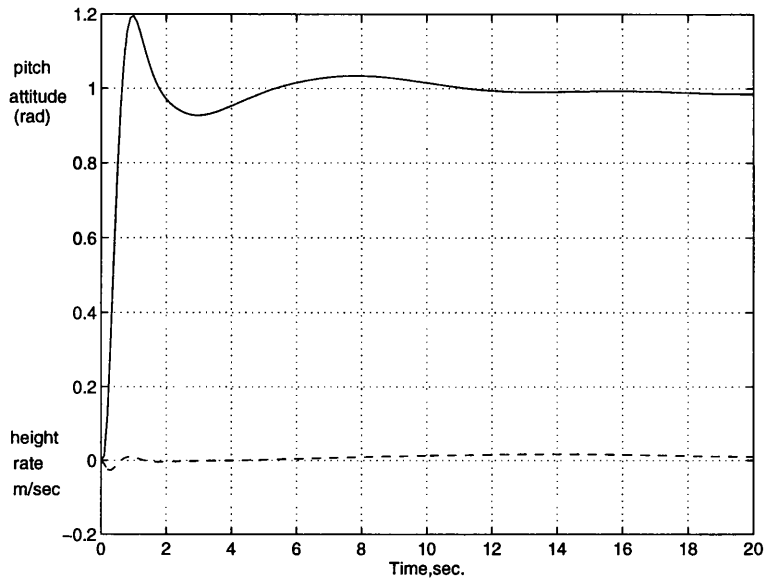

Figure 7.58: Time responses of pitch attitude and height rate to unity step change in input 2 (higher order model)

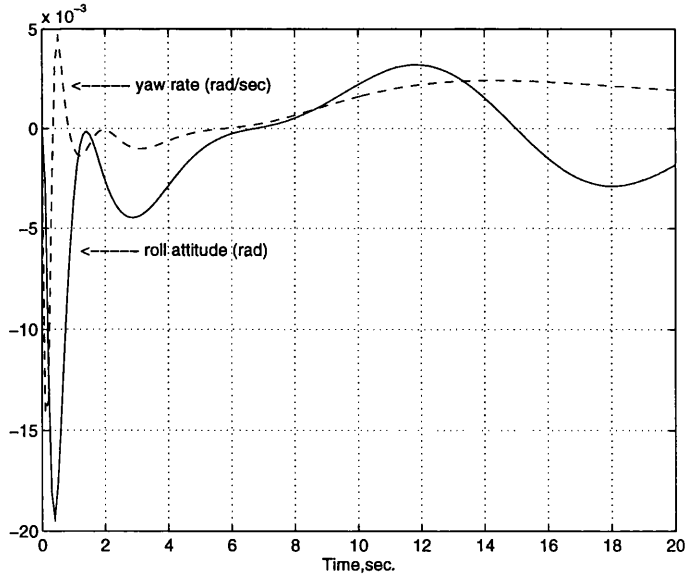

Figure 7.59: Time responses of roll attitude and yaw rate to unity step changes in input 2 (higher order model)

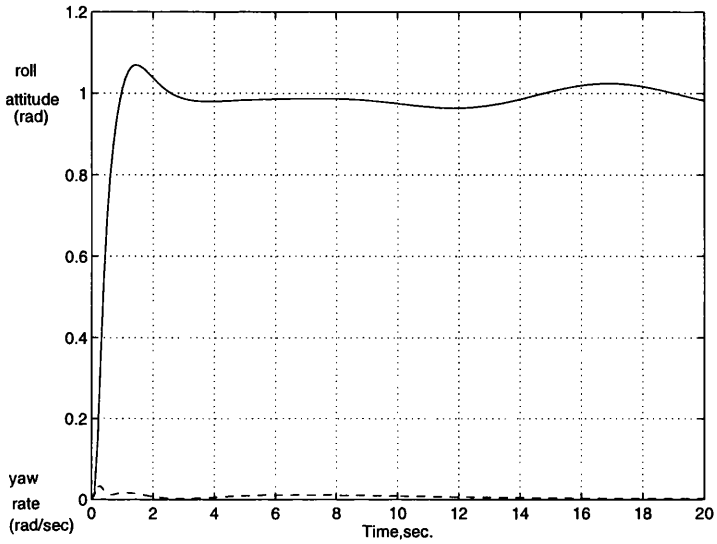

Figure 7.60: Time responses of roll attitude and yaw rate to unity step change in input 3 (higher order model)

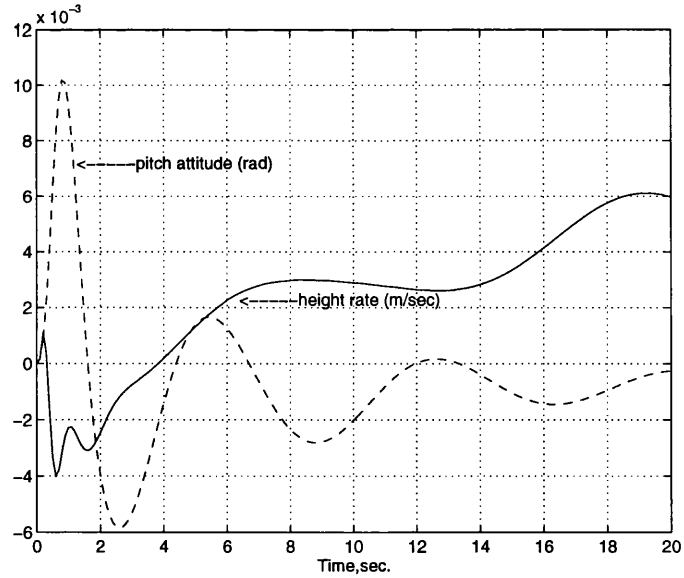

Figure 7.61: Time responses of height rate and pitch attitude to unity step change in input 3 (higher order model)

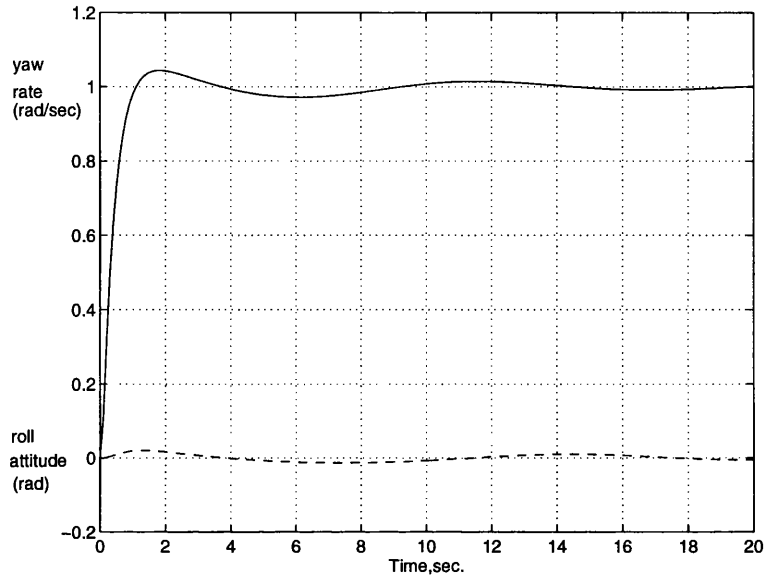

Figure 7.62: Time responses of roll attitude and yaw rate to unity step changes in input 4 (higher order model)

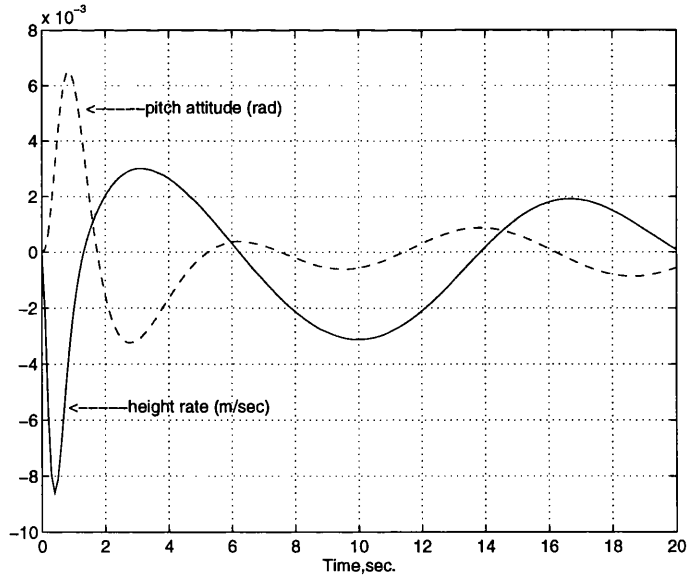

Figure 7.63: Time responses of height rate and pitch attitude to unity step changes in input 4 (higher order model)

7.8 Conclusions

Following the results of Chapters 4-6, the ICD control system for the helicopter in hover was designed. The resulting control system is summarised in the block diagram of Figure(7.64). Similar to the two previous designs, it was necessary to improve the structure of the system model before the design of the actual feedback controller. It was found that despite an apparent natural decoupling characteristic, due to almost exact RHP pole-zero cancellations, the system is strongly coupled. Also, it was found that in comparison to the forward flight models, the system model in hover does not present sensitivity problems. So, in order to eliminate the structural and robustness problems introduced by the almost exact RHP pole-zero cancellations, a weak feedback $H(s)$ and a post-compensator $P(s)$ were designed. Once these structural problems were removed, it was found that the system decouples, *for design purposes* , at the channel crossover frequencies. Hence, the feedback controller matrix $K(s)$ was designed on the basis of the diagonal elements $g_{ii}(s)$ of the amended system. In order to reduce the cross coupling responses and to meet Level 1 handling qualities a pre-filter $P_r(s)$ was introduced.

As the design is based on a low-order rigid body model, the control system was evaluated by applying the full design to a higher-order model which includes low-order approximations of the actuators and rotor dynamics. It was found that requirements of robustness and performance (within Level 1 handling qualities), were satisfied. It is necessary to note that the small differences between the low-order and high-order models at low frequency do no represent any problem as they are at frequencies well below the channel crossover frequencies where the controller gains are high. Also, similar to the designs of Chapters 4-6, the elements of the control system for the helicopter in hover in Figure(7.64) are sparse; $M(s)$ has only one entry, $P(s)$ consists of 1's and 0's and one non-unity off diagonal entry and $K(s)$ has four diagonal entries.

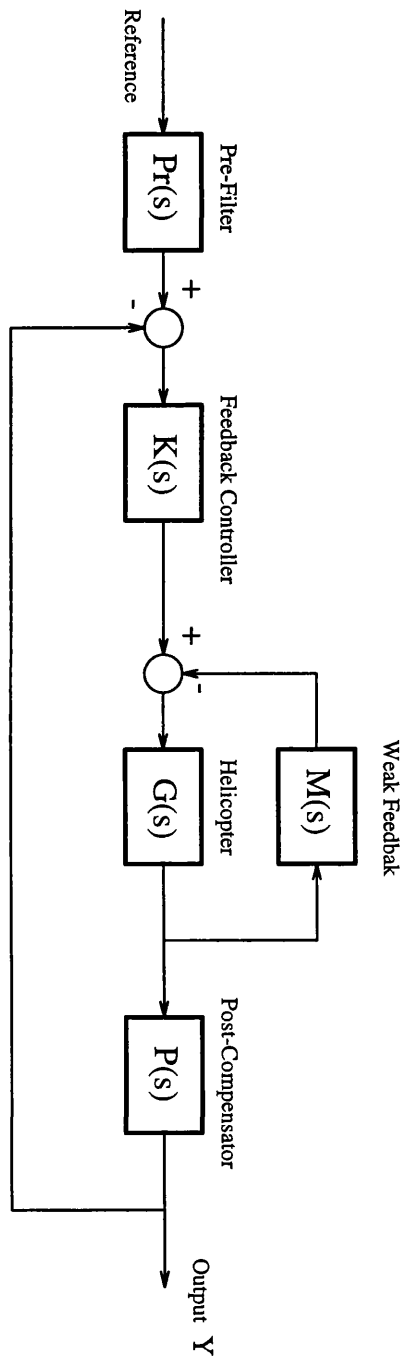

Figure 7.64: ICD Flight control system of the helicopter in hover.

Chapter 8

Conclusions

Despite the fact that the helicopter flight control problem has been substantially studied with highly successful results, it remains a very challenging problem. This is not only because of the complexity of the system and the highly subjective requirements or specifications of design, but also because of the characteristics of the models selected as the basis of design and the way the problem is tackled: *design followed by analysis* . In this way, one of the objectives of this thesis has been to examine in a fundamental way the characteristics of the model that can facilitate or impede the subsequent control design. The methodology of analysis is the engineering approach known as Individual Channel Design (ICD), O'Reilly and Leithead [27, 13, 15, 16, 14, 18, 17]. The reasons why this approach is considered an appropriate framework to be applied to the helicopter control problem are, a) transparency ,i.e, it is possible to determine the structural and robustness characteristics (loop-interaction and RHP poles and zeros) by simple Nyquist and Bode type indicators; b) because the single channel decomposition arises directly from the customer specifications (handling qualities) which can be analysed directly through the use Bode diagrams; c) it provides the necessary conditions to use the highly successful classical gain and phase margins as a measures of performance and robustness for strongly coupled multivariable systems; and d) Although ICD is not a design method *per se* , it is indeed a very powerful and flexible tool for

design, so it should lead to improved control system design, the second objective of the present work.

These objectives were meet in such a way that through the use of ICD it was possible to determine the inherent problems of the helicopter model system which were easily removed by ICD techniques, resulting in a control system for the helicopter flight control problem which satisfied Level 1 handling qualities. Throughout, the ICD analysis found that the helicopter system model presents structural problems which may result in lack of robustness and performance. These problems are in addition with those associated to the unmodelled rotor and actuators dynamics. Furthermore, these problems *can not* be remedied by simple feedback.

Three flight regimes were selected: forward flight at 80 knots and 30 knots, and hover. The models for these flight conditions, derived from HELISTAB, Padfield [28], are in the form of linear state space representations with associated transfer-function matrices with almost RHP pole-zero cancellations. This is a problem which will affect the helicopter model system in any flight condition mainly because the helicopter is open-loop unstable. As indicated by Leithead and O'Reilly [18], models obtained originally in a state space representation present particular problems; specifically the introduction of fictitious pole-zero cancellations either in the right half plane (RHP) or left half plane (LHP). Those in the LHP due to their stable characteristics do not present any problem. However, those in the RHP represent a serious robustness problem. They are either unobservable or uncontrollable; second, they can not be ignored or directly cancelled without compromising robustness. These restrictions arise from the fact that despite being fictitious, there is a high risk of cancelling real RHP poles or zeros, and because exact cancellations *cannot* be always guaranteed. On the other hand, it is recalled that this models arise from a linearisation which may change or modify some dynamical characteristics, i.e, it is not always possible to know whether a RHP cancellation is real or not, Isidori [10]. Therefore, *weak* feedbacks which leave the

system virtually unchanged, were designed in order to change the almost RHP pole-zero cancellations to benign almost LHP pole-cancellations. This results in the elimination of the robustness problems associated with the almost RHP pole-zero cancellations. Also, the *weak* feedbacks were designed in such a way that they do not introduce additional robustness problems, Leithead and O'Reilly [18].

For the case of the forward flight regime, the conclusions are divided in terms of the low speed (30 knots) and the high speed (80 knots) flight conditions. For forward flight at 80 knots, it was found that the system decomposes, *for design purposes,* into lateral and longitudinal dynamics. Hence, the control system design was carried out by two independent designs, one for the lateral dynamics and one for the longitudinal dynamics. In was also found that the lateral dynamics present excessive structural sensitivity at frequencies close to the channel crossover frequencies. Additional to this problem, the lateral dynamics are also affected by the introduction of RHPZ's at frequencies close to the channel crossover frequencies when the design specifications are satisfied. These problems are solved using pre-compensation and a new application for feedforward control, Leithead and O'Reilly [16, 17]. Once these structural problems were solved, feedback controllers were designed. In order to further reduce the cross-coupling terms in the overall closed-loop system, a pre-filter was required. The final design was evaluated on the basis of the full $4x4$ system and it was found that the control system satisfies Level 1 handling qualities specifications.

The forward flight at 30 knots presents substantial differences with respect to the 80 knots case. First, it was found that it does not decompose into lateral and longitudinal dynamics. Therefore, this condition is treated as a full $4x4$ control problem. Second, the sensitivity problems, unlike the 80 knots case, arise at very low frequency which may results in the introduction of RHPZ's in any of the open-loop channels (at frequencies well below the channels crossover frequencies) with

the subsequent lost of stability. Following the results obtained in the 80 knots case, a pre-compensator and a feedforward controller were designed to solve these problems. Again, once the structural problems were removed, a diagonal feedback controller which satisfies the design requirements was designed. Also, similar to the 80 knots case, in order to reduce the cross-coupling terms it was necessary to introduce a pre-filter.

This design was also assessed in terms of a higher-order model which includes approximations of the rotor and actuator dynamics. It was found that the control system was capable of maintaining robustness and performance within Level 1 handling qualities specifications. This was possible by the fact that through the use of ICD it is possible to determine how these unmodelled dynamics affect (mainly by phase lags) the frequency responses of the channels. So, the channels were designed with sufficient phase and gain margins which minimise these effects.

As indicated by Manness *et al* [21], it is of interest to know whether or not a particular method of control design can be used to design a scheduling control scheme for the helicopter problem. Thus, the 30 knots design was also assessed along a range of different speeds (20 to 40 knots). In this case it was found that the control system can maintain robustness and performance only from 25 to 35 knots, i.e, for an interval of 10 knots. This does not satisfy the criterion of 20 knots establish by Manness *et al* [21]. However, it was also found that the modifications required for the control system to guarantee robustness and performance from 20 to 40 knots are minimal. Therefore, ICD can be use to design a scheduling control system for the helicopter control problem.

It is well known that the dynamical behaviour of the helicopter changes substantially between the forward flight condition and the hover. Hence, the ICD design for the hover condition shows substantial differences as compared to the forward flight conditions. It was found that (apart from the almost RHP pole-zero cancellation already explained) the helicopter system model in hover does not

present structural problems. Moreover, it can be considered decoupled, *for design purposes,* at the required channel crossover frequencies. Therefore, the feedback controller was designed only on the basis of the diagonal elements of the transfer-function matrix. This design also requires a pre-filter to reduce the cross-coupling terms to satisfy Level 1 handling qualities specifications.

Similar to the 30 knots design the control system for the helicopter in hover was assessed in terms of a higher-order model which also includes approximations of the rotor and actuators dynamics. Again, it was found that the control system can maintain performance and robustness within Level 1 handling qualities specifications.

8.1 Suggestions for further work

It should be noted that only one set of outputs (one for each regime) was considered in this work. Therefore, it is necessary to extend this work to models with different sets of outputs. Also, different flight conditions with more demanding manoeuvres should be analysed. For instance, the forward flight regime with a small lateral velocity may result in substantial changes in the coupling characteristics of the system model with respect to those reported here. Also, it was assumed that the outputs of the models are signals that can be directly measured; that is, they are not signals obtained by a linear combination of the states via the output matrix C. Otherwise, the system would originally be a system with 4 inputs and 8 outputs which is transformed to a 4-input 4-output system by a post-compensator, namely the matrix C. If this is the case, then it is necessary to analyse the robustness implications of this post-compensation. This is not a trivial analysis due to the fact that the original system will be non-square for which the ICD approach has as yet to be developed. Also, further refinements of the multivariable control designs in the light of assessment against nonlinear models containing rotor and actuator dynamics are required.

Towards the design of a scheduling control strategy it is also necessary to extend the control system design to more flight conditions or velocities. This would require the analysis of the possible effects in the changes of different control modes. For instance, the effect of the change of flight conditions, which require the change of the controller accordingly, may result in *bumping* during the transition between different control modes. But it can be proved that this effect and its elimination depends heavily on the scheduling method used as this process determines the nominal value of the control inputs.

In order to determine the possibilities of *real* applications, it is necessary to investigate how the compensators (elements of the control system) can be implemented. Because digital compensator have many advantages over analog ones, it is preferable to design digital compensators to control analog plants. There are two approaches to carrying out the design. In the first approach, an analog compensator is designed and then it is transformed into a digitial one. The second approach first transforms analog plants into a digital plants and then carries out design using digital techniques. The first approach performs discretisation after design; the second approach performs discretisation before design. Therefore, the digital implementation of the controller could be addressed considering the study of several methods, for instance: Impulse-Invariance Method, Step-Invariance Method and Frequency domain transformations such as Forward Approximation, Backward Approximation, Trapezoid Approximation and Pole-Zero Mapping, Chen [4]. The effectiveness of each method could lead to an extensive analysis procedure and simulation exercise.

Also, in order to facilitate this analysis, it is necessary to reduce the order of the SISO elements of the controllers of the present work. This could be achieve by calculating the multivariable structure functions and the individual channel frequency responses (Nyquist and Bode graphs) by a frequency evaluation instead

of a matrix transfer function evaluation. This would require the use of the *nest* characteristic of the multivariable structure function, Leithead and O'Reilly [14], in order to determine the channel structures.

Finally, the effects of gusts on the control system can be investigated by determining the main characteristics of their dynamics. These are described as stochastic process. Their spectrum and magnitude are obtained by statistical methods. Some of the most known representations are those described in Carr [3] and McLean [23]. This models could be used to analise the gust effects by applying sensitivity analysis.

Appendix A

Appendix

A.1 System model at 20 knots forward flight

$$G_{20}(s) = \begin{bmatrix} G_1(s) \\ \dots \\ G_2(s) \end{bmatrix} \tag{A.1}$$

where

$$G_1(s) = \frac{1}{\triangle} \begin{bmatrix} 1148.2240 & 58.2711 & -0.01147 & 4.38009 \\ -15.489 \pm 69.5858i & -40.7222 \pm 60.4774i & 1226.2096 & 145.3581 \\ -15.898 \pm 35.5184i & 16.8920 \pm 52.3018i & 487.6015 \pm 846.89 & -15.7065 \pm 69.5516i \\ -25.0000 & -15.8399 \pm 35.5528i & -15.8414 \pm 35.5364i & -15.8534 \pm 35.5389i \\ -8.5956 \pm 10.1625i & -25.0000 & -31.8131 & -8.2473 \pm 11.2115i \\ -12.6000 & -8.0151 \pm 10.1068i & -25.0000 & -13.2019 \\ -12.6000 & -12.6000 & -2.1932 \pm 13.1058i & -12.6014 \\ -9.9272 & -0.2139 \pm 0.7237i & -12.6000 & -12.5993 \pm 0.0012i \\ -5.8420 & -0.5644 & -12.6000 & -4.0042 \\ -0.5354 \pm 0.6683i & -0.0727 & -0.0502 \pm 1.0599i & 1.6052 \\ 0.2564 \pm 0.3730i & 0.0831 & -0.5616 & -0.5263 \\ -0.1023 & -12.6000 & -0.3132 & 0.1944 \\ & & 0.0703 & 0.0663 \\ 21.5834 & 1.0952 & -0.0002 & -17.6991 \\ -8.2923 \pm 73.5181i & -325.8799 & -69.93 \pm 45835i & -15.797 \pm 69.629i \\ -13.6451 \pm 35.1460i & 139.298 \pm 242.39i & -15.841 \pm 35.535i & -15.853 \pm 35.538i \\ -36.0964 & -15.8413 \pm 35.5471i & -31.5696 & -8.1860 \pm 11.3334i \\ -25.0000 & -25.0000 & -25.0000 & -13.2440 \\ -7.6167 \pm 11.8743i & -8.0157 \pm 10.1241i & -1.9716 \pm 13.3705i & -12.6033 \\ -12.6000 & -12.6000 & -12.6000 & -12.5983 \pm 0.0029i \\ -12.6000 & -12.6000 & -0.0502 \pm 1.0520i & -4.1164 \\ -0.6263 \pm 0.1281i & -0.2161 \pm 0.7238i & -0.3773 & 1.6042 \\ 0.6264 & -0.3739 & -0.3206 & -0.3710 \\ -0.0870 & -0.0713 & -0.0081 & 0.2023 \\ 0.0146 & -0.0003 & -12.6000 & -0.0125 \end{bmatrix} \quad \text{(A.2)}$$

$$G_2(s) = \frac{1}{\triangle} \begin{bmatrix}
202.9475 & 10.2965 & -0.0013 & -359.6270 \\
-15.1545 \pm 68.7226i & -200.5100 & -5100.1 & -15.5008 \pm 69.6809i \\
-15.5573 \pm 35.4095i & 173.9039 & 3362.5 & -15.8535 \pm 35.5388i \\
-25.0000 & -15.8752 \pm 35.5522i & 1350.3 & -8.4684 \pm 10.3228i \\
-9.5655 \pm 9.2434i & -27.8418 & -15.8540 \pm 35.5450i & -12.9459 \\
-12.6000 & -25.0000 & -25.0000 & -12.6009 \\
-11.9066 & -12.6000 & -14.1258 & -12.5996 \pm 0.0008i \\
-2.9956 & -12.6000 & -12.6000 & -2.8328 \\
-0.1828 \pm 0.5737i & -4.6603 \pm 6.2481i & -1.8570 \pm 0.5447i & -0.1419 \pm 0.5580i \\
0.1462 \pm 0.4890i & -1.0966 & 0.6591 \pm 1.3147i & 0.1881 \pm 0.4952i \\
-0.1167 & 0.0075 \pm 1.1690i & 0.0469 \pm 0.5092i & -0.2790 \\
-12.6000 & 0.5823 \pm 0.5616i & -0.3754 & \\
 & -0.1697 & -12.6000 & \\
 & & & \\
-0.0983 & -0.0050 & 0.0002 & 3.2409 \\
-359.4916 & -204.57 \pm 810.30i & -33172 & -15.4899 \pm 69.6534i \\
-18.3033 \pm 67.4735i & -15.8734 \pm 35.5539i & 32779 & -15.8534 \pm 35.5387i \\
-15.6952 \pm 34.7784i & -25.0000 & -15.8537 \pm 35.5452i & -20.5037 \\
-25.0000 & -24.0952 & -25.0000 & -8.6007 \pm 10.2721i \\
-10.3600 \pm 8.6999i & 5.8245 \pm 11.1899i & 6.7572 \pm 10.9278i & -12.9385 \\
-12.6001 & -12.6000 & -13.8372 & -12.6032 \pm 0.0055i \\
-12.5999 & -12.6000 & -12.6000 & -12.5937 \\
-11.0480 & -4.5474 \pm 5.3308i & -2.2187 & -2.8108 \\
-3.2469 & 0.0838 \pm 0.8698i & 0.0744 \pm 0.3711i & 0.0787 \pm 0.4847i \\
0.0680 \pm 0.5314i & -0.4290 & -0.5513 & -0.3244 \\
-0.2221 & -0.1310 & -0.3802 & 0.0621 \\
-0.0887 & & -12.6000 &
\end{bmatrix} \tag{A.3}$$

with the characteristic polynomial

$$\begin{aligned}
\triangle \;=\; & [1, -15.4990 \pm 69.6653i, -15.8535 \pm 35.5387i, -12.9489, -8.4879 \pm 10.4445i, \\
& -2.8474, -0.2431 \pm 0.8019i, 0.1527 \pm 0.5376i, -0.1060, -0.3564, \\
& -12.6000, -12.6000, -12.6000, -25.0000]
\end{aligned} \tag{A.4}$$

A.2 System model at 25 knots forward flight

$$G_{25}(s) = \begin{bmatrix} G_1(s) \\ \dots \\ G_2(s) \end{bmatrix} \tag{A.5}$$

where

$$G_1(s) = \frac{1}{\triangle} \begin{bmatrix} 1134.7 & 76.6750 & -0.0115 & 4.2314 \\ -15.4758 \pm 69.5584i & -34.4358 \pm 58.4857i & -1119.4 & 129.0422 \\ -15.9127 \pm 35.5070i & 10.6416 \pm 48.3770i & 546.12 \pm 817.51i & -15.7061 \pm 69.5378i \\ -25.0000 & -15.8297 \pm 35.5653i & -15.8321 \pm 35.5292i & -15.8539 \pm 35.5337i \\ -8.6920 \pm 10.0864i & -25.0000 & -31.9132 & -8.2659 \pm 11.2540i \\ -12.6000 & -8.0176 \pm 10.1003i & -25.0000 & -13.0446 \\ -12.6000 & -12.6000 & -2.2911 \pm 13.0175i & -12.6005 \pm 0.0008i \\ -7.7736 \pm 1.0240i & -0.2453 \pm 0.8310i & -12.6000 & -12.5991 \\ -0.5494 \pm 0.7692i & -0.6686 & -0.0852 \pm 1.1130i & -4.3562 \\ 0.2232 \pm 0.3379i & 0.0822 & -0.6658 & 1.9560 \\ -0.0575 & -0.0582 & -0.2883 & -0.6162 \\ & -12.6000 & 0.0733 & 0.1379 \\ & & -12.6000 & 0.0692 \\ & & & \\ 20.4352 & 1.3807 & -0.000178 & -16.1225 \\ -6.0407 \pm 77.1411i & -299.0550 & -14.125 \pm 47020i & -15.8188 \pm 69.6182i \\ -13.2692 \pm 35.367i & 125.83 \pm 227.74i & -15.8320 + 35.5280i & -15.8538 \pm 35.5337i \\ -41.9216 & -15.8327 \pm 35.5479i & -31.4433 & -8.2027 \pm 11.4298i \\ -25.0000 & -25.0000 & -25.0000 & -13.0672 \\ -7.4132 \pm 11.9424i & -8.0181 \pm 10.1223i & -1.9491 + 13.3530i & -12.6040 \\ -12.6000 & -12.6000 & -12.6000 & -12.5980 \pm 0.0034i \\ -12.6000 & -12.6000 & -0.0844 + 1.1043i & -4.5373 \\ -0.6103 \pm 0.4203i & -0.2473 \pm 0.8313i & -0.4230 & 1.9445 \\ 0.5910 & -0.4192 & -0.2946 & -0.4109 \\ -0.0796 & -0.0582 & -0.0103 & 0.1440 \\ -0.0013 & -0.0059 & -12.6000 & -0.0127 \end{bmatrix} \tag{A.6}$$

$$G_2(s) = \frac{1}{\triangle} \begin{bmatrix}
193.5056 & 13.0718 & -0.0011 & -347.0616 \\
-14.7829 \pm 68.2944i & -175.8084 & -5482.3 & -15.5055 \pm 69.6805i \\
-15.4219 \pm 35.3651i & 149.9671 & 4360.1 & -15.8540 \pm 35.5334i \\
-25.0000 & -15.8929 \pm 35.5565i & 1075.1 & -8.4595 \pm 10.3092i \\
-10.4287 \pm 8.8284i & 28.7769 & -15.8549 \pm 35.5443i & -12.9341 \\
-12.6000 & -25.0000 & -25.0000 & -12.6007 \pm 0.0013i \\
-12.6000 & -12.6000 & -14.1663 & -12.5985 \\
-11.0681 & -12.6000 & -12.6000 & -2.9074 \\
-3.1900 & -4.7249 \pm 6.4021i & -1.8907 \pm 0.6511i & -0.1304 \pm 0.5372i \\
-0.1989 \pm 0.5573i & 0.0458 \pm 1.2921i & 0.6709 \pm 1.3556i & 0.1538 \pm 0.4578i \\
0.0967 \pm 0.4746i & -1.0357 & 0.0450 \pm 0.5118i & -0.2568 \\
-0.0206 & 0.5307 \pm 0.1973i & -0.4035 & \\
 & -0.0139 & -12.6000 & \\
 & & & \\
-0.0915 & -0.0062 & 0.00027 & 3.1277 \\
-495.9449 & -274.38 \pm 707.15i & -30092 & -15.4922 \pm 69.6546i \\
-18.0581 \pm 66.3057i & -15.8894 \pm 35.5592i & 30027 & -15.8540 \pm 35.5333i \\
-15.5477 \pm 34.6682i & -25.0000 & -15.8543 \pm 35.5448i & -27.4717 \\
-25.0000 & -24.7634 & -25.0000 & -8.5432 \pm 10.2604i \\
-11.3444 \pm 8.4467i & 7.4376 \pm 10.0682i & 9.0734 \pm 9.1537i & -12.9327 \\
-12.6000 & -12.6000 & -13.8794 & -12.6026 \\
-12.6000 & -12.6000 & -12.6000 & -12.5987 \pm 0.0022i \\
-10.0760 & -4.5912 \pm 5.5546i & -2.1863 & -2.8885 \\
-3.4788 & 0.1053 \pm 0.8919i & -0.6986 & 0.0670 \pm 0.4595i \\
0.0517 \pm 0.5089i & -0.4451 & 0.0950 \pm 0.3486i & -0.3319 \\
-0.2275 & -0.0439 & -0.4024 & 0.0587 \\
-0.0757 & & -12.600 &
\end{bmatrix} \tag{A.7}$$

with the characteristic polynomial

$$\begin{aligned}
\triangle \;=\; & [1, -15.5036 \pm 69.6649i, -15.8540 \pm 35.5334i, -12.9354, -8.4851 \pm 10.4353i, \\
& -2.9286, -0.2673 \pm 0.8943i, 0.1242 \pm 0.5174i, -0.0509, -0.3679, \\
& -12.6000, -12.6000, -12.6000, -25.0000]
\end{aligned} \tag{A.8}$$

A.3 System model at 35 knots forward flight

$$G_{35}(s) = \begin{bmatrix} G_1(s) \\ \dots \\ G_2(s) \end{bmatrix} \tag{A.9}$$

where

$$G_1(s) = \frac{1}{\triangle} \begin{bmatrix}
1169.9 & 136.9330 & -0.0045 & 3.96 \\
-15.4443 \pm 69.5027i & -20.0671 \pm 61.1973i & -1455.2 & 80.0010 \\
-15.9309 \pm 35.4750i & -15.9287 \pm 35.6663i & 714.94 \pm 955.88i & -15.6924 \pm 69.4832i \\
-25.0000 & -3.3614 \pm 33.9132i & -15.7870 \pm 35.4984i & -15.8542 \pm 35.5098i \\
-8.9296 \pm 9.9900i & -25.0000 & -32.4002 & -8.2859 \pm 11.3871i \\
-12.6000 & -8.0154 \pm 10.0714i & -25.0000 & -12.8226 \\
-12.6000 & -12.6000 & -2.6383 \pm 12.6465i & -12.6013 \pm 0.0023i \\
-7.4509 \pm 2.8025i & -12.6000 & -12.6000 & -12.5974 \\
-0.5292 \pm 1.1313i & -0.3546 \pm 1.1833i & -0.2363 \pm 1.3289i & -4.7277 \\
0.0212 \pm 0.3069i & -1.0778 & -1.0837 & 2.6015 \\
-0.0030 & -0.0357 & -0.1889 & -0.9467 \\
 & 0.0433 & 0.0392 & 0.0712 \\
 & & -12.6000 & 0.0382 \\
 & & & \\
17.9987 & 2.1077 & -0.000014 & -12.3560 \\
-0.9399 \pm 90.0745i & -253.5250 & -15.084 \pm 165815.2i & -15.9021 \pm 69.5734i \\
-53.8152 & 102.89 \pm 205.45i & 15.7882 \pm 35.4911i & -15.8538 \pm 35.5101i \\
-12.9563 \pm 35.7873i & -15.7884 \pm 35.5535i & -31.0648 & -8.2328 \pm 11.7514i \\
-25.0000 & -25.0000 & -25.0000 & -12.8106 \\
-7.0472 \pm 12.0602i & -8.0274 \pm 10.1166i & -1.8822 \pm 13.2671i & -12.6037 \pm 0.0066i \\
-12.6000 & -12.6000 & -12.6000 & -12.5926 \\
-0.4906 \pm 0.9329i & -0.3577 \pm 1.1834i & -12.6000 & -5.0658 \\
-0.0076 \pm 0.0933i & -0.5653 & -0.2315 \pm 1.3178i & 2.3869 \\
-0.0090 & -0.0261 \pm 0.0007i & -0.5713 & -0.5364 \\
-12.6000 & -12.6000 & -0.1949 & 0.0781 \\
 & & -0.0163 & -0.0146
\end{bmatrix} \tag{A.10}$$

$$G_2(s) = \frac{1}{\triangle} \begin{bmatrix}
163.9249 & 19.2158 & -0.00037 & -324.8023 \\
-13.0675 \pm 66.6011i & -140.2564 & -10648 & -15.5155 \pm 69.6759i \\
-14.8761 \pm 35.3298i & 116.3674 & 9872.8 & -15.8541 \pm 35.5089i \\
-25.0000 & -15.9807 \pm 35.5744i & 727.8088 & -8.4489 \pm 10.2463i \\
-14.7334 \pm 8.0081i & -31.1149 & -15.8575 \pm 35.5408i & -12.8626 \\
-12.6000 & -25.0000 & -25.0000 & -12.6012 \\
-5.2225 \pm 0.9254i & -12.6000 & -14.2682 & -12.5994 \pm 0.0010i \\
-0.2051 \pm 0.4943i & -4.8375 \pm 6.9528i & -12.6000 & -3.1603 \\
0.0575 \pm 0.4786i & 0.2967 \pm 1.7870i & -12.6000 & -0.0844 \pm 0.4850i \\
-0.0252 & 0.9439 & -2.0068 \pm 0.9672i & 0.0738 \pm 0.3437i \\
-12.6000 & -0.9485 & 0.6867 \pm 1.4523i & -0.2567 \\
 & -0.0339 \pm 0.3197i & 0.0429 \pm 0.4666i & \\
 & -12.6000 & -0.4674 & \\
 & & & \\
-0.0759 & -0.0089 & 0.00015 & 2.9271 \\
-898.2193 & -480.92 \pm 451.26i & -40295 & -15.4970 \pm 69.6560i \\
-16.8912 \pm 63.0040i & -15.9682 \pm 35.5812i & 40216 & -48.2573 \\
-14.8577 \pm 34.3816i & -26.7881 & -15.8551 \pm 35.5420i & -15.8541 \pm 35.5089i \\
-25.0000 & -25.0000 & 26.1298 & -8.4867 \pm 10.2242i \\
-15.7848 \pm 7.9140i & 11.6470 \pm 2.3234i & -25.0000 & -12.8628 \\
-12.6000 & -12.6000 & -14.0108 & -12.6035 \\
-5.0702 \pm 1.6539i & -4.6702 \pm 6.3535i & -12.6000 & -12.5983 \pm 0.0030i \\
0.0624 \pm 0.4717i & 0.3533 \pm 0.9147i & -12.6000 & -3.1519 \\
-0.3335 & -0.4594 & 6.5408 & 0.0618 \pm 0.3947i \\
-0.0099 & 0.0778 & -1.6273 \pm 0.2908i & -0.3715 \\
-12.6000 & -12.6000 & -0.4290 & 0.0447 \\
 & & 0.1276 \pm 0.3064i &
\end{bmatrix} \tag{A.11}$$

with the characteristic polynomial

$$\begin{aligned}
\triangle \;=\; & [1, -15.5129 \pm 69.6600i, -15.8541 \pm 35.5088i, -12.8621, -8.4899 \pm 10.3868i, \\
& -3.1919, -0.3626 \pm 1.2306i, 0.0864 \pm 0.4339i, -0.0016, -0.3925, \\
& -12.6000, -12.6000, -12.6000, -25.0000]
\end{aligned} \tag{A.12}$$

A.4 System model at 40 knots forward flight

$$G_{40}(s) = \begin{bmatrix} G_1(s) \\ \dots \\ G_2(s) \end{bmatrix} \tag{A.13}$$

where

$$G_1(s) = \frac{1}{\Delta} \begin{bmatrix} 1204.5 & 160.8735 & -0.0068 & 4.0279 \\ -15.4469 \pm 69.4963i & -18.3203 \pm 63.4942i & -1217.4 & -15.6775 \pm 69.4664i \\ -15.9324 \pm 35.4634i & -15.9929 \pm 35.5965i & 596.30 \pm 812.73i & 66.0211 \\ -25.0000 & -4.9383 \pm 28.6443i & -15.7661 \pm 35.4862i & -15.8542 \pm 35.4990i \\ -8.9383 \pm 10.0292i & -25.0000 & -32.7598 & -8.2824 \pm 11.4187i \\ -12.6000 \pm 0.0000i & -8.0109 \pm 10.0566i & -25.0000 & -12.8237 \\ -7.3971 \pm 2.5486i & -12.6000 \pm 0.0000i & -2.8077 \pm 12.4641i & -12.6009 \pm 0.0015i \\ -0.5306 \pm 1.2690i & -0.3936 \pm 1.3084i & -12.6000 \pm 0.0000i & -12.5983 \\ -0.0441 \pm 0.2936i & -1.2638 & -0.2925 \pm 1.4242i & -4.6642 \\ -0.0000 & -0.0324 & -1.2761 & 2.7558 \\ 1.1000 & 0.0292 & -0.1573 & -1.0843 \\ 1.1000 & 1.1000 & 0.0252 & 0.0616 \\ 1.1000 & 1.1000 & 1.1000 & 0.0245 \\ & & & \\ 17.6853 & 2.3626 & -0.000014 & -11.8770 \\ 0.5279 \pm 93.1448i & -242.5445 & -14.626e \pm 51603i & -15.9271 \pm 69.5557i \\ -57.1007 & 97.330 \pm 199.86i & -15.7683 \pm 35.4743i & -15.8536 \pm 35.4995i \\ -12.8415 \pm 35.9109i & -15.7668 \pm 35.5573i & -30.9814 & -8.2429 \pm 11.8552i \\ -25.0000 & -25.0000 & -25.0000 & -12.8242 \\ -7.0400 \pm 12.0222i & -8.0339 \pm 10.1156i & -1.8687 \pm 13.2384i & -12.6053 \\ -12.6000 & -12.6000 & -12.6000 & -12.5973 \pm 0.0045i \\ -0.4769 \pm 1.1129i & -0.3974 \pm 1.3081i & -12.6000 & -5.0250 \\ -0.0800 \pm 0.0937i & -0.6050 & -0.2861 \pm 1.4124i & 2.3957 \\ -0.0155 & -0.0253 + 0.0056i & -0.6122 & -0.5681 \\ -12.6000 & -12.6000 & -0.1634 & 0.0701 \\ & & -0.0182 & -0.0166 \\ & & 1.1000 & \end{bmatrix} \tag{A.14}$$

$$G_2(s) = \frac{1}{\triangle} \begin{bmatrix}
163.9249 & 19.2158 & -0.00037 & -324.8023 \\
-12.5317 \pm 65.8947i & -133.5188 & -8702.3 & -15.5154 \pm 69.6719i \\
-14.6187 \pm 35.3543i & 110.2134 & 7991.3 & -15.8540 \pm 35.4978i \\
-25.0000 & -16.0245 \pm 35.5817i & 663.7575 & -8.4537 \pm 10.2226i \\
-16.0368 \pm 8.0210i & -31.8050 & -15.8586 \pm 35.5390i & -12.8221 \\
-12.6000 & -25.0000 & -25.0000 & -12.6010 \pm 0.0017i \\
-12.6000 & -12.6000 & -14.2952 & -12.5980 \\
-4.7711 \pm 1.9392i & -4.8403 \pm 7.1414i & -12.6000 \pm 0.0000i & -3.2520 \\
0.0740 \pm 0.4958i & 0.3782 \pm 1.9783i & -2.0492 \pm 1.0628i & -0.0778 \pm 0.4737i \\
-0.1861 \pm 0.4591i & -0.9306 & 0.6900 \pm 1.4729i & 0.0745 \pm 0.3281i \\
-0.1061 & 0.8659 & -0.4775 & -0.2863 \\
 & -0.0493 \pm 0.3103i & 0.0435 \pm 0.4487i & \\
 & -12.6000 & & \\
 & & & \\
-0.0731 & -0.0098 & 0.00030 & 2.9772 \\
-1014.4 & -540.01 \pm 342.82i & -29136 & -15.4961 \pm 69.6541i \\
-16.5758 \pm 62.1235i & -16.0078 \pm 35.5905i & 29052 & -55.1825 \\
-14.5193 \pm 34.2956i & -27.4298 & -15.8556 \pm 35.5403i & -15.8539 \pm 35.4978i \\
-25.0000 & -25.0000 & 32.4249 & -8.4865 \pm 10.2054i \\
-17.1454 \pm 7.8464i & 18.7807 & -25.0000 & -12.8221 \\
-12.6000 & -12.6000 & -14.0483 & -12.6049 \\
-4.6976 \pm 2.2716i & -4.6711 \pm 6.6091i & -12.6000 & -12.5976 \pm 0.0042i \\
0.0825 \pm 0.4662i & 6.9276 & -12.6000 & -3.2461 \\
-0.3658 & 0.5145 \pm 0.8691i & 5.3482 & 0.0668 \pm 0.3841i \\
0.0232 & -0.4476 & -1.6882 \pm 0.5808i & -0.3848 \\
-12.6000 & 0.0844 & -0.4247 & 0.0377 \\
 & -12.6000 & 0.1265 \pm 0.3003i &
\end{bmatrix} \tag{A.15}$$

with the characteristic polynomial

$$\begin{aligned}
\triangle \;=\; & [1, -15.5127 \pm 69.6559i, -15.8540 \pm 35.4977i, -12.8221, -8.4993 \pm 10.3681i, \\
& -3.2830, -0.3995 \pm 1.3511i, 0.0861 \pm 0.4130i, -0.0031, -0.3971, \\
& -12.6000, -12.6000, -12.6000, -25.0000]
\end{aligned} \tag{A.16}$$

Bibliography

[1] ANONYMOUS. Aeronautical design standard-handling qualities requirements for military rotorcraft. *ADS-33C, United States Army aviation Systems Command, St. Louis, Mo. Directorate for Engineering, U.S.A.*, 1989.

[2] S.L. BUCKINGHAM and G.D. PADFIELD. Piloted simulations to explore helicopter advanced control systems. *Royal Aerospace Establishment, Thecnical report 86022*, 1986.

[3] SUSAN CARR. Siso h_∞ control of and advanced short take off and landing aircraft, icu-301. *ICU-University of Strathclyde, U.K.*, 1991.

[4] CHI-TSONG CHEN. *Control System Design.* Saunders College Publishing, 1993.

[5] R.T.N CHEN and W.S HINDSON. Influence of high order dynamics on helicopter flight control system bandwidth. *Journal of Gidance and Control*, 9:190–197, 1986.

[6] C.VERDE, J. LICEAGA-CASTRO, J. O'REILLY, and W.E. LEITHEAD. Structural and robustness issues in helicopter flight control. *Proc. IMA Internat. Conference on Control: Modelling Computation, Information, UMIST, U.K.*, 1992.

[7] D.F. ENNS. Multivariable flight control for an attack helicopter. *IEEE Control Systems Magazine*, 7:34–38, 1987.

[8] G. HUGHES, M.A MANNESS, and D.J. MURRAY-SMITH. Eigenstructure assignment for handling qualities in helicopter flight control law design. *Proceedings of 16th European Rotorcraft Forum, Glasgow, U.K.*, 1990.

[9] C. INMOCENTI, M.and STANZIOLA. Performance-robustness trade-off of eigenstructure assignment applied to rotorcraft. *Aeronautical Journal*, 94:124–131, 1990.

[10] ALBERTO ISIDORI. *Non-linear Control Systems.* Springer-Verlang, 1989.

[11] GRIBBLE J.J. Linear quadratic gaussian/loop transfer recovery for a helicopter in low speed flight. *Journal of Guidance, Control and Dynamics*, 16:754–761, 1993.

[12] GIORGIO LARDINELLI. *L'ELICOTTERO.* Mario Stavolta Editore, 1978.

[13] W.E. LEITHEAD and J. O'REILLY. Performance issues in the individual channel design of 2-input 2-output systems: Part 1 - structural issues. *International Journal of Control*, 54:47–82, 1991.

[14] W.E. LEITHEAD and J. O'REILLY. M-input m-output feedback control by individual channel design. *International Journal of Control*, 56:1347–1398, 1992.

[15] W.E. LEITHEAD and J. O'REILLY. Performance issues in the individual channel design of 2-input 2-output systems: Part 2 - robustness issues. *International Journal of Control*, 55:3–47, 1992.

[16] W.E. LEITHEAD and J. O'REILLY. Performance issues in the individual channel design of 2-input 2-output systems: Part 3 - non-diagonal control and related issues. *International Journal of Control*, 55:265–312, 1992.

[17] W.E. LEITHEAD and J. O'REILLY. New roles for feedforward in multivariable control by individual channel design. *International Journal of Control*, 57:1357–1386, 1993.

[18] W.E. LEITHEAD and J. O'REILLY. Investigation of the icd structure of systems defined by state-space models. *International Journal of Control*, 60:71–89, 1994.

[19] J. LICEAGA-CASTRO, C.VERDE, J. O'REILLY, and W.E. LEITHEAD. Helicopter flight control by individual channel design. *IEE Proc., Part D, accepted for publication*, 1994.

[20] J. LICEAGA-CASTRO, J. O'REILLY, and W.E. LEITHEAD. Neo-classical helicopter flight control. *Submitted to 1995 American control conference, Seattle*, 1995.

[21] M.A MANNESS, J.J GRIBBLE, and D.J. MURRAY-SMITH. Multivariable methods for helicopters flight control law design. *Proceedings of 16th European Rotorcraft Forum, Glasgow, U.K.*, 1990.

[22] M.A MANNESS and D.J. MURRAY-SMITH. Aspects of multivariable control law designs for helicopters using eigenstructure assignment. *Journal of American Helicopter Society*, 37:18–32, 1992.

[23] DONALD McLEAN. *Automatic Flight Control Systems.* Prentice-Hall, 1990.

[24] D. McRUER, I. ASHKENAS, and D. GRAHAM. *Aircraft Dynamics and Automatic Control.* Princeton University Press, 1973.

[25] DONAL M.LAYTON. *Helicopter performance.* Matrix series in mechanical and aeronautical engineering, 1984.

[26] ROBERT C. NELSON. *Flight stability and automatic control.* MacGraw-Hill Book Company, 1989.

[27] J. O'REILLY and W.E. LEITHEAD. Multivariable control by individual channel design. *International Journal of Control.*, 54:1–46, 1991.

[28] G.D. PADFIELD. A theoretical model of helicopter flight mechanics for application to piloted simulation. *Royal Aircraft Establishment, Technical Report 81048*, 1981.

[29] J. SMITH. An analysis of helicopter flight mechanics part 1, user's guide to software package helistab. *Royal Aircraft Establishment (Bedford), TM FS(B) 569*, 1984.

[30] M.B. TISCHLER. Digital control of highly augmented combat rotorcraft. *NASA Technical Memorandum 88346, USA AVSCOM Tecnical report 87-A-5*, 1987.

[31] M.B. TISCHLER. Assessment of digital flight control for advanced combat rotorcraft. *Journal of American Helicopter Society*, 34:66–76, 1989.

[32] B.K. TOWNSEND. The application of quadratic optimal cooperative control systems to a ch-47 helicopter. *Proceedings of 12th European Rotorcraft Forum, Garmisch-Partenkirchen, Germany*, 1986.

[33] PROUTY RAYMOND W. *Helicopter performance, stability and control.* PWS Publishers, Boston., 1973.

[34] D. WALKER and I. POSTLETHWAITE. Full authority active control system design for a high performance helicopter. *Proceedings of 16th European Rotorcraft Forum, Glasgow, U.K.*, 1990.

[35] A. YUE and I. POSTLETHWAITE. Improvement of helicopter handling qualities using h_∞ optimization. *IEE proceedings Pt. D*, 137:115–129, 1990.